

---

*NEAR-INFRARED LIGHT ACTIVATED LIPID-BASED  
DRUG DELIVERY SYSTEMS FOR THE TREATMENT OF  
AGE-RELATED MACULAR DEGENERATION*

---

A thesis submitted for the degree of

DOCTOR OF PHILOSOPHY

By

Joanne D. Du

Bachelor of Pharmaceutical Sciences (Honours)



**MONASH UNIVERSITY**

Drug Delivery, Disposition and Dynamics

Monash Institute of Pharmaceutical Sciences

Melbourne, Victoria, Australia

**2018**

*Dedicated to my kind parents,*

*Garry To Ha Du and Chun Yuk Chan*

## COPYRIGHT NOTICE

---

© Joanne Du (2018).

I certify that I have made all reasonable efforts to secure copyright permissions for third party content included in this thesis and have not knowingly added copyright content to my work without the owner's permission.

## DECLARATION OF AUTHORSHIP

---

In accordance with Monash University Doctorate Regulation, the following declarations are made.

I hereby declare that this thesis contains no material which has been accepted for the award of any other degree or diploma at any university or equivalent institution and that, to the best of my knowledge and belief, this thesis contains no material previously published or written by another person, except where due reference is made in the text of the thesis.

This thesis includes three original papers published in peer reviewed journals and one manuscript in preparation. In addition, two second author publications were published with co-authors that are related, but did not contribute to the thesis research, are included in the Appendix. The core theme of the thesis is phospholipid-based liquid crystalline nanomaterials in drug delivery. The ideas, development and writing up of all the papers in the thesis were the principal responsibility of myself, the candidate, working within the Drug Delivery, Disposition and Dynamics unit under the supervision of Professor Ben Boyd.

The inclusion of co-authors in the published papers reflects the fact that this work came from active collaborations and acknowledges input into team-based research.

Signature:

A solid black rectangular box redacting the signature of the author.

Print Name:

JOANNE DU

Date:

30/03/2018

## THESIS INCLUDING PUBLISHED WORKS DECLARATION

In the case of Chapters 1, 3, 4 and 5, my contribution to the work involved the following:

Thesis chapter and publication title	Status	Nature and extent of candidate's contribution	Co-author	
			Names	Monash student
Chapter 1. Lipid-based drug delivery systems in the treatment of wet age-related macular degeneration	Published (Drug Deliv. Transl. Res. 2016)	75 % Concept, literature research and manuscript preparation	1. Wye-Khay Fong	No
			2. Suzanne Caliph	No
			3. Ben J. Boyd	No
Chapter 3. Phospholipid-based self-assembled mesophase systems for light-activated drug delivery	Published (Phys. Chem. Chem. Phys. 2015)	75 % Research design, data collection and analysis, and manuscript preparation	1. Wye-Khay Fong	No
			2. Stefan Salentinig	No
			3. Suzanne Caliph	No
			4. Adrian Hawley	No
			5. Ben J. Boyd	No
Chapter 4. Naphthalocyanine as a photothermal actuator for lipid-based drug delivery systems	Published (J. Phys. Chem. B)	80 % Research design, data collection and analysis, and manuscript preparation	1. Linda Hong	Yes
			2. Angel Tan	No
			3. Ben J. Boyd	No
Chapter 5. Light-activated release of aflibercept from a phospholipid-based liquid crystalline system	In Preparation	75 % Research design, data collection and analysis, and manuscript preparation	1. Wye-Khay Fong	No
			2. Eric Hanssen	No
			3. Suzanne Caliph	No
			4. Ben J. Boyd	No

I have not renumbered sections of published and in preparation papers in order to generate a consistent presentation within the thesis.

Candidate's signature:



Date: 30/03/2018

The undersigned hereby certify that the above declaration correctly reflects the nature and extent of the student's and co-authors' contributions to this work. In instances where I am not the responsible author I have consulted with the responsible author to agree on the respective contributions of the authors.

Main Supervisor's signature:



Date: 30/3/2018

## PUBLICATIONS DURING ENROLMENT

---

**J. D. Du** *et al.* Naphthalocyanine as a new photothermal actuator for lipid-based drug delivery systems. *J. Phys. Chem. B* **2018**, 122 (5), 1766-1770.

S. Jia, **J.D. Du** *et al.* Investigation of Donor Acceptor Stenhouse Adducts as New Visible Wavelength-Responsive Switching Elements for Lipid-Based Liquid Crystalline Systems, *Langmuir*. **2017**, 33 (9), 2215-2221

M.D.J. Quinn, T. Wang, **J.D. Du** *et al.* Graphene as a photothermal actuator for control of lipid mesophase structure, *Nanoscale*. **2017**, 9, 341-348.

**J. D. Du** *et al.* Lipid-based drug delivery systems in the treatment of wet age-related macular degeneration. *Drug Deliv. Transl. Res.* **2016**, 6, 781-792.

M.D.J. Quinn, **J. D. Du** *et al.* Lipid liquid-crystal phase change induced through near-Infrared Irradiation of entrained graphene particles. *Langmuir*. **2015**, 31 (24), 6605-6609.

**J. D. Du** *et al.* Phospholipid-based self-assembled mesophase systems for light-activated drug delivery, *Phys. Chem. Chem. Phys.* **2015**, 17, 14021-14027.

**J. D. Du** *et al.* A novel approach to enhance the mucoadhesion of lipid drug nanocarriers for improved drug delivery to the buccal mucosa. *Int. J. Pharm.* **2014**, 471 (1-2), 358-365.

## MANUSCRIPT IN PREPARATION

---

**Joanne D. Du**, Wye-Khay Fong, Eric Hanssen, Suzanne M. Caliph and Ben J. Boyd. Light-activated release of aflibercept from a phospholipid-based liquid crystalline system.

**Joanne D. Du**, Anna C. Pham, Suzanne M. Caliph, Kirstan A. Vessey, Erica L. Fletcher and Ben J. Boyd. Passive targeting to the leaky vasculature in age-related macular degeneration

Angel Tan, Linda Hong, **Joanne D. Du**, Ben J. Boyd. Self-assembled nanostructured lipid systems: Is there a link between structure and cytotoxicity?

## ACKNOWLEDGEMENTS

---

First and foremost, a big thank you to my main supervisor, Professor Ben Boyd, for all the guidance and opportunities he had given me during these few years. I like to express my appreciation to my co-supervisors, Doctor Wye-Khay Fong and Doctor Suzanne Caliph for their assistance and support whenever things do not go as it should. I need to express my gratitude to the guys at the Australian Synchrotron for their help with the experimental set-up on the SAXS/WAXS beamline. The research included in this thesis was supported by an Australian Government Research Training Program Scholarship.

To the Boyd family, present and past, a big thank you for keeping me sane throughout this journey. I would also like to let the rest of my friends know how much I appreciated those impromptu gatherings, which was like a temporary escape from all the built up stress. To my best friend, you have been with me through ups and downs, I am so grateful to have you in my life and I hope that I can continue to rely on you in the near future. I sincerely thank my family and my cousin, Kathy Chan, for tolerating my selfishness during this tough journey and always supporting me, even though I know you all never truly understood what I was doing. Lastly, I want to tell Robert Cheng, I am DONE! I hope you are still proud of me and will continue to look after us from above.

For those who are pursuing this path, please do not take things for granted. Treasure every moment and make the most out of every opportunity, as they will add to the value of your future.

# CONTENTS

---

COPYRIGHT NOTICE .....	ii
DECLARATION OF AUTHORSHIP .....	iii
THESIS INCLUDING PUBLISHED WORKS DECLARATION .....	iv
PUBLICATIONS DURING ENROLMENT .....	v
MANUSCRIPT IN PREPARATION .....	v
ACKNOWLEDGEMENTS.....	vi
CONTENTS .....	vii
LIST OF FIGURES .....	ix
ABBREVIATIONS.....	xi
ABSTRACT .....	xii
CHAPTER ONE: INTRODUCTION .....	1
Declaration for Chapter One .....	2
1. A statement of the problem.....	3
1.1. About age-related macular degeneration (AMD).....	4
1.2. Current treatments for wet AMD .....	6
1.3. Limitations associated with anti-VEGF therapies .....	9
1.4. Opportunities of emerging delivery systems for treatment of AMD.....	10
1.5. Stimuli-responsive systems for ‘on-demand’ drug delivery .....	18
1.6. Hypothesis .....	24
1.7. Project Objectives .....	24
1.8. References.....	26
CHAPTER TWO: GENERAL MATERIALS AND METHODS .....	34
2.1. Materials.....	35
2.1.1. Lipid components .....	35
2.1.2. Near-infrared responsive actuators .....	36
2.1.3. General materials.....	37
2.2. Methods.....	37
2.2.1. General preparation.....	37
2.2.2. Phase characterisation.....	37
2.2.3. Drug release experiment .....	41
2.3. References.....	44
CHAPTER THREE: LIGHT-RESPONSIVE PHOSPHOLIPID-BASED SYSTEM.....	45
Prologue to Chapter Three .....	46
Declaration for Chapter Three .....	46
3. Phospholipid-Based Self-Assembled Mesophase Systems for Light-Activated Drug Delivery .....	47
3.1. Abstract.....	47
3.2. Introduction .....	48
3.3. Materials and Methods .....	51
3.4. Results and Discussion.....	53
3.5. Conclusion .....	61
3.6. Acknowledgements .....	61
3.7. References.....	62
3.8. Supplementary Information .....	64

CHAPTER FOUR: COMPARISON OF DIFFERENT PHOTOTHERMAL ACTUATORS .....	66
Prologue to Chapter Four .....	67
Declaration for Chapter Four .....	67
4. Naphthalocyanine as a New Photothermal Actuator for Lipid-Based Drug Delivery Systems .....	68
4.1. Abstract.....	68
4.2. Introduction .....	69
4.3. Materials and Methods .....	70
4.4. Results.....	72
4.5. Conclusion .....	78
4.6. Acknowledgements .....	78
4.7. References.....	79
4.8. Supplementary Information .....	82
CHAPTER FIVE: LIGHT-ACTIVATED RELEASE FROM PHOSPHOLIPID-BASED SYSTEM .....	83
Prologue to Chapter Five.....	84
Declaration for Chapter Five .....	84
5. Light-Activated Release of Aflibercept from a Phospholipid-Based Liquid Crystalline System.....	85
5.1. Abstract.....	85
5.2. Introduction .....	86
5.3. Material.....	88
5.4. Methods .....	88
5.5. Results and Discussion.....	91
5.6. Conclusion .....	98
5.7. Acknowledgement.....	98
5.8. References.....	99
5.9. Supplementary Information .....	101
CHAPTER SIX: SUMMARY AND OUTLOOK.....	104
6.1. Summary of Findings .....	105
6.2. Future Directions .....	108
6.3. References.....	113
APPENDIX:.....	115

## LIST OF FIGURES

---

1.1.	Schematic of the eye and its barriers in ocular drug delivery.....	4
1.2.	Schematic of normal retina vs. diseased retina with wet age-related macular degeneration .....	6
1.3.	Common self-assembled phases and their corresponding critical packing parameter. The abbreviated phases are as follows: inverse micellar, inverse micellar cubic, inverse hexagonal, inverse bicontinuous cubic, lamellar, normal bicontinuous cubic, normal hexagonal, normal micellar cubic phase and normal micellar .....	20
1.4.	Schematic illustrating how changing the lyotropic liquid crystalline structure can control the release rate of drug. The lyotropic liquid crystalline structures picture on the right are the fast releasing inverse bicontinuous cubic phase, in comparison to the slow releasing phases: inverse hexagonal, inverse micellar cubic and inverse micellar phase. A range of methods can be used to impart stimuli-responsiveness in these systems to switch between slow and fast releasing structures.....	21
1.5.	Schematic of how a NIR-light triggered lipid ‘depot’ could reduce the frequency of intravitreal injections by repeated triggered release of a dose of drug using a laser, to replace regular intravitreal injections.....	22
2.1.	Schematic of drug release experiment for aflibercept .....	45
3.1.	Schematic of desired liquid crystalline system with a phase transition from lamellar phase to bicontinuous cubic phase and its corresponding drug release profile controlled using NIR laser and GNR.....	53
3.2.	Literature phase behaviour of the POPE + cholesterol system in excess water with increasing cholesterol.....	54
3.3.	Phase behaviour of the POPE + cholesterol system in excess water with increasing cholesterol in this study.....	57
3.4.	Small-angle X-ray scattering profiles for 20 mol% cholesterol in POPE from A) literature and B) this study. The annotations of peaks in Figure 3.4B indicate the lamellar phase at low temperatures, and the inverse hexagonal phase at high temperature .....	57
3.5.	Comparison of SAXS scattering profiles from the POPE system with and without cholesterol (20 mol%) and PEG-DSPE (10 mol%) in excess water.....	59
3.6.	Effect of GNR on equilibrium structure of POPE bulk system in excess water A) Temperature dependent phase diagram and B) the lattice parameter of the lipid systems in the presence of 0 nM, 0.3 nM and 3 nM GNR is plotted against temperature.....	61
3.7.	Effect of NIR laser irradiation on apparent temperature of the POPE system in excess water containing 0 nM and 3 nM GNR.....	62
3.8.	SAXS scattering data for POPE and PEG-lipid system in excess water with 3 nM GNR at equilibrium temperatures and after NIR irradiation.....	63
SI 3.1.	Effect of GNR on equilibrium structure of PHYT bulk system. a) Temperature dependent phase diagram and b) the lattice parameter of the lipid systems in the presence of 0 nM, 0.3 nM and 3 nM GNR is plotted against thermostat-controlled temperature.....	67

SI 3.2.	Effect of NIR laser irradiation on apparent temperature of the PHYT system containing 0 nM and 0.3 nM GNR.....	68
SI 3.3.	UV/Vis absorbance of GNR solutions with the maximum SPR peak of 825 nm...	68
4.1.	Effect of NIR irradiation on the structure of PHYT and POPE-based system maintained at 37 °C. A) PHYT + SiNC, B) Blank PHYT, C) POPE + SiNC and D) Blank POPE. The red curves indicate the time points exposed to NIR irradiation .....	75
4.2.	Temperature-dependent phase behaviour for PHYT system containing A) SiNC determined in this study, B) increasing concentration of gold nanorods and C) graphene nanosheets.....	77
4.3.	Effect of NIR irradiation on the apparent temperature for the PHYT and POPE systems. A) PHYT + SiNC, B) POPE + SiNC, C) PHYT + graphene and D) POPE + gold nanorods .....	79
SI 4.1.	Absorbance spectrum of SiNC incorporated PHYT and POPE system, with a maximum absorbance around 790 nm.....	84
5.1.	Temperature sequence of X-ray diffraction patterns for DLPC:2LA-water dispersions from the literature at 20 bar.....	89
5.2.	Temperature sequence of X-ray diffraction patterns for DLPC:2LA-water dispersions from the this study at atmospheric pressure.....	94
5.3.	Temperature-dependent phase behaviour of DLPC:2LA system in excess water, DLPC:2LA with aflibercept, DLPC:2LA with gold nanorods and DLPC:2LA with silicon naphthalocyanine .....	95
5.4.	Difference in morphology of DLPC:2LA liposomes with A) SiNC, B) SiNC with aflibercept, C) aflibercept only, and D, E and F) aflibercept with GNR. Rigid faceted lipid bilayers are present in A and B.....	96
5.5.	SAXS scattering profile of time-resolved activation of DLPC:2LA with a) gold nanorods, which transitions from $L_{\alpha}$ to $V_2/H_2$ , and b) silicon naphthalocyanine, exhibiting a phase transition from $L_{\alpha}$ to $V_2$ .....	97
5.6.	Release of aflibercept (Eylea) from DLPC:2LA vesicles, passive release, DLPC:2LA vesicles with gold nanorods and silicon naphthalocyanine with and without NIR irradiation, and the recovery of aflibercept .....	99
SI 5.1.	Confirmation of hydrophobisation by comparing the absorbance scan of PEGylated GNR and hydrophobised GNR in THF.....	103
SI 5.2.	Quantification of Eylea using standard curve of known concentration vs. absorbance at 280 nm.....	104
SI 5.3.	Encapsulation efficiency of DLPC:2LA samples with GNR, SiNC and without photoactuators.....	104
SI 5.4.	SAXS scattering profile of time-resolved activation of aflibercept-loaded DLPC:2LA without NIR-responsive agents.....	105
SI 5.5.	Absorbance spectrum of DLPC:2LA, with SiNC and with GNR.....	105
6.1.	Schematic comparing liposomes behaviour depending on their surface characteristics.....	114
6.2.	Schematic showing the accumulation of stealth liposomes via EPR effect.....	115

## ABBREVIATIONS

---

Aflibercept	Eylea®, an anti-VEGF drug that inhibits the VEGF protein
AMD	Age-related macular degeneration
CNV	Choroidal neovascularisation
CPP	Critical packing-parameter
Cryo-TEM	Cryogenic transmission electron microscopy
DLPC	1,2-Dilauroyl-sn-glycero-3-phosphocholine
ELISA	Enzyme-linked immunosorbent assay
EPR	Enhanced permeation and retention
GNR	Gold nanorods
GRAS	Generally recognised as safe
H <sub>1</sub>	Normal hexagonal
H <sub>2</sub>	Inverse hexagonal
I <sub>1</sub>	Normal micellar cubic phase
I <sub>2</sub>	Inverse micellar cubic
L <sub>1</sub>	Normal micellar
L <sub>2</sub>	Inverse micellar
LA	Lauric acid
LC	Liquid crystal or liquid crystalline
L <sub>α</sub>	Lamellar
MPS	Mononuclear phagocyte system
NIR	Near-infrared
PBS	Phosphate buffered saline
PDT	Photodynamic therapy
PEG	Polyethylene glycol
PEG-DSPE	1,2-distearoyl-sn-glycero-3-phosphoethanolamine-N-amino(polyethylene glycol)-2000]
PHYT	Phytantriol (3,7,11,15-tetramethylhexadecane-1,2,3-triol)
POPE	1-Palmitoyl-2-oleoyl-sn-glycero-3-phosphoethanolamine
RPE	Retinal pigment epithelium
SAXS	Small angle X-ray scattering
SiNC	Silicon 2,3-naphthalocyanine bis(trihexylsilyloxiide)
SPR	Surface plasmon resonances
SPR	Surface plasmonic resonance
Tapp	Apparent temperature
THF	Tetrahydrofuran
UV	Ultraviolet
V <sub>1</sub>	Normal bicontinuous cubic
V <sub>2</sub>	Bicontinuous cubic
VEGF	Vascular endothelial growth factor

## ABSTRACT

---

Recent advances in drug delivery technology have amplified potential opportunities to treat the debilitating diseases that affect the posterior segment of the eye in a less invasive and more efficient manner. Current methods for drug delivery to the back of the eye are hindered by many barriers and limitations. As a result, to treat the most common posterior eye disease in the developed world, age-related macular degeneration, patients require frequent intravitreal injections that are costly and highly invasive. Considerable efforts have been directed towards developing new materials to optimise drug delivery by reducing the frequency of the intravitreal injections. Phospholipid-based liquid crystalline nanomaterials are of great interest as they are biocompatible, process low toxicity and can encapsulate drugs with different physicochemical properties. These materials also provide an opportunity to design delivery systems that have the potential to release drug on-demand. Depending on the liquid crystalline nanostructure, the rate at which drug is released can be manipulated to induce a slow to fast drug release profile. An ideal stimulus to control the transformation of the nanostructure is using near-infrared light as it can be applied externally to safely penetrate through the eye to activate the release of drug from the liquid crystalline system. This thesis presents phospholipid-based liquid crystalline systems which have been rendered near-infrared light responsive by incorporation of particular and molecular photoactuators. The utilisation of advance synchrotron small angle X-ray scattering technique revealed changes to the lipid packing upon irradiation and transformations between the different self-assembled nanostructures. The nanostructures and where the photoactuators are located was verified using cryogenic transmission electron microscopy. The effect of manipulating the nanostructure was further explored by quantifying the release using affinity chromatography. The desirable lamellar to bicontinuous cubic phase transformation was found to exhibit a slow to fast release profile. A short thirty second exposure resulted corresponded to an almost complete release of encapsulated drug. Although the system requires optimisation to replace the repeated intravitreal injections with multiple light-activated doses for an extended period of at least 6 months, the understanding achieved in this thesis was a fundamental step to eventually translate these systems for pharmaceutical applications.

CHAPTER ONE:  
INTRODUCTION

## Declaration for Chapter One

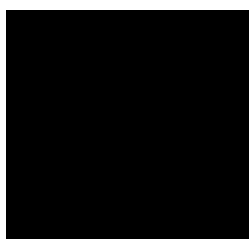
This chapter contains sections reproduced from a review article that was published as: Du, J. D.; Fong, W.-K.; Caliph, S.; Boyd, B. J., Lipid-Based Drug Delivery Systems in the Treatment of Wet Age-Related Macular Degeneration. Drug Delivery Translational Research 2016, 6, 781-792. The original submission can be found in the Appendix. The review provides an overview on the emerging delivery systems with an emphasis upon on-demand delivery systems as they have greater potential to overcome the current limitations. This chapter focuses on how lipid-based delivery systems can improve treatment of exudative age-related macular degeneration and culminates with the hypotheses and aims of this project.

For Chapter One, the nature and extent of contribution to the work was as follows:

<b>Name</b>	<b>Nature of contribution</b>	<b>Extent of contribution</b>
Joanne D. Du	Concept, research of literature, evaluated the gap in the literature and preparation of manuscript	75 %
Wye-Khay Fong	Co-supervisor, provided input into the preparation of manuscript	10 %
Suzanne Caliph	Co-supervisor, provided input into the preparation of manuscript	5 %
Ben J. Boyd	Main supervisor, provided input into the preparation of manuscript	10 %

The undersigned hereby declare that the above declaration correctly reflects the nature and extent of candidate and co-author contributions:

Candidate's signature:



Date: 30/3/2018

Main supervisor's signature:

Date: 30/3/2018

## 1. A statement of the problem

Age-related macular degeneration is an inflammation of the macula that is estimated to cause irreversible vision impairment and blindness in 196 million aged individuals by the year 2020.<sup>1</sup> The exudative disease progresses due to choroidal neovascularization, where new blood vessels rapidly grow and eventually damage the retinal pigment endothelial layer that is responsible for maintaining the functionality of photoreceptor cells, visual pigment transport and protection, formation of blood-retinal barrier in conjunction with the vascular endothelium, and immune defence of the macula.<sup>2</sup> The abnormal neovasculature has been predominantly attributed to an overexpression of vascular endothelial growth factor (VEGF). Currently, only palliative treatment is available which uses drugs that inhibit VEGF, also known as anti-VEGF drugs. The anti-VEGF treatments are costly, highly invasive and requires bi-monthly bolus injections directly into the vitreous humour of the eye owing to the limited uptake and ocular penetration.<sup>3</sup> Considerable efforts have been directed toward improving visual outcomes by designing new therapeutic molecules and controlling relevant pathogenetic factors.<sup>4-5</sup> The issue is not a shortage of good drugs but a lack of effective drug delivery systems. Intensive research has resulted in potential innovative nanotherapies that can provide a practical, more specific and less invasive approach to revolutionise future pharmaceutical treatment.<sup>6</sup> In particular, self-assembled systems such as lipid-based liquid crystalline materials have been rendered stimuli-responsive through the incorporation of novel materials to activate drug release on-demand.<sup>7</sup> Such systems have potential to reduce the frequency of intravitreal injections. Near-infrared light is an ideal stimulus for ophthalmic applications as it can be easily applied externally and can safely penetrate through biological components. Therefore, this thesis focuses on designing a near-infrared light responsive liquid crystalline system for on-demand delivery of the current anti-VEGF drugs.

### 1.1. About age-related macular degeneration (AMD)

Millions of people suffer from ocular diseases and AMD remains to be the leading cause of irreversible vision impairment and blindness in Australia, the United States and Europe.<sup>1,8-9</sup> Treatment of ocular diseases is one of the most challenging due to numerous anatomical and physiological barriers that limits the delivery of drugs (Figure 1.1). The eye is a highly complex and protected organ divided into two segments: 1) Anterior segment consisting of cornea, conjunctiva, iris, ciliary body, aqueous humour and lens; 2) Posterior segment including sclera, retina, choroid and vitreous humour.

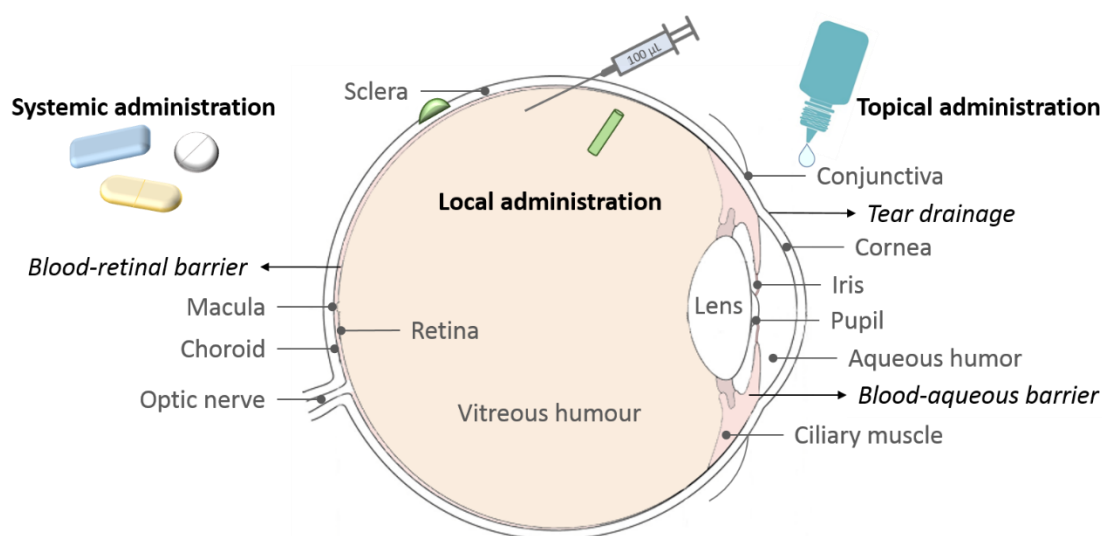


Figure 1.1 Schematic of the eye and its barriers in ocular drug delivery.

The main challenge in ophthalmic drug delivery is to overcome the tight-junctions of the blood-aqueous barrier and the blood-retinal barrier, which limits drug penetrations to the anterior and posterior segment, respectively. Ophthalmic drugs can be delivered via topical, systemic and local administration. Topical delivery in the form of eye drops will require penetration through the blood-aqueous barrier. The blood-aqueous barrier consists of the endothelium of the ciliary blood vessels and ciliary nonpigmented endothelium, both preventing drug entry into the intraocular tissues and aqueous humour.<sup>10</sup> Systemic delivery via intravenous injections requires drugs to transport through the outer blood-retinal barrier, which is represented by the retinal pigment epithelium (RPE), a layer underneath the neurosensory region of the retina. The RPE is a “tight” ion transporting barrier that restricts transcellular transport of polar solutes from the choroid, while the inner blood-retinal barrier including the

endothelium of the retinal vessels, offers considerable resistance to systemic penetration of drugs.<sup>11</sup> As a consequence of the limited ocular penetration, local administration such as intravitreal injections and ocular implants are more suitable for posterior eye diseases. Local administered drugs can by-pass the barriers to deliver the therapeutics directly into the vitreous cavity, near the site of action.

AMD is a posterior eye disease that affects the macular region of the retina resulting in the loss of central vision by causing damage to the RPE. This layer is responsible for nourishing the photoreceptors in the retina via the main blood supply to the eye, the choroid vasculature, as well as removing waste products from photoreceptor cells, and visual pigment transport and regeneration.<sup>12</sup> The Bruch's membrane separates the RPE and the choroid layer which can thicken with age, slowing the transport of metabolites and consequently the formation of subretinal deposits called, 'drusen'. The extent of accumulation of drusen under the RPE and the amount of hypopigmentary or hyperpigmentary changes of the RPE are characteristics of AMD.<sup>13-14</sup> As the disease progresses, severe vision loss occurs in one of two forms:

1) Dry AMD or geographic atrophy, which results in a gradual reduction of central vision over many years owing to the progressive atrophy of the RPE, choriocapillaris and photoreceptors.

2) Wet AMD or neovascular AMD occurs due to choroidal neovascularisation (CNV). This occurs when endothelial cells proliferate in the choroid and angiogenic blood vessels enter the RPE through a break in the Bruch's membrane and rapidly grow under the retina into the subretinal pigment epithelium or the subretinal space as illustrated in Figure 1.2.<sup>14</sup> Leakage of fluids and bleeding from the vessels causes fibrous scarring and leads to a rapid loss of central vision.

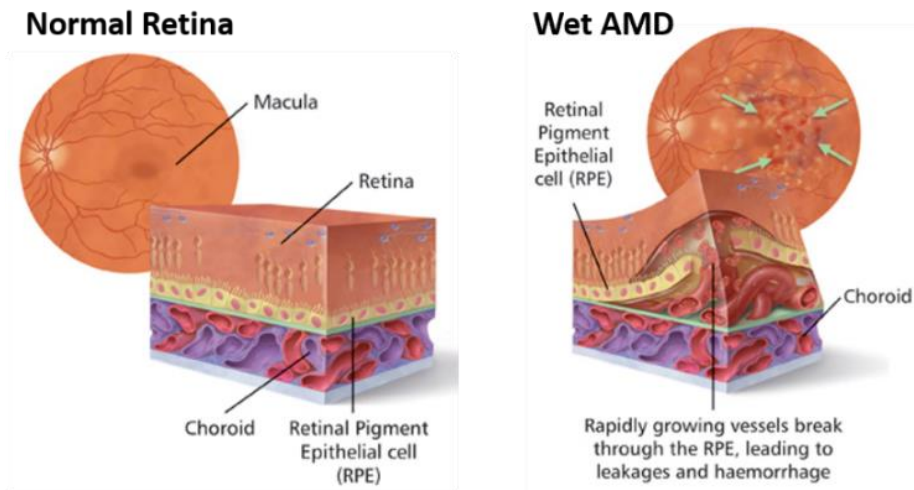


Figure 1.2 Schematic of normal retina vs. diseased retina with wet age-related macular degeneration (AMD).<sup>6</sup>

### 1.2. Current treatments for wet AMD

There are only palliative treatments available for wet AMD. Until the early 2000, photocoagulation and photodynamic therapies (PDT) with verteporfin (Visudyne®) was used to prevent or delay loss of visual acuity in eyes that have CNV. Photocoagulation is a thermal laser treatment that uses either krypton red (647 nm) or argon green (514 nm) laser. The lasers deliver intense photocoagulation burns that extend 100 µm beyond the perimeter of the lesion.<sup>15-16</sup> PDT was used as a minimally invasive treatment involving light activation of light-sensitive molecules after intravenous administration that localise in the neovasculature in the eye. Upon activation using a low-energy laser, reactive oxygen species are produced and these destroy target cells resulting in closure of the abnormal blood vessels.<sup>17</sup> Although these light-based treatments did delay the development of CNV, they are restricted to well-defined classic lesions (about 50 % of CNV lesion) and most cases required retreatments, which have been associated with high risks of immediate visual loss and adverse effects.<sup>13</sup> As such, these treatments have been largely replaced with vascular endothelial growth factor inhibitors.

The abnormal neovasculature creating unusual leaky blood vessels has been predominantly attributed to an overexpression of vascular endothelial growth factor (VEGF),<sup>18</sup> also known as VEGF-A. VEGF-A is a dimeric glycoprotein that interacts with two tyrosine kinase receptors, VEGFR-1 and VEGFR-2 located primarily on endothelial

cells.<sup>19</sup> To slow this progress, drugs that block this protein, anti-VEGF drugs, were developed and was first approved for the symptomatic treatment of neovascular AMD by the US Food and Drug Administration (FDA) in 2004. There are also other actives in addition to the anti-VEGF based treatments that are currently in clinical development to inhibit both VEGF and VEGF gene expression <sup>20</sup>, such as tyrosine kinase inhibitors and nucleotides. Corticosteroids and anti-inflammatory drugs such as triamcinolone <sup>21-</sup> <sup>22</sup> have also been investigated for angiogenic ocular diseases, however, the risks of elevated intraocular pressure, glaucoma and cataracts makes such treatment less desirable.<sup>23</sup> It has been recently postulated that controlling cholesterol levels in the eye via the use of statins or nucleic acid based therapies will also result in the successful treatment of AMD <sup>24</sup>.

Current FDA-approved anti-VEGF treatments including pegaptanib (Macugen™, Eyetech and Pfizer), ranibizumab (Lucentis®, Genentech/Novartis) and aflibercept (Eylea®, Regeneron and Bayer). The first anti-VEGF therapy, pegaptanib, was a 28-base ribonucleic acid aptamer that was covalently linked to two branched 20 kD polyethylene glycol moieties. The VEGF-A gene is organised into eight exons on chromosome 6p21 and alternate gene splicing can generate nine isoforms. Pegaptanib was developed to bind and block the activity of the most prevalent isoform, VEGF<sub>165</sub>. Pegaptanib stabilised vision in 70 % of patients, which was better than the 55 % of patients that received placebo in phase III randomised trial.<sup>25</sup> However, there were cases of adverse events in 890 patients during the first year of the trial, with the most serious being endophthalmitis (1.3 %), traumatic injury to the lens (0.6 %) and retinal detachment (0.7 %), which lead to severe loss of visual acuity in 0.1% of patients treated with pegaptanib.

Ranibizumab was the second anti-VEGF therapy approved by the FDA in 2006. Ranibizumab is a recombinant, humanised monoclonal antibody fragment that neutralises all forms of VEGF-A. Ranibizumab was shown to prevent vision loss and improve mean visual acuity. At 12 months, 94.6 % of patients given 0.5 mg of ranibizumab lost fewer than 15 letters, in comparison to 62.2 % of patients that received placebo injections. In the same group that received ranibizumab, 33.8 % of the patient was able to improve their visual acuity by 15 or more letters, as compared to 5.0 % of the

sham-injection group.<sup>26</sup> The benefit in visual acuity was maintained at 24 months, with low rate of serious adverse events in the 716 patients. During 24 months of the trial, endophthalmitis (1.0 %) and serious uveitis (1.3 %) was identified in patients given ranibizumab.

Prior to the approval of ranibizumab, bevacizumab (Avastin®, Genentech) has been used as an off-label alternative treatment. Bevacizumab is a full monoclonal antibody that was approved for metastatic colon cancer in 2004. Similar to ranibizumab, it binds to all isoforms of VEGF-A, and is derived from the same mouse monoclonal antibody precursor. Early reports showed comparable efficacy to ranibizumab but at a much lower price, leading to its use by some ophthalmologist.

Aflibercept, also known in the scientific literature as VEGF Trap-Eye, is the newest anti-VEGF agent approved in 2011 and now the most commonly used treatment. It is a recombinant fusion protein, consisting of the binding portion of human VEGF receptor 1 and 2 extracellular domains fused to the Fc portion of human IgG1.<sup>27</sup> The binding portions were selected due to their high affinity for VEGF-A, VEGF-B and placental growth factor. Aflibercept has high binding affinity to all isomers of the VEGF-A family, in particular, its affinity for VEGF<sub>165</sub> is 94 times greater than ranibizumab and approximately 120 times higher than bevacizumab.<sup>28</sup> Also, in comparison to 48 kD for ranibizumab and 148 kD for bevacizumab, aflibercept has an intermediate size of approximately 115 kD.<sup>29</sup> Its size and high affinity increased the intravitreal half-life of aflibercept (4.7 days), in comparison to the half-life of 2.88 days for ranibizumab,<sup>30</sup> and is estimated that the binding capacity 79 days after injection is equivalent to the bind capacity of ranibizumab 30 days after injection.<sup>28</sup> Although anti-VEGF drugs are effective, they are large macromolecules that have limited uptake and ocular penetration. Similar to the other anti-VEGF treatments, patients that received aflibercept were identified with severe adverse events at similar frequencies, which is the result of the frequent intravitreal injections.

### 1.3. Limitations associated with anti-VEGF therapies

While the anti-VEGF drugs are effective in controlling the symptoms of neovascular AMD, their delivery is far from efficient reducing patient compliance. Owing to the size and a short residence time of anti-VEGF drugs, high concentration of anti-VEGF drugs need to be administered directly into the vitreous humour on a regular basis. When administered, elimination of drug may occur via the anterior or posterior route. The anterior route eliminates the drug via diffusion into the aqueous from the vitreous humour, aqueous turnover and uveal blood flow. The posterior route elimination involves drug transport across the blood-retina barrier, which is dependent on the permeability of the drug or active transport mechanisms.<sup>10</sup> Large hydrophilic drugs are primarily eliminated by the anterior route as they cannot penetrate across the blood-retina barrier.<sup>31-32</sup> The concentration of anti-VEGF drugs declines in an exponential fashion over 29 days.<sup>30</sup> Therefore, most of the administered drug in a single injection is cleared without exerting a therapeutic effect within a month.

Many of the severe adverse events observed during clinical trials of anti-VEGF treatments are due to the intravitreal injections, including risk of vitreous hemorrhage, retinal detachment and the development of cataracts.<sup>33-34</sup> Intravitreal injections require a high degree of sterility to prevent infection and if not performed correctly, can result in endophthalmitis, which in extreme cases can require vitrectomy to treat. The frequent intravitreal injections also carries high financial burden for instance, both aflibercept and ranibizumab costs approximately US\$2000 per intravitreal dose. Although, some ophthalmologists have used bevacizumab as the cheapest anti-VEGF treatment at about US\$50.<sup>35</sup> Bevacizumab has not been subjected to formal clinical trials and hence, remains an unapproved option not subsidised by health providers consequently limiting its adoption. With aging populations in many industrialised countries, the financial implications for health budgets of the individual as well as the economy are critical, and likely to be unsustainable with the current long-term anti-VEGF treatment regime. Given the current limitation of anti-VEGF therapies, there is an urgent need for a more cost effective and safer alternative to the current intravitreal treatments.

#### 1.4. Opportunities of emerging delivery systems for treatment of AMD

Since the introduction of anti-VEGF therapy, substantial efforts have been made towards improving the current treatments by reducing the frequency of intravitreal administration. Since FDA approval in 2011, aflibercept quickly became the main treatment for wet AMD as it was developed to reduce the treatment burden on patients by increasing the dosing regimen to 8 weeks. Other options to extend the duration of action have been investigated. One chemical entity that shows promise utilises polyethylene glycol (PEG), which have been widely applied because of its long half-life in the blood and low interaction with other organs.<sup>36</sup> EYE001, is a PEG-conjugated oligonucleotide that shows a high specificity and affinity to VEGF<sub>165</sub> and has an estimated terminal half-life of 84 hours in the vitreous humour after intravenous injection.<sup>37</sup> However, stabilisation of vision was only seen in 26.7 % of patients at 3 months with only one dose.<sup>37</sup> Considering the time required for clinical translation and approval for new chemical entities, the limitations of anti-VEGF treatments are unlikely to be overcome through molecular modification of the drug itself.

Individualised anti-VEGF treatment regimens such as ‘as-needed therapy’ and the ‘treat-and-extend strategy’ have also been investigated to find a safer and more cost-effective alternative to the traditional monthly treatments, however, the frequency of treatment remains high for most patients.<sup>19</sup> The main biopharmaceutical challenge in the treatment of AMD therefore is to improve the delivery of the currently available therapies. There is an increasing interest in the use of smart materials for active drug delivery in order to selectively target the posterior segment of the eye. As a result, there has been considerable effort directed towards the development of novel delivery systems, in particular, sustained-release systems of already approved anti-VEGF drugs to ultimately reduce the required frequency of intravitreal injections. Thus, novel materials for more effective delivery of drugs are emerging to overcome these barriers.

Ideally, new proposed treatments for AMD aim to either reduce the frequency of the highly effective but highly invasive intravitreal injections, or provide greater patient

compliance via a safer route of administration. Much attention has been directed towards implanted polymeric intravitreal devices<sup>38</sup> and liposomal systems (Table 1).

#### 1.4.1. Polymeric delivery systems

Polymers are a popular means of modifying the availability of drug after administration to provide a slow release effect. Drug-containing polymer systems for this purpose fall into two general classes – non-biodegradable implants, and biodegradable implants. Non-biodegradable implants have the advantage of providing very long term sustained release of drug, however, the device is often limited by the need to be surgically implanted, and removed and replaced when the drug load is depleted. Surgical implantation procedures have also been known to cause other acute and long-term complications such as retinal detachment and suprachoroidal and vitreous haemorrhage.<sup>39</sup> Therefore, non-biodegradable implants can only be practical if the device can be tolerated within the eye for an extended period of time. On the other hand, soft biodegradable implants do not require removal, and may be amenable to injection as a non-surgical procedure. To date, there are four products on the market for posterior segment delivery (Vitrasert<sup>®</sup>, Retisert<sup>®</sup>, Ozurdex<sup>®</sup> and Iluvien<sup>®</sup>), which uses polymeric devices to provide a sustained release effect for small compounds. However, there are no polymeric products currently available for the delivery of anti-VEGF drugs.

An alternative class of biocompatible polymeric devices for the delivery of anti-VEGF drugs are hydrogels. Hydrogels have been investigated because like some conventional polymer implants, they have a macroporous structure that sustains the release of the macromolecular drugs after implantation.<sup>40</sup> However, translation of hydrogels as drug delivery systems in products is still in its infancy, where further studies are required to completely understand the effect of the shape, size and site of placement of the hydrogel implant on drug delivery. Although recent advancements in the field of polymeric nanoparticle-based drug delivery have been shown to overcome some of the limitations of the current anti-VEGF treatments in various preclinical studies.<sup>41</sup> Substantial clinical translation are required before these polymeric devices can become a product.

### 1.4.2. Liposomal delivery systems

Given the potential difficulties in translation of new polymeric systems for extended treatment of wet AMD, it is our contention that new developments in drug delivery approaches are more likely to come from lipid-based materials such as liposomes (nanoparticles with a spherical bilayer structure which encloses an inner aqueous compartment). There are more than two decades of research on liposomes and many products already on the market, and of specific interest, a number of recent reviews have summarised the developments of liposomal research in the field of ocular delivery (Table 1). This thesis will focus on the potential for lipid-based systems, including liposomes to improve the treatment of wet AMD with an emphasis on novel lipid-based systems to provide on-demand drug delivery.

Table 1 Recent literature detailing liposomal systems for ophthalmic drug delivery.

<b>Title of review</b>	<b>Year</b>	<b>Ref.</b>
Light activated liposomes: Functionality and prospects in ocular drug delivery	2016	42
Liposomes in topical ophthalmic drug delivery: An update	2016	43
Delivery strategies for treatment of age-related ocular diseases: From a biological understanding to biomaterial solutions	2015	44
Drug delivery techniques for treating age-related macular degeneration	2014	45
Liposomes and nanotechnology in drug development: focus on ocular targets	2014	46
Nanotherapy for posterior eye diseases	2014	47
Drug delivery implants in the treatment of vitreous inflammation	2013	48
Liposomes for intravitreal drug delivery: A state of the art	2012	49
Recent applications of liposomes in ophthalmic drug delivery	2011	50
A review of implantable intravitreal drug delivery technologies for the treatment of posterior segment eye diseases	2010	51

Liposomes are one of the most commonly known lyotropic liquid crystalline structures. They are vesicular nanoparticles that are spontaneously formed by the self-assembly of amphiphilic phospholipids in excess water. The lipid bilayer encloses an inner aqueous compartment that can encapsulate hydrophilic molecules, including peptide and proteins, indicating their applicability to encapsulate anti-VEGF biological drugs. The biodegradable and biocompatible nature of phospholipids makes these attractive for ophthalmic delivery. There are nine clinical trials determining the safety and efficacy of liposomal systems in treatment of ocular conditions including dry eyes, ocular hypertension, glaucoma, intraocular retinoblastoma, blepharitis and macular edema.<sup>52</sup> Therefore, in comparison to polymeric devices which have only been used in preclinical studies for ocular applications, this section will explain how liposomes can provide a greater potential to improve the treatment of AMD via a number of mechanisms, including sustaining drug release via extended intraocular retention time, minimising adverse events through targeted delivery and reducing the invasiveness of the anti-VEGF treatment.

#### 1.4.3. Extending therapeutic duration by increasing drug retention

Liposomes have been shown to alter the biopharmaceutical behaviour of drugs in ocular delivery.<sup>53-54</sup> Specifically for treatment of AMD, liposomes have been shown to sustain release of actives (Table 2). Abrishami *et al.* showed liposomes could increase the residence time of anti-VEGF biological drugs after intravitreal administration. Liposomes containing bevacizumab were retained in the vitreous humour at five times higher concentration than free drug over 42 days. These liposomal carriers are expected to provide sufficient concentration of therapeutic drug for over 6 weeks.<sup>55</sup> Such a system will have limited uptake given the current treatment, aflibercept requires retreatment after 8 weeks. Although it provided a step change in reducing the frequency of administration, a significantly longer duration (> 2 months) of drug retention at the site of AMD will be more suitable. Other recent studies have shown that liposomal systems can efficiently deliver the active to the site of action resulting in a reduction in CNV area, however, the effect was recorded 14 days after laser photocoagulation because the extent of CNV is usually the greatest and most favourable for observation at this time

point. As such, sustained release was assumed from previous literature,<sup>49</sup> and in some cases, with the support of *in vitro* release studies.<sup>56-57</sup>

Table 2 Liposomes intended to improve treatment of AMD by sustaining release of active.

Description	Route of Administration	Drug category	Observation	Year	Ref.
Negatively charged liposomes	Subconjunctival administration.	Anti-VEGF	A sustained release duration of 21 days <i>in vitro</i>	2017	58
Surface modified liposomes	Topical delivery	Anti-inflammatory	Improved the physical stability, sustained release over 60 days <i>in vitro</i>	2012	56
Nanoliposomes	Intravitreal injection	Anti-VEGF	Sustained bevacizumab in the vitreous body <i>in vivo</i> (in rabbits over 40 days)	2009	55

#### 1.4.4. Selective delivery to the target site

Liposomal delivery systems have also been shown to provide enhanced delivery to the site of action using various targeting ligands. Delivery of some therapeutic agents, such as nucleotides, is generally problematic because it has difficulty penetrating biological barriers resulting in low delivery efficiency at the target site.<sup>59</sup> Problematic agents can be encapsulated in ligand-conjugated liposomes to target specific cells at the site of CNV, as detailed in Table 3. Recent *in vitro* data found that cationic PEGylated liposomes modified with the RGD oligopeptide can efficiently carry siRNA for downregulating VEGF expression in RPE cells,<sup>59-60</sup> and a PEGylated liposomal system has been shown to facilitate intracellular delivery of an anti-VEGF to RPE cells in rat models.<sup>61</sup> Efficient delivery of actives selectively to the site of CNV allows enhanced therapeutic efficacy causing significant reduction of CNV area. Currently, only intravitreally administered formulations into rats have been investigated and thus, the clinical benefits in extending the duration between injections remains uncertain.

Table 3 Liposomes used to improve treatment of AMD by enhancing cellular interactions.

Description	Route of Administration	Drug category	Observation	Toxicology	Year	Ref.
Vector-mediated liposomes	Intravitreal injection	Angiogenesis inhibitor	Adenoviral vector mediated liposomes efficiently delivered tristetraproline, suppressed CNV <i>in vivo</i> (rat) after 14 days and decreased VEGF mRNA expression	Possible systemic toxicity due to adenoviral vectors	2014	62
Peptide modified PEGylated liposomes	Intravitreal injection	Angiogenesis inhibitor	YSA peptide selectively targeted EphA2 in neovasculatures, increased intracellular delivery efficiency and enhanced the therapeutic efficacy against CNV in rats after 14 days	Toxicity at injection site may be due to oxygen radicals of doxorubicin	2012	57
Peptide modified PEGylated liposomes	<i>(in vitro)</i>	Nucleotide	Efficiently carry siRNA, downregulated VEGF expression in RPE cells <i>in vitro</i>	N/A	2011, 2013	59-60
PEGylated cationic liposomes	Intravitreal injection	Nucleotide	Efficiently protected siRNA load, facilitated intracellular delivery and caused a reduction of CNV area <i>in vivo</i> (rat) after 14 days	Cationic surface charge may induce inflammation	2011	61
Peptide modified liposomes	Intravitreal injection	Tyrosine-kinase inhibitor	Inhibitory effects of SU5416 was enhanced and sustained by APRPG-liposomes resulting in CNV reduction <i>ex vivo</i> (in rats after 14 days)	VEGF inhibition can affect healthy tissues	2011	63

#### 1.4.5. Providing a less invasive route of administration

Liposomes potentially allow a less invasive route of administration for anti-VEGF treatment, avoiding intravitreal injections (Table 4). Firstly, liposomal formulations have been studied for their effectiveness following topical administration.<sup>56, 64-65</sup> Although this route may not result in reduced frequency of administration, by avoiding intravitreal injections, topical application of a liposomal formulation could provide a significant improvement in patient compliance and safety.

Recently, a topically administered bevacizumab-liposome system has shown potential as a non-invasive alternative for ocular instillation. Topical administration such as eye drops, is the most common and arguably preferred therapeutic approach owing to its non-invasive nature. Davis *et al.* showed, using *in vivo* rat and rabbit studies, that liposomes can overcome the corneal barriers and enhance the delivery of encapsulated bevacizumab to the posterior segment of the eye after topical application by incorporation of an anionic phospholipid-binding protein, annexin A5.<sup>64</sup> However, ocular bioavailability of the drug is usually less than 5 % of the topically applied dose, which confines the use topical administration to treating diseases that affects the anterior segment of the eye.<sup>33</sup> This is due to the limited volume of administration, rapid tear drainage and the significantly hindered permeation of hydrophilic drugs and macromolecules through physical barriers such as cornea, conjunctiva, blood-aqueous barrier and sclera.<sup>66</sup> The consequent low bioavailability of the drug would require frequent administration, and the lack of control over the actual dose delivered to the posterior segment can lead to higher systemic exposure, potentially limiting its use as an approved AMD treatment.

Anti-VEGF therapy has become the latest standard treatment for AMD, however, long-term inhibition of VEGF has been associated with higher risks of mortality, incident myocardial infarction, bleeding, and incident stroke,<sup>67</sup> and is thought that the previously used PDT treatment may be more suitable in this regard. However, similar to topical administration, only 1 to 5 % of systemically administered drug enters the vitreous chamber due to the blood-retinal barrier.<sup>10</sup> For drugs to cross these rate-limiting barriers, it needs optimum membrane partition characteristics or be a substrate

suitable for active transporters through the RPE or the endothelium of blood vessels. Consequently, it is proposed that a compromise between the two may provide new opportunities in therapy, where systemic administration of liposomes loaded with a photodynamic therapy agent can be used to reduce the frequency of administration by intravitreal injection through alternating therapeutic approaches to treatment. Recent liposomal research successfully improved the previous liposomal PDT by reducing CNV lesion size with minimal tissue damage.<sup>68-69</sup> Therefore, it has been suggested that improvement of PDT or a combination therapy of alternating PDT and anti-VEGF treatments may reduce the need for intravitreal injections and may be more suitable for selected patients at risk from extended VEGF inhibition.

Table 4 Liposomes used to improve treatment of AMD by avoiding intravitreal injections for administration.

Route of Administration	Description	Drug category	Observation	Toxicology	Year	Ref.
Topical delivery	Protein associated anionic liposomes	Anti-VEGF	Annexin A5 enhanced permeation through the retina after 5 days, significantly enhancing bioavailability <i>in vivo</i> (rat/rabbits)	No adverse events	2014	64
	Surface modified liposomes	Anti-inflammatory	Effective retinal delivery of diclofenac by promoting non-corneal drug penetration <i>in vivo</i> (rabbits)	N/A	2012	56
	Submicron-sized liposomes	Potent free radical scavenger	Inhibition of light-induced and oxidative stress-induced retinal damage and prevented shrinkage of the outer nuclear layer	Low toxicity	2011	65, 70
Intravenous injections	Single unilamellar liposomes	Photodynamic therapy (PDT)	Significantly reduced CNV lesions with minimal tissue damage	Low inflammatory reaction and skin phototoxicity	2015	68
	Cationic liposomes	Photodynamic therapy (PDT)	Neovascular obliteration as effective as Visudyne <sup>®</sup> but induced less tissue damage after 10 days	Less pronounced PDT-associated retinal damage	2013	69
	Peptide grafted cationic polymerized liposomes	Angiogenesis inhibitor	Targeted gene delivery lead to a reduction in size and leakage of CNV <i>in vivo</i> (rat) starting at 5 days after CNV creation	Low possibility of systemic side effects	2011	71

In summary, intravitreal injections of anti-VEGF drugs remain the most effective treatment option for AMD, yet, there are many limitations in terms of safety, affordability and adherence. Lipid systems present alternative approaches to polymers with clear capacity to improve the treatment of AMD. Especially in consideration of their biocompatibility and translatability, the track record of safe use of liposomes in other diseases provides a significant advantage over other materials. Liposomes have been used in the design of safe and cost-effective delivery systems, but have not yet to be made it into products for intravitreal delivery of anti-VEGF compounds to improve treatment effectiveness or duration in the clinic for treatment of ocular diseases. Although liposomal formulations are commercially available and the production methods have been improving over time,<sup>72</sup> their applications are usually limited by development cost, the need to optimise the production method for new formulations, limited delivery due to blocking by biological barriers, and of greater concern, their unadjustable or uncontrollable release rate.<sup>73</sup> Liposomes can either encapsulate the drug and thus, must retain their drug payload with minimal drug leakage,<sup>74</sup> or be designed for burst-release, where the drug can be bound to the surface of the nanocarriers using surface modifiers.<sup>75</sup> For the encapsulation strategy, premature drug leakage, the diffusion controlled release of the drug and the low permeability of large macromolecules, limits their application as drug carriers. Liposomal formulation can be designed to possess efficient and stable encapsulation with minimal drug leakage while in circulation, such as Doxil<sup>®</sup>. These carriers however, may be cleared without releasing their drug loading thereby reducing its therapeutic effect. In tumours, the overexpression of phospholipases<sup>76</sup> is mainly responsible for the breakdown of the bilayer and release of the therapeutic payload.<sup>77-78</sup> It remains uncertain whether enzymatic activity would be sufficient in AMD to induce substantial leakage. Therefore, there is likely to be a role to play for stimuli-responsive systems that enable 'on-demand' drug release.

### 1.5. Stimuli-responsive systems for 'on-demand' drug delivery

Controlling the release of drug can potentially reduce the frequency of intravitreal injections, improve systemic safety by actively controlling the rate of drug release and provide a less invasive treatment option. Stimuli-responsive systems have been explored

in the context of ocular delivery to deliver drugs ‘on-demand’, when required.<sup>38, 79</sup> These ‘smart’ materials have been designed to respond to an endogenous or external stimulus to cause the initiation, increase, decrease or cessation of drug release from within the matrix. Polymeric implants that are responsive to an electric current,<sup>80</sup> light<sup>81</sup> or a magnetic field<sup>82</sup> to achieve tuneable drug release have been explored for delivery to the eye, however, translation of polymeric devices to viable treatments are still in their infancy. This thesis will focus on lipid systems, particularly liposomes and other lyotropic liquid crystalline materials, which have also been rendered stimuli-responsive, and ongoing efforts to evaluate their application to the problem of AMD are discussed below.

### 1.5.1. Stimuli-responsive lipid-based systems

Lipid-based liquid crystalline nanoparticles are soft materials with a complex internal nanostructure that is formed by the self-assembly of some unique polar amphiphilic lipids in excess of water. These structures have been demonstrated to be effective carriers to improve the delivery of molecules with varying physicochemical properties,<sup>83-86</sup> provide the mechanism for sustained-release,<sup>87</sup> and protection from degradation when the drug is encapsulated. The most common liquid crystalline structures include the lamellar phase ( $L_{\alpha}$ ), inverse hexagonal phase ( $H_2$ ) and the bicontinuous cubic phase ( $V_2$ ). Of these three structures, liposomes are the most commonly known lyotropic lipid self-assembly presented as a spherical bilayer structure resulting from the dispersion of lamellar phase ( $L_{\alpha}$ ). The critical packing-parameter (CPP) concept, which was introduced by Israelachvili *et al.*, can be used to understand how the geometry of surfactants and lipids can dictate the type of self-assembled system formed using Equation 1.

$$CPP = V_s / (a_o l) \quad (1)$$

Where,  $V_s$  is the hydrophobic chain volume,  $a_o$  is the head group area and  $l$  is the hydrophobic chain length.<sup>88</sup> This parameter is affected by different factors including the concentration and chemical structure of the lipid as well as environmental factors such as temperature,<sup>7</sup> water content,<sup>89</sup> ionic strength,<sup>90</sup> and pH.<sup>91-92</sup> When CPP is less than 1, normal phases form, where the hydrophobic chains face towards the core of the

structure. For values greater than 1, inverse or reverse phase forms such that the hydrophobic chains face away from the aqueous core (Figure 1.3). By convention, curvatures are taken to be positive if the head group surface curves toward the hydrocarbon. Normal phases have a next positive mean curvature (Type 1), while inverse phases have negative curvature (Type 2). The sequence of phases exhibited by lipid systems as thermodynamic parameters are changed tends to follow a monotonic sequence of phases running from positive to negative curvature.<sup>93</sup>

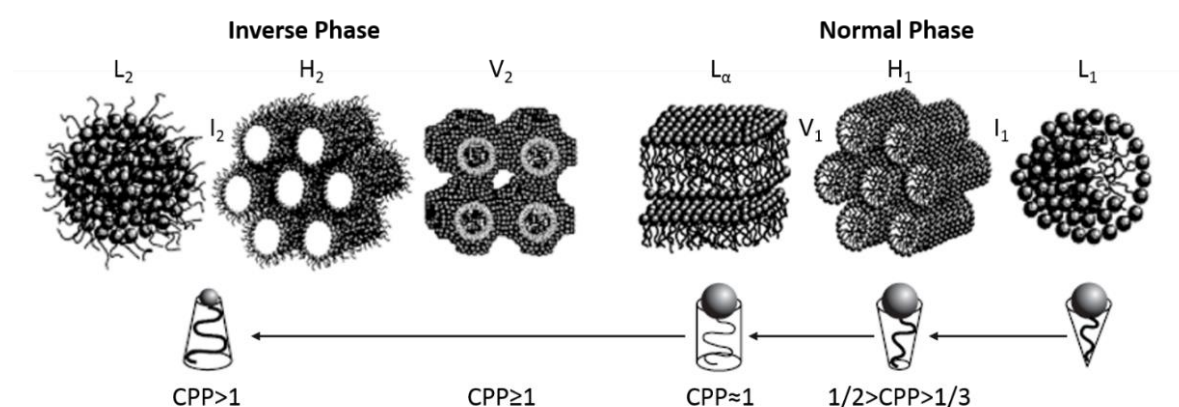


Figure 1.3 Common self-assembled phases and their corresponding critical packing parameter. The abbreviated phases are as follows: inverse micellar ( $L_2$ ), inverse micellar cubic ( $I_2$ ), inverse hexagonal ( $H_2$ ), inverse bicontinuous cubic ( $V_2$ ), lamellar ( $L_\alpha$ ), normal bicontinuous cubic ( $V_1$ ), normal hexagonal ( $H_1$ ), normal micellar cubic phase ( $I_1$ ) and normal micellar ( $L_1$ ). Adapted from <sup>94</sup>.

These self-assembled phases can be modified to transition from one phase to another depending on the packing of amphiphilic lipids, presence of additives and environmental factors,<sup>88</sup> or in the context of on-demand drug delivery under a wide range of stimuli. It is known that the phase structure being either “open” or “closed” dictates the rate of drug release as illustrated in Figure 1.4.<sup>95</sup> For example, the  $H_2$  phase displays a much slower release than  $V_2$  phase owing to the smaller water channels and closed rod-like micellar structure.<sup>89, 95</sup> Likewise, the closed nature of  $L_\alpha$  phase, which enables the encapsulation of drug, will show slow or no drug release in comparison to the  $V_2$  phase. It is envisioned that lipid-based systems can be designed to be responsive and deliver drug ‘on-demand’. These systems will exhibit little or no drug release in the

'off' state, but when stimulated, a phase transition occurs, activating release of drug until it is switched off. This process can be repeated to release pulses of drug on demand, and would be more suitable for long-term delivery. As such, the reversibility of the system is an important attribute in order to provide pulsatile release for repeated treatments. In other words, the liquid crystalline systems should have the ability to return to its original, slow release state when the stimulus is removed.

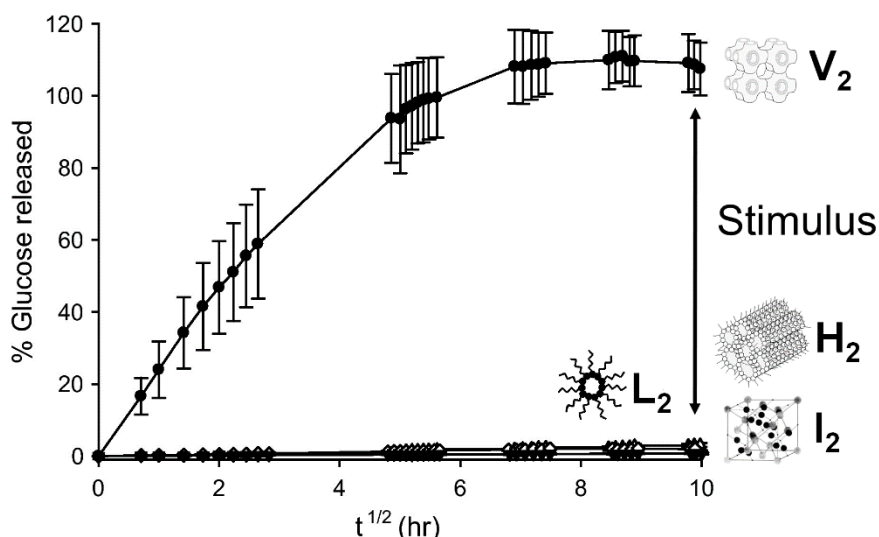


Figure 1.4 Schematic illustrating how changing the lyotropic liquid crystalline structure can control the release rate of drug. The lyotropic liquid crystalline structures picture on the right are the fast releasing inverse bicontinuous cubic phase ( $V_2$ ), in comparison to the slow releasing phases: inverse hexagonal phase ( $H_2$ ), inverse micellar cubic phase ( $I_2$ ) and inverse micellar phase ( $L_2$ ). A range of methods can be used to impart stimuli-responsiveness in these systems to switch between slow and fast releasing structures.<sup>6</sup>

### 1.5.2. Stimuli to activate drug release

There are a number of scenarios where triggered release of drug from these lipid systems for treatment of wet AMD may be foreseen to be advantageous, illustrated schematically in Figure 1.5. In the simplest case, responsive liposomes would release their cargo selectively when they encounter the stimulus either due to a change in the permeability of the bilayers or via a transition of the phase structure. Temperature has been used as a stimulus for on-demand drug delivery from lyotropic lipid systems,<sup>96-97</sup> however

temperature-responsive systems are not considered practical for controlling release of drug in the eye because of the lack of specificity in heat source leading to potential for accidental activation of drug release. Alternatively, magnetic<sup>98</sup> and light<sup>99-100</sup> sensitive materials can be incorporated into the lyotropic liquid crystal matrix to enable external control over drug release, making them more suitable for on-demand applications. For ocular applications in the posterior segment, where the liposome has been intravitreally injected, or been delivered via the systemic circulation as described above, light as a trigger would be a useful stimulus. Light-sensitive liposomes have been extensively studied previously for biological applications,<sup>101</sup> however, it does not appear that such systems have been used in the treatment of AMD.



Figure 1.5 Schematic of how a NIR-light triggered lipid ‘depot’ could reduce the frequency of intravitreal injections by repeated triggered release of a dose of drug using a laser, to replace regular intravitreal injections.<sup>6</sup>

### 1.5.3. Methods for imparting light responsiveness in materials

Light activation provides a very broad range of adjustable parameters such as wavelength, duration, beam diameter and intensity that can be used to optimise and control the dose of the actives released, when required. To this end, there are numerous papers on ultraviolet (UV) activated liposomes systems.<sup>102-103</sup> However, UV activated systems risk damage to the eye through intense UV exposure. Specifically, UV-B (280-315 nm) and UV-C (100-280 nm) are absorbed at the ocular surface, are poorly transmitted through tissue such as the cornea, and consequently have not been shown to be successful *in vivo*.<sup>104</sup> With the suitability for clinical applications in mind, although UV-A (315-400 nm) is able to penetrate pass the lens, the near infrared (NIR) region

around 650 nm to 900 nm that has the lowest absorption coefficient with water, lipids and haemoglobin,<sup>105</sup> is the best light source for triggered drug delivery. NIR irradiation can penetrate tissues up to 50 mm deep,<sup>106</sup> rendering it amenable for ophthalmic, subcutaneous and deeper tissue applications.

Recent research has reported that liposomes can be made responsive to NIR irradiation.<sup>107-108</sup> Several nanosized photothermal agents including gold nanoparticles<sup>100, 109-110</sup> and graphene derivatives<sup>111</sup> have been explored as actuators as they can be tuned to absorb light in the NIR range and have been shown to efficiently convert the light into thermal energy to exhibit a change in the lipid structure. However, these particle-based actuators present problems with uncertainty about their location relative to the lipid material<sup>99, 112</sup> or aqueous phase<sup>111</sup>, and the potential for the nanosized agents to dissociate after administration, resulting in a reduction of the photothermal effect and limiting the practicality of these materials. To overcome this concern, an alternative small molecule photoactuator that can remain within the phospholipid structure and can elicit a photothermal effect similar to other known nanosized agents may be more desirable. Silicon 2,3-naphthalocyanine bis(trihexylsilyloxy) (SiNC) is of particular interest as it is a low molecular weight photosensitiser currently under investigation as a potential fluorescence imaging and phototherapeutic agent.<sup>113-114</sup> It is expected that light-responsive systems will have utility for delivery to the posterior segment as injectable 'depot' systems, as dispersed particles for ease of administration. The depot strategy allows for storage of multiple doses of drug, replacing say 12 months requirement of drug, but able to be administered as a single injection. The volume of the single injection will be restricted to below 0.1 mL to avoid adverse events such as increased intraocular pressure.<sup>115</sup> The system will need to be optimised to release a fixed dose of active repeatedly at intervals determined by symptom recurrence, throughout the 12 month period by fine tuning the NIR exposure time and the concentration of NIR agent in the system. Therefore, there at least exists potential to achieve a less frequent administration in the treatment of AMD if pulsatile, repeat administration can be achieved using a reversible stimuli-responsive lyotropic phospholipid-based systems.

## 1.6. Hypothesis

The overarching hypothesis that come from the above introduction is that the internal nanostructure of phospholipid-based systems can be rendered photo-sensitive through inclusion of near-infrared light responsive agents to allow for stimuli-responsive drug release of aflibercept via external activation.

- a. That the light-activated phase transition are reversible to provide pulsatile release of encapsulated drug.
- b. That a small molecule photosensitiser will exhibit a similar photothermal response to a particle-based actuator.
- c. That a slow to fast release profile will be demonstrated by the lamellar to bicontinuous cubic phase transition in the liquid crystal system.

## 1.7. Project Objectives

The aim of this project is to formulate an 'on-demand' drug delivery system that can be externally and non-invasively activated to release encapsulated drug via light activation.

The aims to be achieved in order to address the above hypotheses are listed below:

1. Design a phospholipid-based system that will provide reversible transitions between the lamellar and bicontinuous cubic phase.
2. Determine the effect of near-infrared agents on phase behaviour in the phospholipid-based systems.
3. Determine the amount of drug encapsulated within the phospholipid-based systems and whether drug release can be stimulated using near-infrared irradiation.

Chapter Two is a relevant materials and experimental techniques section that further describes and justifies their use in this thesis. The experimental chapters, Chapter Three, Four and Five, have been ordered systematically.

Chapter Three is the first experimental chapter that consists of a published article entitled “Phospholipid-Based Self-Assembled Mesophase Systems for Light-Activated Drug Delivery”. This chapter demonstrated that phospholipid-based systems could be rendered photo-sensitive through the inclusion of a particle-based photoactuator, gold nanorods. Although the NIR-activated phase transition was contrary to literature, NIR light induced reversible disruption to the lipid packing.

Chapter Four builds on the previous chapter and probes the similarities and difference of alternative NIR-responsive agents. This chapter contains a reproduction of the publication entitled “Naphthalocyanine as a New Photothermal Actuator for Lipid-Based Drug Delivery Systems”. The published article compared the photothermal effect of the molecular photosensitiser, SiNC, to literature particle-based actuators, GNR and graphene.

Chapter Five is a manuscript in preparation that investigated the release of the commonly used anti-VEGF therapy, aflibercept, from a light-responsive phospholipid-based system. Both the molecular and particle-based actuators were incorporated into another phospholipid-based system, which was confirmed to exhibit the lamellar to cubic phase transition. Upon near infrared irradiation, the phase transition occur which corresponded to the activation of aflibercept release.

The thesis is concluded in Chapter Six with an overall summary of the project and recommendations for future directions.

## 1.8. References

1. Wong, W. L.; Su, X.; Li, X.; Cheung, C. M. G.; Klein, R.; Cheng, C.-Y.; Wong, T. Y., Global prevalence of age-related macular degeneration and disease burden projection for 2020 and 2040: a systematic review and meta-analysis. *Lancet* **2014**, *2*, 106-116.
2. Sparrow, J. R.; Hicks, D.; Hamel, C. P., The retinal pigment epithelium in health and disease. *Current Molecular Medicine* **2010**, *10* (9), 802-823.
3. Balaratnasingam, C.; Dhrami-Gavazi, E.; McCann, J. T.; Ghadiali, Q.; Freund, K. B., Aflibercept: a review of its use in the treatment of choroidal neovascularization due to age-related macular degeneration. *Clinical Ophthalmology (Auckland, N.Z.)* **2015**, *9*, 2355-2371.
4. Ishikawa, M.; Jin, D.; Sawada, Y.; Abe, S.; Yoshitomi, T., Future therapies of wet age-related macular degeneration. *J. Ophthalmol.* **2015**, *2015*, 138070.
5. Holz, F. G.; Schmitz-Valckenberg, S.; Fleckenstein, M., Recent developments in the treatment of age-related macular degeneration. *J. Clin. Invest.* **2014**, *124*, 1430-1438.
6. Du, J. D.; Fong, W.-K.; Caliph, S.; Boyd, B. J., Lipid-based drug delivery systems in the treatment of wet age-related macular degeneration. *Drug Deliv. Transl. Res.* **2016**, *6*, 781-792.
7. Fong, W.-K.; Hanley, T.; Boyd, B. J., Stimuli responsive liquid crystals provide 'on-demand' drug delivery in vitro and in vivo. *J. Control. Release* **2009**, *135*, 218-26.
8. Resnikoff, S.; Pascolini, D.; Etya'ale, D.; Kocur, I.; Pararajasegaram, R.; Pokharel, G. P.; Mariotti, S. P., Global data on visual impairment in the year 2002. *Bulletin of the World Health Organization* **2004**, *82* (11), 844-51.
9. Group, T. E. D. P. R., Causes and prevalence of visual impairment among adults in the United States. *Arch. Ophthalmol.* **2004**, *122* (4), 477-485.
10. Vadlapudi, A. D.; Cholkar, K.; Dasari, S. R.; Mitra, A. K., Ocular drug delivery. Mitra, A. K., Ed. Burlington, MA : Jones & Bartlett Learning: 2015; pp 219-263.
11. Hughes, P. M.; Olejnik, O.; Chang-Lin, J.-E.; Wilson, C. G., Topical and systemic drug delivery to the posterior segments. *Adv. Drug Deliv. Rev.* **2005**, *57* (14), 2010-2032.
12. Bonilha, V. L.; Rayborn, M. E.; Bhattacharya, S. K.; Gu, X.; Crabb, J. S.; Crabb, J. W.; Hollyfield, J. G., The retinal pigment epithelium apical microvilli and retinal function. *Adv. Exp. Med. Biol.* **2006**, *572*, 519-524.
13. Coleman, H. R.; Chan, C.-C.; Ferris Iii, F. L.; Chew, E. Y., Age-related macular degeneration. *Lancet* **2008**, *372* (9652), 1835-1845.
14. Ozaki, E.; Campbell, M.; Kiang, A.-S.; Humphries, M.; Doyle, S. L.; Humphries, P., Inflammation in age-related macular degeneration. In *Retinal Degenerative Diseases*, Ash, J. D.; Grimm, C.; Hollyfield, J. G.; Anderson, R. E.; LaVail, M. M.; Bowes Rickman, C., Eds. Springer New York: 2014; Vol. 801, pp 229-235.
15. Group, M. P. S., Laser photocoagulation of subfoveal recurrent neovascular lesions in age-related macular degeneration: Results of a randomized clinical trial. *Arch. Ophthalmol.* **1991**, *109* (9), 1232-1241.
16. Group, M. P. S., Krypton laser photocoagulation for idiopathic neovascular lesions: Results of a randomized clinical trial. *Arch. Ophthalmol.* **1990**, *108* (6), 832-837.
17. Kawczyk-Krupka, A.; Bugaj, A. M.; Potempa, M.; Wasilewska, K.; Latos, W.; Sieroń, A., Vascular-targeted photodynamic therapy in the treatment of neovascular

- age-related macular degeneration: Clinical perspectives. *Photodiagnosis Photodyn. Ther.* **2015**, *12* (2), 161-175.
18. Aiello, L. P.; Pierce, E. A.; Foley, E. D.; Takagi, H.; Chen, H.; Riddle, L.; Ferrara, N.; King, G. L.; Lois, E. H. S., Suppression of retinal neovascularization in vivo by inhibition of vascular endothelial growth factor (VEGF) using soluble VEGF-receptor chimeric proteins. *Proc. Natl. Acad. Sci. U.S.A.* **1995**, *92* (23), 10457-10461.
  19. Kovach, J. L.; Schwartz, S. G.; Flynn, H. W.; Scott, I. U., Anti-VEGF treatment strategies for wet AMD. *J. Ophthalmol.* **2012**, *2012*, 786870.
  20. Tolentino, M. J.; Dennrick, A.; John, E.; Tolentino, M. S., Drugs in Phase II clinical trials for the treatment of age-related macular degeneration. *Expert Opin. Drug Deliv.* **2014**, *24* (2), 183-199.
  21. Araújo, J.; Nikolic, S.; Egea, M. A.; Souto, E. B.; Garcia, M. L., Nanostructured lipid carriers for triamcinolone acetonide delivery to the posterior segment of the eye. *Colloids Surf. B Biointerfaces* **2011**, *88* (1), 150-157.
  22. Araújo, J.; Garcia, M. L.; Mallandrich, M.; Souto, E. B.; Calpena, A. C., Release profile and transscleral permeation of triamcinolone acetonide loaded nanostructured lipid carriers (TA-NLC): in vitro and ex vivo studies. *Nanomedicine* **2012**, *8* (6), 1034-1041.
  23. Boyer, D. S.; Hopkins, J. J.; Sorof, J.; Ehrlich, J. S., Anti-vascular endothelial growth factor therapy for diabetic macular edema. *Ther. Adv. Endocrinol. Metab.* **2013**, *4* (6), 151-169.
  24. Pikuleva, I. A.; Curcio, C. A., Cholesterol in the retina: the best is yet to come. *Prog. Retin. Eye Res.* **2014**, *0*, 64-89.
  25. Gragoudas, E. S.; Adamis, A. P.; Cunningham, E. T.; Feinsod, M.; Guyer, D. R., Pegaptanib for neovascular age-related macular degeneration. *N. Engl. J. Med.* **2004**, *351* (27), 2805-2816.
  26. Rosenfeld, P. J.; Brown, D. M.; Heier, J. S.; Boyer, D. S.; Kaiser, P. K.; Chung, C. Y.; Kim, R. Y., Ranibizumab for neovascular age-related macular degeneration. *N. Engl. J. Med.* **2006**, *355* (14), 1419-1431.
  27. Ohr, M.; Kaiser, P. K., Intravitreal aflibercept injection for neovascular (wet) age-related macular degeneration. *Exp. Opin. Pharmacother.* **2012**, *13*, 585-591.
  28. Stewart, M. W., What are the half-lives of ranibizumab and aflibercept (VEGF Trap-eye) in human eyes? Calculations with a mathematical model. *Eye Reports* **2011**, *1:e5*, 1-14.
  29. Stewart, M. W., Aflibercept (VEGF Trap-eye): the newest anti-VEGF drug. *Br. J. Ophthalmol.* **2012**, *96* (9), 1157.
  30. Bakri, S. J.; Snyder, M. R.; Reid, J. M.; Pulido, J. S.; Ezzat, M. K.; Singh, R. J., Pharmacokinetics of intravitreal ranibizumab (Lucentis). *Ophthalmol.* **2007**, *114* (12), 2179-2182.
  31. Meyer, C. H.; Krohne, T. U.; Holz, F. G., Intraocular pharmacokinetics after a single intravitreal injection of 1.5 mg versus 3.0 mg of bevacizumab in humans. *Retina* **2011**, *31* (9), 1877-84.
  32. Li, S. K.; Hao, J.; Liu, H.; Lee, J.-H., MRI Study of Subconjunctival and Intravitreal Injections. *J. Pharm. Sci.* **2012**, *101* (7), 2353-2363.
  33. Short, B. G., Safety evaluation of ocular drug delivery formulations: techniques and practical considerations. *Toxicol. Pathol.* **2008**, *36* (1), 49-62.
  34. Wong, T. Y.; Liew, G.; Mitchell, P., Clinical update: new treatments for age-related macular degeneration. *Lancet* **370** (9583), 204-206.

35. Steinbrook, R., The price of sight — ranibizumab, bevacizumab, and the treatment of macular degeneration. *N. Engl. J. Med.* **2006**, 355 (14), 1409-1412.
36. Kimura, H.; Yasukawa, T.; Tabata, Y.; Ogura, Y., Drug targeting to choroidal neovascularization. *Adv. Drug. Deliv. Rev.* **2001**, 52 (1), 79-91.
37. Group, E. S., Preclinical and phase 1A clinical evaluation of an anti-VEGF pegylated aptamer (EYEO01) for the treatment of exudative age-related macular degeneration. *Retina* **2002**, 22 (2), 143-52.
38. Yasin, M. N.; Svirskis, D.; Seyfoddin, A.; Rupenthal, I. D., Implants for drug delivery to the posterior segment of the eye: A focus on stimuli-responsive and tunable release systems. *J. Control. Release* **2014**, 196, 208-221.
39. Lim, J. I.; Wolitz, R. A.; Dowling, A. H.; Bloom, H. R.; Irvine, A. R.; Schwartz, D. M., Visual and anatomic outcomes associated with posterior segment complications after ganciclovir implant procedures in patients with AIDS and cytomegalovirus retinitis. *Am. J. Ophthalmol.* **1999**, 127 (3), 288-93.
40. Ninawe, P. R.; Hatziaavramidis, D.; Parulekar, S. J., Delivery of drug macromolecules from thermally responsive gel implants to the posterior eye. *Chem. Eng. Sci.* **2010**, 65 (18), 5170-5177.
41. Bisht, R.; Mandal, A.; Jaiswal Jagdish, K.; Rupenthal Ilva, D., Nanocarrier mediated retinal drug delivery: overcoming ocular barriers to treat posterior eye diseases. *Wiley Interdiscip. Rev. Nanomed. Nanobiotechnol.* **2017**, 10 (2), e1473.
42. Lajunen, T.; Nurmi, R.; Kontturi, L.; Viitala, L.; Yliperttula, M.; Murtomäki, L.; Urtti, A., Light activated liposomes: Functionality and prospects in ocular drug delivery. *J. Control. Release* **2016**, 244, 157-166.
43. Agarwal, R.; Iezhitsa, I.; Agarwal, P.; Abdul Nasir, N. A.; Razali, N.; Alyautdin, R.; Ismail, N. M., Liposomes in topical ophthalmic drug delivery: an update. *Drug Deliv.* **2016**, 23 (4), 1075-1091.
44. Delplace, V.; Payne, S.; Shoichet, M., Delivery strategies for treatment of age-related ocular diseases: From a biological understanding to biomaterial solutions. *J. Control. Release* **2015**, 219, 652-668.
45. Schwartz, S. G.; Scott, I. U.; Flynn, H. W.; Stewart, M. W., Drug delivery techniques for treating age-related macular degeneration. *Expert Opin. Drug Deliv.* **2013**, 11 (1), 61-68.
46. Honda, M.; Asai, T.; Oku, N.; Araki, Y.; Tanaka, M.; Ebihara, N., Liposomes and nanotechnology in drug development: focus on ocular targets. *Int. J. Nanomedicine* **2013**, 8, 495-504.
47. Kaur, I. P.; Kakkar, S., Nanotherapy for posterior eye diseases. *J. Control. Release* **2014**, 193, 100-112.
48. Wang, J.; Jiang, A.; Joshi, M.; Christoforidis, J., Drug delivery implants in the treatment of vitreous inflammation. *Mediators Inflamm.* **2013**, 2013, 780634.
49. Bochot, A.; Fattal, E., Liposomes for intravitreal drug delivery: A state of the art. *J. Control. Release* **2012**, 161 (2), 628-634.
50. Mishra, G. P.; Bagui, M.; Tamboli, V.; Mitra, A. K., Recent applications of liposomes in ophthalmic drug delivery. *J. Drug Deliv.* **2011**, 2011, 14.
51. Choonara, Y. E.; Pillay, V.; Danckwerts, M. P.; Carmichael, T. R.; du Toit, L. C., A review of implantable intravitreal drug delivery technologies for the treatment of posterior segment eye diseases. *J. Pharm. Sci.* **2010**, 99 (5), 2219-2239.

52. ClinicalTrials.gov [Internet]. Bethesda (MD): National Library of Medicine (US). 2000- [cited 2016 April 14]. *NLM Identifier: NCT00535054, NCT02420834, NCT01987323, NCT02466399, NCT02599688, NCT00072384, NCT00335738, NCT01115192, NCT02006147. Available from: <http://clinicaltrials.gov>.*
53. Natarajan, J. V.; Ang, M.; Darwitan, A.; Chattopadhyay, S.; Wong, T. T.; Venkatraman, S. S., Nanomedicine for glaucoma: liposomes provide sustained release of latanoprost in the eye. *Int. J. Nanomedicine* **2012**, *7*, 123-131.
54. Habib, F. S.; Fouad, E. A.; Abdel-Rhman, M. S.; Fathalla, D., Liposomes as an ocular delivery system of fluconazole: in-vitro studies. *Acta Ophthalmol.* **2010**, *88* (8), 901-904.
55. Abrishami, M.; Zarei-Ghanavati, S.; Soroush, D.; Rouhbakhsh, M.; Jaafari, M.; Malaekheh-Nikouei, B., Preparation, characterization, and in vivo evaluation of nanoliposomes-encapsulated bevacizumab (avastin) for intravitreal administration. *Retina* **2009**, *29* (1), 699-703.
56. Fujisawa, T.; Miyai, H.; Hironaka, K.; Tsukamoto, T.; Tahara, K.; Tozuka, Y.; Ito, M.; Takeuchi, H., Liposomal diclofenac eye drop formulations targeting the retina: Formulation stability improvement using surface modification of liposomes. *International Journal of Pharmaceutics* **2012**, *436* (1-2), 564-567.
57. Wang, J.-l.; Liu, Y.-l.; Li, Y.; Dai, W.-b.; Guo, Z.-m.; Wang, Z.-h.; Zhang, Q., EphA2 targeted doxorubicin stealth liposomes as a therapy system for choroidal neovascularization in rats. *Invest. Ophthalmol. Vis. Sci.* **2012**, *53* (11), 7348-7357.
58. Joseph, R. R.; Tan, D. W. N.; Ramon, M. R. M.; Natarajan, J. V.; Agrawal, R.; Wong, T. T.; Venkatraman, S. S., Characterization of liposomal carriers for the trans-scleral transport of ranibizumab. *Sci. Rep.* **2017**, *7*, 16803.
59. Chen, C.-W.; Lu, D.-W.; Yeh, M.-K.; Shiau, C.-Y.; Chiang, C.-H., Novel RGD-lipid conjugate-modified liposomes for enhancing siRNA delivery in human retinal pigment epithelial cells. *Int. J. Nanomedicine* **2011**, *6*, 2567-2580.
60. Chen, C.-W.; Yeh, M.-K.; Shiau, C.-Y.; Chiang, C.-H.; Lu, D.-W., Efficient downregulation of VEGF in retinal pigment epithelial cells by integrin ligand-labeled liposome-mediated siRNA delivery. *Int. J. Nanomedicine* **2013**, *8*, 2613-2627.
61. Liu, H. A.; Liu, Y. L.; Ma, Z. Z.; Wang, J. C.; Zhang, Q., A lipid nanoparticle system improves siRNA efficacy in RPE cells and a laser-induced murine CNV model. *Invest. Ophthalmol. Vis. Sci.* **2011**, *52* (7), 4789-94.
62. Cho, Y. W.; Han, Y. S.; Chung, I. Y.; Kim, S. J.; Seo, S. W.; Yoo, J. M.; Park, J. M., Suppression of laser-induced choroidal neovascularization by intravitreal injection of tristetraprolin. *Int. J. Ophthalmol.* **2014**, *7* (6), 952-958.
63. Honda, M.; Asai, T.; Umemoto, T.; Araki, Y.; Oku, N.; Tanaka, M., Suppression of choroidal neovascularization by intravitreal injection of liposomal su5416. *Arch. Ophthalmol.* **2011**, *129* (3), 317-321.
64. Davis, B. M.; Normando, E. M.; Guo, L.; Turner, L. A.; Nizari, S.; O'Shea, P.; Moss, S. E.; Somavarapu, S.; Cordeiro, M. F., Topical delivery of avastin to the posterior segment of the eye in vivo using annexin A5-associated liposomes. *Small* **2014**, *10* (8), 1575-1584.
65. Shimazaki, H.; Hironaka, K.; Fujisawa, T.; Tsuruma, K.; Tozuka, Y.; Shimazawa, M.; Takeuchi, H.; Hara, H., Edaravone-loaded liposome eyedrops protect against light-induced retinal damage in mice. *Invest. Ophthalmol. Vis. Sci.* **2011**, *52* (10), 7289-7297.

66. Maurice, D. M.; Mishima, S., Ocular pharmacokinetics. In *Pharmacology of the Eye*, Sears, M., Ed. Springer Berlin Heidelberg: 1984; Vol. 69, pp 19-116.
67. Curtis, L. H.; Hammill, B. G.; Schulman, K. A.; Cousins, S. W., Risks of mortality, myocardial infarction, bleeding, and stroke associated with therapies for age-related macular degeneration. *Arch. Ophthalmol.* **2010**, *128* (10), 1273-1279.
68. Li, T.; Hou, X.; Deng, H.; Zhao, J.; Huang, N.; Zeng, J.; Chen, H.; Gu, Y., Liposomal hypocrellin B as a potential photosensitizer for age-related macular degeneration: pharmacokinetics, photodynamic efficacy, and skin phototoxicity in vivo. *Photochem. Photobiol. Sci.* **2015**, *14* (5), 972-981.
69. Gross, N.; Ranjbar, M.; Evers, C.; Hua, J.; Martin, G.; Schulze, B.; Michaelis, U.; Hansen, L. L.; Agostini, H. T., Choroidal neovascularization reduced by targeted drug delivery with cationic liposome-encapsulated paclitaxel or targeted photodynamic therapy with verteporfin encapsulated in cationic liposomes. *Mol. Vis.* **2013**, *19*, 54-61.
70. Hironaka, K.; Inokuchi, Y.; Fujisawa, T.; Shimazaki, H.; Akane, M.; Tozuka, Y.; Tsuruma, K.; Shimazawa, M.; Hara, H.; Takeuchi, H., Edaravone-loaded liposomes for retinal protection against oxidative stress-induced retinal damage. *Eur. J. Pharm. Biopharm.* **2011**, *79* (1), 119-125.
71. Salehi-Had, H.; Roh, M. I.; Giani, A.; Hisatomi, T.; Nakao, S.; Kim, I. K.; Gragoudas, E. S.; Vavvas, D.; Guccione, S.; Miller, J. W., Utilizing targeted gene therapy with nanoparticles binding alpha v beta 3 for imaging and treating choroidal neovascularization. *PLoS ONE* **2011**, *6* (4), e18864.
72. Mozafari, M. R., Liposomes: an overview of manufacturing techniques. *Cell Mol. Biol. Lett.* **2005**, *10* (4), 711-9.
73. Martiel, I.; Sagalowicz, L.; Mezzenga, R., Phospholipid-based nonlamellar mesophases for delivery systems: Bridging the gap between empirical and rational design. *Adv. Colloid Interface Sci.* **2014**, *209*, 127-143.
74. Gabizon, A.; Shmeeda, H.; Barenholz, Y., Pharmacokinetics of Pegylated Liposomal Doxorubicin. *Clin. Pharmacokinet.* **2003**, *42* (5), 419-436.
75. Natarajan, J. V.; Nugraha, C.; Ng, X. W.; Venkatraman, S., Sustained-release from nanocarriers: a review. *J. Control. Release* **2014**, *193*, 122-138.
76. Mounier, C. M.; Wendum, D.; Greenspan, E.; Fléjou, J. F.; Rosenberg, D. W.; Lambeau, G., Distinct expression pattern of the full set of secreted phospholipases A<sub>2</sub> in human colorectal adenocarcinomas: sPLA<sub>2</sub>-III as a biomarker candidate. *Br. J. Cancer* **2008**, *98*, 587.
77. Jiang, W.; Lionberger, R.; Yu, L. X., In vitro and in vivo characterizations of PEGylated liposomal doxorubicin. *Bioanalysis* **2011**, *3* (3), 333-344.
78. Ponce, A.; Wright, A.; Dewhirst, M.; Needham, D., Targeted bioavailability of drugs by triggered release from liposomes. *Future Lipidol.* **2006**, *1* (1), 25-34.
79. Mura, S.; Nicolas, J.; Couvreur, P., Stimuli-responsive nanocarriers for drug delivery. *Nat. Mater.* **2013**, *12* (11), 991-1003.
80. Li, P.-Y.; Shih, J.; Lo, R.; Saati, S.; Agrawal, R.; Humayun, M. S.; Tai, Y.-C.; Meng, E., An electrochemical intraocular drug delivery device. *Sens. Actuators A Phys.* **2008**, *143* (1), 41-48.
81. Peng, K.; Tomatsu, I.; van den Broek, B.; Cui, C.; Korobko, A. V.; van Noort, J.; Meijer, A. H.; Spaink, H. P.; Kros, A., Dextran based photodegradable hydrogels formed via a Michael addition. *Soft Matter* **2011**, *7* (10), 4881-4887.

82. Pirmoradi, F. N.; Jackson, J. K.; Burt, H. M.; Chiao, M., On-demand controlled release of docetaxel from a battery-less MEMS drug delivery device. *Lab on a Chip* **2011**, *11* (16), 2744-2752.
83. Lee, K. W. Y.; Nguyen, T.-H.; Hanley, T.; Boyd, B. J., Nanostructure of liquid crystalline matrix determines in vitro sustained release and in vivo oral absorption kinetics for hydrophilic model drugs. *Int J Pharm* **2009**, *365* (1-2), 190-199.
84. Phan, S.; Fong, W.-K.; Kirby, N.; Hanley, T.; Boyd, B. J., Evaluating the link between self-assembled mesophase structure and drug release. *Int J Pharm* **2011**, *421* (1), 176-182.
85. Clogston, J.; Caffrey, M., Controlling release from the lipidic cubic phase. Amino acids, peptides, proteins and nucleic acids. *J Contr Release* **2005**, *107* (1), 97-111.
86. Malmsten, M., Soft drug delivery systems. *Soft Matter* **2006**, *2*, 760.
87. Nguyen, T.-H.; Hanley, T.; Porter, C. J. H.; Boyd, B. J., Nanostructured liquid crystalline particles provide long duration sustained-release effect for a poorly water soluble drug after oral administration. *J. Control. Release* **2011**, *153*, 180-6.
88. Israelachvili, J. N.; Mitchell, D. J.; Ninham, B. W., Theory of Self-Assembly of Hydrocarbon Amphiphiles into Micelles and Bilayers. *J. Chem. Soc. Faraday Trans.* **1976**, *72*, 1525-1568.
89. Dong, Y.-D.; Dong, A. W.; Larson, I.; Rappolt, M.; Amenitsch, H.; Hanley, T.; Boyd, B. J., Impurities in commercial phytantriol significantly alter its lyotropic liquid-crystalline phase behavior. *Langmuir* **2008**, *24*, 6998-7003.
90. Muir, B. W.; Zhen, G.; Gunatillake, P.; Hartley, P. G., Salt induced lamellar to bicontinuous cubic phase transitions in cationic nanoparticles. *J. Phys. Chem. B* **2012**, *116*, 3551-6.
91. Du, J. D.; Liu, Q.; Salentinig, S.; Nguyen, T.-H.; Boyd, B. J., A novel approach to enhance the mucoadhesion of lipid drug nanocarriers for improved drug delivery to the buccal mucosa. *Int. J. Pharm.* **2014**, *471* (1-2), 358-365.
92. Negrini, R.; Fong, W. K.; Boyd, B. J.; Mezzenga, R., pH-responsive lyotropic liquid crystals and their potential therapeutic role in cancer treatment. *Chem Commun* **2015**, *51* (30), 6671-6674.
93. Tate, M. W.; Eikenberry, E. F.; Turner, D. C.; Shyamsunder, E.; Gruner, S. M., Nonbilayer phases of membrane lipids. *Chem. Phys. Lipids* **1991**, *57* (2), 147-164.
94. Holmberg, K.; Jönsson, B.; Kronberg, B.; Lindman, B., *Surfactants and polymers in aqueous solution*. John Wiley & Sons, Ltd: 2003.
95. Phan, S.; Fong, W.-K.; Kirby, N.; Hanley, T.; Boyd, B. J., Evaluating the link between self-assembled mesophase structure and drug release. *Int. J. Pharm.* **2011**, *421*, 176-182.
96. Li, L.; ten Hagen, T. L. M.; Schipper, D.; Wijnberg, T. M.; van Rhooen, G. C.; Eggermont, A. M. M.; Lindner, L. H.; Koning, G. A., Triggered content release from optimized stealth thermosensitive liposomes using mild hyperthermia. *J. Control. Release* **2010**, *143* (2), 274-279.
97. Yeo, S. Y.; de Smet, M.; Langereis, S.; Vander Elst, L.; Muller, R. N.; Grüll, H., Temperature-sensitive paramagnetic liposomes for image-guided drug delivery: Mn<sup>2+</sup> versus [Gd(HPDO<sub>3</sub>A)(H<sub>2</sub>O)]. *Biochim. Biophys. Acta* **2014**, *1838* (11), 2807-2816.
98. Arruebo, M.; Fernández-Pacheco, R.; Ibarra, M. R.; Santamaría, J., Magnetic nanoparticles for drug delivery. *Nano Today* **2007**, *2*, 22-32.

99. Fong, W.-K.; Hanley, T. L.; Thierry, B.; Kirby, N.; Boyd, B. J., Plasmonic nanorods provide reversible control over nanostructure of self-assembled drug delivery materials. *Langmuir* **2010**, *26*, 6136-6139.
100. Fong, W.-K.; Hanley, T. L.; Thierry, B.; Kirby, N.; Waddington, L. J.; Boyd, B. J., Controlling the nanostructure of gold nanorod-lyotropic liquid-crystalline hybrid materials using near-infrared laser irradiation. *Langmuir* **2012**, *28*, 14450-14460.
101. Yavlovich, A.; Smith, B.; Gupta, K.; Blumenthal, R.; Puri, A., Light-sensitive lipid-based nanoparticles for drug delivery: design principles and future considerations for biological applications. *Mol. Membr. Biol.* **2010**, *27* (7), 364-81.
102. Leung, S. J.; Romanowski, M., Light-activated content release from liposomes. *Theranostics* **2012**, *2* (10), 1020-1036.
103. Yavlovich, A.; Singh, A.; Tarasov, S.; Capala, J.; Blumenthal, R.; Puri, A., Design of liposomes containing photopolymerizable phospholipids for triggered release of contents. *J. Therm. Anal. Calorim.* **2009**, *98* (1), 97-104.
104. Bisht, R.; Jaiswal, J. K.; Chen, Y.-S.; Jin, J.; Rupenthal, I. D., Light-responsive in situ forming injectable implants for effective drug delivery to the posterior segment of the eye. *Expert Opin. Drug Deliv.* **2016**, *13* (7), 953-962.
105. Weissleder, R.; Ntziachristos, V., Shedding light onto live molecular targets. *Nat. Med.* **2003**, *9* (1), 123-128.
106. Barun, V. V.; Ivanov, A. P.; Volotovskaya, A. V.; Ulashchik, V. S., Absorption spectra and light penetration depth of normal and pathologically altered human skin. *J. Appl. Spectrosc.* **2007**, *74* (3), 430-439.
107. Cao, J.; Huang, S.; Chen, Y.; Li, S.; Li, X.; Deng, D.; Qian, Z.; Tang, L.; Gu, Y., Near-infrared light-triggered micelles for fast controlled drug release in deep tissue. *Biomaterials* **2013**, *34* (26), 6272-6283.
108. Fong, W.-K.; Hanley, T. L.; Thierry, B.; Tilley, A.; Kirby, N.; Waddington, L. J.; Boyd, B. J., Understanding the photothermal heating effect in non-lamellar liquid crystalline systems, and the design of new mixed lipid systems for photothermal on-demand drug delivery. *Phys. Chem. Chem. Phys.* **2014**, *16* (45), 24936-24953.
109. Kwon, H. J.; Byeon, Y.; Jeon, H. N.; Cho, S. H.; Han, H. D.; Shin, B. C., Gold cluster-labeled thermosensitive liposomes enhance triggered drug release in the tumor microenvironment by a photothermal effect. *J. Control. Release* **2015**, *216*, 132-139.
110. Du, J. D.; Fong, W.-K.; Salentinig, S.; Caliph, S. M.; Hawley, A.; Boyd, B. J., Phospholipid-based self-assembled mesophase systems for light-activated drug delivery. *Phys. Chem. Chem. Phys.* **2015**, *17*, 14021-14027.
111. Quinn, M. D. J.; Wang, T.; Du, J. D.; Boyd, B. J.; Hawley, A.; Notley, S. M., Graphene as a Photothermal Actuator for Control of Lipid Mesophase Structure. *Nanoscale* **2017**, *9*, 341-348.
112. Lee, J. H.; Shin, Y.; Lee, W.; Whang, K.; Kim, D.; Lee, L. P.; Choi, J. W.; Kang, T., General and Programmable Synthesis of Hybrid Liposome/Metal Nanoparticles. *Sci. Adv.* **2016**, *2*, e1601838.
113. Taratula, O.; Schumann, C.; Duong, T.; Taylor, K. L.; Taratula, O., Dendrimer-encapsulated naphthalocyanine as a single agent-based theranostic nanoplatform for near-infrared fluorescence imaging and combinatorial anticancer phototherapy. *Nanoscale* **2015**, *7*, 3888-3902.
114. Taratula, O.; Doddapaneni, B. S.; Schumann, C.; Li, X.; Bracha, S.; Milovancev, M.; Alani, A. W. G.; Taratula, O., Naphthalocyanine-based biodegradable polymeric

nanoparticles for image-guided combinatorial phototherapy. *Chem. Mater.* **2015**, *27*, 6155-6165.

115. Kotliar, K.; Maier, M.; Bauer, S.; Feucht, N.; Lohmann, C.; Lanzl, I., Effect of intravitreal injections and volume changes on intraocular pressure: clinical results and biomechanical model. *Acta Ophthalmol.* **2007**, *85* (7), 777-781.

CHAPTER TWO:  
GENERAL MATERIALS AND  
METHODS

## 2.1. Materials

### 2.1.1. Lipid components

Phytantriol (3,7,11,15-tetramethylhexadecane-1,2,3-triol) was a gift from DSM Nutritional Products (Kaiseraugst, Switzerland). 1,2-Dilauroyl-sn-glycero-3-phosphocholine (DLPC), 1-palmitoyl-2-oleoyl-sn-glycero-3-phosphoethanolamine (POPE) and 1,2-distearoyl-sn-glycero-3-phosphoethanolamine-N-[amino- (polyethylene glycol)-2000] (PEG-DSPE) were purchased from Avanti Polar Lipids (Alabaster, USA). Lauric acid ( $\geq 98\%$ ) and cholesterol from Sigma-Aldrich (St. Louis, USA).

Phytantriol (PHYT) is a generally recognized as safe (GRAS) excipient used in personal care products and is an established platform known to be responsive to photothermal stimuli. PHYT in excess water forms the bicontinuous cubic ( $V_2$ ) in ambient temperature, and transforms to the inverse hexagonal ( $H_2$ ) and inverse micellar ( $L_2$ ) phase at high temperatures. PHYT with a minimum purity of 95 % was used to ensure the phase transition occurs around 60 °C.<sup>1</sup> The release of hydrophilic compounds from the  $V_2$  phase have been shown to be significantly faster than from the  $H_2$  phase.<sup>2</sup> Although the phase behaviour will result in a release profile that is not ideal for on-demand drug release application, its phase transition have been shown to be both reversible and reproducible with the use of near-infrared (NIR) light activation to particle-based photoactuators.

An ideal release profile would be a phospholipid system that can transition from the  $L_\alpha$  to  $V_2$  phase to exhibit a slow to fast release profile with an increase in temperature, and ultimately upon the application of a NIR stimulus. Phospholipids are the main component of cell membranes, therefore phospholipid-based carriers are suitable drug delivery purposes because of their biocompatible and biodegradable nature. When the phase behaviours of individual lipid species are studied, roughly half of the naturally occurring lipids form non-lamellar phases.<sup>3</sup> Due to the balance between headgroup area and tail volume, which strongly dictates the packing of the lipid molecules at the amphiphile/water interface, the formation of the  $V_2$  phase is more stringent and is less frequently encountered than the  $H_2$  phase. There are limited known phospholipid-based systems that exhibits the  $L_\alpha$  to  $V_2$  phase transition.

This thesis investigates two phospholipid systems: POPE system with 20 mol% cholesterol, and DLPC and lauric acid (LA) at a 1:2 molar ratio.

1) In the first instance, POPE with increasing proportions of cholesterol was investigated as the  $L_\alpha$  to  $V_2$  phase transition were previously identified at high temperature in mixtures containing less than 30 mol% cholesterol.<sup>4</sup> Specifically,  $V_2$  phases were observed for the POPE system with 20 mol% cholesterol at temperatures above 60 °C.<sup>4</sup> Consequently, it was this ratio that was utilised.

2) DLPC:2LA at 20 bar pressure was found to transition from  $L_\alpha$  to  $V_2$  phase at 41 °C, and subsequently, a coexisting  $V_2$  and  $H_2$  phase was observed between 50 and 65 °C. Due to their reported transformations being ideal for on-demand purposes, further investigation into their phase behaviour and photothermal response was necessary.

### 2.1.2. Near-infrared responsive actuators

Methyl conjugated Gold Nanorods<sup>TM</sup> with an aspect ratio of 4.2 (length, 42 nm; width, 10 nm) were purchased from Nanopartz (Loveland, USA). The measured surface plasmon resonances (SPR) was 825 nm. PEGylated Gold NanoRods with an aspect ratio of 4.3 (length, 47.8 nm; width, 11.2 nm) were purchased from NanoHybrids Inc. (Texas, USA). The measured SPR was 814 nm. Silicon 2,3-naphthalocyanine bis(trihexylsilyloxy) (SiNC) was purchased from Sigma-Aldrich (St. Louis, USA).

Gold nanorods (GNR) at the concentration of 0.3 nM and 3 nM were selected to probe the photothermal response of particle-based actuators in phospholipid-based systems. Recent studies using PHYT system have shown that the addition of 3 nM GNR with a surface plasmon resonances (SPR) at 780 nm in water, induces heating of approximately 50 °C when irradiated for 10 sec at 808 nm.<sup>5</sup> A lower concentration was also included, however, the change in phase structure was not observed on inclusion of 0.3 nM in the PHYT system.

SiNC was selected for its enhanced absorption in the 750-800 nm spectral range and can be efficiently activated with NIR light to generate reactive oxygen species, which have been shown to be useful for safe and effective photodynamic therapy (PDT) and bioimaging.<sup>6</sup> SiNC has also been incorporated into the design of contact lenses.

SiNC have been gaining attention as a functional pigment that absorbs lights and was shown to have UV-blocking capabilities.<sup>7</sup>

### 2.1.3. General materials

Eylea® (Regeneron/Bayer) was a gift from Dr Devinder Chauhan (Ophthalmic Surgeon, Retina Doctor). Pluronic® F108 stabilizer, 1-dodecanthiol ( $\geq 98\%$ ), glycine ( $\geq 98\%$ ) were purchased from Sigma-Aldrich (St. Louis, USA). Tris Ultra Pure Grade with a purity  $>99.9\%$ , was purchased from Astrala Scientific Pty Ltd (NSW, Australia). Hydrochloric acid (1 M), dimethyl sulfoxide and dry tetrahydrofuran (THF) were purchased from Merck (VIC, Australia). Phosphate buffered saline (PBS) at pH 7.4 was made using analytical reagent quality salts including 137 mM sodium chloride (Chem-Supply, Australia), 10 mM di-sodium hydrogen orthophosphate and 2.7 mM potassium dihydrogen orthophosphate (APS Ajax Finechem, Australia). All materials were used without further purification. Water used in these studies was obtained from a Millipore Milli-Q purification system (Billerica, USA).

## 2.2. Methods

### 2.2.1. General preparation

A thin-film hydration method was used to prepare the lipid-based samples with and without NIR-responsive actuators. Lipids and NIR-responsive agents were weighed in the appropriate molar ratios and dissolved in chloroform or THF. The mixture was then dried under a stream of nitrogen gas for 3 hr, then under vacuum overnight at 40-50°C to ensure complete removal of solvent. The lipid mixture was hydrated with appropriate volumes of PBS (with 1 w/w% Pluronic® F108 stabiliser, if required). Dispersed samples were subjected to ultrasonication (S220 Focused-ultrasonicator, Covaris, USA) for 15 min (40 s pulses, peak power: 250.0 and duty factor: 30.2). The samples were allowed to equilibrate for  $>24$  hr prior to phase characterisation and release experiments.

### 2.2.2. Phase characterisation

The foundation for the work carried out during this project was phase characterisation experiments of lipid-based formulations using small angle X-ray scattering (SAXS). The phase behaviour of these lipid systems was evaluated at equilibrium and dynamically

using time-resolved synchrotron SAXS to observe the effect of photothermal heating via NIR activation. Subsequent techniques were later employed to confirm the morphology of the system and to investigate the release of drug. Justifications of the chosen techniques are provide provided below, further details are included in the experimental chapters three, four and five.

#### 2.2.2.1. Small angle X-ray scattering (SAXS)

The liquid crystal (LC) structures were assessed using SAXS to qualitatively identify and confirm the internal nanostructure formed from various lipid compositions. SAXS measurements were performed at the Australian Synchrotron.<sup>8</sup> SAXS has become the most recognised technique for the characterisation of bulk and dispersed liquid crystals and other colloidal structures in solution as it provides non-invasive morphological information of structures.<sup>9</sup> Typically, SAXS with a scattering angle ( $\theta$ ) of less than  $10^\circ$ , provides structural information for samples in the size range of one to several hundreds of nanometres in size. Moreover, synchrotron X-ray source delivers higher flux than regular bench-top instruments, which enables probing of structures in a time resolved manner. As such, synchrotron SAXS was the primary technique used throughout this thesis to elucidate the structural evolution of these lipidic self-assembled systems in real-time.

SAXS experiments probe the LC structure with a well-collimated X-ray beam at a specific wavelength ( $\lambda$ ), which is then scattered according to the distribution of electron densities in the samples. The variations in the intensity of the scattered X-rays are measured as a function of the scattering angle ( $\theta$ ), which results in a unique scattering pattern.<sup>9-10</sup> These scattering patterns can be described using the Bragg's Law; Equation 1:

$$2d \sin\theta = n\lambda \quad (1)$$

Where  $d$  represents the interplanar spacing and  $n$  is an integer. The angular scattering intensity provides morphological information on the structures with a spatial dimension. The scattering pattern is often expressed as a plot of intensity versus the magnitude of the scattering vector,  $q$ , by Equation 2 and these plots were reduced with

the use of the in-house developed software package, scatterBrain<sup>11</sup>. A silver behenate standard (d-spacing = 58.38 Å) was used for the q range calibration.

$$q = \frac{4\pi}{\lambda} \sin(\theta/2) \quad (2)$$

The relative positions and spacing of the Bragg peaks correlate to fixed Miller indices, which are used to identify the phase structures present.<sup>9</sup> The scattering vector at which the peaks occur is then used to calculate the interplanar spacing,  $d$ , between two reflecting planes of the liquid crystal phase according to Equation 3:

$$d = 2\pi/q \quad (3)$$

The mean lattice parameter of a system is a measure of the internal phase structure and can be calculated using the calculated  $d$  value, the absolute position of the peaks and applying the appropriate scattering law for the phase structure present as shown in Table 1, with the exception of the inverse micellar phase ( $L_2$ ), which is evidenced by a broad peak between 0.15 and 0.20 Å.

Table 1 SAXS reflection laws of liquid crystal mesophases that was investigated

Name		Space Group	Spacing Ratios
Lamellar phase		$L_\alpha$	1:2:3:4
Bicontinuous cubic phase ( $V_2$ )	Diamond	$Pn3m$	$\sqrt{2} : \sqrt{3} : \sqrt{4} : \sqrt{6}$
	Primitive	$Im3m$	$\sqrt{2} : \sqrt{4} : \sqrt{6} : \sqrt{8}$
Inverse hexagonal phase ( $H_2$ )		$P6m$	1: $\sqrt{3}$ : $\sqrt{4}$

A global change in temperature cannot be detected upon irradiation of these systems because the localized heating that causes changes in lipid packing is rapidly dissipated through the material. In time-resolved measurements, the photothermal effect requires the use of the apparent temperature ( $T_{app}$ ). By utilising the lattice parameters calculated from the temperature-dependent equilibrium data, a calibration plot of the lattice parameter vs. temperature can be used to convert the effect of irradiation on the lipid systems to  $T_{app}$ .<sup>12</sup> The calculated  $T_{app}$  acts as a measure of disruption of lipid packing during irradiation, which is used to compare the magnitude of change in lipid packing and effectiveness between the different near-infrared actuator incorporated lipid systems.

#### a) Equilibrium experiments

The equilibrium lyotropic phase behaviour of LC systems have been well studied as these systems can often be dispersed to form nanoparticles which retains the internal structure of the nondispersed phase. As such, the equilibrium phase behaviour in an excess of water were first investigated to confirm the nanostructures and the phase transition temperature, which may vary due to the use of different sources of phospholipids. The equilibrium experiments was also used to determine whether the concentration of the added NIR-responsive actuators will affect the general phase behaviour of the phospholipids. Briefly, the structure of dispersion samples were determined with increasing temperature from 25 to 80 °C. The samples were allowed to equilibrate for 10 min for every 5 degrees interval. One second acquisitions at 100 % flux was used to ensure full resolution of peaks. The equilibrium results were then used to construct a calibration plot for use in dynamic experiments.

#### b) Dynamic experiments

Dynamic experiments were conducted to monitor the change in structure upon NIR irradiation. A Class IIIB fibre coupled laser system (Changchun New Industries, China) with the power output at 400 mW and a wavelength ( $\lambda$ ) of 808 nm was used to illuminate the samples externally. The acquisition time was reduced to 0.1 s at 20 % flux to avoid radiation damage from the synchrotron beam during data accumulation. Data was obtained at intervals of every 8-10 s data for up to 8 min in order to have a time-

resolved indication of the effect of irradiation upon nanostructure. No change in structure was observed for blank phospholipid samples when exposed to the same dose of X-ray radiation. The SAXS scattering patterns were acquired before, during and after near-infrared activation.

#### 2.2.2.2. Cryogenic transmission electron microscopy (cryo-TEM)

Cryo-TEM was used to verify the nanostructure formed by the different phospholipid-based dispersions with and without NIR responsive elements. Cryogenic method was chosen over normal TEM as it avoids introducing artefacts that can form during sample preparation such as the staining, fixation and adsorption process. Cryo-TEM is a common technique used to visualise the nanostructure of self-assembled systems. The images captured the disposition of the NIR-responsive agents relative to the lipid bilayer and confirmed the vesicular morphology in the absence of Bragg peaks in the SAXS data. The cryo-TEM experiments were conducted by Associate Professor Eric Hanssen at the Bio21 Molecular Science and Biotechnology Institute (Melbourne). This technique requires the sample to be vitrified to preserve their structure in their native environment. Briefly, dispersed samples are loaded on a carbon grid supported by a copper grid. The sample is then blotted dried to obtain a thin liquid film, which is then immediately quenched in liquid ethane at  $-180\text{ }^{\circ}\text{C}$  and transferred to liquid nitrogen at  $-196\text{ }^{\circ}\text{C}$  to ensure immediate vitrification. The grid is then viewed by electron microscopy at low doses to prevent sample damage. The detailed method can be found in Chapter Five, section 5.6.

#### 2.2.3. Drug release experiment

Current methods that have been used to measure drug release from lipid-based systems includes the use of dialysis and pressure ultrafiltration. Both methods utilise a membrane with a specific molecular weight cut-off (MWCO) to separate the smaller free drug molecules from the lipid carriers that are generally 100 nm in size. A recent release study using dialysis found that *ex vivo* transport experiments showed slower ranibizumab transport kinetics in comparison with *in vitro* results.<sup>13</sup> It is expected that greater difference will be seen *in vivo* as the release obtained using equilibrium dialysis is often dictated by diffusion through the artificial membrane. Samples are removed

from the receptor compartment at appropriate time intervals, generally in hours or days, making it difficult to resolve the actual release of drug from the delivery system. As a consequence, pressure ultrafiltration that utilises a constant stream of inert gas to apply pressure at a constant flow rate of around 1 mL/min, provides benefits over the commonly used dialysis methods.<sup>14</sup> However, the temporal resolution of the pressure ultrafiltration method is limited by the time, which is in the order of minutes, taken to remove a sample of sufficient volume for analysis. Generally, to ensure that the concentration of drug in the ultrafiltrate sample is representative of that in the free solution, the initial volumes are discarded which will be the void volume of the apparatus. Although both techniques have been used previously, it was deemed unsuitable for the release studies of aflibercept.

The main problems encountered using the above method was co-elution of the liposomes and aflibercept. Aflibercept is a dimeric glycoprotein with a protein molecular weight of 96.9 kD ( $C_{4318}H_{6788}N_{1164}O_{1304}S_{32}$ , 2 x 431 amino acids). It contains approximately 15% glycosylation to give a total molecular weight of 115 kD. A MWCO of over 100 kD not only allowed the drug to cross through the membrane, but also the liposomes, which are polydispersed soft materials. Therefore, an alternative purification method was designed in order to conduct a release experiment that can selectively separate and quantify free aflibercept.

Affinity chromatography is a common technique used to purify anti-bodies. The method designed to separate the free aflibercept utilises Protein A Spin Trap (GE Healthcare Australia Pty. Ltd., Australia). Each spin unit consists of a small scale pre-packed column with Protein A Sepharose™ High Performance resin designed for rapid purification of IgG antibodies due to the high affinity for the Fc portion. Free aflibercept with exposed Fc portion binds to Protein A, allowing the aflibercept-encapsulated carriers to be separated and collected for further activation studies. The general method is summarised in Figure 2.1. Briefly, the process involves incubating the liposomal dispersion to allow binding of the free aflibercept to Protein A in PBS pH 7.4. After collecting the encapsulated liposomes, the free aflibercept can then be eluted using 400 µL of the acidic debinding buffer. To preserve the integrity of the protein, the eluate is collected into 100 µL of neutralising buffer. The neutralised eluate is then quantified

using UV-Vis spectrometry at 280 nm, which measures the aromatic amino acids (mainly tyrosine and tryptophan) in the protein.

Although Enzyme-Linked Immunosorbent Assay (ELISA) is commonly used to determine the efficacy of anti-VEGF drugs, it was not used in this experiment. ELISA is a convenient and precise method with commercial products such as the Invitrogen Human VEGF ELISA kit (Life Technologies, USA) that is readily available with a sensitivity of <5 pg/mL. However, each assay will typically take 4 h to perform and the presence of anti-VEGF drugs may interfere with the measurements.<sup>15</sup> Therefore, UV-Vis spectrometer was used in this instance as the absorbance data can be obtain within minutes. The full experimental method can be found in Chapter Five, section 5.4.3.

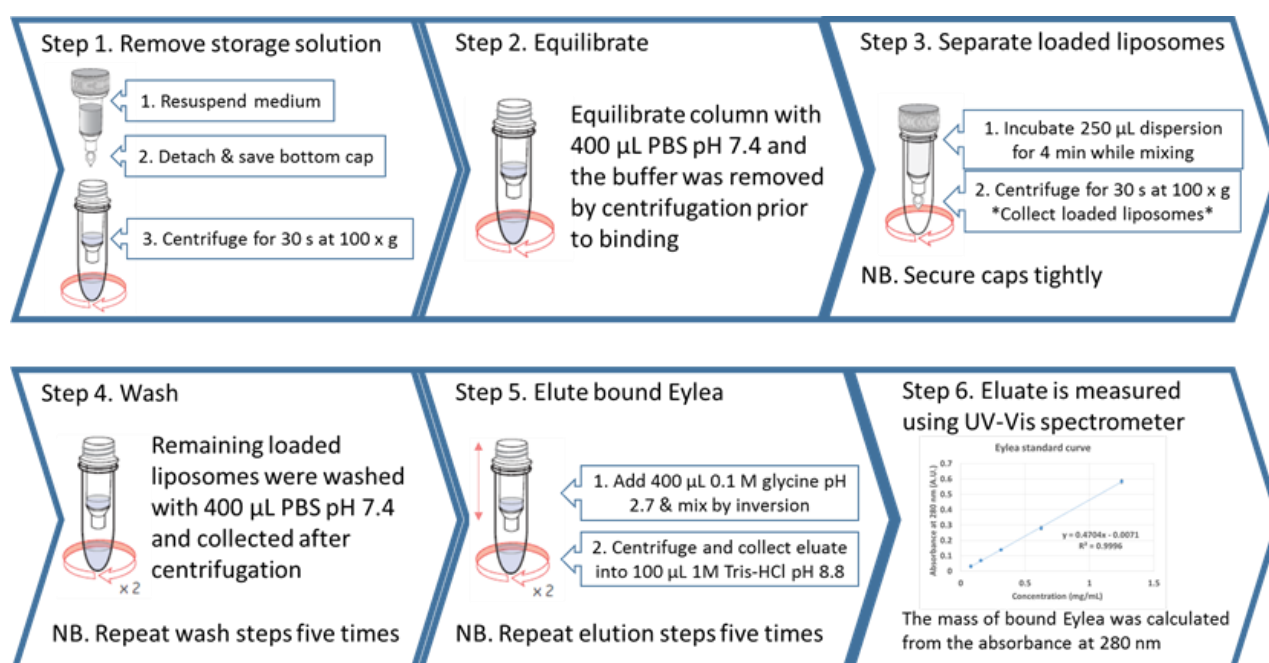


Figure 2.1 Schematic of drug release experiment for aflibercept (Eylea®).

Table 2 The concentration and pH of the buffers used in the release studies.

<b>Binding Buffer</b>	Phosphate buffered saline (PBS), pH 7.4 (See 2.1.3)
<b>Debinding Buffer</b>	0.1 M glycine-HCl, pH 2.7
<b>Neutralising Buffer</b>	1 M Tris-HCl, pH 9.0

## 2.3. References

1. Dong, Y.-D.; Dong, A. W.; Larson, I.; Rappolt, M.; Amenitsch, H.; Hanley, T.; Boyd, B. J., Impurities in commercial phytantriol significantly alter its lyotropic liquid-crystalline phase behavior. *Langmuir* **2008**, *24*, 6998-7003.
2. Fong, W.-K.; Hanley, T.; Boyd, B. J., Stimuli responsive liquid crystals provide 'on-demand' drug delivery in vitro and in vivo. *J. Control. Release* **2009**, *135*, 218-26.
3. Tate, M. W.; Eikenberry, E. F.; Turner, D. C.; Shyamsunder, E.; Gruner, S. M., Nonbilayer phases of membrane lipids. *Chem. Phys. Lipids* **1991**, *57* (2), 147-164.
4. Wang, X.; Quinn, P. J., Cubic phase is induced by cholesterol in the dispersion of 1-palmitoyl-2-oleoyl-phosphatidylethanolamine. *Biochim. Biophys. Acta* **2002**, *1564*, 66-72.
5. Fong, W.-K.; Hanley, T. L.; Thierry, B.; Kirby, N.; Boyd, B. J., Plasmonic nanorods provide reversible control over nanostructure of self-assembled drug delivery materials. *Langmuir* **2010**, *26*, 6136-6139.
6. Schmidt-Erfurth, U.; Hasan, T., Mechanisms of action of photodynamic therapy with verteporfin for the treatment of age-related macular degeneration. *Surv. Ophthalmol.* **2000**, *45* (3), 195-214.
7. Sung, A. Y.; Kim, T.-H., Preparation and characterization of ophthalmic polymers containing silicon nanoparticles. *Korean J. Chem. Eng.* **2012**, *29* (9), 1272-1278.
8. Kirby, N. M.; Mudie, S. T.; Hawley, A. M.; Cookson, D. J.; Mertens, H. D. T.; Cowieson, N.; Samardzic-Boban, V., A low-background-intensity focusing small-angle X-ray scattering undulator beamline. *J. Appl. Crystallogr.* **2013**, *46*, 1670-1680.
9. Hyde, S. T., *Identification of Lyotropic Liquid Crystalline Mesophases*. John Wiley & Sons, Ltd: 2001; p 299-332.
10. Boyd, B. J.; Dong, Y.-D.; Rades, T., Nonlamellar liquid crystalline nanostructured particles: Advances in materials and structure determination. *J. Liposome Res.* **2009**, *19*, 12-28.
11. Mudie, S. T. *ScatterBrain*, V2.30; Australian Synchrotron: Australia.
12. Fong, W.-K.; Hanley, T. L.; Thierry, B.; Kirby, N.; Waddington, L. J.; Boyd, B. J., Controlling the nanostructure of gold nanorod-lyotropic liquid-crystalline hybrid materials using near-infrared laser irradiation. *Langmuir* **2012**, *28*, 14450-14460.
13. Joseph, R. R.; Tan, D. W. N.; Ramon, M. R. M.; Natarajan, J. V.; Agrawal, R.; Wong, T. T.; Venkatraman, S. S., Characterization of liposomal carriers for the trans-scleral transport of Ranibizumab. *Sci. Rep.* **2017**, *7* (1), 16803.
14. Boyd, B. J., Characterisation of drug release from cubosomes using the pressure ultrafiltration method. *Int. J. Pharm.* **2003**, *260* (2), 239-247.
15. Takahashi, H.; Nomura, Y.; Nishida, J.; Fujino, Y.; Yanagi, Y.; Kawashima, H., Vascular endothelial growth factor (VEGF) concentration is underestimated by enzyme-linked immunosorbent assay in the presence of anti-VEGF drugs. *Invest. Ophthalmol. Vis. Sci.* **2016**, *57* (2), 462-466.

CHAPTER THREE:  
LIGHT-RESPONSIVE  
PHOSPHOLIPID-BASED SYSTEM

## Prologue to Chapter Three

---

Phospholipids can be rendered photo-responsive with gold nanorods, allowing external activation of drug release that can be used in various applications such as ocular delivery. This chapter introduces the potential of a phospholipid-based system that was recently reported to exhibit the desirable phase behaviour for stimuli-responsive drug release and the work presented has been published as: Du, J. D.; Fong, W.-K.; Salentinig, S.; Caliph, S. M.; Hawley, A.; Boyd, B. J., Phospholipid-Based Self-Assembled Mesophase Systems for Light-Activated Drug Delivery. *Physical Chemistry Chemical Physics* 2015, 17, 14021-14027.

## Declaration for Chapter Three

For Chapter Three, the nature and extent of contribution to the work was as follows:

<b>Name</b>	<b>Nature of contribution</b>	<b>Extent of contribution</b>
Joanne D. Du	Research design, performance of data collection and analysis, and preparation of manuscript	75 %
Wye-Khay Fong	Co-supervisor, provided input into the preparation of manuscript	5 %
Stefan Salentinig	Provided input into the preparation of manuscript	5 %
Suzanne Caliph	Co-supervisor, provided input into the preparation of manuscript	5 %
Adrian Hawley	Provided input into the preparation of manuscript	5 %
Ben J. Boyd	Main supervisor, provided input into the preparation of manuscript	5 %

The undersigned hereby declare that the above declaration correctly reflects the nature and extent of candidate and co-author contributions:

Candidate's signature:



Date: 30/3/2018

Main supervisor's signature:



Date: 30/3/2018

### 3. Phospholipid-Based Self-Assembled Mesophase Systems for Light-Activated Drug Delivery

Joanne D. Du<sup>1</sup>, Wye-Khay Fong<sup>1,2</sup>, Stefan Salentinig<sup>1</sup>, Suzanne Caliph<sup>1</sup>, Adrian Hawley<sup>3</sup> and Ben J. Boyd<sup>1,4</sup>

<sup>1</sup>Drug Delivery, Disposition and Dynamics, Monash Institute of Pharmaceutical Sciences, Monash University (Parkville Campus), 381 Royal Parade, Parkville, VIC, 3052, Australia

<sup>2</sup>Food and Soft Materials Science, Institute of Food, Nutrition & Health, ETH Zurich, Schmelzbergstrasse 9, 8092 Zürich, Switzerland

<sup>3</sup>SAXS/WAXS beamline, Australian Synchrotron, 800 Blackburn Rd, Clayton, VIC 3168, Australia

<sup>4</sup>ARC Centre of Excellence in Convergent Bio-Nano Science and Technology, Monash Institute of Pharmaceutical Sciences, Monash University (Parkville Campus), 381 Royal Parade, Parkville, VIC 3052, Australia

First Published: 01 May 2015

Citation: *Phys. Chem. Chem. Phys.* 2015, 17, 14021-14027.

DOI: 10.1039/C5CP01229E

#### 3.1. Abstract

The manipulation of the structure of phospholipid-based mesophases to induce a slow to fast drug release profile has potential for use in therapeutic situations where continuous absorption of drug is not desirable and, to reduce the frequency of injection for short acting or rapidly cleared drugs in treatments for diseases such as macular degeneration. This study had two aims; firstly to confirm the phase behaviour of 20 mol% cholesterol in 1-palmitoyl-2-oleoyl-sn-glycero-3-phosphoethanolamine (POPE), which was previously reported to transition from lamellar (slow release) to bicontinuous cubic (fast release) phase with increasing temperature. Contrary to literature, no

bicontinuous cubic phase was observed but a transition to the inverse hexagonal phase occurred at all POPE:cholesterol ratios investigated. The second aim was to render these mesophases responsive to near-infrared laser (NIR) irradiation by incorporation of gold nanorods (GNR) incorporated into the POPE system to induce photothermal heating. The inclusion of 3 nM GNR in POPE systems induced reversible disruption of lipid packing equivalent to increasing the temperature to 55 °C when irradiated for 30 s. This study confirmed that although the previously published phase behaviour was not correct, GNR and NIR can be used to manipulate the self-assembled mesophases in phospholipid-based systems and highlights the potential for a phospholipid-based light-activated drug delivery system.

### 3.2. Introduction

Many amphiphilic lipids such as phospholipids and monoglycerides spontaneously self-assemble to form ordered thermodynamically stable liquid crystalline (LC) mesophases in excess water. Lipid-based LC systems have been gaining interest in the field of drug delivery, the most common being the lamellar ( $L_{\alpha}$ ) phase which forms nanoparticles, termed liposomes, when dispersed. Liposomes composed from phospholipids are suitable drug delivery vehicles as they are biocompatible, possess low toxicity and can encapsulate both hydrophilic and lipophilic drugs.<sup>1</sup> However, their rapid clearance from circulation by mononuclear phagocyte system (MPS) limits their utility *in vivo*. Polyethylene glycol (PEG) grafted lipids are often used to provide a non-fouling coating to the nanoparticle to inhibit protein binding and reduce non-specific removal from the circulatory system by decreasing uptake by MPS.<sup>2</sup> The consequent long circulation behaviour can assist particle uptake through the leaky vasculature in tumours, termed the enhanced permeation and retention (EPR) effect. The nanoparticles can readily permeate and be retained within the tumour site due to the poorly formed leaky vasculature with gaps up to several hundreds of nanometres in size and compromised or absent lymphatic drainage.<sup>3</sup> There is increasing evidence that the EPR effect may be relevant not only in tumour tissues but also in inflammation.<sup>3, 4</sup> Hence, having a stimuli-responsive element included in stealth particles to activate release at a specific location may provide improved selectivity and reduce toxicity. In order for this LC system to be

more responsive, it is critical to actively control the rate of drug release, which may be achieved through the manipulation of self-assembled nanostructures.

Previous studies have shown that the nanostructure of the mesophase in self-assembled lipid systems is important in determining the drug release rate due to the state of the aqueous channels being either open or closed.<sup>5</sup> The inverse hexagonal ( $H_2$ ) phase displays a slower release than the bicontinuous cubic ( $V_2$ ) phase due to the smaller water channels and closed rod-like micellar structure.<sup>5, 6</sup> Likewise, the closed nature of the  $L_\alpha$  phase when it is dispersed as liposomes, enables the encapsulation of drug, and is expected to provide slow or no drug release in comparison to the  $V_2$  phases. Thus, it is hypothesised that through the manipulation of the self-assembled nanostructure from  $L_\alpha$  to  $V_2$  phase, drug release can be triggered to switch “on” and “off”, and may have potential in providing external control over drug delivery. Consequently, systems that can be triggered to exhibit this phase behaviour may be particularly useful for on-demand drug delivery.

Temperature has been used as a stimulus to induce transitions between LC structures and has provided an avenue to manipulate drug release.<sup>7</sup> However, there is a major limitation to using temperature directly as the stimulus, as there is no specificity in the heat source which leads to a high potential for accidental activation of drug release. Previous studies have shown that incorporation of gold nanorods (GNR) into the lipid matrix can provide remote heating through the photothermal effect and trigger the phase transitions upon near-infrared (NIR) irradiation.<sup>8</sup> NIR radiation has been reported to penetrate tissues up to 50 mm deep,<sup>9</sup> suggesting a light-sensitive LC system has potential for various applications such as ophthalmic, subcutaneous and deeper tissue applications. Hence the broad aim of this study was to develop LC systems which will undergo the lamellar to cubic phase transition when stimulated with a NIR laser (Figure 3.1).

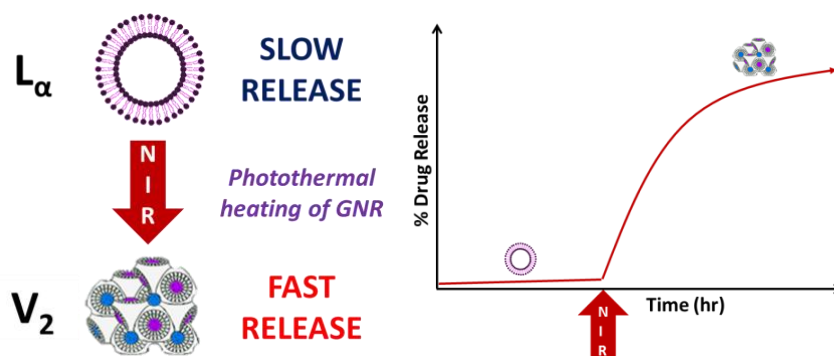


Figure 3.1 Schematic of desired liquid crystalline system with a phase transition from lamellar phase ( $L_\alpha$ ) to bicontinuous cubic phase ( $V_2$ ) and its corresponding drug release profile controlled using NIR laser and GNR.

In previous studies, GNR were embedded in phytantriol cubic phase and irradiated with NIR however, the reversible transition from  $V_2$  to  $H_2$  obtained provides a fast to slow drug release profile, which is not useful for stimulated drug delivery purposes.<sup>8</sup> Therefore, it is necessary to explore other lipid systems. It was reported that the 1-palmitoyl-2-oleoyl-sn-glycero-3-phosphoethanolamine (POPE) + cholesterol system in water transitions from  $L_\alpha$  to either  $H_2$  or  $V_2$  phase with increasing temperature depending on cholesterol content (Figure 3.2).<sup>10</sup> Specifically, as reported in the literature phase diagram in Figure 3.2, a system containing POPE with 20 mol% of cholesterol was expected to exhibit a  $L_\alpha$  to the diamond  $V_2$  phase (Pn3m with the ratio of reciprocal d-spacing of  $\sqrt{2} : \sqrt{3} : \sqrt{4} : \sqrt{6} : \sqrt{8} : \sqrt{9} : \sqrt{10}$ ) at approximately 60 °C (represented by the arrow in Figure 3.2), which should exhibit the desired drug release profile, and PEGylation of the lamellar particles should provide favourable circulation behaviour. Hence in this study, the phase behaviour of these lipid systems was evaluated using small angle X-ray scattering (SAXS) at equilibrium and dynamically using time-resolved synchrotron SAXS observed the effect of photothermal heating via NIR activation of encapsulated GNR. The equilibrium phase diagram for the POPE + cholesterol in water systems was first investigated to determine the robustness of the baseline phase behaviour with different source of POPE and cholesterol. The effect of subsequent addition of PEG-phospholipid to the lipid mixture on the phase behaviour was then evaluated and finally, the responsiveness of the system on incorporation of GNR to NIR irradiation was then demonstrated.

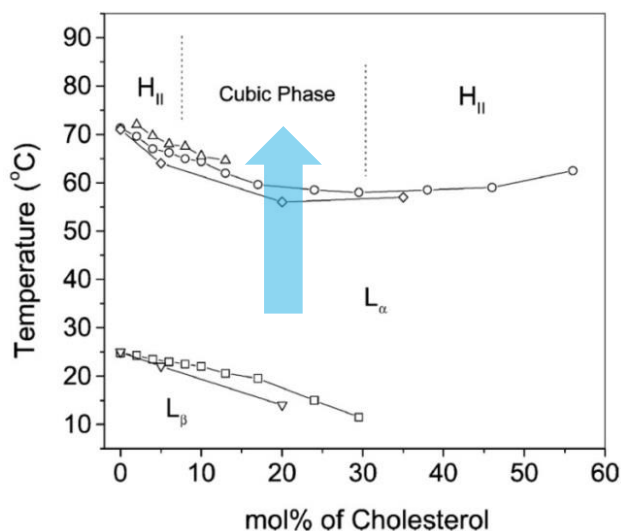


Figure 3.2 Literature phase behaviour of the POPE + cholesterol system in excess water with increasing cholesterol (mol% cholesterol in POPE + cholesterol mixture). Reproduced with permission from Ref<sup>10</sup>.

### 3.3. Materials and Methods

#### 3.3.1. Materials

1-palmitoyl-2-oleoyl-sn-glycero-3-phosphoethanolamine (POPE) and 1,2-distearoyl-sn-glycero-3-phosphoethanolamine-N-[amino(polyethylene glycol)-2000] (PEG-DSPE) was purchased from Avanti Polar Lipids (Alabaster, USA). Cholesterol was purchased from Sigma-Aldrich (St. Louis, USA). Methyl conjugated Gold Nanorod<sup>TM</sup> with an aspect ratio of 4.2 (length, 42 nm; width, 10 nm) were purchased from Nanopartz (Loveland, CO). The measured surface plasmonic resonance (SPR) is 825 nm. Phytantriol (3,7,11,15-tetramethylhexadecane-1,2,3-triol) was a gift from DSM Nutritional Products (Kaiseraugst, Switzerland), with a minimum purity of 95%. All materials were used without further purification. Sodium chloride (Chem-Supply, Australia), disodium hydrogen orthophosphate and potassium dihydrogen orthophosphate (APS Ajax Finechem, Australia) and HCl (1M) (Merck, Australia) were of analytical reagent quality. Water used in these studies was obtained from a Millipore Milli-Q purification system (Billerica, USA). Phosphate buffered saline (PBS) was prepared by dissolving 8.0 g of sodium chloride, 0.19 g of potassium dihydrogen phosphate and 2.38 g of disodium hydrogen phosphate in sufficient water to produce 1000 mL and the pH adjusted to 7.4.

### 3.3.2. General procedure for LC preparation

Lipids were weighed in the appropriate mole ratios (0-40 mol% cholesterol in POPE  $\pm$ 10 mol% PEG-DSPE) dissolved in chloroform. The mixture was then dried under a stream of nitrogen gas for 3 hr, then under vacuum overnight at 40°C to ensure complete removal of solvent. The lipid mixture was then hydrated in a 20:1 (w/w) ratio (for dispersion) or a 1:1 (w/w) ratio (for bulk) with PBS and was allowed to equilibrate for >24 hr before investigation using SAXS. Gold nanorod solution was diluted with PBS to 0, 0.3 and 3 nM concentration and was added to the dried bulk lipid sample.

### 3.3.3. Phase characterisation of POPE and cholesterol systems

The LC structures were assessed using small angle X-ray scattering (SAXS) to qualitatively identify and confirm the internal nanostructure formed from various lipid compositions. SAXS measurements were performed at the SAXS/WAXS beam line at the Australian Synchrotron.<sup>11</sup> The synchrotron X-ray beam was tuned to a wavelength of 1.127 Å (11.0 keV) at a camera to detector distance of 1034.97 mm which gave the  $q$ -range  $0.0176 < q < 1.016 \text{ \AA}^{-1}$ , where  $q$  is the length of the scattering vector, defined by  $q = (4\pi/\lambda) \sin(\theta/2)$ , is the wavelength and  $\theta$  the scattering angle. A silver behenate standard (d-spacing = 58.38 Å) was used for the  $q$  range calibration. The 2D SAXS patterns were acquired within 1 s using a Pilatus 1M detector with active area 169 x 179 mm<sup>2</sup> and with a pixel size of 172  $\mu\text{m}$ . Equilibrated dispersion samples were transferred into 1.5 mm diameter glass capillaries, placed in the temperature controlled capillary holder and the SAXS profiles were determined with increasing temperature. Acquisition time for equilibrated samples was 1 s. Bulk samples were used in dynamic activation experiments which allow detection of phase changes when stimulated using NIR in real time. A Class IIIB fibre coupled laser system (MDL-808) with the power output at 400 mW at a wavelength  $\lambda = 808 \text{ nm}$  (Changchun New Industries, China) was mounted 20 cm from the sample at a tangential angle to the X-ray beam and samples were illuminated remotely by a computer control system. Scattering patterns were acquired for 1 s, every 10 s for 2 min. The two dimensional scattering patterns were integrated into the one-dimensional scattering function  $I(q)$  using the in-house developed software package scatterBrain. Scattering curves are plotted as a function of relative intensity,  $I$ , versus  $q$  and phase structures were identified by indexing the Bragg peaks to known relative

spacing ratios.<sup>12</sup> The apparent temperature ( $T_{app}$ ) of the matrix during irradiation in the presence or absence of GNR was determined using a 'calibration' plot of the lattice parameter vs. temperature of the matrix from the equilibrium SAXS results.<sup>8</sup>

### 3.4. Results and Discussion

#### 3.4.1. Phase behaviour of POPE and cholesterol dispersions

The phase diagram for the POPE and cholesterol systems in excess aqueous solution was determined using SAXS (Figure 3.3). The lamellar ( $L_\alpha$ ) phase in excess water was found to transition to the inverse hexagonal ( $H_2$ ) phase in excess water with increasing temperature and the phase transition temperature reduced with increasing cholesterol concentration. From the literature (Figure 3.2), POPE with cholesterol in the concentration range between 10-30 mol% was reported to transition from  $L_\alpha$  to  $V_2$  at approximately 60 °C; in this study, the  $V_2$  phase was not observed.<sup>10</sup> On reflection, there are apparent inconsistencies between the SAXS profiles presented by Wang *et al.* reproduced in Figure 3.4A. The figure shows coexisting phases from around 50 °C up to the highest temperature, which is not reflected in the derived phase diagram, dominated by the single  $L_\alpha$  phase (Figure 3.2).

Additionally, an unusual peak in Figure 3.4A can be noticed at high temperature and was indexed as a peak that corresponds to the  $V_2$  phase. However, this peak was not observed in recent data (Figure 3.4B) suggesting that the unusual peak may be an artefact of impurities in the sample or a detector/integration anomaly, resulting in inaccurate phase identification. The pure POPE sample was found to transition to the  $H_2$  phase above 70 °C, as previously reported.<sup>13</sup> The addition of 20 mol% of cholesterol provided a similar effect to that on addition of 2.5 mol% of vitamin E, such that the  $H_2$  peak first appeared at 44 °C.<sup>13</sup> This implies that cholesterol, like vitamin E, is able to reduce the transition temperature to close to physiological temperature.<sup>13, 14</sup> This is unfavourable in this drug delivery system as an unintentional phase transition may occur *in vivo*. Therefore, subsequent dynamic studies were conducted with POPE alone without added cholesterol, where the phase transition occurs at higher temperature.

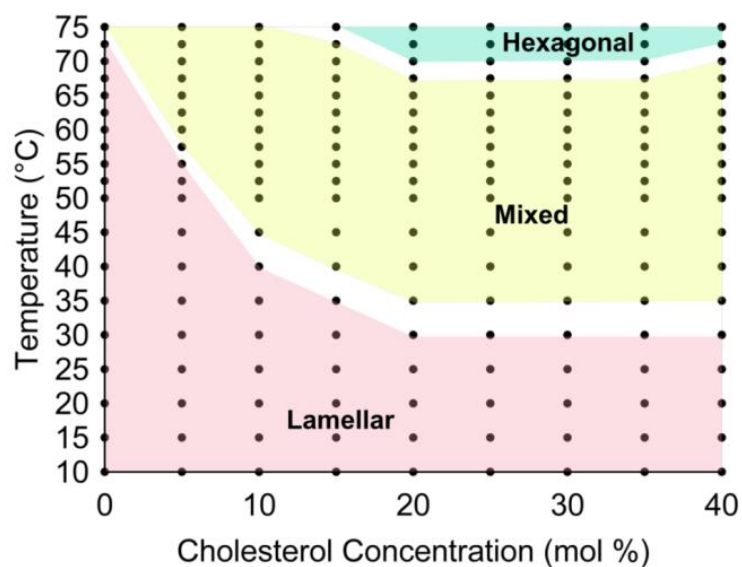


Figure 3.3 Phase behaviour of the POPE + cholesterol system in excess water with increasing cholesterol (mol% cholesterol in POPE + cholesterol mixture) in this study.

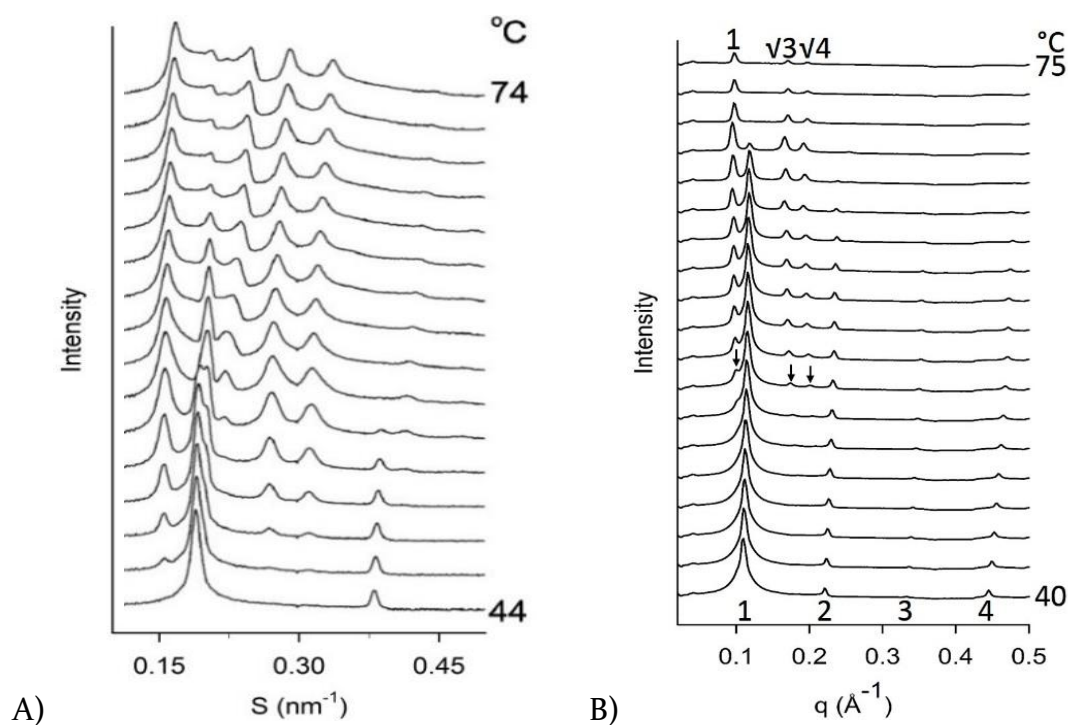


Figure 3.4 Small-angle X-ray scattering profiles for 20 mol% cholesterol in POPE from A) literature (reproduced with permission from Ref<sup>10</sup>) and B) this study. The annotations of peaks in Figure 3.4B indicate the lamellar phase at low temperatures (peaks at spacing 1, 2, 3, 4), and the inverse hexagonal phase at high temperature (1,  $\sqrt{3}$ ,  $\sqrt{4}$ ).

### 3.4.2. Effect of PEG-lipid in POPE dispersions

As mentioned, polyethylene glycol (PEG) grafted lipids can be incorporated into liposomes to assist in targeted drug delivery and longer circulation of rapidly cleared drugs. Therefore, the effect of addition of PEG-DSPE at 10 mol% to the POPE system was also investigated. This level of PEG-lipid is commonly used to provide a ‘stealth’ coating for liposomes as it has been shown to decrease MPS uptake by 90%.<sup>1</sup> The addition of PEG-lipid was found to facilitate dispersion and stabilize the  $L_{\alpha}$  phase. POPE with 20 mol% of cholesterol formed the  $H_2$  structure at approximately 30°C, 40°C lower than pure POPE. With the addition of PEG-lipid, both POPE systems with and without cholesterol formed the  $L_{\alpha}$  phase. Unexpectedly, both systems did not exhibit the phase transition to  $H_2$  phase at high temperatures (Figure 3.5) despite the differences in phase transition temperature, suggesting that the  $L_{\alpha}$  phase was highly stabilized due to the addition of the PEG-lipid. It should also be noted that the  $L_{\alpha}$  peaks became more defined with increasing temperatures suggesting that multi-lamellar structures were likely to be present. The critical packing-parameter (CPP) concept can be used to understand how the  $L_{\alpha}$  phase was formed using Equation 1,

$$\text{Equation 1: } CPP = \frac{V_s}{a_0 l}$$

Where,  $V_s$  is the hydrophobic chain volume,  $a_0$  is the head group area and  $l$  is the hydrophobic chain length.<sup>15</sup> The geometry of the POPE formed lamellar structure ( $1/2 \leq CPP < 1$ ) due to the double hydrophobic tail, whereas the geometry of the PEG-lipid form more spherical micellar structures ( $CPP < 1/3$ ) since the  $a_0$  is large. At higher temperature, the steric repulsion of the large PEG-lipid head group decreases, increasing the CPP, causing more ordered lamellar structures to form.

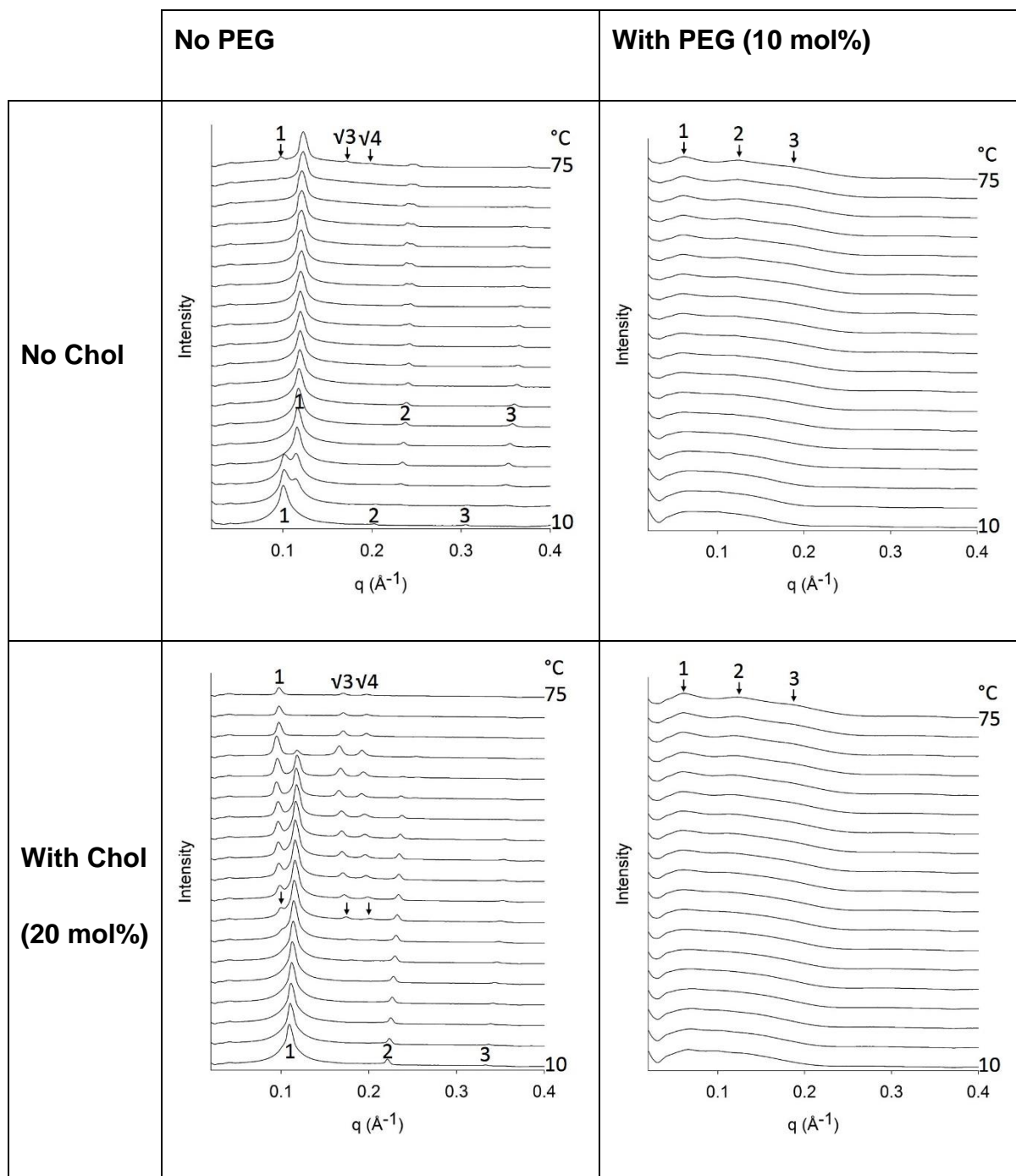


Figure 3.5 Comparison of SAXS scattering profiles from the POPE system with and without cholesterol (20 mol%) and PEG-DSPE (10 mol%) in excess water.

### 3.4.3. Effect of GNR on phase behaviour without irradiation in bulk liquid crystalline systems

The effect of GNR incorporation on the equilibrium phase behaviour of the bulk LC systems was evaluated in order to be able to quantify the effect of laser-activated photothermal heating.<sup>8</sup> The phytantriol LC system was used to compare the effect of incorporating the hydrophilic GNR with previous studies using hydrophobic GNR. Consistent with previous literature,<sup>8</sup> the presence of GNR did not substantially change the lattice parameter, phase structure or transition temperature for the phytantriol system despite the difference in hydrophobicity (SI 1 and 2). Likewise, the addition of GNR to the POPE system did not significantly influence the phase behaviour of the matrices as illustrated in Figure 3.6A, as all three matrices transitioned from  $L_{\alpha}$  to  $H_2$  phase upon an increase in temperature. The incorporation of GNR did however have a subtle effect on the phase transition temperature causing the formation of a region of coexisting  $L_{\alpha}$  and  $H_2$  phases in excess water to occur at lower temperature (approximately 5 °C lower) and broadening of the temperature range for the mixed phase region. The lattice parameters vs. temperature calibration plots for determining the apparent temperature on laser irradiation are shown in Figure 3.6B. A noticeable difference was observed in the lattice parameter for the  $H_2$  phase of the POPE systems at high temperature, but not for the  $L_{\alpha}$  phase (Figure 3.6). This suggests that the changes in lattice parameter for the  $H_2$  phase are affected by the addition of GNR, although the exact relationship with change in GNR concentration is not yet clear. The calibration curves can thus be applied to any GNR concentration up to 3 nM to estimate the apparent temperature of the matrices during irradiation in the  $L_{\alpha}$  phase region, or at the specific concentrations measured in the  $H_2$  region.

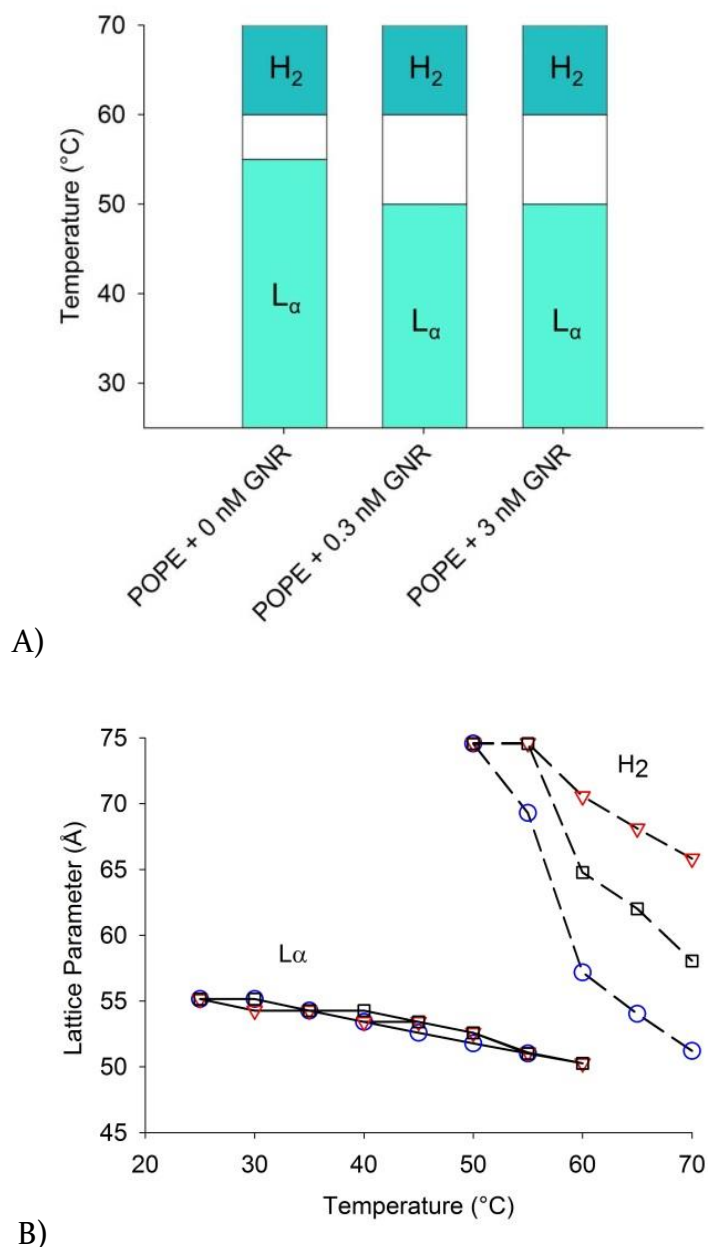


Figure 3.6 Effect of GNR on equilibrium structure of POPE bulk system in excess water A) Temperature dependent phase diagram and B) the lattice parameter of the lipid systems in the presence of 0 nM ( $\circ$ ), 0.3 nM ( $\nabla$ ) and 3 nM ( $\square$ ) GNR is plotted against temperature. Corresponding phases are indicated as follow: dashed line for  $H_2$  phase and a solid line for  $L_\alpha$  phase.

### 3.4.4. Effect of NIR irradiation

The effect of irradiation of the matrices containing GNR on the nanostructure of the LC systems was finally evaluated using time-resolved SAXS. Figure 3.7 illustrates that incorporation of GNR imparted photo-sensitivity to the lipid systems.

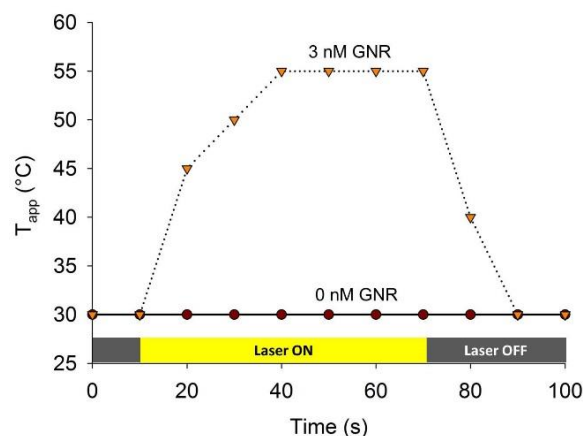


Figure 3.7 Effect of NIR laser irradiation on apparent temperature ( $T_{app}$ ) of the POPE system in excess water containing 0 nM (●) and 3 nM (▼) GNR.

In the absence of GNR, the  $L_{\alpha}$  phase was observed for the POPE systems in excess water on irradiation, precluding non-specific heating by the laser, which is consistent with previous studies.<sup>8</sup> Inclusion of a low concentration of GNR (0.3 nM) in POPE did not induce a change in phase structure on irradiation (see SI) therefore a higher concentration (3 nM) was used in further experimentation. For the POPE system in excess water, a photothermal heating effect was observed, and 30 s of irradiation induced disruption of lipid packing equivalent to increasing the apparent temperature to 55 °C. The duration of irradiation required to achieve this level of disruption was much greater than previous reports for the phytantriol system.<sup>8</sup> This may be due to the use of different GNR functionality and/or difference in heat capacity of the material.<sup>16</sup> It has been reported that the GNR can be tuned by varying the size and aspect ratio of the gold nanoparticles to absorb at a specific wavelength,<sup>17</sup> which will allow optimization of the photothermal effect and prevent accidental activation. In this study, the SPR peak of the GNR was measured to be 825 nm (SI 3), meaning that the photothermal heating is expected to be less effective when irradiated using the 808 nm NIR diode laser.

The study was further extended to investigate the reversibility of POPE, PEG-lipid and GNR system in excess water. Figure 3.8 clearly shows that the nanostructure of the mesophase pre-irradiation is of  $L_{\alpha}$  phase at 30 °C. Upon irradiation, the system retained its  $L_{\alpha}$  structure until 20 s of exposure. The peaks are broad in the dynamic study due to the lack of time for the structures to fully equilibrate. It is also evident that the peaks corresponding to the  $H_2$  phase are forming at 20 sec. By utilising the lattice parameters calculated from the equilibrium phase behaviour, the  $T_{app}$  of the matrix at different irradiation times were calculated. The presence of  $H_2$  peaks corresponds to a  $T_{app}$  of 70 °C. Therefore, 20 s of irradiation was shown to induce an increase of about 40°C in the PEGylated POPE and GNR system. Upon cessation of irradiation, the system returned only partially to the initial  $L_{\alpha}$  phase however, complete reversibility of the system was not observed suggesting further equilibration time may be necessary due to a supercooling effect as reported previously.<sup>18</sup> PEGylation was incorporated as it may increase the residence time of the phospholipid-based carriers when delivered to the site of inflammation, such as the macula for age-related macular degeneration. However, PEGylation negates the phase transition upon heating and may not be necessary when delivering intravitreally.

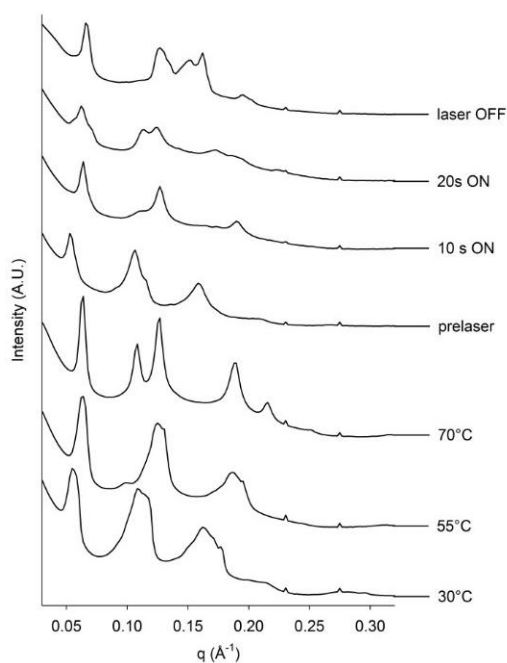


Figure 3.8 SAXS scattering data for POPE and PEG-lipid system in excess water with 3 nM GNR at equilibrium temperatures (30, 55 and 70 °C) and after NIR irradiation.

### 3.5. Conclusion

This study presents the phase behaviour of the cholesterol / POPE system in excess water. Contrary to previous reports, the H<sub>2</sub> phase was observed rather than the reported L<sub>α</sub> to V<sub>2</sub> phase transition between 10-30 mol% cholesterol. The addition of cholesterol (20 mol%) was shown to reduce the transition temperature by 40°C when comparing to the pure POPE + water system. The addition of PEG-lipids to the POPE system in excess water facilitated dispersion and stabilized the L<sub>α</sub> phase. Addition of a low concentration of GNR to the phospholipid systems imparted photo-sensitivity without compromising the integrity of the mesophases. The phase transition resulting from the photothermal heating was reversible for the non-PEGylated POPE + water system. These findings suggest the potential of this biocompatible composition as a photo-responsive system suitable for drug delivery.

### 3.6. Acknowledgements

The authors thank the Australian Research Council for funding under the Future Fellowships Scheme for BJB and the Discovery Projects Scheme for SS. This research was conducted in part on the SAXS/WAXS beamline at the Australian Synchrotron.

## 3.7. References

1. Immordino, M. L.; Dosio, F.; Cattel, L., Stealth liposomes: review of the basic science, rationale, and clinical applications, existing and potential. *Int. J. Nanomedicine* 2006, 1 (3), 297-315.
2. Yamauchi, H.; Yano, T.; Kato, T.; Tanaka, I.; Nakabayashi, S.; Higashi, K.; Miyoshi, S.; Yamada, H., Effects of sialic acid derivative on long circulation time and tumor concentration of liposomes. *Int. J. Pharm.* 1995, 113 (2), 141-148.
3. Maeda, H.; Nakamura, H.; Fang, J., The EPR effect for macromolecular drug delivery to solid tumors: Improvement of tumor uptake, lowering of systemic toxicity, and distinct tumor imaging in vivo. *Adv. Drug Deliv. Rev.* 2013, 65 (1), 71-79.
4. Kimura, H.; Yasukawa, T.; Tabata, Y.; Ogura, Y., Drug targeting to choroidal neovascularization. *Adv. Drug Deliv. Rev.* 2001, 52 (1), 79-91.
5. Phan, S.; Fong, W.-K.; Kirby, N.; Hanley, T.; Boyd, B. J., Evaluating the link between self-assembled mesophase structure and drug release. *Int. J. Pharm.* 2011, 421, 176-182.
6. Dong, Y.-D.; Dong, A. W.; Larson, I.; Rappolt, M.; Amenitsch, H.; Hanley, T.; Boyd, B. J., Impurities in commercial phytantriol significantly alter its lyotropic liquid-crystalline phase behavior. *Langmuir* 2008, 24, 6998-7003.
7. Fong, W.-K.; Hanley, T.; Boyd, B. J., Stimuli responsive liquid crystals provide 'on-demand' drug delivery in vitro and in vivo. *J. Control. Release* 2009, 135, 218-26.
8. Fong, W.-K.; Hanley, T. L.; Thierry, B.; Kirby, N.; Boyd, B. J., Plasmonic nanorods provide reversible control over nanostructure of self-assembled drug delivery materials. *Langmuir* 2010, 26, 6136-6139.
9. Barun, V. V.; Ivanov, A. P.; Volotovskaya, A. V.; Ulashchik, V. S., Absorption spectra and light penetration depth of normal and pathologically altered human skin. *J. Appl. Spectrosc.* 2007, 74 (3), 430-439.
10. Wang, X.; Quinn, P. J., Cubic phase is induced by cholesterol in the dispersion of 1-palmitoyl-2-oleoyl-phosphatidylethanolamine. *Biochim. Biophys. Acta* 2002, 1564, 66-72.
11. Kirby, N. M.; Mudie, S. T.; Hawley, A. M.; Cookson, D. J.; Mertens, H. D. T.; Cowieson, N.; Samardzic-Boban, V., A low-background-intensity focusing small-angle X-ray scattering undulator beamline. *J. Appl. Crystallogr.* 2013, 46, 1670-1680.
12. Hyde, S. T., Identification of Lyotropic Liquid Crystalline Mesophases. John Wiley & Sons, Ltd: 2001; p 299-332.
13. Wang, X.; Quinn, P. J., The structure and phase behaviour of alpha-tocopherol-rich domains in 1-palmitoyl-2-oleoyl-phosphatidylethanolamine. *Biochimie* 2006, 88 (12), 1883-8.
14. Dong, Y.-D.; Larson, I.; Hanley, T.; Boyd, B. J., Bulk and dispersed aqueous phase behavior of phytantriol: effect of vitamin E acetate and F127 polymer on liquid crystal nanostructure. *Langmuir* 2006, 22, 9512-8.
15. Israelachvili, J. N.; Mitchell, D. J.; Ninham, B. W., Theory of Self-Assembly of Hydrocarbon Amphiphiles into Micelles and Bilayers. *J. Chem. Soc. Faraday Trans.* 1976, 72, 1525-1568.
16. Fong, W.-K.; Hanley, T. L.; Thierry, B.; Tilley, A.; Kirby, N.; Waddington, L. J.; Boyd, B. J., Understanding the photothermal heating effect in non-lamellar liquid

crystalline systems, and the design of new mixed lipid systems for photothermal on-demand drug delivery. *Phys. Chem. Chem. Phys.* 2014, 16 (45), 24936-24953.

17. Alkilany, A. M.; Thompson, L. B.; Boulos, S. P.; Sisco, P. N.; Murphy, C. J., Gold nanorods: Their potential for photothermal therapeutics and drug delivery, tempered by the complexity of their biological interactions. *Adv. Drug Deliv. Rev.* 2012, 64 (2), 190-199.

18. Dong, Y.-D.; Tilley, A. J.; Larson, I.; Lawrence, M. J.; Amenitsch, H.; Rappolt, M.; Hanley, T.; Boyd, B. J., Nonequilibrium effects in self-assembled mesophase materials: unexpected supercooling effects for cubosomes and hexosomes. *Langmuir* 2010, 26, 9000-9010.

## 3.8. Supplementary Information

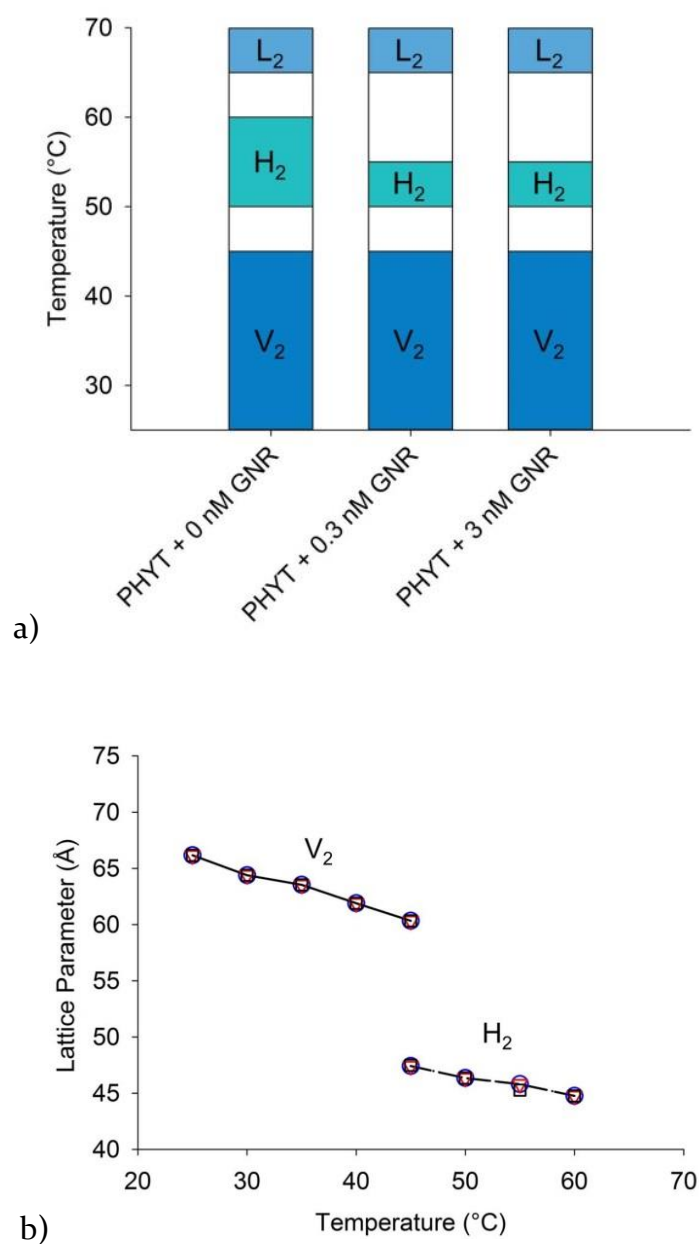


Figure SI 3.1 Effect of GNR on equilibrium structure of PHYT bulk system. a) Temperature dependent phase diagram and b) the lattice parameter of the lipid systems in the presence of 0 nM ( $\circ$ ), 0.3 nM ( $\nabla$ ) and 3 nM ( $\square$ ) GNR is plotted against thermostat-controlled temperature. Corresponding phases are indicated as follow: dashed line for  $H_2$  phase and a solid line for  $V_2$  phase.

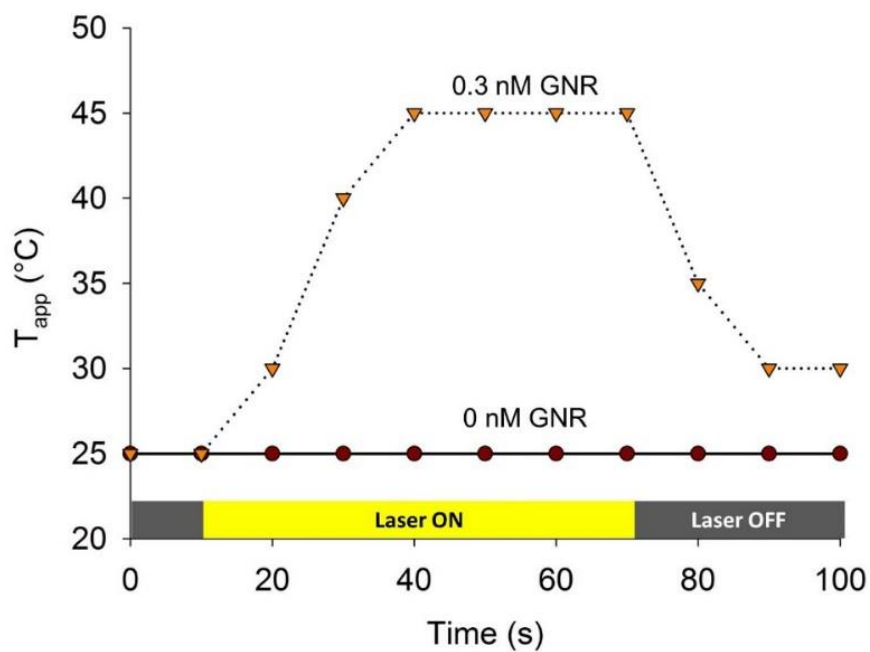


Figure SI 3.2 Effect of NIR laser irradiation on apparent temperature ( $T_{app}$ ) of the PHYT system containing 0 nM ( $\bullet$ ) and 0.3 nM ( $\blacktriangledown$ ) GNR.

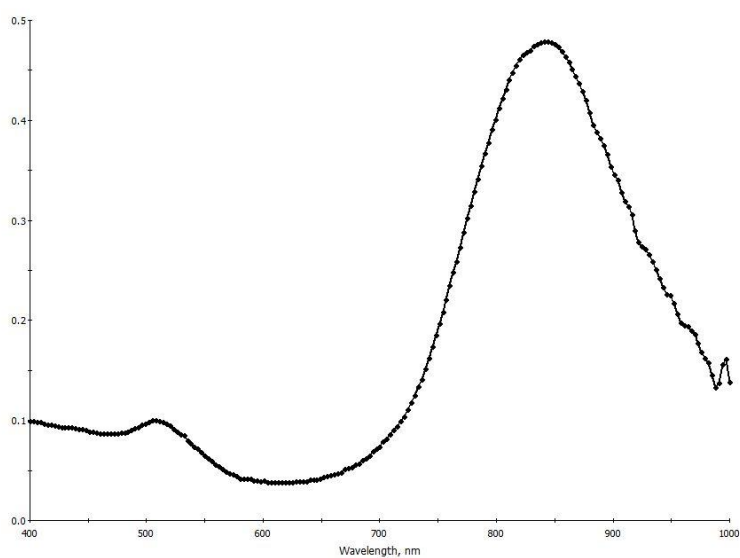


Figure SI 3.3 UV/Vis absorbance of GNR solutions with the maximum SPR peak of 825 nm

CHAPTER FOUR:  
COMPARISON OF DIFFERENT  
PHOTOTHERMAL ACTUATORS

## Prologue to Chapter Four

---

Near-infrared (NIR) light is the safest source for ophthalmic applications. There are many NIR-responsive agents investigated to control the release of drugs from lipid carriers because the localised photothermal heating would not affect the surrounding tissues of the eye. However, their photothermal effect is often limited due to their size. In this chapter, a molecular photosensitiser and the currently used nanosized NIR-responsive agents were incorporated into established lipid platforms, including the POPE+Chol system mentioned in Chapter Three, to compare the photothermal effect in hope to overcome the existing limitations. Although the phase behaviour of the lipid platforms investigated in this chapter is not ideal for on-demand drug delivery, the photo-activated phase transitions were found to be reversible suggesting the potential for the agents investigated to be useful photoactuators. This chapter contains a reproduction of the following publication: Du, J. D.; Hong, L.; Tan, A.; Boyd, B. J., Naphthalocyanine as a New Photothermal Actuator for Lipid-Based Drug Delivery Systems. *Journal of Physical Chemistry B* 2018, 122 (5), 1766-1770.

## Declaration for Chapter Four

For Chapter Four, the nature and extent of contribution to the work was as follows:

Name	Nature of contribution	Extent of contribution
Joanne D. Du	Research design, performance of data collection and analysis, and preparation of manuscript	80%
Linda Hong	Assisted in synchrotron experiments, collated data and made figures, and provided input into the preparation of manuscript	5 %
Angel Tan	Provided input into the preparation of manuscript	5 %
Ben J. Boyd	Main supervisor, provided input into the preparation of manuscript	10 %

The undersigned hereby declare that the above declaration correctly reflects the nature and extent of candidate and co-author contributions:

Candidate's signature:



Date: 30/3/2018

Main supervisor's signature:



Date: 30/3/2018

## 4. Naphthalocyanine as a New Photothermal Actuator for Lipid-Based Drug Delivery Systems

Joanne D. Du, Linda Hong, Angel Tan and Ben J. Boyd\*

Drug Delivery, Disposition and Dynamics, Monash Institute of Pharmaceutical Sciences, Monash University (Parkville Campus), 381 Royal Parade, Parkville, VIC 3052, Australia

ARC Centre of Excellence in Convergent Bio-Nano Science and Technology, Monash Institute of Pharmaceutical Sciences, Monash University (Parkville Campus), 381 Royal Parade, Parkville, VIC 3052, Australia

First Published: January 9, 2018

Citation: *J. Phys. Chem. B* 2018, 122 (5), 1766-1770.

DOI: 10.1021/acs.jpcc.7b12234

### 4.1. Abstract

One approach to address the substantial global burden of ocular diseases such as aged related macular degeneration is using light-activated drug delivery to obviate the need for highly invasive and frequent need for costly intravitreal injections. To enable such systems, new light responsive materials are required. This communication reports the use of silicon 2,3-naphthalocyanine bis(trihexylsilyloxy) (SiNC), a small molecule photosensitizer as a new actuator for triggering light responsive lipid-based drug delivery systems. Small angle X-ray scattering was used to confirm that the addition of SiNC imparted light sensitivity to the lipid systems, resulting in a complete phase transition within 20 s of near infrared irradiation. The phase transition was also reversible, suggesting potential for on-demand drug delivery. When compared to the phase transitions induced using alternative light responsive actuators, gold nanorods and graphene, there were some differences in phase behaviour. Namely, the phytantriol with SiNC system transitioned directly to the inverse micellar phase, skipping the intermediate inverse hexagonal structure. The photodynamic properties and efficiency

in controlling the release of drug suggest that SiNC-actuated lipid systems have potential to reduce the burden of repeated intravitreal injections.

## 4.2. Introduction

Age-related macular degeneration (AMD) is a chronic eye disease that requires bi-monthly intravitreal injections to deliver inhibitors of the vascular endothelial growth factor (anti-VEGF) to slow the neovascularization that causes irreversible vision impairment and blindness in patients.<sup>1</sup> The highly invasive, frequent and costly treatments are a substantial global burden, estimated to affect 196 million older people by 2020, increasing to 288 million by 2040.<sup>2</sup>

Considerable efforts have been directed towards reducing the burden of the current anti-VEGF treatment.<sup>3-4</sup> Lipid-based liquid crystalline nanostructures including the lamellar phase ( $L_{\alpha}$ ), bicontinuous cubic phase ( $V_2$ ), inverse hexagonal phase ( $H_2$ ) and inverse micellar phase ( $L_2$ ) are of increasing interest for ophthalmic delivery due to their biocompatibility and the ability to control drug release. Depending on the state of the aqueous channels being either open or closed, the release of encapsulated drugs can be either fast or slow, respectively.<sup>5-7</sup> The inverted phase structures are of particular interest in drug delivery applications due to their potential for encapsulation of hydrophilic compounds in the internalized aqueous compartments, and because of their thermodynamic stability to dilution, which together confer favourable controlled release properties.

Recently, photo-sensitive ‘actuators’ have been incorporated into these structures to control the rate of drug release through manipulation of the nanostructure via an external light source.<sup>8-12</sup> Materials that have a strong absorbance in the near-infrared (NIR) region are of particular interest as near infrared light can safely penetrate biological tissues due to its low absorption coefficient with water, lipids, and haemoglobin, and the penetration depth of up to 50 mm deep suggests potential for activation of systems implanted into the back of the eye. Several nanosized photothermal agents including gold nanoparticles<sup>13-15</sup> and graphene derivatives<sup>16</sup> have been explored as actuators as they can be tuned to absorb light in the NIR range and have been shown to efficiently convert the light into thermal energy to exhibit a change

in the lipid structure. However, these particle-based actuators present problems with uncertainty about their location relative to the lipid material<sup>17-18</sup> or aqueous phase<sup>16</sup>, and the potential for the nanosized agents to dissociate after administration, resulting in a reduction of the photothermal effect and limiting the practicality of these materials.

Naphthalocyanine is a low molecular weight photosensitiser currently under investigation as a potential fluorescence imaging and phototherapeutic agent.<sup>19-23</sup> It is hypothesized in this study that this small molecule photosensitiser will be embedded within the lipid structure to elicit a photothermal effect similar to other known nanosized agents, enabling activated release of encapsulated anti-VEGF therapy. This determines the potential use of SiNC as an actuator in two heat-sensitive lipid systems based on phytantriol (3,7,11,15-tetramethylhexadecane-1,2,3-triol)<sup>24-26</sup> and 1-palmitoyl-2-oleoyl-sn-glycero-3-phosphoethanolamine mixed with cholesterol (POPE)<sup>27</sup>, that were previously investigated using particle-based photothermal agents. Phytantriol forms a bicontinuous cubic phase in excess water which transitions to an inverted hexagonal phase at elevated temperatures, while the POPE system transitions from a lamellar to an inverted hexagonal phase at elevated temperatures.

### 4.3. Materials and Methods

Phytantriol (PHYT; 3,7,11,15-tetramethylhexadecane-1,2,3-triol) was purchased from DSM Nutritional Products (Kaiseraugst, Switzerland). 1-Palmitoyl-2-oleoyl-sn-glycero-3-phosphoethanolamine (POPE) was purchased from Avanti Polar Lipids (Alabaster, USA). Silicon 2,3-naphthalocyanine bis(trihexylsilyloxy) (SiNC) and cholesterol were purchased from Sigma-Aldrich (St. Louis, USA). Lipid dispersions were prepared by dissolving PHYT with 5 mol% SiNC and POPE with 20 mol% cholesterol and 10 mol% SiNC in THF and the solution was then dried under a stream of nitrogen gas for 3 h, then under vacuum overnight at 50 °C to ensure complete removal of solvent. Blank lipid samples were prepared in the same manner without SiNC. The peak absorbance of SiNC in lipid systems was observed around 790 nm (Refer to Figure SI 4.1). The lipid film was then hydrated in a 20:1 (w/w) ratio with PBS containing 1 w/w% Pluronic® F108 stabiliser at pH 7.4. The lipid dispersions were allowed to equilibrate for 24 h before

investigation using small angle X-ray scattering (SAXS) at the Australian Synchrotron to qualitatively identify the internal nanostructure formed *in situ*.<sup>28</sup>

The synchrotron X-ray beam was tuned to a wavelength of 0.954 Å (13.0 keV) at a camera to detector distance of 964.4 mm which gave the q-range of the scattering vector from 0.0176 to 1.016 Å<sup>-1</sup>. A silver behenate standard (d-spacing = 58.38 Å) was used for the q range calibration. For equilibrium measurement, samples were transferred into 1.5 mm diameter glass capillaries and the 2D SAXS patterns were acquired using a Pilatus 1M detector with active area 169 to 179 mm<sup>2</sup> and with a pixel size of 172 μm. For the temperature-dependent results, the samples were placed in a temperature-controlled capillary holder, and heated from 25 to 80 °C at 5 °C intervals with equilibration for 10 min at each temperature prior to acquisition. The acquisition time was 1 s at 100 % flux. In time-resolved measurements, a Class IIIB fibre coupled laser system (MDL-808) with the power output at 400 mW at 808 nm (Changchun New Industries, China) was mounted 5 cm from the sample at a tangential angle to the X-ray beam and samples in a temperature controlled capillary holder were allowed to equilibrate for 10 min at 37 °C before they were illuminated remotely by a computer control system. SAXS patterns were collected before, during and after laser activation. The acquisition time was 0.1 s at intervals of every 8-10 s at 20 % flux for 2 min to avoid radiation damage from the synchrotron beam during data accumulation. The two dimensional scattering patterns were integrated into the one dimensional scattering function I(q) using the in-house developed software package, scatterBrain.<sup>29</sup> Scattering curves are plotted as a function of relative intensity, I, versus q and phase structures were identified by indexing the Bragg peaks to known relative spacing ratios.<sup>30-31</sup> The lamellar phase (L<sub>α</sub>) shows reflections at spacing ratios of 1:2:3:4, bicontinuous cubic phase (V<sub>2</sub>) can be identified by the reflection spacing of  $\sqrt{2}$ :  $\sqrt{3}$ :  $\sqrt{4}$ :  $\sqrt{6}$  (Pn3m), inverse hexagonal phase (H<sub>2</sub>) has a spacing ratio of 1:  $\sqrt{3}$ :  $\sqrt{4}$  and inverse micellar phase (L<sub>2</sub>) is evident by a broad peak between 0.15 and 0.20 Å. The apparent temperature (T<sub>app</sub>) of the lipid system during irradiation was determined using a calibration plot of the lattice parameter vs. temperature using the temperature-dependent SAXS results, where the lattice parameter is a measure of the internal phase structure calculated from the relative peak positions.

#### 4.4. Results

The effect of NIR irradiation on the nanostructure was evaluated using time-resolved small angle X-ray scattering (SAXS). After reduction to express the SAXS data as intensity versus magnitude of the scattering vector, the structures were identified by the spacing of the Bragg peaks and lattice parameters were calculated by the relative positions of the peaks. Figure 4.1 illustrates the time dependence of NIR irradiation on structure when SiNC is incorporated in the PHYT and POPE systems. The PHYT + SiNC system (Figure 4.1A) transitioned from the bicontinuous cubic phase (indicated by the indexed peak positions at  $\sqrt{2}$ ,  $\sqrt{3}$ ,  $\sqrt{4}$ ,  $\sqrt{6}$ ) to the inverse micellar phase (characterised by the broad hump at  $q \sim 0.17 \text{ \AA}^{-1}$ ) with less than 10 s irradiation, and reverted back to the original cubic phase within 30 s of ceasing the irradiation. The POPE + SiNC (Figure 4.1C) system was less sensitive than the PHYT system, retaining the equilibrium  $L_{\alpha}$  structure (indicated by peaks at spacing ratios 1:2:3) until 20 s of irradiation. The system converted to the  $H_2$  phase, indicated by the peaks at ratios 1:  $\sqrt{3}$ :  $\sqrt{4}$ . Approximately 40 s after ceasing the irradiation, the  $H_2$  transitioned back to the starting  $L_{\alpha}$  structure. No change in structure was observed upon irradiation for lipid systems without SiNC, as evident in Figure 4.1B and D.

To better understand the dynamic behaviour of these systems, and to determine any effect of the SiNC on self-assembly in the absence of NIR light, equilibrium temperature ramps were conducted in the presence of SiNC, where the SAXS patterns were acquired at fixed increasing temperatures, and the lattice parameter calculated for the phases present at each temperature.

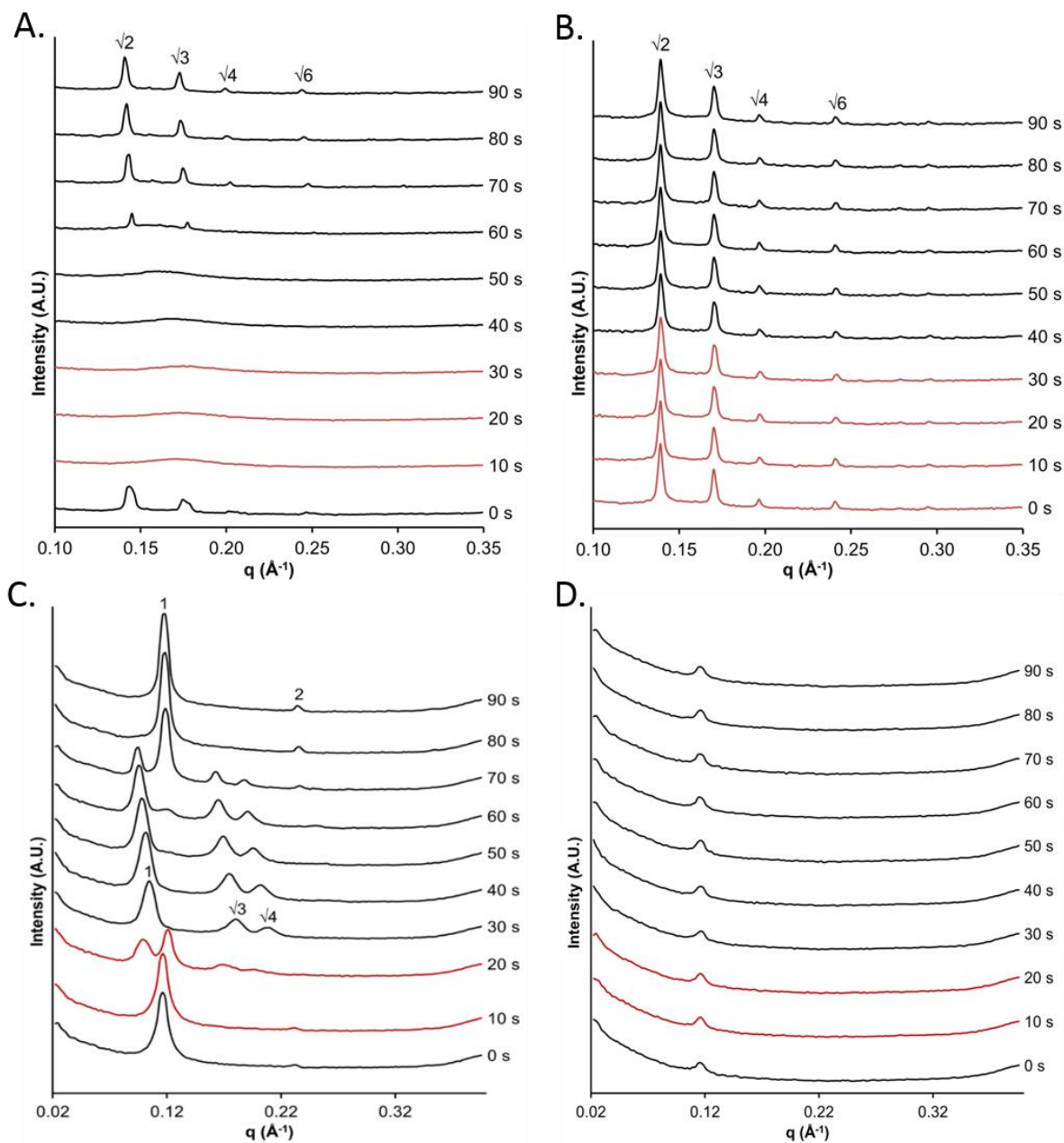


Figure 4.1 Effect of NIR irradiation on the structure of PHYT and POPE-based system maintained at 37 °C. A) PHYT + SiNC, B) Blank PHYT, C) POPE + SiNC and D) Blank POPE. The red curves indicate the time points exposed to NIR irradiation.

The equilibrium phase behaviour of the PHYT-based cubic phase in the presence of SiNC is seen in Figure 4.2A, where a phase transition from the  $V_2$  phase to the  $L_2$  phase occurred at approximately 55 °C. Previous temperature ramps studied in the absence of, and on inclusion of the hydrophobic gold nanorods<sup>17</sup> and graphene nanosheets<sup>16</sup> as the photothermal actuator showed an intermediate  $H_2$  phase between approximately 45 and 65 °C (Figure 4.2B and C). It is known that an increase in temperature induces the formation of more hydrophobic structures due to an increase in the effective volume of the hydrophobic tails.<sup>32</sup> However, it is also known that the formation of the  $H_2$  phase is energetically disfavoured due to the requirement to fill geometric voids at the vertices where hydrophobic tails meet in the structure between the hexagonally packed water-filled rods.<sup>33</sup> The transition directly to the  $L_2$  phase without transitioning through the disfavoured  $H_2$  structure has been observed previously for PHYT-based dispersions in the absence of hydrophobic additives,<sup>34</sup> but not for bulk phase samples which was the format for the comparator gold nanorod and graphene containing systems. This suggests that SiNC does not act as a hydrophobic additive, essentially leaving the packing of the lipids unaffected until irradiated with NIR light.

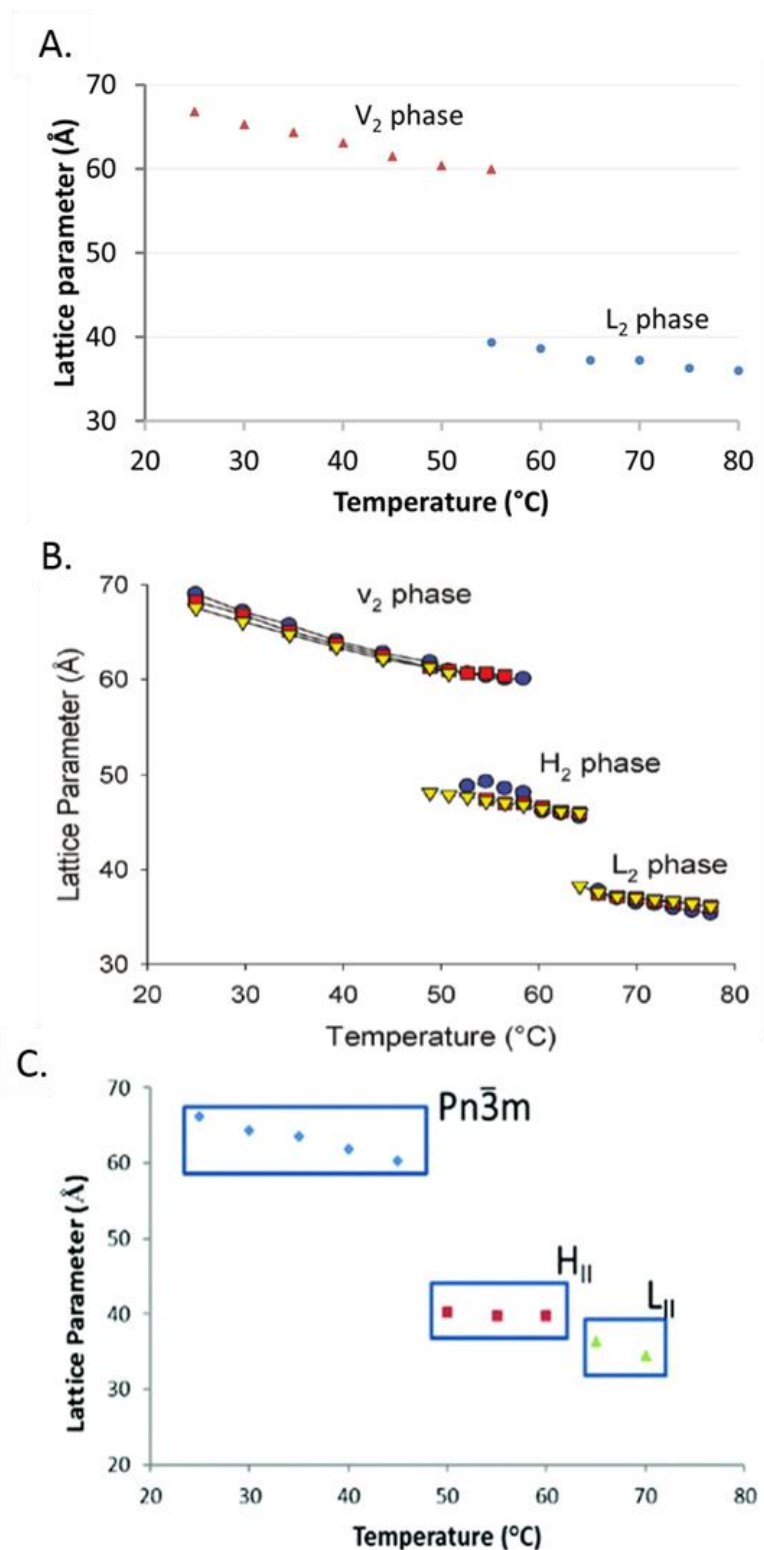


Figure 4.2 Temperature-dependent phase behaviour for PHYT system containing A) SiNC determined in this study, B) increasing concentration of gold nanorods<sup>17</sup> and C) graphene nanosheets<sup>16</sup>. Reproduced with permission from American Chemical Society and the Royal Society of Chemistry.

By utilising the lattice parameters calculated from the temperature-dependent equilibrium data in Figure 4.2 as a calibration curve,<sup>13</sup> the effect of irradiation on the lipid systems can be converted to the apparent temperature ( $T_{app}$ ) of the lipid system at each acquisition time (Figure 4.3). The  $T_{app}$  is a measure of disruption of lipid packing under the stimulus, and allows comparison of efficiency (magnitude of change in lipid packing) and effectiveness (required concentration) across different photoactuator systems. It should be noted that a global change in temperature cannot be detected on irradiation of these systems – the localised heating that causes changes in lipid packing is rapidly dissipated through the material.

The magnitude of change in  $T_{app}$  suggests that a much lower concentration of SiNC might be able to be used to stimulate the phase transition of both PHYT and POPE systems. The  $L_2$  peak for the PHYT + SiNC system at 60 s of irradiation corresponded to a  $T_{app}$  of 80 °C (Figure 4.3A). Therefore, 60 s irradiation of the PHYT system with SiNC induced an increase of approximately 40 °C, which is similar to the previously studied PHYT + graphene system (Figure 4.3C).

Similar to the PHYT + SiNC system, the POPE + SiNC system showed a rapid increase in  $T_{app}$  of 40 °C within 30 s of irradiation (Figure 4.3B). The actuation by SiNC in this case was more effective than inclusion of gold nanorods at 3 nM in past work, which reached a maximum increase of 25 °C with 30 s of irradiation (Figure 4.3D). SiNC is proposed to provide a greater photothermal effect as its photothermal effect can more readily affect the lipid molecules as it is embedded within the lipid structure, whereas the other actuators would suffer some dissipation of heat through the aqueous regions and as a result, be overall less effective actuators.

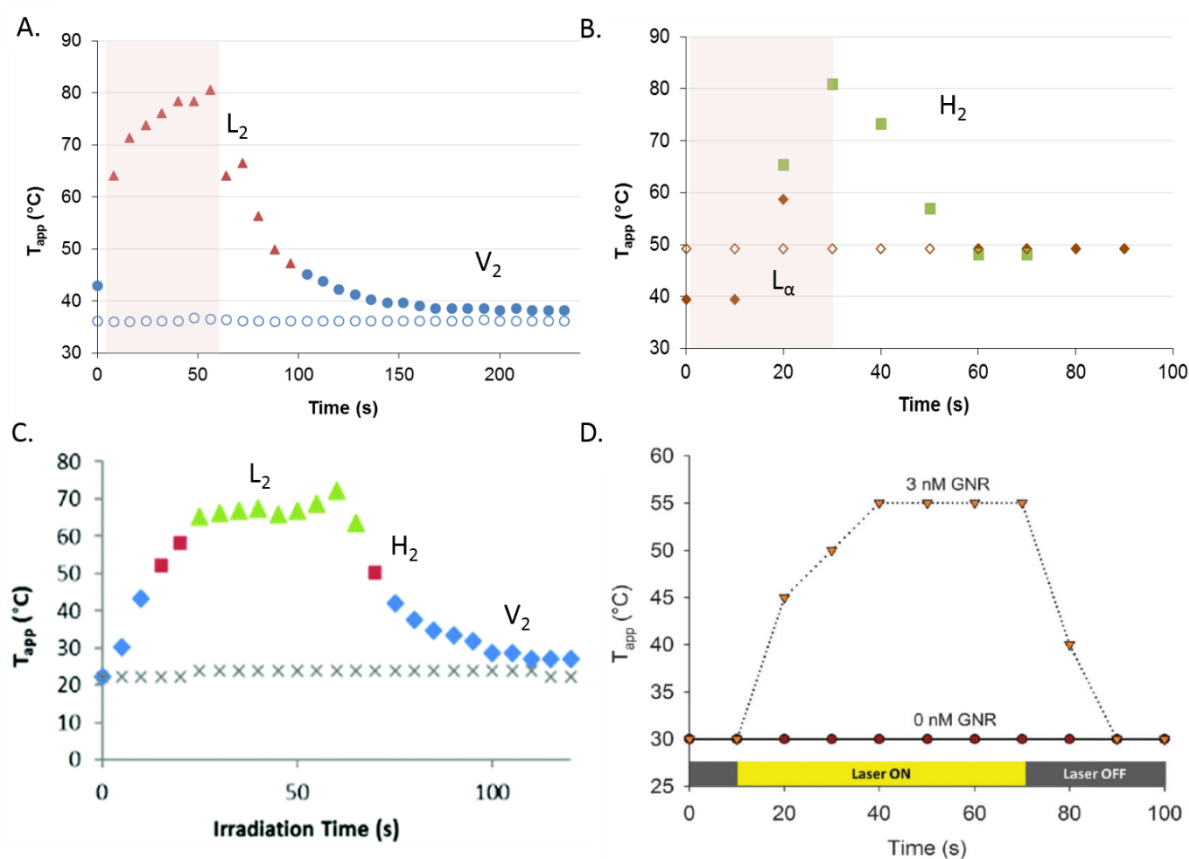


Figure 4.3 Effect of NIR irradiation on the apparent temperature ( $T_{app}$ ) for the PHYT and POPE systems. A) PHYT + SiNC (open circle = blank PHYT), B) POPE + SiNC (open circle = blank POPE), C) PHYT + graphene<sup>16</sup> (X = blank PHYT) and D) POPE + gold nanorods<sup>15</sup> (closed circle = blank POPE). Reproduced with permission from The Royal Society of Chemistry and the PCCP Owner Societies.

#### 4.5. Conclusion

In conclusion, the molecular actuator, SiNC, was shown for the first time to impart photothermal sensitivity to lipid systems. The SiNC-containing lipid systems required a shorter irradiation time to elicit a complete phase transition than the equivalent systems containing gold nanorods or graphene. The lipids studied in this communication were selected because they are established platforms known to be responsive to other photothermal stimuli. It is recognised however that their phase behaviour will result in a release profile that is not ideal for on-demand drug release application, as they tend to transition to the slow-releasing inverse hexagonal and inverse micellar phase structures. An ideal release profile would be a lipid system that can transition from the  $L_{\alpha}$  to  $V_2$  phase to exhibit a slow to fast release profile with an increase in temperature/NIR stimulus, and such lipid systems are currently under investigation .

#### 4.6. Acknowledgements

BJB is the recipient of an Australian Research Council Future Fellowship. This research was undertaken on the SAXS/WAXS beamline at the Australian Synchrotron, VIC. JDD is supported through an Australian Government Research Training Program Scholarship. These experiments were conducted on the SAXS/WAXS beamline at the Australian Synchrotron. The research was supported by the ARC Centre of Excellence in Convergent Bio-Nano Science and Technology.

## 4.7. References

1. Ohr, M.; Kaiser, P. K., Intravitreal aflibercept injection for neovascular (wet) age-related macular degeneration. *Exp. Opin. Pharmacother.* **2012**, *13*, 585-591.
2. Wong, W. L.; Su, X.; Li, X.; Cheung, C. M. G.; Klein, R.; Cheng, C.-Y.; Wong, T. Y., Global prevalence of age-related macular degeneration and disease burden projection for 2020 and 2040: a systematic review and meta-analysis. *Lancet* **2014**, *2*, 106-116.
3. Ishikawa, M.; Jin, D.; Sawada, Y.; Abe, S.; Yoshitomi, T., Future therapies of wet age-related macular degeneration. *J. Ophthalmol.* **2015**, 138070.
4. Holz, F. G.; Schmitz-Valckenberg, S.; Fleckenstein, M., Recent developments in the treatment of age-related macular degeneration. *J. Clin. Invest.* **2014**, *124*, 1430-1438.
5. Lajunen, T.; Nurmi, R.; Kontturi, L.; Viitala, L.; Yliperttula, M.; Murtomäki, L.; Urtti, A., Light activated liposomes: functionality and prospects in ocular drug delivery. *J. Control. Release* **2016**, *244*, Part B, 157-166.
6. Delplace, V.; Payne, S.; Shoichet, M., Delivery strategies for treatment of age-related ocular diseases: from a biological understanding to biomaterial solutions. *J. Control. Release* **2015**, *219*, 652-668.
7. Du, J. D.; Fong, W.-K.; Caliph, S.; Boyd, B. J., Lipid-based drug delivery systems in the treatment of wet age-related macular degeneration. *Drug Deliv. Transl. Res.* **2016**, *6*, 781-792.
8. Li, H.; Yang, X.; Zhou, Z.; Wang, K.; Li, C.; Qiao, H.; Oupicky, D.; Sun, M., Near-infrared light-triggered drug release from a multiple lipid carrier complex using an all-in-one strategy. *J. Control. Release* **2017**, *261*, 126-137.
9. Eastoe, J.; Vesperinas, A., Self-assembly of light-sensitive surfactants. *Soft Matter* **2005**, *1*, 338-347.
10. Miranda, D.; Lovell, J. F., Mechanisms of light-induced liposome permeabilization. *Bioeng. Transl. Med.*, **2016**, *1*, 267-276.
11. Rwei, A. Y.; Zhan, C.; Wang, B.; Kohane, D. S., Multiply repeatable and adjustable on-demand phototriggered local anesthesia. *J. Control. Release* **2017**, *251*, 68-74.
12. Carter, K. A.; Shao, S.; Hoopes, M. I.; Luo, D.; Ahsan, B.; Grigoryants, V. M.; Song, W.; Huang, H.; Zhang, G.; Pandey, R. K., Porphyrin-phospholipid liposomes permeabilized by near-infrared light. *Nat. Commun.* **2014**, *5*, 3546.
13. Fong, W.-K.; Hanley, T. L.; Thierry, B.; Kirby, N.; Waddington, L. J.; Boyd, B. J., Controlling the nanostructure of gold nanorod-lyotropic liquid-crystalline hybrid materials using near-infrared laser irradiation. *Langmuir* **2012**, *28*, 14450-14460.
14. Kwon, H. J.; Byeon, Y.; Jeon, H. N.; Cho, S. H.; Han, H. D.; Shin, B. C., Gold cluster-labeled thermosensitive liposomes enhance triggered drug release in the tumor microenvironment by a photothermal effect. *J. Control. Release* **2015**, *216*, 132-139.
15. Du, J. D.; Fong, W.-K.; Salentinig, S.; Caliph, S. M.; Hawley, A.; Boyd, B. J., Phospholipid-based self-assembled mesophase systems for light-activated drug delivery. *Phys. Chem. Chem. Phys.* **2015**, *17*, 14021-14027.
16. Quinn, M. D. J.; Wang, T.; Du, J. D.; Boyd, B. J.; Hawley, A.; Notley, S. M., Graphene as a photothermal actuator for control of lipid mesophase structure. *Nanoscale* **2017**, *9*, 341-348.

17. Fong, W.-K.; Hanley, T. L.; Thierry, B.; Kirby, N.; Boyd, B. J., Plasmonic nanorods provide reversible control over nanostructure of self-assembled drug delivery materials. *Langmuir* **2010**, *26*, 6136-6139.
18. Lee, J. H.; Shin, Y.; Lee, W.; Whang, K.; Kim, D.; Lee, L. P.; Choi, J. W.; Kang, T., General and programmable synthesis of hybrid liposome/metal nanoparticles. *Sci. Adv.* **2016**, *2*, e1601838.
19. Taratula, O.; Schumann, C.; Duong, T.; Taylor, K. L.; Taratula, O., Dendrimer-encapsulated naphthalocyanine as a single agent-based theranostic nanoplatform for near-infrared fluorescence imaging and combinatorial anticancer phototherapy. *Nanoscale* **2015**, *7*, 3888-3902.
20. Taratula, O.; Doddapaneni, B. S.; Schumann, C.; Li, X.; Bracha, S.; Milovancev, M.; Alani, A. W. G.; Taratula, O., Naphthalocyanine-based biodegradable polymeric nanoparticles for image-guided combinatorial phototherapy. *Chem. Mater.* **2015**, *27*, 6155-6165.
21. Camerin, M.; Rello-Varona, S.; Villanueva, A.; Rodgers, M. A. J.; Jori, G., Metallo-naphthalocyanines as photothermal sensitizers for experimental tumours: in vitro and in vivo studies. *Lasers Surg. Med.* **2009**, *41*, 665-673.
22. Zhang, Y.; Lovell, J. F., Recent applications of phthalocyanines and naphthalocyanines for imaging and therapy. *Wiley Interdiscip. Rev. Nanomed. Nanobiotechnol.* **2017**, *9*, e1420.
23. Zhang, Y.; Hong, H.; Sun, B.; Carter, K.; Qin, Y.; Wei, W.; Wang, D.; Jeon, M.; Geng, J.; Nickles, R. J., Surfactant-stripped naphthalocyanines for multimodal tumor theranostics with upconversion guidance cream. *Nanoscale* **2017**, *9*, 3391-3398.
24. Dong, Y.-D.; Dong, A. W.; Larson, I.; Rappolt, M.; Amenitsch, H.; Hanley, T.; Boyd, B. J., Impurities in commercial phytantriol significantly alter its lyotropic liquid-crystalline phase behavior. *Langmuir* **2008**, *24*, 6998-7003.
25. Mulet, X.; Boyd, B. J.; Drummond, C. J., Advances in drug delivery and medical imaging using colloidal lyotropic liquid crystalline dispersions. *J. Colloid Interface Sci.* **2013**, *393*, 1-20.
26. Fong, W.-K.; Negrini, R.; Vallooran, J. J.; Mezzenga, R.; Boyd, B. J., Responsive self-assembled nanostructured lipid systems for drug delivery and diagnostics. *J. Colloid Interface Sci.* **2016**, *484*, 320-339.
27. Winter, R.; Erbes, J.; H. Templer, R.; M. Seddon, J.; Syrykh, A.; A. Warrender, N.; Rapp, G., Inverse bicontinuous cubic phases in fatty acid/phosphatidylcholine mixtures: the effects of pressure and lipid composition. *Phys. Chem. Chem. Phys.* **1999**, *1*, 887-893.
28. Kirby, N. M.; Mudie, S. T.; Hawley, A. M.; Cookson, D. J.; Mertens, H. D. T.; Cowieson, N.; Samardzic-Boban, V., A low-background-intensity focusing small-angle x-ray scattering undulator beamline. *J. Appl. Crystallogr.* **2013**, *46*, 1670-1680.
29. Mudie, S. T. *ScatterBrain*, V2.30; Australian Synchrotron: Australia.
30. Boyd, B. J.; Dong, Y.-D.; Rades, T., Nonlamellar liquid crystalline nanostructured particles: advances in materials and structure determination. *J. Liposome Res.* **2009**, *19*, 12-28.
31. Hyde, S. T., *Identification of lyotropic liquid crystalline mesophases*. John Wiley & Sons, Ltd: 2001; p 299-332.
32. Israelachvili, J. N.; Mitchell, D. J.; Ninham, B. W., Theory of self-assembly of hydrocarbon amphiphiles into micelles and bilayers. *J. Chem. Soc. Faraday Trans.* **1976**, *72*, 1525-1568.

33. Rappolt, M.; Hickel, A.; Bringezu, F.; Lohner, K., Mechanism of the lamellar/inverse hexagonal phase transition examined by high resolution x-ray diffraction. *Biophys. J.* **2003**, *84*, 3111-3122.
34. Dong, Y.-D.; Tilley, A. J.; Larson, I.; Lawrence, M. J.; Amenitsch, H.; Rappolt, M.; Hanley, T.; Boyd, B. J., Nonequilibrium effects in self-assembled mesophase materials: unexpected supercooling effects for cubosomes and hexosomes. *Langmuir* **2010**, *26*, 9000-9010.

## 4.8. Supplementary Information

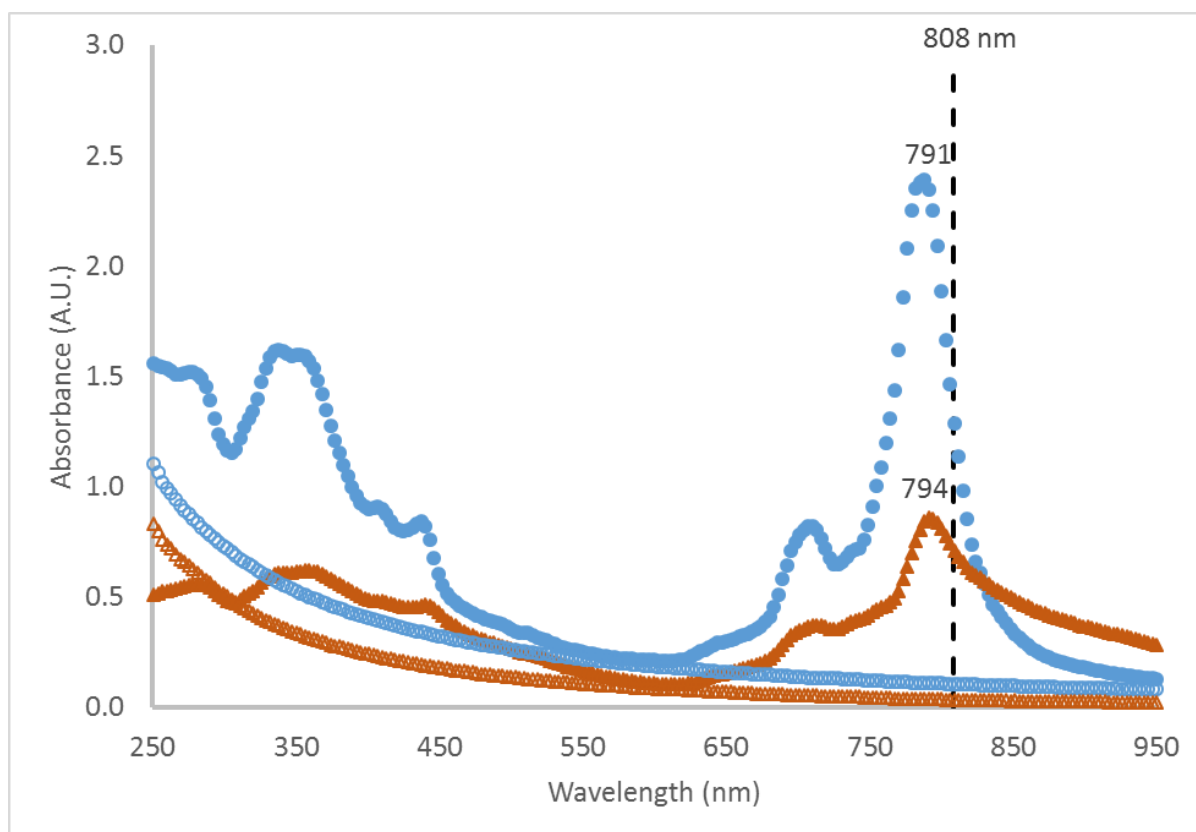


Figure SI 4.1. Absorbance spectrum of SiNC incorporated PHYT (●) and POPE system (▲), with a maximum absorbance around 790 nm. Open symbols represent the absorbance of blank lipid systems.

CHAPTER FIVE:  
LIGHT-ACTIVATED RELEASE FROM  
PHOSPHOLIPID-BASED SYSTEM

## Prologue to Chapter Five

---

A stimuli-responsive system have potential to overcome the current limitation of anti-VEGF treatment by reducing the costly, highly invasive and frequent intravitreal injections. In this chapter, a phospholipid and fatty acid system was investigated as the previous phospholipid-based system investigated in Chapter Three did not exhibit the desired phase behaviour. To gain insight to the release profile of the phospholipid and fatty acid system upon near infrared irradiation, aflibercept was encapsulated and the release of aflibercept was evaluated using an affinity chromatography method. The work is presented as a manuscript in preparation.

## Declaration for Chapter Five

The nature and extent of contribution to the work described below was as follows:

<b>Name</b>	<b>Nature of contribution</b>	<b>Extent of contribution</b>
Joanne D. Du	Research design, performance of data collection and analysis, and preparation of manuscript	75%
Wye-Khay Fong	Co-supervisor, provided input into the preparation of manuscript	5 %
Eric Hanssen	Conducted the cryo-TEM experiments	5 %
Suzanne M. Caliph	Co-supervisor, provided input into the preparation of manuscript	5 %
Ben J. Boyd	Main supervisor, provided input into the preparation of manuscript	10 %

The undersigned hereby declare that the above declaration correctly reflects the nature and extent of candidate and co-author contributions:

Candidate's signature:



Date: 30/3/2018

Main supervisor's signature:



Date: 30/3/2018

## 5. Light-Activated Release of Aflibercept from a Phospholipid-Based Liquid Crystalline System

Joanne D. Du<sup>1,3</sup>, Wye-Khay Fong<sup>2</sup>, Eric Hanssen<sup>3</sup>, Suzanne M. Caliph<sup>1</sup> and Ben J. Boyd<sup>1,4</sup>

<sup>1</sup> Drug Delivery, Disposition and Dynamics, Monash Institute of Pharmaceutical Sciences, Monash University (Parkville Campus), 381 Royal Parade, Parkville, VIC 3052, Australia

<sup>2</sup> Adolphe Merkle Institute, University of Fribourg, Chemin des Verdiers 4, 1700 Fribourg, Switzerland

<sup>3</sup> The Bio21 Molecular Science and Biotechnology Institute, 30 Flemington Road, Parkville, VIC 3052, Australia

<sup>4</sup> ARC Centre of Excellence in Convergent Bio-Nano Science and Technology, Monash Institute of Pharmaceutical Sciences, Monash University (Parkville Campus), 381 Royal Parade, Parkville, VIC 3052, Australia

### 5.1. Abstract

Intravitreal injections of aflibercept are currently used for the treatment of aged-related macular degeneration. The treatment-associated burden reduces patient compliance that can lead to blindness. This paper reports a light-sensitive phospholipid-based system that can provide a more sustainable and less invasive treatment for this chronic disease. The results confirms that the activation of incorporated near-infrared (NIR) responsive agents, namely gold nanorods and silicon naphthalocyanine, can control the release of aflibercept from phospholipid-based vesicles. The almost complete release of aflibercept from the vesicles can be activated when exposed to 30 s of NIR irradiation causing a phase transition to the bicontinuous cubic phase. The dynamic release of aflibercept was quantified with the use of affinity chromatography, enabling rapid analysis. Further studies are required to optimise the light-sensitive systems, nonetheless, such a system has the potential to become less invasive and provide a depot for controlled drug delivery over time.

## 5.2. Introduction

Aflibercept (Eylea®) is a recombinant fusion protein consisting of the binding portion of human VEGF receptor 1 and 2 extracellular domains fused to the Fc portion of human IgG1. Currently, aflibercept is used to treat neovascular age-related macular degeneration (AMD) and is administered via intravitreal injection with a loading dose of three monthly injections followed by a dose every eight weeks thereafter.<sup>1</sup> The multiple intravitreal injections are necessary due to the high clearance rate from the posterior segment of the eye, and as a consequence, the active exhibits short intraocular retention time.<sup>2-3</sup> AMD is the most common chronic eye disease that causes blindness in older adults residing in developed countries.<sup>4</sup> The disease causes degenerative changes in the retinal pigment epithelial cells that promotes the development of chronic inflammation in the retina and choroid.<sup>5</sup> Most severe vision loss occurs as the disease progressively damages the retinal pigment epithelium due to choroidal neovascularization at the site of inflammation. Aflibercept is a palliative treatment that inhibits the action of vascular endothelial growth factor (VEGF), the predominant cause of choroidal neovascularisation.<sup>6</sup> Although intravitreal injections are effective, they have low patient compliance due to associated risks of other ocular problems and are likely to be unsustainable due to the long term financial burden for the individual, their families and the economy.<sup>7</sup> An on-demand controlled release delivery system can address these limitations by extending the dosing frequency of aflibercept, while reducing the frequency of the intravitreal injections and their corresponding treatment-associated side effects.<sup>8</sup>

This paper proposes the use of a self-assembled phospholipid-based liquid crystalline (LC) nanostructured particle that can be activated to release intravitreally administered drugs when required. Specialised lipids self-assemble in aqueous environments to form particles with complex internal nanostructures that control the release rate of drugs depending on the nanostructure formed; specifically the open or closed nature of the aqueous channels.<sup>9</sup> This study investigates the utility of a phospholipid-based system as a stimuli-responsive drug delivery matrix that can transition from the closed lamellar ( $L_{\alpha}$ ) phase to the open bicontinuous cubic ( $V_2$ ) phase. Specifically, a system based upon the combination of 1,2-dilauroyl-sn-glycero-3-

phosphocholine (DLPC) and lauric acid (LA) at a 1:2 molar ratio was investigated as shown in Figure 5.1. Under pressure (20 bar), DLPC:2LA dispersions at 41 °C were found to form the  $V_2$  phase with the  $Im\bar{3}m$  space group corresponding to spacing ratio  $\sqrt{2} : \sqrt{4} : \sqrt{6}$ , which later transitions to the  $Pn\bar{3}m$   $V_2$  phase, with a spacing ratio of  $\sqrt{2} : \sqrt{3} : \sqrt{4} : \sqrt{6}$ , coexisting with the inverse hexagonal ( $H_2$ ) phase.<sup>10</sup> The DLPC:2LA system is expected to exhibit little or no drug release as the drugs are encapsulated in the closed  $L_\alpha$  structure, however, drug release can be triggered via a phase transition to the open  $V_2$  structure.

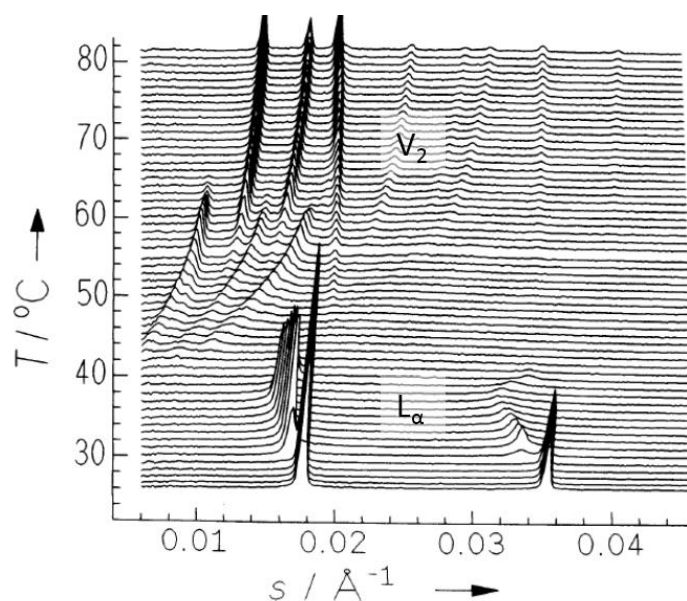


Figure 5.1 Temperature sequence of X-ray diffraction patterns for DLPC:2LA-water dispersions from the literature at 20 bar, reproduced from <sup>10</sup> with permission from the PCCP Owner Societies.

In this study, near-infrared (NIR) light sensitive agents were incorporated into the DLPC:2LA system in order to provide a mean for on-demand manipulation. NIR light has been proposed as a biocompatible stimulus due to its safety profile and penetration depth of up to 50 mm,<sup>11</sup> leading to its used in ophthalmic therapies<sup>12</sup>. Two types of NIR-responsive agents, a small molecule photosensitiser namely silicon 2,3-naphthalocyanine bis(trihexylsilyloxy) (SiNC)<sup>13</sup>, and plasmonic gold nanorods (GNR),<sup>14</sup> have been incorporated into phospholipid-based LC system to impart photosensitivity. It is hypothesised that upon NIR irradiation, the photothermal heating effect will cause a phase change, and subsequent release of a unit dose of drug, mimicking the repeat injections. Hence, the frequency of injections will be reduced by

replacing the repeated injections with a non-invasive on-demand release strategy. Ideally, the repeated intravitreal injections will be replaced by the light-activated doses for an extended period of at least 6 months.

### 5.3. Material

1,2-Dilauroyl-sn-glycero-3-phosphocholine (DLPC) with >99% purity was purchased from Avanti Polar Lipids (Alabaster, USA). Silicon 2,3-naphthalocyanine bis(trihexylsilyloxy) (SiNC), lauric acid (LA), tris(2-carboxyethyl)phosphine hydrochloride ( $\geq 98\%$ ), 1-dodecanthiol ( $\geq 98\%$ ) and glycine ( $\geq 98\%$ ) was purchased from Sigma-Aldrich (St. Louis, USA). Tris(hydroxymethyl)aminomethane, Ultra Pure Grade (>99.9 %) was purchased from Astrala Scientific Pty Ltd (NSW, Aus). PEGylated Gold NanoRods (GNR) with an aspect ratio of 4.3 (length, 47.8 nm; width, 11.2 nm) were purchased from NanoHybrids Inc. (Texas, USA), with the measured surface plasmonic resonance (SPR) of 814 nm. Eylea® (Regeneron/Bayer) was a gift from Dr Devinder Chauhan (Vision Eye Institute, AUS). HCl (1 M), dimethyl sulfoxide and dry tetrahydrofuran were purchased from Merck (VIC, Australia). Sodium chloride (Chem-Supply, Australia), di-sodium hydrogen orthophosphate and potassium dihydrogen orthophosphate (APS Ajax Finechem, Australia) were of analytical reagent quality. All materials were used without further purification. Water used in these studies was obtained from a Millipore Milli-Q purification system (Billerica, USA).

### 5.4. Methods

#### General procedure for the preparation of lipid dispersion

A thin-film hydration method was used to prepare the lipid dispersions with and without a NIR-responsive agent. Briefly, DLPC and LA at 1:2 mole ratio were weighed and dissolved in the absence of the NIR-responsive element with THF. The NIR responsive formulations had either 3 nM hydrophobised GNR in THF (Figure SI 5.1) or 10 mol% SiNC in THF, added to the lipid solution. The mixture was then dried under a stream of nitrogen gas for 3 h, then under vacuum overnight at 50 °C to ensure complete removal of solvent. The lipid mixture was subsequently hydrated with PBS (pH 7.4) at 1:9 (w/w) ratio in order to obtain a 10 % w/w lipid dispersion. The mixture was then

homogenised by ultrasonication (S220 Focused-ultrasonicator (Covaris, USA)) for 15 min (40 s pulses, peak power of 250 and duty factor of 30.2).

#### 5.4.1. Structural analysis of lipid dispersions using small angle X-ray scattering (SAXS)

The lipid structure in excess water was probed using small angle X-ray scattering (SAXS) at the Australian Synchrotron.<sup>15</sup> The temperature-dependent and time-resolved activation experiments were conducted according to the methods previously described.<sup>14, 16</sup> The synchrotron X-ray beam was modified to a wavelength of 0.954 Å (13.0 keV) at a camera to detector distance of 964.4 mm, which gave the q-range of the scattering vector from 0.0176 to 1.016 Å<sup>-1</sup>. For the temperature-dependent experiments, results were acquired after 10 min equilibration at 5 °C intervals from 25 to 80 °C, with an acquisition time of 1 s at 100 % flux. The time-resolved experiments were activated using a Class IIIB fibre coupled laser system (MDL-808) with the power output at 400 mW at 808 nm (Changchun New Industries, China), that was mounted 5 cm from the sample at a tangential angle to the X-ray beam. The samples were allowed to equilibrate for 10 min at 37 °C in a temperature controlled capillary holder before they were illuminated remotely by a computer control system for 30 to 60 s. Time-resolved results were acquired every 10 s, 0.1 s acquisitions at 20 % flux to avoid radiation damage from the synchrotron beam during data accumulation. SAXS patterns were collected before, during and after laser activation. The resultant scattering patterns were converted to a plot of relative intensity (I) versus the magnitude of the scattering vector (q). The ratio of reciprocal spacings of the Bragg peaks were indexed to elucidate the lipid structure.

#### 5.4.2. Morphology of nanostructures using cryogenic transmission electron microscopy (cryo-TEM)

The vesicular structures of lipid dispersions was further verified using cryo-TEM. Samples were diluted by 20-folds with PBS (pH 7.4) and vitrification process was conducted using a Vitrobot Mark III (FEI, Eindhoven, Netherlands) to maintain an ambient humidity of 80% and the temperature at 22°C. Briefly, aliquots (3 µL) of the sample were pipetted onto copper grids (200-mesh) coated with perforated carbon film (Lacey carbon film: ProSciTech, Qld, Australia), which were rendered hydrophilic via

glow discharge using nitrogen. After 15 s adsorption time, the grid was blotted for 2 s and plunged into liquid ethane cooled by liquid nitrogen. Frozen grids were stored in liquid nitrogen until required. The samples were examined using a Gatan 626 cryoholder (Gatan, Pleasanton, CA, USA) and Tecnai F30 Transmission Electron Microscope (FEI, Eindhoven, Netherlands) at an operating voltage of 300 kV. A low dose electron dose of 10-15 electrons/Å<sup>2</sup> was used for all imaging and the images were recorded using a FEI CETA 4k x 4k CMOS camera.

### 5.4.3. Encapsulation and release of aflibercept loaded vesicles

Aflibercept (Eylea®) diluted with PBS to 4 mg/mL, was added to lipid dispersions with and without NIR-responsive actuators at a 1:1 ratio to obtain a 5 % w/w lipid dispersion, which was then extruded 21 times through a 100 nm membrane filter (Avanti Polar Lipids, USA) to promote encapsulation of aflibercept. The SiNC lipid dispersion was centrifuged at 7378 x g for 10 min prior to extrusion to remove excess solid SiNC.

The free aflibercept was then separated from the aflibercept-loaded vesicles using Protein A Spin Trap (GE Healthcare Australia Pty. Ltd., Australia), a small scale pre-packed column with Protein A Sepharose™ High Performance. The columns are designed for rapid purification of IgG antibodies, such that the Fc portion of aflibercept will bind to the Protein A. The affinity purification is coupled with UV-Vis spectrometry to enable rapid analysis for *in situ* activation and quantification of the fusion protein. Briefly, the storage solution was removed from the column, and was washed three times using 400 µL PBS (pH 7.4) via centrifugation for 30 s at 100 x g. After the final wash spin, ensuring complete removal of PBS, 250 µL of aflibercept-lipid dispersion (5 w/w% lipid, 2 mg/mL aflibercept) was applied onto the washed column, was sealed by capping the end and incubated for at least 4 min with gentle mixing. The aflibercept-encapsulated vesicles were collected via centrifugation for 30 s at 100 x g for subsequent activation studies. The column was then washed four times with 400 µL PBS to collect the remaining aflibercept-encapsulated vesicles. The free aflibercept was debound from the Protein A column by eluting four times using 400 µL 0.1 M glycine solution (pH 2.7) into 100 µL of neutralising solution (1 M Tris-HCl, pH 8.8). To quantify the amount of free aflibercept, the eluates were transferred into UV transparent 96-well plates and the UV

absorbance at 280 nm was measured using an Enspire® Multilabel Plate Reader (PerkinElmer, USA), which detects the aromatic amino acids (mainly tyrosine and tryptophan) in the protein. The mass of free aflibercept were determined for each eluate using a standard curve (Figure SI 5.2), which was constructed using known concentration of aflibercept diluted with Glycine/Tris buffer (1:4) at pH ~7. The encapsulation efficiency (%EE) was  $27 \pm 4.5$  % (n=4) for GNR-vesicles and  $40 \pm 20$  % (n=4) for SiNC-vesicles (Figure SI 5.3), which was calculated using Eq.1.

$$\text{Eq. 1. } \%EE = 100 \times \frac{(\text{Applied} - \text{Free aflibercept (mg)})}{\text{Applied aflibercept (mg)}}$$

The aflibercept-loaded vesicles were subjected to 0 or 30 s NIR irradiation using a Class IIIB fibre coupled laser system (MDL-808) with the power output at 400 mW at a wavelength of 808 nm (Changchun New Industries, China) and the free aflibercept was quantified using the Protein A column described above. All activation experiments were done within 2 days after the initial encapsulation process. The percentage released was calculated using Eq. 2.

$$\text{Eq. 2. } \% \text{ Release} = 100 \times \frac{\text{Free aflibercept (mg)}}{\text{Encapsulated aflibercept (mg)}}$$

Free aflibercept in PBS solution (2 mg/mL) was quantified in the same manner to act as the positive control showing a  $96 \pm 1.3$  % recovery (Figure 5.5, Free Eylea Solution). All samples were conducted in triplicates (n=3). Statistical differences between the data sets were assessed using a one-way ANOVA post-hoc Tukey analysis of variance.

## 5.5. Results and Discussion

### 5.5.1. Phase behaviour of DLPC:2LA

The phase behaviour of DLPC:2LA dispersions were determined using SAXS (Figure 5.2). DLPC:2LA system was confirmed to transition from vesicles (dispersed  $L_{\alpha}$  phase) to coexisting  $V_2$  and  $H_2$  phase in excess water above 40 °C. The transition temperature is similar to the literature value around 41 °C however, the coexistence with  $H_2$  phase with the spacing ratio  $1:\sqrt{3}:\sqrt{4}$ , was only observed between 50 to 65 °C. This slight difference in phase behaviour may be attributed to the experiments being performed at

ambient pressures as opposed to the 20 bar pressure used in the literature studies<sup>10</sup>. Pressure suppresses the movement of the hydrocarbon chain, more so than the head group section, favouring the formation of structures with less negative curvature ( $V_2$  phase).<sup>17</sup> The  $L_\alpha$  to  $V_2 + H_2$  transition temperature of the lipid only matrix is close to physiological temperature, which may limit its use “as is” due to the possibility of accidental activation. However, the encapsulation of aflibercept into the DLPC:2LA system showed an increase in the phase transition temperature to 50 °C, suggesting that the amphiphilic nature of the aflibercept protein makes it surface active, and consequently, the protein associates strongly with the lipidic bilayer. In Figure 5.3, the addition of NIR-responsive agents in DLPC:2LA system was also investigated and consistent with previous literature, GNR did not change the phase structure or transition temperature.<sup>14</sup> Conversely, the incorporation of SiNC did have a subtle effect on the phase structure, causing the formation of the coexisting  $H_2$  phase to occur at a higher temperature. This slight change in the lipid packing may be attributed to the small molecule being embedded within the phospholipid structure, which is different to the SiNC and phytantriol-based system from literature.<sup>13</sup> Further investigation into the morphology of the light-sensitive DLPC:2LA vesicles are required.

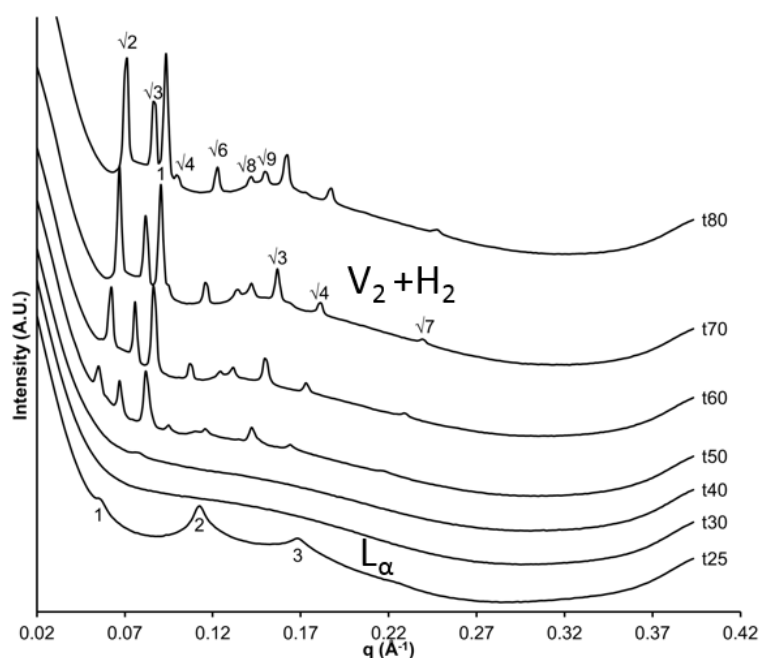


Figure 5.2 Temperature sequence of X-ray diffraction patterns for DLPC:2LA-water dispersions from this study at atmospheric pressure.

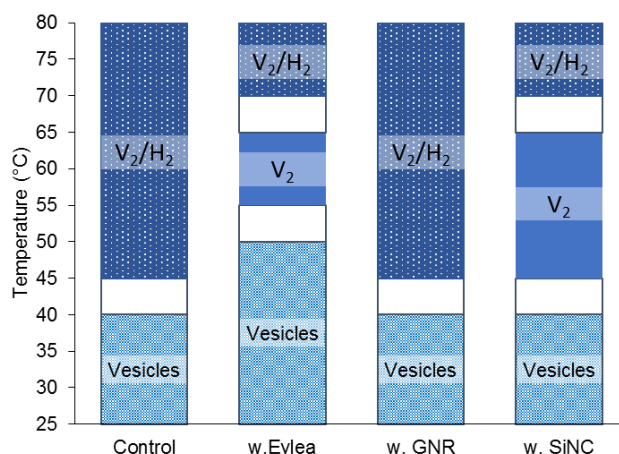


Figure 5.3 Temperature-dependent phase behaviour of DLPC:2LA system in excess water (control), DLPC:2LA with aflibercept (w. Eylea), DLPC:2LA with gold nanorods (w. GNR) and DLPC:2LA with silicon naphthalocyanine (w. SiNC).

### 5.5.2. Effect of NIR agent on the morphology

The nanostructure of the particles was further investigated using cryo-TEM in order to confirm the vesicular structure of the formulations (Figure 5.4). The incorporation of SiNC with and without aflibercept, displayed a polyhedral faceted lipid bilayer morphology, which is similar to previously explored temperature-sensitive liposomes loaded with magnetic resonance imaging contrast agents.<sup>18-19</sup> The faceting indicates that addition of the small molecules caused the lipid bilayer to become more rigid.<sup>20</sup> A recent study has found that addition of cholesterol, which is known to increase the packing and rigidity of phospholipid bilayers,<sup>21</sup> can double the encapsulation efficiency in comparison to just phospholipid vesicles.<sup>22</sup> The average encapsulation for SiNC-vesicles (around 40 %) was found to be similar to the reported cholesterol-vesicles (about 43 %) <sup>22</sup>. The control, DLPC:2LA vesicles are spherical (Figure 5.4C) and the spherical structure is maintained when GNR are incorporated (Figure 5.4 D, E and F). Although the spherical morphology of the liposome is maintained in the presence of GNR, the distribution of the GNR varies which may result in a reduction in photothermal effect. Therefore, the use of the smaller SiNC may provide a more consistent effect despite the change in morphology. The photothermal effect of these NIR-responsive phospholipid systems were further investigated by quantifying the release of encapsulated aflibercept when irradiated.

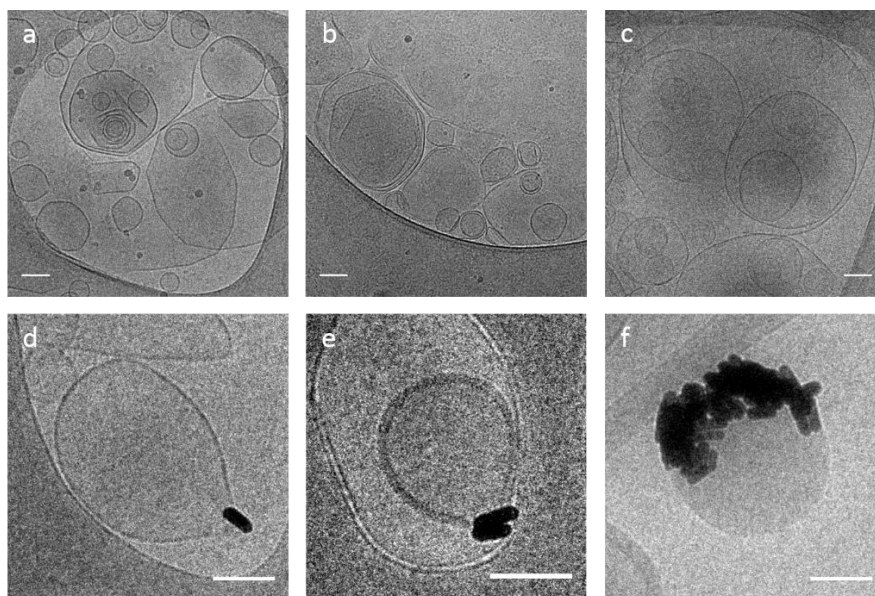


Figure 5.4 Difference in morphology of DLPC:2LA liposomes with A) SiNC, B) SiNC with aflibercept, C) aflibercept only, and D, E and F) aflibercept with GNR. Rigid faceted lipid bilayers are present in A and B. (scale bar = 100 nm)

### 5.5.3. Effect of NIR irradiation on phase behaviour

The effect of irradiation on the nanostructure of aflibercept-loaded DLPC:2LA system containing NIR agents was evaluated using time-resolved SAXS. No change the vesicular structure were observed upon NIR irradiation of DLPC:2LA vesicles in the absence of NIR-responsive agents, as evident in Figure SI 5.4. Figure 5.5 illustrates that incorporation of both GNR and SiNC imparted photo-sensitivity to the phospholipid-based vesicles. Within 30 s of irradiation, both NIR agents induced a disruption of the lipid packing to form the  $V_2$  phase, equivalent to increasing the apparent temperature to above 60 °C as shown in Figure 5.5. The duration of irradiation required was similar to the previous reports for the 1-palmitoyl-2-oleoyl-sn-glycero-3-phosphoethanolamine system with gold nanorods.<sup>14</sup> The reversibility of the photothermal effect was evident such that after a short relaxation period, the activated phase transition to the  $V_2$  phase returned to the starting vesicle structure. The GNR incorporated system took less than 1 min to transition from the  $V_2$  phase back to vesicles, which is faster than the system with SiNC, taking about 4 min. This may be caused by the supercooling effect, which suppresses the phase transition after heating.<sup>23</sup> While the inverse hexagonal  $H_2$  phase was only observed in the later irradiation cycles for the GNR incorporated system.<sup>24</sup>

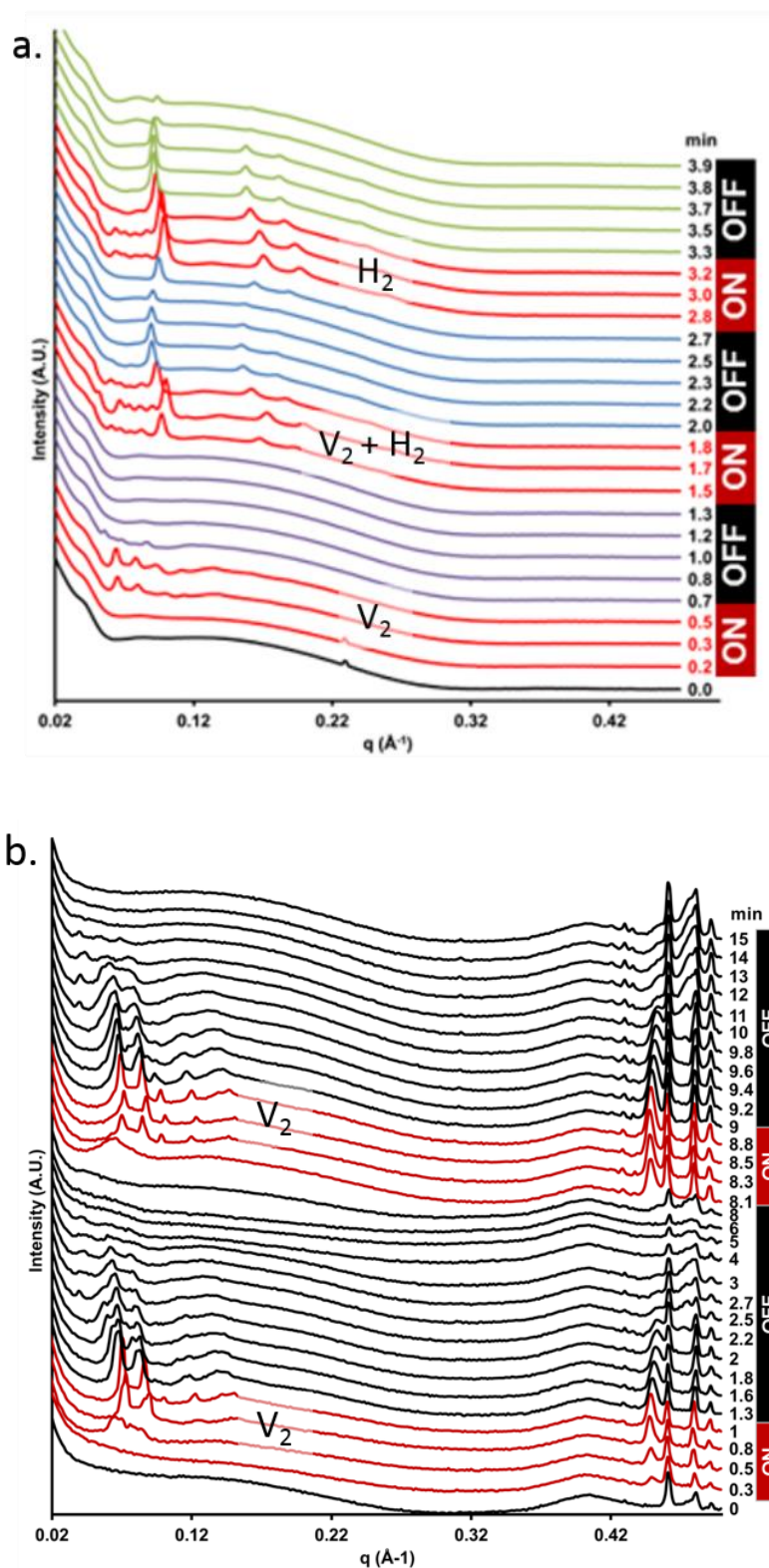


Figure 5.5 SAXS scattering profile of time-resolved activation of DLPC:2LA with a) gold nanorods (GNR), which transitions from  $L_\alpha$  to  $V_2/H_2$ , and b) silicon naphthalocyanine (SiNC), exhibiting a phase transition from  $L_\alpha$  to  $V_2$ .

#### 5.5.4. Effectiveness of NIR activation

A significant release of aflibercept was observed only upon NIR irradiation as illustrated in Figure 5.6. The addition of NIR-responsive agents to the DLPC:2LA vesicles demonstrated a slight increase in release of aflibercept without NIR irradiation, however, this change is not statistically significant in comparison to the control. Previously, activation of bacteriochlorophyll, using 800 nm light at 300 mW, corresponded to 100 % liposomal content released in 20 min.<sup>25</sup> The light-mediated release from liposomes with gold nanoparticles have also been shown to require approximately 30 min to reach 60-80 % content release.<sup>26</sup> In this study, a short 30 s exposure resulted in over 80 % release. The activation of GNR-vesicles significantly boosted the release of the loaded aflibercept ( $p=0.0008$ )  $90 \pm 9.8$  %, which is higher than the activated SiNC-vesicles ( $84 \pm 8.1$  %,  $p=0.0014$ ). Activating the phase transition to the fast releasing  $V_2$  phase is essential for effective release. Slower release were observed in previous studies involving phosphatidylcholine-based (egg lecithin and 1,2-distearoyl-sn-glycero-3-phosphocholine) liposomes due to their a strong tendency to maintain the  $L_\alpha$  structure, thereby releasing the contents via an increase in the permeability of the liposomal membrane.<sup>27</sup> The polyhedral faceted morphology of SiNC-vesicles did not affect the efficacy of the NIR activation however, the concentration of NIR agent and their absorption at the 808 nm wavelength used may have caused the photothermal heating to be less effective. The greater release observed may be attributed to the peak absorbance of the NIR-responsive agents in the phospholipid-based system. The absorption maximum of GNRs was measured to be 832.5 nm with a maxima at 1.4 A.U., which was higher than SiNC, with a maximum about 1 A.U. at 791 nm, when measured using UV-Vis spectrometry (see Figure SI 5.5). Similar high release of encapsulated contents with an initial release of  $87.5 \pm 14.4$ % (on day one) was reported for cholesterol-vesicles.<sup>28</sup> In the control formulation in this study, aflibercept remained encapsulated in the DLPC:2LA vesicles without NIR-responsive actuators, after 14 d, indicated by the similar background release detected. Although, further studies are required to increase the loading capacity of the light-sensitive vesicles while reducing the overall volume in order to deliver a bolus dose that can last for an extended period, this study confirmed

that NIR irradiation can be used to externally activate the release of drugs from the light-sensitive DLPC:zLA vesicles.

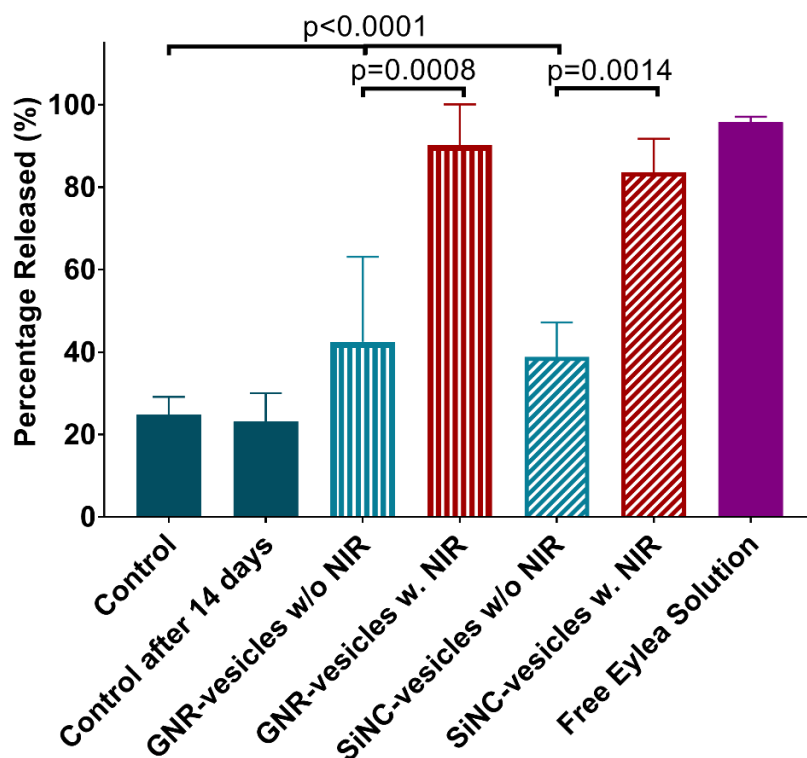


Figure 5.6 Release of aflibercept (Eylea) from DLPC:zLA vesicles (Control), passive release (Control after 14 days), DLPC:zLA vesicles with gold nanorods (GNR-vesicles) and silicon naphthalocyanine (SiNC-vesicles) with and without NIR irradiation, and the recovery of aflibercept (Free Eylea Solution) (n=3).

The release experiments employed a novel method for the quantification of aflibercept. It has been demonstrated that Protein A spin columns can be used as an alternative assay to rapidly quantify the dynamic release of anti-VEGF drugs. Although statistical significant results ( $p < 0.0001$ ) were obtained within 20 min using the Protein A spin columns, this affinity assay requires further optimisation. The current method removed the free aflibercept within minutes of incubation however, it utilises centrifugation that caused leakage from the encapsulated vesicles, owing to the friction through the resin. A low centrifugation speed of 100 x g was used throughout the experiment that resulted in a background release of around 30 %. This can be improved

by utilising a longer affinity column coupled with a peristaltic pump to control the flow rate of the buffer solution.

## 5.6. Conclusion

The DLPC:2LA system was confirmed to transition from the slow releasing lamellar ( $L_{\alpha}$ ) phase, to the fast releasing bicontinuous cubic ( $V_2$ ) phase. The incorporation of NIR-responsive actuators, GNR and SiNC, imparted NIR light sensitivity to the phospholipid-based systems. The vesicles with SiNC exhibited facettings, which is different to the spherical morphology of the control DLPC:2LA vesicles and the vesicles with GNR, which resulted in an increase in encapsulation. NIR light activation was crucial to activate the release of aflibercept from the light-sensitive vesicles. Such systems have potential to reduce the frequency of intravitreal injections, improve systemic safety by actively controlling the rate of drug release and provide a less invasive treatment option suitable for ocular delivery.

## 5.7. Acknowledgement

This research was undertaken on the SAXS/WAXS beamline at the Australian Synchrotron, VIC. JDD is supported through an Australian Government Research Training Program Scholarship. These experiments were conducted on the SAXS/WAXS beamline at the Australian Synchrotron. The research was supported by the ARC Centre of Excellence in Convergent Bio-Nano Science and Technology. WKF is supported by the Swiss National Science Foundation through the National Center of Competence in Research Bio-Inspired Materials. We would like to thank Dr Devinder Chauhan from the Vision Eye Institute, Australia for gifting the aflibercept, and Dr Rodrigo Morales from Monash University, Australia for gifting the Protein A spin trap used in these experiments.

## 5.8. References

1. Ohr, M.; Kaiser, P. K., Intravitreal aflibercept injection for neovascular (wet) age-related macular degeneration. *Exp. Opin. Pharmacother.* **2012**, *13*, 585-591.
2. Bakri, S. J.; Snyder, M. R.; Reid, J. M.; Pulido, J. S.; Ezzat, M. K.; Singh, R. J., Pharmacokinetics of intravitreal ranibizumab (Lucentis). *Ophthalmol.* **2007**, *114* (12), 2179-2182.
3. Stewart, M. W., What are the half-lives of ranibizumab and aflibercept (VEGF Trap-eye) in human eyes? Calculations with a mathematical model. *Eye Reports* **2011**, *1:e5*, 1-14.
4. Wong, W. L.; Su, X.; Li, X.; Cheung, C. M. G.; Klein, R.; Cheng, C.-Y.; Wong, T. Y., Global prevalence of age-related macular degeneration and disease burden projection for 2020 and 2040: a systematic review and meta-analysis. *Lancet* **2014**, *2*, 106-116.
5. Kauppinen, A.; Paterno, J. J.; Blasiak, J.; Salminen, A.; Kaarniranta, K., Inflammation and its role in age-related macular degeneration. *Cell. Mol. Life Sci.* **2016**, *73*, 1765-1786.
6. Balaratnasingam, C.; Dhrami-Gavazi, E.; McCann, J. T.; Ghadiali, Q.; Freund, K. B., Aflibercept: a review of its use in the treatment of choroidal neovascularization due to age-related macular degeneration. *Clinical Ophthalmology (Auckland, N.Z.)* **2015**, *9*, 2355-2371.
7. Du, J. D.; Fong, W.-K.; Caliph, S.; Boyd, B. J., Lipid-based drug delivery systems in the treatment of wet age-related macular degeneration. *Drug Deliv. Transl. Res.* **2016**, *6*, 781-792.
8. Schweizer, D.; Serno, T.; Goepferich, A., Controlled release of therapeutic antibody formats. *European Journal of Pharmaceutics and Biopharmaceutics* **2014**, *88* (2), 291-309.
9. Phan, S.; Fong, W.-K.; Kirby, N.; Hanley, T.; Boyd, B. J., Evaluating the link between self-assembled mesophase structure and drug release. *Int. J. Pharm.* **2011**, *421*, 176-182.
10. Winter, R.; Erbes, J.; H. Templer, R.; M. Seddon, J.; Strykh, A.; A. Warrender, N.; Rapp, G., Inverse bicontinuous cubic phases in fatty acid/phosphatidylcholine mixtures: the effects of pressure and lipid composition. *Phys. Chem. Chem. Phys.* **1999**, *1*, 887-893.
11. Barun, V. V.; Ivanov, A. P.; Volotovskaya, A. V.; Ulashchik, V. S., Absorption spectra and light penetration depth of normal and pathologically altered human skin. *J. Appl. Spectrosc.* **2007**, *74* (3), 430-439.
12. Newman, D. K., Photodynamic therapy: current role in the treatment of chorioretinal conditions. *Eye* **2016**, *30* (2), 202-210.
13. Du, J. D.; Hong, L.; Tan, A.; Boyd, B. J., Naphthalocyanine as a new photothermal actuator for lipid-based drug delivery systems. *J. Phys. Chem. B* **2018**, *122* (5), 1766-1770.
14. Du, J. D.; Fong, W.-K.; Salentinig, S.; Caliph, S. M.; Hawley, A.; Boyd, B. J., Phospholipid-based self-assembled mesophase systems for light-activated drug delivery. *Phys. Chem. Chem. Phys.* **2015**, *17*, 14021-14027.
15. Kirby, N. M.; Mudie, S. T.; Hawley, A. M.; Cookson, D. J.; Mertens, H. D. T.; Cowieson, N.; Samardzic-Boban, V., A low-background-intensity focusing small-angle X-ray scattering undulator beamline. *J. Appl. Crystallogr.* **2013**, *46*, 1670-1680.

16. Fong, W.-K.; Hanley, T.; Boyd, B. J., Stimuli responsive liquid crystals provide 'on-demand' drug delivery in vitro and in vivo. *J. Control. Release* **2009**, *135*, 218-26.
17. Brooks, N. J.; Ces, O.; Templer, R. H.; Seddon, J. M., Pressure effects on lipid membrane structure and dynamics. *Chem. Phys. Lipids* **2011**, *164* (2), 89-98.
18. Yeo, S. Y.; de Smet, M.; Langereis, S.; Vander Elst, L.; Muller, R. N.; Grull, H., Temperature-sensitive paramagnetic liposomes for image-guided drug delivery: Mn<sup>2+</sup> versus [Gd(HPDO<sub>3</sub>A)(H<sub>2</sub>O)]. *Biochim. Biophys. Acta* **2014**, *1838* (11), 2807-2816.
19. Chiu, G. N. C.; Abraham, S. A.; Ickenstein, L. M.; Ng, R.; Karlsson, G.; Edwards, K.; Wasan, E. K.; Bally, M. B., Encapsulation of doxorubicin into thermosensitive liposomes via complexation with the transition metal manganese. *J. Control. Release* **2005**, *104* (2), 271-288.
20. Kuntsche, J.; Horst, J. C.; Bunjes, H., Cryogenic transmission electron microscopy (cryo-TEM) for studying the morphology of colloidal drug delivery systems. *Int. J. Pharm.* **2011**, *417* (1), 120-137.
21. Briuglia, M.-L.; Rotella, C.; McFarlane, A.; Lamprou, D. A., Influence of cholesterol on liposome stability and on in vitro drug release. *Drug Deliv. Transl. Res.* **2015**, *5* (3), 231-242.
22. Joseph, R. R.; Tan, D. W. N.; Ramon, M. R. M.; Natarajan, J. V.; Agrawal, R.; Wong, T. T.; Venkatraman, S. S., Characterization of liposomal carriers for the trans-scleral transport of Ranibizumab. *Sci. Rep.* **2017**, *7* (1), 16803.
23. Dong, Y.-D.; Tilley, A. J.; Larson, I.; Lawrence, M. J.; Amenitsch, H.; Rappolt, M.; Hanley, T.; Boyd, B. J., Nonequilibrium effects in self-assembled mesophase materials: unexpected supercooling effects for cubosomes and hexosomes. *Langmuir* **2010**, *26*, 9000-9010.
24. Rappolt, M.; Hickel, A.; Bringezu, F.; Lohner, K., Mechanism of the lamellar/inverse hexagonal phase transition examined by high resolution X-ray diffraction. *Biophys. J.* **2003**, *84*, 3111-3122.
25. Thompson, D. H.; Gerasimov, O. V.; Wheeler, J. J.; Rui, Y.; Anderson, V. C., Triggerable plasmalogen liposomes: improvement of system efficiency. *Biochim. Biophys. Acta* **1996**, *1279* (1), 25-34.
26. Paasonen, L.; Laaksonen, T.; Johans, C.; Yliperttula, M.; Kontturi, K.; Urtti, A., Gold nanoparticles enable selective light-induced contents release from liposomes. *J. Control. Release* **2007**, *122* (1), 86-93.
27. Martiel, I.; Sagalowicz, L.; Mezzenga, R., Phospholipid-based nonlamellar mesophases for delivery systems: Bridging the gap between empirical and rational design. *Adv. Colloid Interface Sci.* **2014**, *209*, 127-143.
28. Araújo, J.; Garcia, M. L.; Mallandrich, M.; Souto, E. B.; Calpena, A. C., Release profile and transscleral permeation of triamcinolone acetonide loaded nanostructured lipid carriers (TA-NLC): in vitro and ex vivo studies. *Nanomedicine* **2012**, *8* (6), 1034-1041.
29. Orendorff, C. J.; Murphy, C. J., Quantitation of Metal Content in the Silver-Assisted Growth of Gold Nanorods. *J. Phys. Chem. B* **2006**, *110* (9), 3990-3994.

### 5.9. Supplementary Information

#### Hydrophobisation of PEGylated gold nanorods

PEG stabilised gold nanorods with a LSPR of 808nm (25  $\mu$ L, Nanohybrids, TX, USA) were dispersed in THF (975  $\mu$ L). The samples were then washed twice by: sonication (5 min) and centrifugation (10 min, 4150 x g) before the supernatant was aspirated and replaced with fresh THF. After the second wash, dodecanethiol was added at a rate of 9.4  $\mu$ L/mL. Hydrophobisation was then initialised by sonicating the gold nanorods for 10 min before overnight incubation. Both PEGylated and hydrophobised GNR dispersed in THF (1 mL) were loaded into a quartz cuvette (0.5 cm) and were analysed by an absorbance scan from 400 – 1000 nm on the UV-visible spectrophotometer (UV-2700, Shimadzu). The concentration of gold was calculated using the Beer Lambert Law:

$$\text{Eq. 3.} \quad A = \epsilon lc$$

Where A = absorbance,  $\epsilon$  = extinction coefficient (interpolated from <sup>29</sup>), l = path length and c = concentration. As evident in Figure 5.4, the hydrophobisation process have a batch-to-batch variation, which can result in a reduction of photothermal effect to 808 nm.

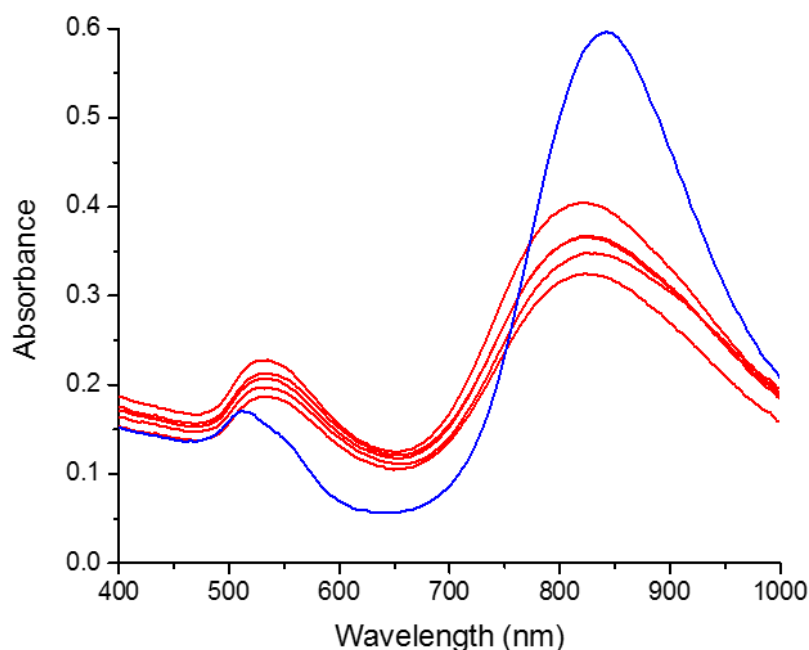


Figure SI 5.1 Confirmation of hydrophobisation by comparing the absorbance scan of PEGylated GNR (Blue) and hydrophobised GNR (Red) in THF.

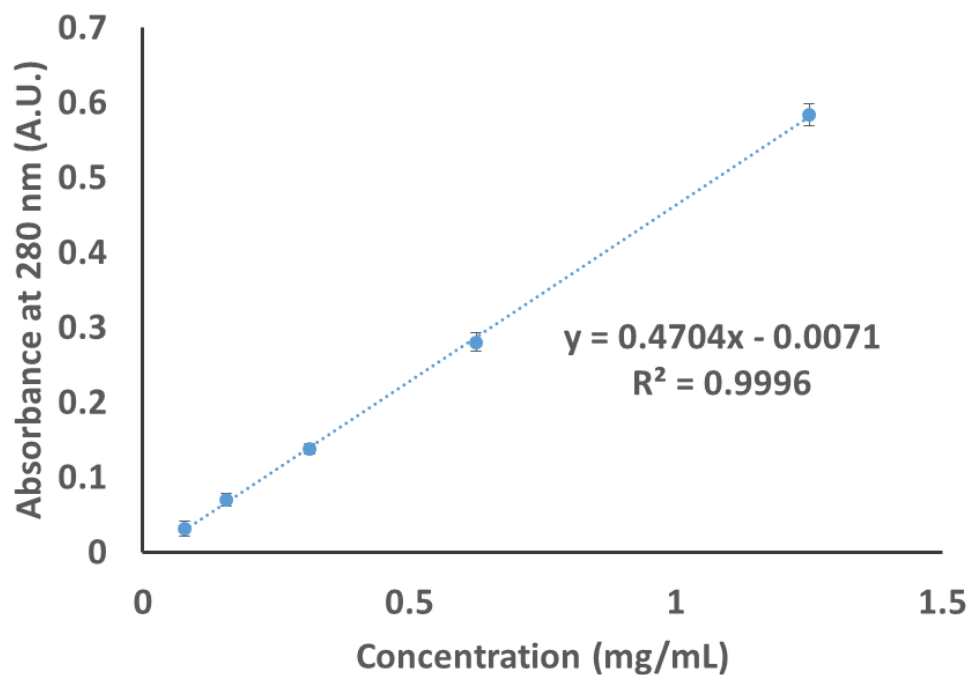


Figure SI 5.2 Quantification of Eylea using standard curve of known concentration vs. absorbance at 280 nm (n=3)

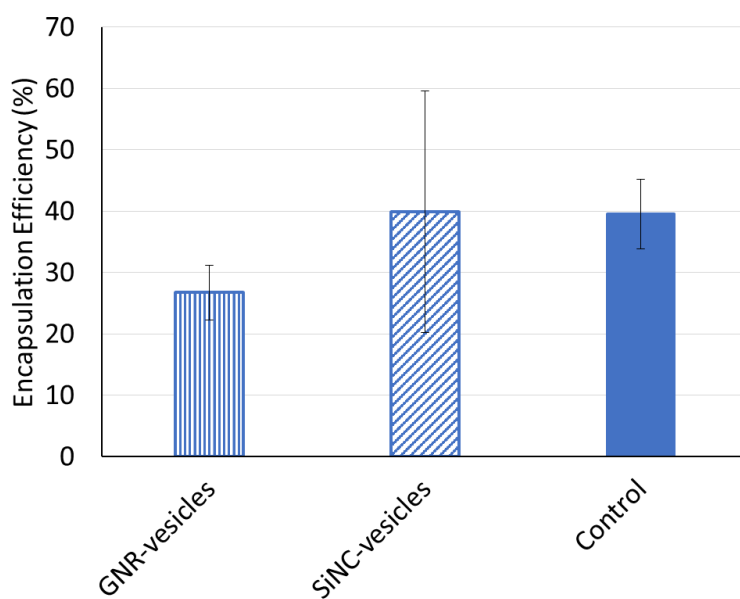


Figure SI 5.3 Encapsulation efficiency of DLPC:zLA samples with GNR, SiNC and without photoactuators (Control) (n=4)

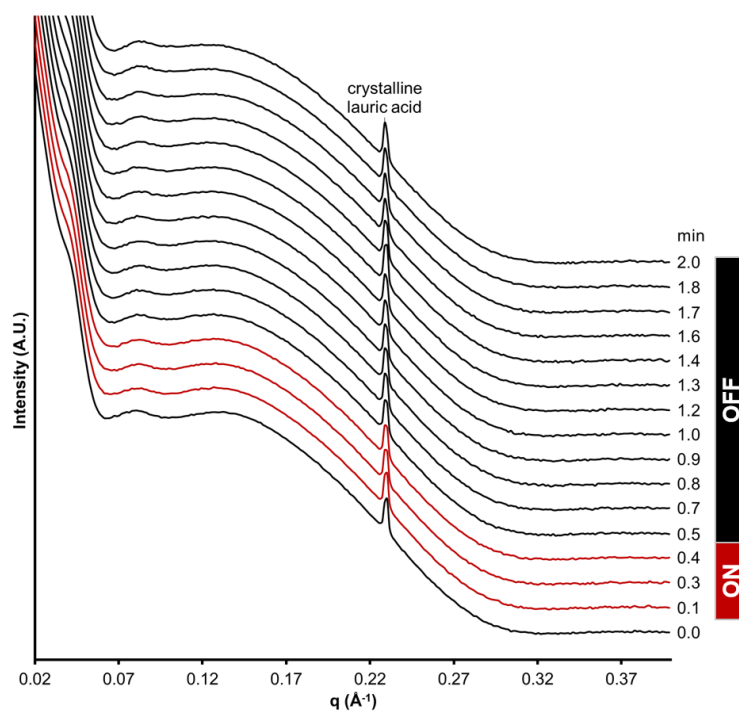


Figure SI 5.4 SAXS scattering profile of time-resolved activation of aflibercept-loaded DLPC:zLA without NIR-responsive agents.

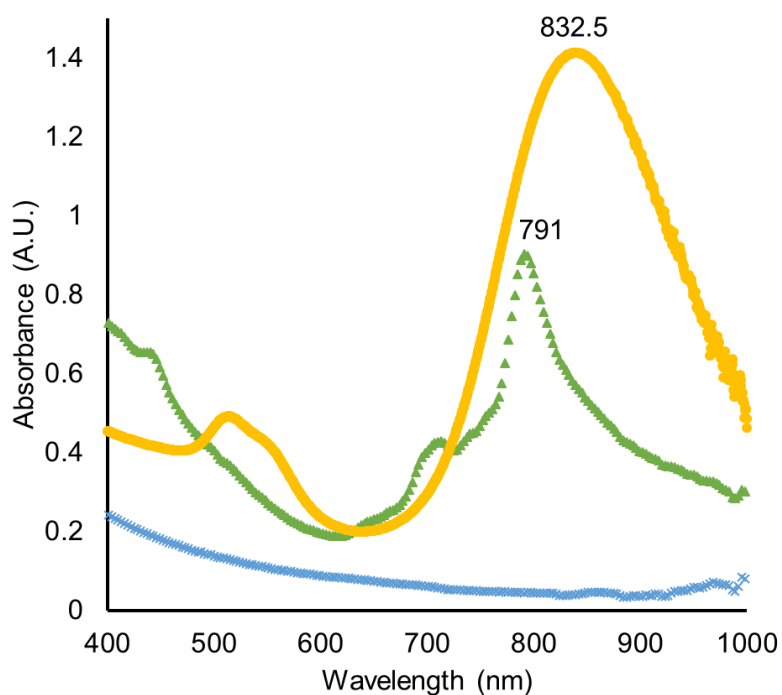


Figure SI 5.5 Absorbance spectrum of DLPC:zLA (X), with SiNC (▲) and with GNR (●)

CHAPTER SIX:  
SUMMARY AND OUTLOOK

## 6.1. Summary of Findings

Considerable efforts have been directed towards improving the current treatments for age-related macular degeneration (AMD) to reduce the substantial global burden caused by this chronic ocular disease. As mentioned in Chapter One, the approach explored in this thesis has been to design a delivery system that can reduce the frequency of the highly invasive and costly intravitreal injections using a pulsatile release strategy. The biodegradable and biocompatible nature of phospholipids, and their ability to self-assemble in excess water to form nanostructures that can be manipulated to control the release of various encapsulate drugs, makes them attractive for ophthalmic delivery. This thesis presents the phase behaviour of light-responsive phospholipid-based liquid crystalline materials that can be externally activated to release a commercially available anti-VEGF drug.

The overarching hypothesis that come from the above introduction is that the internal nanostructure of phospholipid-based systems can be rendered photo-sensitive through inclusion of near-infrared light responsive agents to allow for stimuli-responsive drug release of aflibercept via external activation.

- a. That the light-activated phase transition are reversible to provide pulsatile release of encapsulated drug.
- b. That a small molecule photosensitiser will exhibit a similar photothermal response to a particle-based actuator.
- c. That a slow to fast release profile will be demonstrated by the lamellar to bicontinuous cubic phase transition in the liquid crystal system.

The reversibility of a phospholipid system, 20 mol% cholesterol in 1-palmitoyl-2-oleoyl-sn-glycero-3-phosphoethanolamine (POPE), was investigated in Chapter Three. The phase behaviour of the POPE-based system was previously reported to transition from  $L_{\alpha}$  to  $V_2$  phase with increasing temperature. It was hypothesised that such a system will exhibit a slow to fast drug release profile upon external manipulated in order to activate drug release when required. Contrary to literature, no  $V_2$  phase was observed, instead, a transition to the inverse hexagonal ( $H_2$ ) phase occurred between 10-30 mol%

cholesterol. The  $H_2$  phase has been shown to exhibit a much slower release rate than  $V_2$  phase, due to the smaller water channels and closed rod-like micellar structure. Although the POPE-based system did not exhibit the 'ideal' phase transition from  $L_\alpha$  to  $V_2$ , the  $L_\alpha$  to  $H_2$  phase transition was thought to still have the potential to function as a reversible pulsatile release system and was thus pursued as a proof-of-concept to determine whether phospholipid-based mesophases could be rendered responsive to near-infrared laser (NIR) irradiation. Low concentrations of gold nanorods (GNR) were incorporated into the POPE-based system to induce photothermal heating upon activation. The inclusion of 3 nM GNR in the POPE systems induced reversible disruption of lipid packing, which was found to be equivalent to increasing the apparent temperature of the matrix to 55°C when irradiated for 30 s. The addition of polyethylene glycol was investigated as it may increase the residence time of the phospholipid-based carriers when delivered to the site of inflammation however, it was found to negate the phase transition, exhibiting partial reversibility. An incomplete phase transition will restrict the change in the rate of drug release. This will limit the drug release from the system however, a PEGylated system may not be necessary when delivering intravitreally. Nevertheless, this chapter confirmed that although the previously published phase behaviour was not correct, GNR and NIR could be used to manipulate the self-assembled mesophases in phospholipid-based systems, and highlighted the potential for a phospholipid-based light-activated drug delivery system.

The use of photo-sensitive 'actuators' can provide control over the rate of drug release from lipid-based systems. As such, this thesis focused on incorporating NIR-sensitive materials as this wavelength of light can safely penetrate through some biological barriers and light stimuli can be easily applied externally. The practicality of particle-based actuators, like GNR, may be limited by the reduction of the photothermal effect due to the uncertainty about their distribution relative to the lipid bilayer, and their potential dissociation from the lipid-based carrier after administration. Therefore, alternative NIR light responsive materials were also investigated in order to overcome the issues with particle-based actuators. Although, not included in the main body of this thesis, alternative NIR-responsive agents, namely graphene nanoparticles and

donor-acceptor Stenhouse adducts, were utilised and the corresponding publications are included in the Appendix.

In Chapter Four, the photothermal effect on lipid-based systems for alternative NIR-responsive agents were evaluated. Specifically, a molecular actuator, silicon 2,3-naphthalocyanine bis(trihexylsilyloxy) (SiNC), was compared to particle-based actuators, GNR and graphene. The addition of SiNC within the lipid structure imparted light sensitivity to phytantriol and phospholipid-based liquid crystalline mesophases. Toxicity is not anticipated as the increase in temperature was observed only locally, where the NIR-responsive agents are located on the lipid-based carriers and not globally, suggesting that photothermal heating would not cause damages to surrounding tissues. The SiNC-containing lipid systems required a shorter irradiation time to elicit a complete phase transition when compared to the phase transitions induced using particle-based actuators. The photodynamic properties, efficiency in controlling the phase structure and ultimately, the release of drug, suggest that SiNC-actuated lipid systems have potential to reduce the burden of repeated intravitreal injections. The lipids studied in this chapter were known to transition to the slow-releasing H<sub>2</sub> phase and inverse micellar (L<sub>2</sub>) phase structures. They were selected because they are established platforms known to be responsive to other photothermal stimuli, however, their phase behaviour will result in a release profile that is not ideal for on-demand drug release application. Consequently, a phospholipid-based system with potential to exhibit a slow to fast release profile was investigated in the final experimental chapter of this thesis.

The studies in Chapter Five confirmed that a different phospholipid system based upon the combination of 1,2-dilauroyl-sn-glycero-3-phosphocholine (DLPC) and lauric acid (LA) at a 1:2 molar ratio exhibited the ideal phase transition. It was found that activation of the aflibercept-loaded DLPC:2LA vesicles with 30 s NIR irradiation triggered the phase transition to the V<sub>2</sub> phase and the change in structure corresponded to an almost complete release of encapsulated an anti-VEGF drug. Specifically, the release of aflibercept, encapsulated in DLPC:2LA vesicles with either GNR or SiNC was quantified using the Protein-A Spin Trap. Although significant differences between the release from the control and light-responsive systems was observed, further

optimisation of the method is required. The first suggestion is to reduce the multiple wash sequence when debinding the anti-VEGF drug. This can be achieved by adding an incubation period to allow the resin to equilibrate and reach the low pH that is required for debinding. The wide deviation is due to batch-to-batch variability when purifying individual liposomal samples of 250  $\mu\text{L}$ . Larger affinity columns attached to a peristaltic pump can control the flow rate of the buffer solutions and allow greater loading volumes of liposomal dispersions. This will ultimately reduce the background release while increasing the reproducibility when purifying the encapsulated liposomes. The complete recovery of aflibercept should also be investigated to confirm that the concentration of drug in the supernatant and inside the vesicles adds up to 100 %. This can be achieved by destroying the loaded vesicles using a surfactant solution such as Triton X-100. Nonetheless, the current release results confirmed that the closed  $L_{\alpha}$  structure exhibits little or no drug release as the drugs are encapsulated within the phospholipid-based vesicles, and fast drug release can be triggered via a phase transition to the open  $V_2$  structure.

Overall, the hypotheses were well supported by the conclusions reported in this thesis. The identification of the systems proposed in this thesis is the initial step towards a viable on-demand drug delivery product. Although only one activation cycle was obtained in this thesis, such a system can potentially half the required injection frequency. However, further development is required to translate these phospholipid-based systems into actual products.

## 6.2. Future Directions

There is a growing market to develop novel ophthalmic drug delivery technologies to deliver commercially available drugs in a more cost effective, efficient and patient friendly manner. As mentioned in Chapter One, pulsatile light-responsive drug delivery systems have potential to reduce the frequency of intravitreal injections (as illustrated in Figure 1.5) and will help to avoid complications and poor compliance associated with the current treatment for AMD. The system described in this thesis exhibited a complete burst release of the encapsulated drug, resulting in a maximum of 40% of the recommended therapeutic dose (2 mg) currently administered intravitreally. Due to the

limitation of the current aflibercept intravitreal injections as mentioned in Chapter One, the concentration is in excess and may not necessarily be relevant when utilising the depot strategy. Currently, the system described in Chapter Five have potential to half the frequency of injection as it can be activated once. Further studies are required to verify the efficacy of the system and for it to be practical for pulsatile delivery, this system requires further optimisation in order to deliver multiple doses for an extended period of at least 6 months. It should also be noted that the addition of aflibercept causes an increase in the phase transition temperature as illustrated in Figure 5.2. Therefore, further studies may be required to determine whether a higher concentration of aflibercept is necessary. This is because upon activation, the aflibercept concentration will reduce and may reach a point where the drug loading is completely released due to the drop in transition temperature. Given that the volume of the single injection is restricted to 0.1 mL to avoid adverse events such as increased intraocular pressure, multiple doses can only be achieved by increasing the concentration of encapsulated drug and optimising the duration of irradiation time to obtain the required unit dose per light treatment. This can be achieved by utilising active drug loading methods with higher concentration of aflibercept stock solution, and adjusting the power of the radiation source. After optimising this system, it is highly possible that the system will show therapeutic results in future studies.

While these light-responsive systems are designed for *in vivo* applications and biocompatible phospholipids and NIR elements were used, the compatibility of the combination of the biocompatible materials with relevant biological components are not well understood. The logical progression to translate these new technologies with existing drug into products will require stringent validation using cell culture and/or animal models to conduct *ex vivo* and *in vivo* experiments. Further investigations are required to determine whether there will be changes in activity of the drug, stability of the formulation and safety of the light-sensitive nanomaterial *in vivo*. There have been a number of developed animal models of choroidal neovascularization (CNV) which provide an intermediate step between *in vivo* experimentation and human clinical trials.<sup>1</sup> There are rodent and non-rodent species such as rabbits and primates, however, there is a number of differences in ocular anatomy of common animal models to human

as listed in Table 1. The species that have the most comparative weight of the vitreous humour and length of vitreous path to human (3.9 g and 1.65 cm) is pig at 3.6 g and 1.70 cm, respectively.<sup>2</sup> To test the efficacy of the system as a treatment for AMD, it will best to use the currently accepted disease model of the leaky neovascularization characteristics, which is the laser-induced CNV mice model.<sup>3</sup> While animal studies are deemed necessary, the number of animals used during the whole development process should be reduced when possible. To this date, no standard *in vitro* ocular models are available for studying drug release, permeation, absorption, and ocular toxicity. Considerable efforts have been focused on developing *in vitro* models derived from human cells however, regular 2D cell-based *in vitro* experiments cannot adequately recreate the *in vivo* complexity of the eye.<sup>4</sup> A recent study have demonstrated the possibility of a 3D spheroid culture with corneal endothelial layers.<sup>5</sup> This suggests that a robust 3D ocular biomimetic platform can be established and will most likely be the future for preclinical research in ophthalmology.

Table 1. Ocular anatomy of common animal model species

<b>Eyes from</b>	<b>Axial Length (mm)</b>	<b>Corneal Thickness (mm)</b>	<b>Anterior Chamber Depth (mm)</b>	<b>Lens Thickness (mm)</b>	<b>Ref.</b>
<b>Human</b>	23.92	0.55	3.05	4.0	6
<b>Monkey</b>	17.92	0.55	3.24	2.98	7
<b>Dog</b>	20.8	0.64	4.29	7.85	8
<b>Rabbit</b>	18.1	0.4	2.9	7.9	9
<b>Rat</b>	6.29	0.26	0.88	3.71	10
<b>Mouse</b>	3.37	0.1	0.25	2.0	11

Alternatively, there is a possibility to modify the current phospholipid system to remove the need of intravitreal injections altogether. With the present safety concern of repeated intravitreal injections and long-term anti-VEGF inhibition mentioned in Chapter One, selective delivery to the target site is crucial. Systemic administration of free drug with the intention of treating the posterior segment is currently limited by lack of access of anti-VEGF molecules to the site of disease due to the blood-retina barrier and limited circulatory half-life. One opportunity that is gaining interest is using ‘passive’ targeting of liposomes to the site of AMD. Liposomes in the ‘naked’ unmodified

state (Figure 6.1, left hand side) are rapidly cleared from circulation, whereas those that have been surface modified with a ‘stealth’ polyethylene glycol (PEG) coating display extended systemic residence times. The circulation time could be extended from 30 min to 24-48 h.<sup>12</sup> Stealth liposomes avoid non-specific removal from the circulatory system by the mononuclear phagocyte system (MPS).<sup>13</sup> The PEG coating and consequent long circulation time has been shown to assist particle uptake through leaky vasculature in tumours, attributed to the enhanced permeation and retention (EPR) effect. These nanoparticles can extravasate into tumour sites due to the poorly formed, leaky vasculature, where gaps up to several hundreds of nanometres in size can occur, and in the absence of lymphatic drainage can be retained in the interstitial tissues.<sup>14</sup>

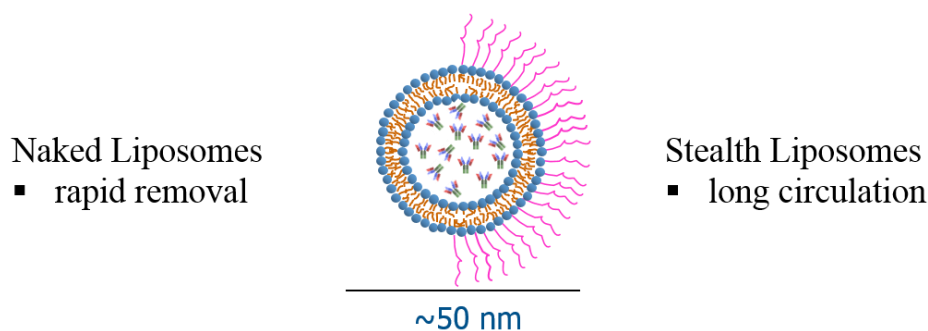


Figure 6.1 Schematic comparing liposomes behaviour depending on their surface characteristics. Reproduced with permission from <sup>15</sup>.

In the case of AMD, the leakiness of the blood vessels that leads to the symptomatic obscuration of vision may present an opportunity for delivery via the EPR effect that is not present in healthy retinal tissues (Figure 6.2). It has been reported that the anatomical characteristics of wet AMD are similar to tumour sites, such that the blood vessels formed during CNV exhibit hyper-permeability with little drainage. For instance, fluorescently labelled polymer (PVA) was shown to accumulate in the retinal tissues of mice with CNV compared to control non-CNV mice.<sup>16</sup> Along similar lines, fluorescent labelled polyion-complexes, PEG-micellar particles approximating 50 nm in size, have also been shown to accumulate in ocular tissues of rats with induced CNV after intravenous administration.<sup>17</sup> Consequently, it could be hypothesized that systemically administered stealth liposomes may deliver anti-VEGF drugs systemically to the macula at greater concentration than administering free drug alone, although the

potential and level of drug accumulation has yet to be realised. The release of the drug from the liposomes will need to be considered due to the low permeability of large macromolecules. As mentioned previously, the overexpression of phospholipases in tumours is responsible for the breakdown of the bilayer and release of the therapeutic payload. It remains uncertain whether enzymatic activity would be sufficient in AMD to induce substantial leakage. Therefore, a stimuli-responsive system such as the one described in this thesis, may be essential for the translation of these lipid carriers to therapeutic products.

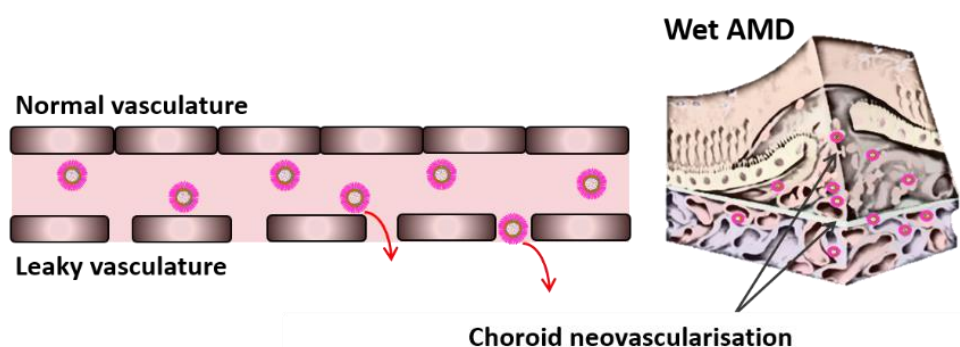


Figure 6.2 Schematic showing the accumulation of stealth liposomes via EPR effect. Reproduced with permission from <sup>15</sup>.

In conclusion, light-responsive lipid-based systems are an emerging technology that can transform the future for pharmaceutical treatments. Since the discovery of liposomes in 1964,<sup>18</sup> significant progress have been made towards commercialisation of further liposomal formulations including improvements in production methods, their colloidal and chemical stability, and their drug encapsulation efficiency. However, their uncontrollable release rate limits their application in long-term drug delivery. The concept to utilise a stimulus to activate and control the release from drug carriers was first introduced for polymeric system around the year 2000.<sup>19-20</sup> Applying a stimulus to lipid-based system have only occurred in the past decade. As such, it is still a novel field and the understanding achieved in this thesis was a fundamental step to eventually translate these systems to products. Future research into these materials will be of great interest and it will be exciting to witness future treatments that utilises this technology to provide a more sustainable, less invasive and longer lasting treatment for other chronic diseases.

## 6.3. References

1. Grossniklaus, H. E.; Kang, S. J.; Berglin, L., Animal models of choroidal and retinal neovascularization. *Prog. Retin. Eye Res.* **2010**, *29* (6), 500-519.
2. Laude, A.; Tan, L. E.; Wilson, C. G.; Lascaratos, G.; Elashry, M.; Aslam, T.; Patton, N.; Dhillon, B., Intravitreal therapy for neovascular age-related macular degeneration and inter-individual variations in vitreous pharmacokinetics. *Prog. Retin. Eye Res.* **2010**, *29* (6), 466-475.
3. Lambert, V.; Lecomte, J.; Hansen, S.; Blacher, S.; Gonzalez, M.-L. A.; Struman, I.; Sounni, N. E.; Rozet, E.; de Tullio, P.; Foidart, J. M.; Rakic, J.-M.; Noel, A., Laser-induced choroidal neovascularization model to study age-related macular degeneration in mice. *Nat. Protoc.* **2013**, *8*, 2197.
4. Shafaie, S.; Hutter, V.; Cook, M. T.; Brown, M. B.; Chau, D. Y. S., In vitro cell models for ophthalmic drug development applications. *Biores. Open Access* **2016**, *5* (1), 94-108.
5. Li, S.; Han, Y.; Lei, H.; Zeng, Y.; Cui, Z.; Zeng, Q.; Zhu, D.; Lian, R.; Zhang, J.; Chen, Z.; Chen, J., In vitro biomimetic platforms featuring a perfusion system and 3D spheroid culture promote the construction of tissue-engineered corneal endothelial layers. *Sci. Rep.* **2017**, *7* (1), 777.
6. Deering, M. F., A photon accurate model of the human eye. *ACM Trans. Graph.* **2005**, *24* (3), 649-658.
7. Lapuerta, P.; Schein, S. J., A four-surface schematic eye of macaque monkey obtained by an optical method. *Vision Research* **1995**, *35* (16), 2245-2254.
8. Mutti, D. O.; Zadnik, K.; Murphy, C. J., Naturally occurring vitreous chamber-based myopia in the Labrador retriever. *Investigative Ophthalmology & Visual Science* **1999**, *40* (7), 1577-1584.
9. Hughes, A., A schematic eye for the rabbit. *Vision Research* **1972**, *12* (1), 123-126.
10. Hughes, A., A schematic eye for the rat. *Vision Research* **1979**, *19* (5), 569-588.
11. Schmucker, C.; Schaeffel, F., A paraxial schematic eye model for the growing C57BL/6 mouse. *Vision Research* **2004**, *44* (16), 1857-1867.
12. Ponce, A.; Wright, A.; Dewhirst, M.; Needham, D., Targeted bioavailability of drugs by triggered release from liposomes. *Future Lipidol.* **2006**, *1* (1), 25-34.
13. Yamauchi, H.; Yano, T.; Kato, T.; Tanaka, I.; Nakabayashi, S.; Higashi, K.; Miyoshi, S.; Yamada, H., Effects of sialic acid derivative on long circulation time and tumor concentration of liposomes. *Int. J. Pharm.* **1995**, *113* (2), 141-148.
14. Maeda, H.; Nakamura, H.; Fang, J., The EPR effect for macromolecular drug delivery to solid tumors: Improvement of tumor uptake, lowering of systemic toxicity, and distinct tumor imaging in vivo. *Adv. Drug Deliv. Rev.* **2013**, *65* (1), 71-79.
15. Du, J. D.; Fong, W.-K.; Caliph, S.; Boyd, B. J., Lipid-based drug delivery systems in the treatment of wet age-related macular degeneration. *Drug Deliv. Transl. Res.* **2016**, *6*, 781-792.
16. Kimura, H.; Yasukawa, T.; Tabata, Y.; Ogura, Y., Drug targeting to choroidal neovascularization. *Adv. Drug Deliv. Rev.* **2001**, *52* (1), 79-91.
17. Ideta, R.; Yanagi, Y.; Tamaki, Y.; Tasaka, F.; Harada, A.; Kataoka, K., Effective accumulation of polyion complex micelle to experimental choroidal neovascularization in rats. *FEBS Letters* **2004**, *557* (1-3), 21-25.

18. Deamer, D. W., From “Banghasomes” to liposomes: A memoir of Alec Bangham, 1921–2010. *FASEB J.* **2010**, *24* (5), 1308-1310.
19. He, C.; Kim, S. W.; Lee, D. S., In situ gelling stimuli-sensitive block copolymer hydrogels for drug delivery. *J. Control. Release* **2008**, *127* (3), 189-207.
20. Gil, E. S.; Hudson, S. M., Stimuli-responsive polymers and their bioconjugates. *Prog. Polym. Sci.* **2004**, *29* (12), 1173-1222.

## APPENDIX:

Original publications included in this section were completed during candidature that were either: (A) adapted for the thesis or (B) did not contribute to the overall coherent flow of the thesis.

# Lipid-based drug delivery systems in the treatment of wet age-related macular degeneration

Joanne D. Du<sup>1</sup> · Wye-Khay Fong<sup>1,2</sup> · Suzanne Caliph<sup>1</sup> · Ben J. Boyd<sup>1,3</sup>

© Controlled Release Society 2016

**Abstract** Recent advances in drug delivery technology have amplified potential opportunities to treat the debilitating diseases that affect the posterior segment of the eye in a less invasive and more efficient manner. Current methods for effective drug delivery to the back of the eye are hindered by many barriers and limitations. As a consequence, considerable efforts have been directed towards developing new materials to selectively deliver drug directly to the target site. This review focuses on lipid-based delivery systems which show promise in improving treatment for the most common disease of the posterior segment of the eye in the developed world, age-related macular degeneration, with an emphasis upon on-demand delivery systems as they have greater potential to overcome the current limitations.

**Keywords** Age-related macular degeneration · Lipids · Liposomes · Intravitreal · Stimuli responsive

## Introduction

Treatment of diseases that affect the posterior segment of the eye remains highly challenging due to the numerous anatomical

and physiological barriers which normally protect the eye from harm, such as the cornea and conjunctiva, the blood-aqueous barrier, the blood-retinal barrier and the barrier effect imparted by the inner limiting membrane that lines the neurosensory retina/vitreous interface. In particular, age-related macular degeneration (AMD) is the leading cause of irreversible vision impairment and blindness in Australia, the USA and Europe. It is a disease that affects over 30 million people worldwide [1–3]. The preferred therapeutic approach for drug delivery to the eye is eye drops; however, for delivery to the posterior section of the eye, periocular injections, systemic intravenous injections and intravitreal injections are typically required, the latter being the most effective technique as it delivers therapeutics directly into the vitreous, near the site of action. Although intravitreal injections are effective, they are highly invasive and have many limitations including patient non-compliance issues and risk of vitreous haemorrhage, retinal detachment and the development of cataracts [4–6]. Thus, novel materials for safer and more effective delivery of drugs are emerging to overcome these barriers.

This review focuses specifically on lipid nanotherapies for the treatment of wet AMD (Fig. 1). Briefly, this disease affects the macular region of the retina resulting in the loss of central vision by causing damage to the retinal pigment epithelium (RPE), a layer underneath the neurosensory region of the retina. The RPE is responsible for nourishing the photoreceptors in the retina via the main blood supply to the eye, the choroid vasculature, as well as removing waste products from photoreceptor cells, and visual pigment transport and regeneration [8]. The Bruch's membrane separates the RPE and the choroid layer which can thicken with age, slowing the transport of metabolites and consequently the formation of subretinal deposits called 'drusen'. The extent of accumulation of drusen under the RPE and the amount of hypopigmentary or hyperpigmentary changes of the RPE are characteristics of

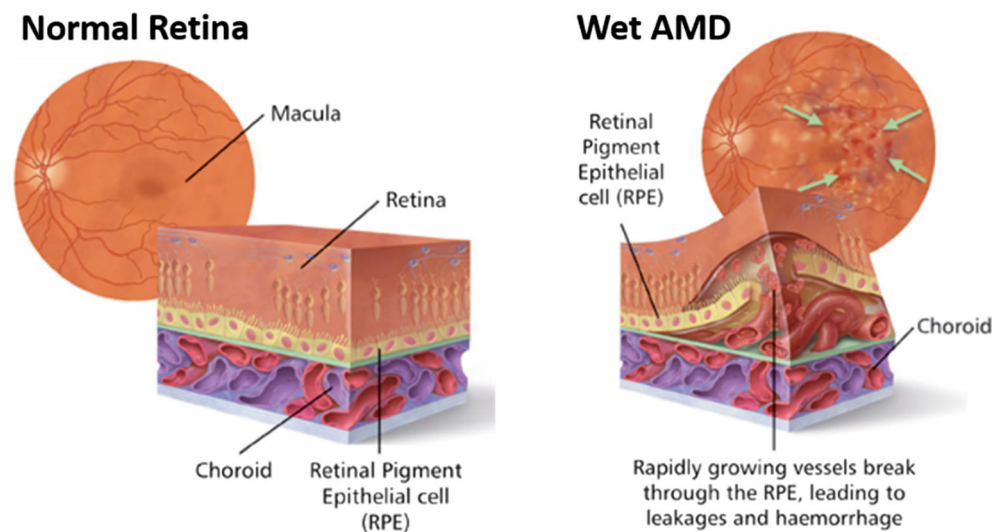
✉ Ben J. Boyd  
ben.boyd@monash.edu

<sup>1</sup> Drug Delivery, Disposition and Dynamics, Monash Institute of Pharmaceutical Sciences, Monash University (Parkville Campus), 381 Royal Parade, Parkville, VIC 3052, Australia

<sup>2</sup> Department of Health Sciences & Technology, ETH Zürich, 8092 Zürich, Switzerland

<sup>3</sup> ARC Centre of Excellence in Convergent Bio-Nano Science and Technology, Monash Institute of Pharmaceutical Sciences, Monash University (Parkville Campus), 381 Royal Parade, Parkville, VIC 3052, Australia

**Fig. 1** Schematic of normal retina vs. diseased retina with wet age-related macular degeneration (AMD). Adapted with permission from [7]



AMD [4, 9]. In addition, it has been recently shown that ageing impairs the ability of macrophages to effectively efflux intracellular cholesterol, which leads to higher levels of free cholesterol within ageing macrophages, resulting in a phenotype of monocyte that promotes vascular proliferation [10]. As the disease progresses, severe vision loss occurs in one of two forms: (1) dry AMD or geographic atrophy, which results in a gradual reduction of central vision over many years due to the progressive atrophy of the RPE, choriocapillaris and photoreceptors, (2) wet AMD or neovascular AMD occurs due to choroidal neovascularisation (CNV). This occurs when endothelial cells proliferate in the choroid and angiogenic blood vessels enter the RPE through a break in the Bruch's membrane and rapidly grow under the retina into the subretinal pigment epithelium or the subretinal space as illustrated in Fig. 1 [4]. Leakage of fluids and bleeding from the vessels cause fibrous scarring and lead to a rapid loss of central vision.

### Problems associated with current treatment for wet AMD

Currently, only palliative treatment is available for wet AMD. The abnormal neovasculature creating unusual leaky blood vessels has been predominantly attributed to an overexpression of vascular endothelial growth factor (VEGF). To slow this progress, drugs that block this protein, anti-VEGF drugs, were developed. The use of anti-VEGF drugs has been reported since early 2000s in the treatment of neovascularization in cancer and in more recent times for the symptomatic treatment of neovascularization in wet AMD [11].

Anti-VEGF drugs are currently delivered as a bolus intravitreal injection directly into the vitreous due to limited uptake and ocular penetration [12–14]. Although the injection is not painful, the major issues to date are, firstly, the short intraocular retention time of the actives due to the high clearance rate

from the posterior section of the eye. Anti-VEGF drugs have a short residence time in the vitreous humour, thus requiring high frequency of intravitreal administrations, in some cases monthly injections for life. Direct injections of anti-VEGF drugs provide a high local concentration in the ocular tissue, which declines in an exponential fashion over 29 days with a half-life of 2.88 days [15], meaning that most of the administered drug is cleared without exerting any therapeutic effect. Secondly, the injections require a high degree of sterility to prevent infection and, if not performed correctly, can result in endophthalmitis, which in extreme cases require vitrectomy to treat. Long-term anti-VEGF treatment also carries a high financial burden, for instance, Lucentis® (Genentech/Novartis) costs about US\$2000 per treatment [16]. With ageing populations in many industrialised countries, the financial implications for health budgets of the individual as well as the economy are critical and likely to be unsustainable with the current treatment regime. This highlights the need for a cost-effective drug delivery approach that can deliver an effective dose to the ocular treatment site whilst minimising side effects.

Current FDA-approved treatments including pegaptanib (Macugen™, Eyetech and Pfizer) [12], ranibizumab (Lucentis®, Genentech/Novartis) [13] and aflibercept (Eylea®, Regeneron and Bayer) [14] have been shown to successfully control the symptoms of wet AMD when delivered monthly up to 2 years; however, safety and cost concerns still remain. An option to improve the safety and impact on patients receiving anti-VEGF treatment is to reduce the frequency of intravitreal administration. In the absence of a sustained-release material, this would involve increasing the residence time and therapeutic duration of action of the 'free' antibody treatment, which is difficult to achieve, as antibody treatments typically have short residence times in body tissues. The latest anti-VEGF drug, aflibercept (Eylea®, Regeneron and Bayer), was developed to reduce the treatment burden on patients by increasing the dosing regimen to

8 weeks. This is possible due to the higher binding affinity of the molecule in the eye, allowing for a more targeted treatment [14]. However, the high cost (~US\$1850 per dose) remains a limiting factor for adoption of this treatment. Bevacizumab (Avastin<sup>®</sup>, Genentech), a treatment approved for metastatic colon cancer in 2004, has been used as an off-label alternative treatment due to the alleged comparable efficacy with ranibizumab but at a much lower price, where one intravitreal dose of ranibizumab (~US\$2000) is at least 40-fold higher than the cost of bevacizumab (~US\$50) [16]. However, Avastin<sup>®</sup> has not been subjected to formal clinical trials and, hence, remains an unapproved option not subsidised by health providers consequently limiting its adoption. Individualised anti-VEGF treatment regimens such as ‘as-needed therapy’ and the ‘treat-and-extend strategy’ have also been investigated to find a safer and more cost-effective alternative to the traditional monthly treatments; however, the frequency of treatment remains high for most patients [17].

There are also other actives in addition to the anti-VEGF-based treatments that are currently in clinical development to inhibit both VEGF and VEGF gene expression [18], such as tyrosine kinase inhibitors and nucleotides. Corticosteroids and anti-inflammatory drugs such as triamcinolone [19, 20] have also been investigated for angiogenic ocular diseases; however, the risks of elevated intraocular pressure, glaucoma and cataracts make such treatment less desirable [21] and have been excluded from this review.

The main biopharmaceutical challenge in the treatment of AMD therefore is to improve therapy from a patient’s perspective, which will involve reducing the frequency of, or removing altogether the need for, intravitreal injections. This is unlikely to be overcome through molecular modification of the drug itself. It has been recently postulated that controlling cholesterol levels in the eye via the use of statins or nucleic acid-based therapies will also result in the successful treatment of AMD [22]. However, as these drugs have systemic effects and considering the time required for clinical translation, there is an increasing interest in the use of smart materials for active drug delivery in order to selectively target the posterior section of the eye. As a result, there has been considerable effort directed towards the development of novel delivery systems, in particular, sustained-release systems of already approved anti-VEGF drugs to ultimately reduce the required frequency of intravitreal injections.

### Opportunities and limitations of emerging delivery systems for the treatment of AMD

Since the introduction of anti-VEGF therapy, substantial efforts have been made towards the development of new materials to more effectively deliver anti-VEGF drugs in a less invasive manner and at a lower cost. Ideally, new proposed

treatments for AMD aim to either reduce the frequency of the highly effective but highly invasive intravitreal injections or provide greater patient compliance via a safer route of administration. Much attention has been directed towards implanted polymeric intravitreal devices [23] and liposomal systems (Table 1), with the latter being of specific interest due to the biocompatibility of the lipid materials and the ability for controlled drug release.

Polymers are a popular means of modifying the availability of drug after administration to provide a slow release effect. Drug-containing polymer systems for this purpose fall into two general classes—non-biodegradable implants and biodegradable implants. Non-biodegradable implants have the advantage of providing very long-term sustained release of drug; however, the device is often limited by the need to be surgically implanted, and removed and replaced when the drug load is depleted. Surgical implantation procedures have also been known to cause other acute and long-term complications such as retinal detachment and suprachoroidal and vitreous haemorrhage [32]. Therefore, non-biodegradable implants can only be practical if the device can be tolerated within the eye for an extended period of time. On the other hand, soft biodegradable implants do not require removal and may be amenable to injection as a non-surgical procedure. To date, there are a number of products on the ocular delivery market using polymeric devices to provide a sustained-release effect for small molecule steroidal compounds; however, to date, there are no products using these systems for anti-VEGF drugs. An alternative class of biocompatible polymeric devices for the delivery of anti-VEGF drugs is hydrogels. Hydrogels have been investigated because like some conventional polymer implants, they have a macroporous structure that sustains the release of macromolecular drugs after implantation [33]. However, translation of hydrogels as drug delivery systems in products is still in its infancy, where further studies are required to completely understand the effect of the shape, size and site of placement of the hydrogel implant on drug delivery. A recent study has also reported that some charged polymeric nanoparticles can penetrate the vitreal barrier and reach the inner retinal structure [34].

Given the potential difficulties in translation of new polymeric systems for extended treatment of wet AMD, it is our contention that new developments in drug delivery approaches are more likely to come from lipid-based materials such as liposomes (nanoparticles with a spherical bilayer structure which encloses an inner aqueous compartment, see Fig. 2). There are more than two decades of research on liposomes and a number of recent reviews have summarised the developments of liposomal research in the field of ocular delivery (Table 1). This review will focus on the potential for lipid-based systems, including liposomes to improve the treatment of wet AMD with an emphasis on novel lipid-based systems to provide on-demand drug delivery.

**Table 1** Recent reviews detailing liposomal systems for ophthalmic drug delivery

Title of review	Year	Ref.
Delivery strategies for treatment of age-related ocular diseases: from a biological understanding to biomaterial solutions	2015	[24]
Drug delivery techniques for treating age-related macular degeneration	2014	[25]
Liposomes and nanotechnology in drug development: focus on ocular targets	2014	[26]
Nanotherapy for posterior eye diseases	2014	[27]
Drug delivery implants in the treatment of vitreous inflammation	2013	[28]
Liposomes for intravitreal drug delivery: a state of the art	2012	[29]
Recent applications of liposomes in ophthalmic drug delivery	2011	[30]
A review of implantable intravitreal drug delivery technologies for the treatment of posterior segment eye diseases	2010	[31]

## Liposomes as delivery systems for improving the treatment of AMD

Amphiphilic phospholipids often self-assemble to form lipid bilayers that, when dispersed, can form vesicular nanoparticles termed liposomes. The bilayer encloses an inner aqueous compartment that can encapsulate hydrophilic molecules, including peptide and proteins, indicating their applicability to encapsulate anti-VEGF biological drugs. The biodegradable and biocompatible nature of phospholipids makes these attractive for ophthalmic delivery. There are nine clinical trials determining the safety and efficacy of liposomal systems in the treatment of ocular conditions including dry eye, ocular hypertension, glaucoma, intraocular retinoblastoma, blepharitis and macular oedema [35]; however, none are for the treatment of AMD specifically. This section will explain how liposomes can potentially improve the treatment of AMD via a number of mechanisms illustrated schematically in Fig. 2, including sustaining drug release via extended intraocular retention time, minimising adverse events through targeted delivery and reducing the invasiveness of the treatment by providing an alternative route for administration of anti-VEGF drugs.

## Extending therapeutic duration by increasing residence time of drugs

Liposomes have been shown to alter the biopharmaceutical behaviour of drugs in ocular delivery [36, 37]. Specifically for treatment of AMD, liposomes have been shown to sustain release of actives (Table 2). Abrishami et al. showed liposomes can increase the residence time of anti-VEGF biological drugs after intravitreal administration. Liposomes containing bevacizumab were retained in the vitreous humour at five times higher concentration than free drug over 42 days. These liposomal carriers are expected to provide sufficient concentration of therapeutic drug for over 6 weeks [39]. However, such a system might have limited uptake unless a significantly longer duration (>2 months) of drug retention at the site of AMD could be achieved, to provide a step change in reducing the frequency of administration. Other recent studies have shown that liposomal systems can efficiently deliver the active to the site of action resulting in a reduction in CNV area; however, the effect was recorded 14 days after laser photocoagulation because the extent of CNV is usually the greatest and

**Fig. 2** Schematic showing the rationale by which liposomes may improve ocular delivery, depending on their surface characteristics

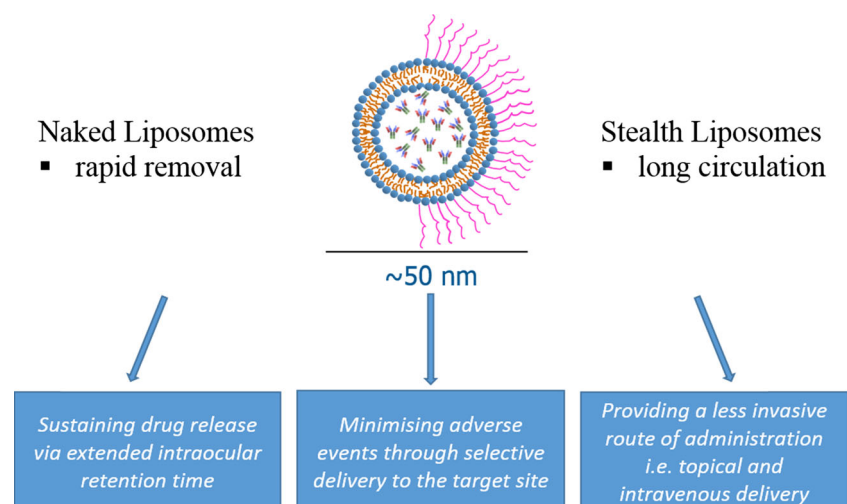


**Table 2** Liposomes intended to improve treatment of AMD by sustaining release of active drug

Description	Route of administration	Drug category	Observation	Year	Ref.
Surface-modified liposomes	Topical delivery	Anti-inflammatory	Improved the physical stability, sustained release over 60 days in vitro	2012	[38]
Nanoliposomes	Intravitreal injection	Anti-VEGF	Sustained bevacizumab release in the vitreous body in vivo (in rabbits over 40 days)	2009	[39]

most favourable for observation at this time point. As such, sustained release was assumed from previous literature [29] and, in some cases, with the support of in vitro release studies [38, 40].

### Selective delivery to the target site through enhanced cellular interaction

Liposomal delivery systems have also been shown to provide enhanced delivery to the site of action using various targeting ligands. Delivery of some therapeutic agents, such as nucleotides, is generally problematic because it has difficulty penetrating biological barriers resulting in low delivery efficiency at the target site [41]. Problematic agents can be encapsulated in ligand-conjugated liposomes to target specific cells at the site of CNV, as detailed in Table 3. Recent in vitro data found that cationic PEGylated liposomes modified with the RGD oligopeptide can efficiently carry siRNA for downregulating VEGF expression in RPE cells [41, 43] and a PEGylated liposomal system has been shown to facilitate intracellular delivery of an anti-VEGF to RPE cells in rat models [44]. Efficient delivery of actives selectively to the site of CNV allows enhanced therapeutic efficacy causing significant reduction of CNV area. Currently, only intravitreally administered formulations into rats have been investigated and, thus, the clinical benefits in extending the duration between injections remain uncertain.

#### *Providing a less invasive route of administration*

Liposomes potentially allow a less invasive route of administration for anti-VEGF treatment, avoiding intravitreal injections (Table 4). Firstly, liposomal formulations have been studied for their effectiveness following topical administration [38, 47, 49], which is the most simple and relatively non-invasive method for ocular drug delivery. Although this route may not result in reduced frequency of administration, by avoiding intravitreal injections, topical application of a liposomal formulation could provide a significant improvement in patient compliance and safety. Recently, a topically administered bevacizumab-liposome system has shown potential as a non-invasive alternative for ocular instillation. Davis et al. showed using in vivo rat and rabbit studies that liposomes can

overcome the corneal barriers and enhance the delivery of encapsulated bevacizumab to the posterior segment of the eye after topical application by incorporating an anionic phospholipid-binding protein, annexin A5 [47]. However, ocular bioavailability of the drug is usually <5 % of the topically applied dose attributed to limited volume of administration, rapid tear drainage and the physical barriers such as the cornea, conjunctiva and sclera [52]. The consequent low bioavailability of the drug would require frequent administration, and the lack of control over the actual dose delivered to the posterior section can lead to higher systemic exposure, potentially limiting its use as an approved AMD treatment.

#### *Photodynamic therapy as an approach to reduce administration frequency*

Anti-VEGF therapy has become the latest standard treatment for AMD; however, long-term inhibition of VEGF has been associated with higher risks of mortality, incident myocardial infarction, bleeding and incident stroke [53] and is thought that the previously used photodynamic therapies (PDT) may be more suitable in this regard. However, PDT drugs such as verteporfin (Visudyne®) have been known to have high risks of immediate visual loss and adverse effects [54], as such, have been largely replaced by anti-VEGF therapies. Consequently, it is proposed that a compromise between the two may provide new opportunities in therapy, where systemic administration of liposomes loaded with a photodynamic therapy agent can be used to reduce the frequency of administration by intravitreal injection through alternating therapeutic approaches to treatment. Briefly, PDT is a minimally invasive treatment involving light activation of light-sensitive molecules after intravenous administration that localise in the neovasculature in the eye. Upon activation using a low-energy laser, reactive oxygen species are produced and these destroy target cells resulting in closure of the abnormal blood vessels. Recent liposomal research successfully improved the previous liposomal PDT by reducing CNV lesion size with minimal tissue damage [46, 48]. Therefore, it has been suggested that improvement of PDT or a combination therapy of alternating PDT and anti-VEGF treatments may reduce the need for intravitreal injections and may be more suitable for selected patients at risk from extended VEGF inhibition.

**Table 3** Liposomes used to improve treatment of AMD by enhancing cellular interactions

Description	Route of administration	Drug category	Observation	Toxicology	Year	Ref.
Vector-mediated liposomes	Intravitreal injection	Angiogenesis inhibitor	Adenoviral vector-mediated liposomes efficiently delivered tristetraprolin, suppressed CNV in vivo (rat) after 14 days and decreased VEGF mRNA expression	Possible systemic toxicity due to adenoviral vectors	2014	[42]
Peptide-modified PEGylated liposomes	Intravitreal injection	Angiogenesis inhibitor	YSA peptide selectively targeted EphA2 in neovasculatures, increased intracellular delivery efficiency and enhanced the therapeutic efficacy against CNV in rats after 14 days	Toxicity at injection site may be due to oxygen radicals of doxorubicin	2012	[40]
Peptide-modified PEGylated liposomes	In vitro	Nucleotide	Efficiently carry siRNA, downregulated VEGF expression in RPE cells in vitro	N/A	2011, 2013	[41, 43]
PEGylated cationic liposomes	Intravitreal injection	Nucleotide	Efficiently protected siRNA load, facilitated intracellular delivery and caused a reduction of CNV area in vivo (rat) after 14 days	Cationic surface charge may induce inflammation	2011	[44]
Peptide-modified liposomes	Intravitreal injection	Tyrosine-kinase inhibitor	Inhibitory effects of SU5416 was enhanced and sustained by APRPG liposomes resulting in CNV reduction ex vivo (in rats after 14 days)	VEGF inhibition can affect healthy tissues	2011	[45]

#### *Passive targeting via systemic circulation to avoid intravitreal injection*

With the present safety concern of repeated intravitreal injections and long-term anti-VEGF inhibition mentioned in the previous section, selective delivery to the target site is crucial. Systemic administration of free drug with the intention of treating the posterior segment is currently limited by lack of access of anti-VEGF molecules to the site of disease due to the blood-retina barrier and limited circulatory half-life. One opportunity that is gaining interest is using ‘passive’ targeting of liposomes to the site of AMD. Liposomes in the ‘naked’ unmodified state (Fig. 2, left-hand side) are rapidly cleared from circulation, whereas those that have been surface modified with a ‘stealth’ polyethylene glycol (PEG) coating display extended systemic residence times. Stealth liposomes avoid non-specific removal from the circulatory system by the mononuclear phagocyte system (MPS) [55]. The PEG coating and consequent long circulation time has been shown to assist particle uptake through leaky vasculature in tumours, attributed to the enhanced permeation and retention (EPR) effect. These nanoparticles can extravasate within tumour sites due

to the poorly formed leaky vasculature, where gaps up to several hundreds of nanometers in size can occur, and in the absence of lymphatic drainage can be retained in the interstitial tissues [56]. In the case of AMD, the leakiness of the blood vessels that leads to the symptomatic obscuration of vision may present an opportunity for delivery via the EPR effect that is not present in healthy retinal tissues (Fig. 3). It has been reported that the anatomical characteristics of wet AMD are similar to tumour sites such that the CNV vessels exhibit hyperpermeability with little drainage. Fluorescently labelled polymer (PVA) accumulated in the retinal tissues of mice with CNV compared to control non-CNV mice [57] (Fig. 4). Along similar lines, fluorescent-labelled polyion complexes, PEG-micellar particles approximating 50 nm in size, have also been shown to accumulate in ocular tissues of rats with induced CNV after intravenous administration [58]. Consequently, it could be hypothesised that systemically administered stealth liposomes may deliver anti-VEGF drugs to the macula at greater concentration than administering free drug alone, although the potential and level of drug accumulation has yet to be realised.

**Table 4** Liposomes used to improve treatment of AMD by avoiding intravitreal injections for administration

Description	Route of administration	Drug category	Observation	Toxicology	Year	Ref.
Single unilamellar liposomes	Intravenous injections	Photodynamic therapy (PDT)	Significantly reduced CNV lesions with minimal tissue damage	Low inflammatory reaction and skin phototoxicity	2015	[46]
Peptide-associated anionic liposomes	Topical delivery	Anti-VEGF	Annexin A5 enhanced permeation through the retina after 5 days, significantly enhancing bioavailability in vivo (rat/rabbits)	No adverse events	2014	[47]
Cationic liposomes	Intravenous injections	Photodynamic therapy (PDT)	Neovascular obliteration as effective as Visudyne® but induced less tissue damage after 10 days	Less pronounced PDT-associated retinal damage	2013	[48]
Surface-modified liposomes	Topical delivery	Anti-inflammatory	Effective retinal delivery of diclofenac by promoting non-corneal drug penetration in vivo (rabbits)	N/A	2012	[38]
Submicron-sized liposomes	Topical delivery	Potent-free radical scavenger	Inhibition of light-induced and oxidative stress-induced retinal damage and prevented shrinkage of the outer nuclear layer	Low toxicity	2011	[49, 50]
Peptide-grafted cationic polymerised liposomes	Intravenous injection	Angiogenesis inhibitor	Targeted gene delivery leads to a reduction in size and leakage of CNV in vivo (rat) starting at 5 days after CNV creation	Low possibility of systemic side effects	2011	[51]

In summary, liposomes have potential to effectively deliver anti-VEGF compounds in a less invasive manner. However, the release of the drug then becomes a concern due to the low permeability of large macromolecules. In tumours, overexpression of phospholipases is mainly responsible for the breakdown of the bilayer and release of the therapeutic payload. It remains uncertain whether enzymatic activity would be sufficient in AMD to induce substantial leakage. Therefore, there is likely to be a role to play for stimuli-responsive systems that enable ‘on-demand’ drug release.

### Stimuli-responsive lipid systems for ‘on-demand’ drug delivery

Controlling the release of drug can potentially reduce the frequency of intravitreal injections, improve systemic safety by actively controlling the rate of drug release and provide a less

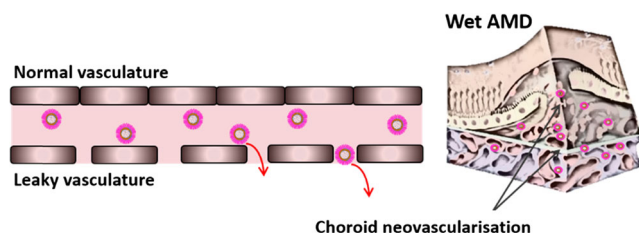
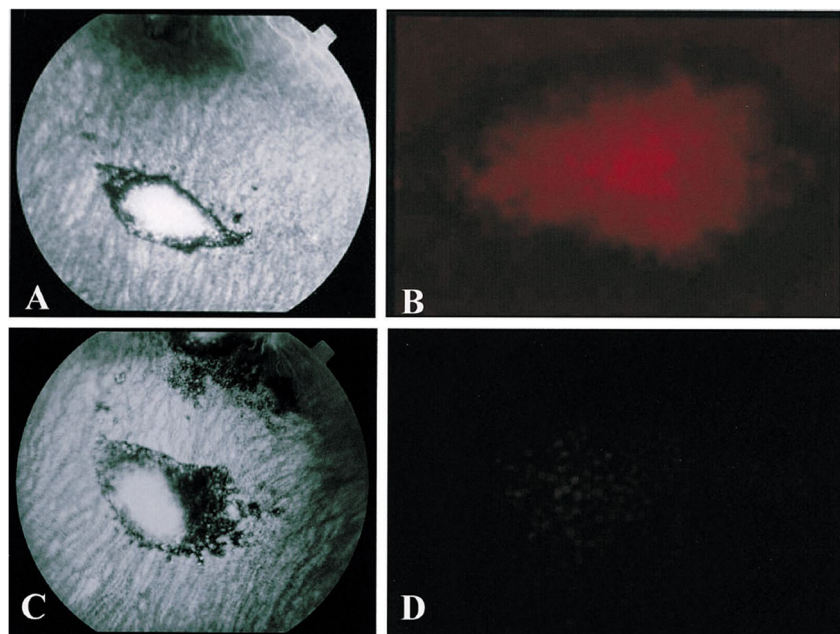


**Fig. 3** Schematic showing the accumulation of stealth liposomes via EPR effect

invasive treatment option. Stimuli-responsive systems have been explored in the context of ocular delivery to deliver drugs ‘on-demand’, when required [23, 59]. These ‘smart’ materials have been designed to respond to an endogenous or external stimulus to cause the initiation, increase, decrease or cessation of drug release from within the matrix. Polymeric implants responsive to an electric current [60], light [61] or a magnetic field [62] to achieve tunable drug release have been explored for delivery to the eye. Lipid systems, particularly liposomes and other lyotropic liquid crystalline materials, have also been rendered stimuli responsive, and ongoing efforts to evaluate their application to the problem of AMD are discussed below.

Liposomes are the simplest case of lyotropic lipid self-assembly presented as a spherical bilayer structure resulting from the dispersion of lamellar phase ( $L_{\alpha}$ ). Other self-assembled geometries have been identified to form from biocompatible lipids in water, a number of which are illustrated in Fig. 5 to the right of the graph, and these lyotropic lipid systems have also been demonstrated to be effective carriers to improve the delivery of molecules with varying physicochemical properties [63–66] and also provide protection from degradation when the drug is encapsulated. Lyotropic liquid crystalline matrices are soft materials with a complex internal nanostructure formed by the self-assembly of some polar amphiphilic lipids in excess of water and provides the mechanism for sustained release [67]. The most common liquid crystalline structures include inverse hexagonal phase ( $H_2$ ) and the bicontinuous cubic phase ( $V_2$ ). These self-assembled phases can be modified to transition from one phase to another

**Fig. 4** Accumulation of fluorescent-labelled polymer in retinal tissues after intravenous administration to mice with CNV, due to an EPR-like effect. The accumulation of RITC–PVA (**b**) and free RITC (**d**) in the subretinal space. RITC was strongly detected by fluorescence microscopy in an eye with RITC–PVA injected (**b**). The area stained with RITC corresponded with CNV revealed as the staining of fluorescein in a late phase of fluorescein angiography (**a**). Most of free RITC was not retained in the CNV lesion (**d**), whereas the fluorescein leakage was intense (**c**). Reproduced with permission from [57].



depending on the packing of amphiphilic lipids, presence of additives and environmental factors [68], or in the context of on-demand drug delivery under a wide range of stimuli.

It is known that the phase structure being either “open” or “closed” dictates the rate of drug release as illustrated in Fig. 5 left-hand side [63]. For example, the  $H_2$  phase displays a much slower release than  $V_2$  phase due to the smaller water channels and closed rod-like micellar structure [63, 69]. Likewise, the closed nature of  $L_\alpha$  phase, which enables the encapsulation of drug, will show slow or no drug release in comparison to both  $H_2$  and  $V_2$  phases. It is envisioned that lipid-based systems can be designed to be responsive and deliver drug ‘on-demand’.

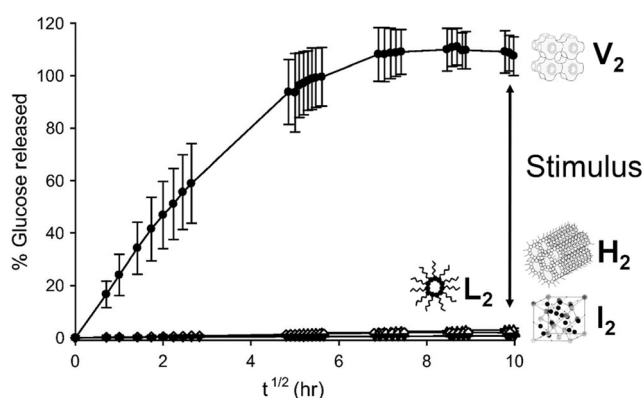


**Fig. 5** Schematic illustrating how changing the lyotropic liquid crystalline structure can control the release rate of drug. The lyotropic liquid crystalline structures on the right are the fast releasing inverse bicontinuous cubic phase ( $V_2$ ), in comparison to the slow releasing phases: inverse hexagonal phase ( $H_2$ ), inverse micellar cubic phase ( $I_2$ ) and inverse micellar phase ( $L_2$ ). A range of methods can be used to impart stimuli responsiveness in these systems to switch between slow and fast releasing structures. Adapted with permission from [63]

These systems will exhibit little or no drug release in the ‘off’ state, but when stimulated, a phase transition occurs, activating the release of drug until it is switched off. This process can be repeated to release pulses of drug on demand and would be more suitable for long-term delivery.

There are a number of scenarios where triggered release of drug from these lipid systems for the treatment of wet AMD may be foreseen to be advantageous, illustrated schematically in Fig. 6. In the simplest case, responsive liposomes would release their cargo selectively when they encounter the stimulus either due to a change in the permeability of the bilayers or via a transition of the phase structure. Phase transitions in lyotropic lipid systems have been induced previously by modifying the lipid packing using stimuli such as temperature [70], water content [69], ionic strength [71] and pH [72, 73]. Temperature has been used as a stimuli for on-demand drug delivery [70] from lyotropic lipid systems [69]; however, temperature-responsive systems are not considered practical for controlling release of drug in the eye, due to lack of specificity in heat source leading to potential for accidental activation of drug release. Alternatively, magnetic- [74] and light-sensitive [75, 76] materials can be incorporated into the lyotropic liquid crystal matrix to enable external control over drug release, making them more suitable for on-demand applications.

For ocular applications in the posterior segment, where the liposome has been intravitreally injected, or been delivered via the systemic circulation as described above, light as a trigger would be a useful stimulus. Light-sensitive liposomes have been extensively studied previously for biological applications [77]; however, it does not appear that such systems have been used in the treatment of AMD. Light activation provides a very broad range of adjustable parameters such as wavelength,

**Fig. 6** Schematic of how a NIR light-triggered lipid ‘depot’ could reduce the frequency of intravitreal injections by repeated triggered release of a dose of drug using a laser, to replace regular intravitreal injections



duration, beam diameter and intensity that can be used to optimise and control the dose of the actives released, when required. To this end, there are numerous papers on ultraviolet (UV)-activated liposome systems [78, 79]. However, UV-activated systems risk damage to the eye through intense UV exposure, and UV is poorly transmitted through tissue such as the cornea, and consequently have not been shown to be successful in vivo. With the suitability for clinical applications in mind, the near-infrared (NIR) region around 650 to 900 nm that has the lowest absorption coefficient with water, lipids and haemoglobin [80] is the best light source for triggered drug delivery and PDT. Recent research has reported liposomes can be made responsive to NIR irradiation [81, 82]. Of particular interest, light-sensitive gold nanorods (GNR) have already been shown to provide remote heating to lyotropic lipid systems and trigger the phase transitions upon NIR irradiation [75, 83]. NIR irradiation can penetrate tissues up to 50 mm deep [84], rendering it amenable for ophthalmic, subcutaneous and deeper tissue applications. Such stimuli-responsive systems are considered to have utility for delivery to the posterior segment as injectable bulk ‘depot’ systems, rather than as particles. The bulk depot allows for storage of multiple doses of drug, replacing, for example, 12 months requirement of drug normally administered as 12 separate injections, with a single injection. The volume of the single injection will be restricted to below 0.1 mL to avoid adverse events such as increased intraocular pressure [85]. The detail behind such a system will clearly need to be elaborated, requiring evaluation of the dose per volume constraints, optimised to release a fixed dose of active repeatedly at intervals determined by symptom recurrence, throughout the 12-month period by fine tuning the NIR exposure time and GNR concentration in the system. However, at least a potential exists to achieve less frequent administration in the treatment of AMD if pulsatile, and repeat administration can be achieved using stimuli-responsive lyotropic lipid systems.

## Conclusion

To this date, intravitreal injections of anti-VEGF drugs remain the most effective treatment option for AMD, yet there are many limitations in terms of safety, affordability and adherence. Liposomes have been used in the design of safe and

cost-effective delivery systems, but have not yet made it into products for intravitreal delivery of anti-VEGF compounds to improve treatment effectiveness or duration in the clinic for treatment of ocular diseases. Stealth liposomes may offer an alternative approach for systemic delivery taking advantage of the enhanced permeability of the neovasculature in wet AMD. Lyotropic liquid crystal systems have potential to also address problems with treatment of AMD, as they can be rendered stimuli-responsive and drug release can be stimulated readily using light, for example. Overall lipid systems present alternative approaches to polymers with clear capacity to improve the treatment of AMD, especially in consideration of their biocompatibility and translatability with the track record of safe use of liposomes in other diseases providing a significant advantage over other materials.

## Compliance with ethical standards

**Conflict of interest** The authors declare that they have no conflict of interest.

## References

1. Resnikoff S, Pascolini D, Etya'ale D, Kocur I, Pararajasegaram R, Pokharel GP, et al. Global data on visual impairment in the year 2002. *Bull World Health Organ.* 2004;82(11):844–51.
2. Group TEDPR. Causes and prevalence of visual impairment among adults in the United States. *Arch Ophthalmol.* 2004;122(4):477–85. doi:10.1001/archophth.122.4.477.
3. Wong WL, Su X, Li X, Cheung CMG, Klein R, Cheng C-Y, et al. Global prevalence of age-related macular degeneration and disease burden projection for 2020 and 2040: a systematic review and meta-analysis. *Lancet.* 2014;2(2):106–16. doi:10.1016/S2214-109X(13)70145-1.
4. Ozaki E, Campbell M, Kiang A-S, Humphries M, Doyle SL, Humphries P. Inflammation in age-related macular degeneration. In: Ash JD, Grimm C, Hollyfield JG, Anderson RE, LaVail MM, Bowes Rickman C, editors. *Retinal degenerative diseases. Advances in experimental medicine and biology.* New York: Springer; 2014. p. 229–35.
5. Short BG. Safety evaluation of ocular drug delivery formulations: techniques and practical considerations. *Toxicol Pathol.* 2008;36(1):49–62.

6. Wong TY, Liew G, Mitchell P. Clinical update: new treatments for age-related macular degeneration. *Lancet*. 2007;370(9583):204–6. doi:10.1016/S0140-6736(07)61104-0.
7. Macular Disease Foundation Australia [Internet]. Schematic of retina. 2004; [cited 2016 February 8]. Available from: www.mdfoundation.com.au.
8. Bonilha VL, Rayborn ME, Bhattacharya SK, Gu X, Crabb JS, Crabb JW, et al. The retinal pigment epithelium apical microvilli and retinal function. *Adv Exp Med Biol*. 2006;572:519–24. doi:10.1007/0-387-32442-9\_72.
9. Coleman HR, Chan C-C, Ferris Iii FL, Chew EY. Age-related macular degeneration. *Lancet*. 2008;372(9652):1835–45. doi:10.1016/S0140-6736(08)61759-6.
10. Sene A, Khan AA, Cox D, Nakamura RE, Santeford A, Kim BM, et al. Impaired cholesterol efflux in senescent macrophages promotes age-related macular degeneration. *Cell Metab*. 2013;17(4):549–61. doi:10.1016/j.cmet.2013.03.009.
11. Group ES. Preclinical and phase 1A clinical evaluation of an anti-VEGF pegylated aptamer (EYE001) for the treatment of exudative age-related macular degeneration. *Retina*. 2002;22(2):143–52.
12. Gragoudas ES, Adamis AP, Cunningham ET, Feinsod M, Guyer DR. Pegaptanib for neovascular age-related macular degeneration. *N Engl J Med*. 2004;351(27):2805–16. doi:10.1056/NEJMoa042760.
13. Rosenfeld PJ, Brown DM, Heier JS, Boyer DS, Kaiser PK, Chung CY, et al. Ranibizumab for neovascular age-related macular degeneration. *N Engl J Med*. 2006;355(14):1419–31. doi:10.1056/NEJMoa054481.
14. Ohr M, Kaiser PK. Intravitreal aflibercept injection for neovascular (wet) age-related macular degeneration. *Exp Opin Pharmacother*. 2012;13(4):585–91. doi:10.1517/14656566.2012.658368.
15. Bakri SJ, Snyder MR, Reid JM, Pulido JS, Ezzat MK, Singh RJ. Pharmacokinetics of intravitreal ranibizumab (Lucentis). *Ophthalmol*. 2007;114(12):2179–82. doi:10.1016/j.opthta.2007.09.012.
16. Steinbrook R. The price of sight—ranibizumab, bevacizumab, and the treatment of macular degeneration. *N Engl J Med*. 2006;355(14):1409–12. doi:10.1056/NEJMp068185.
17. Kovach JL, Schwartz SG, Flynn HW, Scott IU. Anti-VEGF treatment strategies for wet AMD. *J Ophthalmol*. 2012;2012:786870. doi:10.1155/2012/786870.
18. Tolentino MJ, Dennrick A, John E, Tolentino MS. Drugs in phase II clinical trials for the treatment of age-related macular degeneration. *Expert Opin Drug Deliv*. 2014;24(2):183–99. doi:10.1517/13543784.2015.961601.
19. Araújo J, Nikolic S, Egea MA, Souto EB, Garcia ML. Nanostructured lipid carriers for triamcinolone acetate delivery to the posterior segment of the eye. *Colloids Surf B Biointerfaces*. 2011;88(1):150–7. doi:10.1016/j.colsurfb.2011.06.025.
20. Araújo J, Garcia ML, Mallandrich M, Souto EB, Calpena AC. Release profile and transscleral permeation of triamcinolone acetate loaded nanostructured lipid carriers (TA-NLC): in vitro and ex vivo studies. *Nanomedicine*. 2012;8(6):1034–41. doi:10.1016/j.nano.2011.10.015.
21. Boyer DS, Hopkins JJ, Sorof J, Ehrlich JS. Anti-vascular endothelial growth factor therapy for diabetic macular edema. *Ther Adv Endocrinol Metab*. 2013;4(6):151–69. doi:10.1177/2042018813512360.
22. Pikuleva IA, Curcio CA. Cholesterol in the retina: the best is yet to come. *Prog Retin Eye Res*. 2014;41:64–89. doi:10.1016/j.preteyeres.2014.03.002.
23. Yasin MN, Svirskis D, Seyfoddin A, Rupenthal ID. Implants for drug delivery to the posterior segment of the eye: a focus on stimuli-responsive and tunable release systems. *J Control Release*. 2014;196:208–21. doi:10.1016/j.jconrel.2014.09.030.
24. Delplace V, Payne S, Shoichet M. Delivery strategies for treatment of age-related ocular diseases: from a biological understanding to biomaterial solutions. *J Control Release*. 2015;219:652–68. doi:10.1016/j.jconrel.2015.09.065.
25. Schwartz SG, Scott IU, Flynn HW, Stewart MW. Drug delivery techniques for treating age-related macular degeneration. *Expert Opin Drug Deliv*. 2013;11(1):61–8. doi:10.1517/17425247.2013.859135.
26. Honda M, Asai T, Oku N, Araki Y, Tanaka M, Ebihara N. Liposomes and nanotechnology in drug development: focus on ocular targets. *Int J Nanomedicine*. 2013;8:495–504. doi:10.2147/IJN.S30725.
27. Kaur IP, Kakkar S. Nanotherapy for posterior eye diseases. *J Control Release*. 2014;193:100–12. doi:10.1016/j.jconrel.2014.05.031.
28. Wang J, Jiang A, Joshi M, Christoforidis J. Drug delivery implants in the treatment of vitreous inflammation. *Mediat Inflamm*. 2013;2013:780634. doi:10.1155/2013/780634.
29. Bochot A, Fattal E. Liposomes for intravitreal drug delivery: a state of the art. *J Control Release*. 2012;161(2):628–34. doi:10.1016/j.jconrel.2012.01.019.
30. Mishra GP, Bagui M, Tamboli V, Mitra AK. Recent applications of liposomes in ophthalmic drug delivery. *J Drug Deliv*. 2011;2011:14. doi:10.1155/2011/863734.
31. Choonara YE, Pillay V, Danckwerts MP, Carmichael TR, du Toit LC. A review of implantable intravitreal drug delivery technologies for the treatment of posterior segment eye diseases. *J Pharm Sci*. 2010;99(5):2219–39. doi:10.1002/jps.21987.
32. Lim JJ, Wolitz RA, Dowling AH, Bloom HR, Irvine AR, Schwartz DM. Visual and anatomic outcomes associated with posterior segment complications after ganciclovir implant procedures in patients with AIDS and cytomegalovirus retinitis. *Am J Ophthalmol*. 1999;127(3):288–93.
33. Ninawe PR, Hatzivramidis D, Parulekar SJ. Delivery of drug macromolecules from thermally responsive gel implants to the posterior eye. *Chem Eng Sci*. 2010;65(18):5170–7. doi:10.1016/j.ces.2010.06.014.
34. Koo H, Moon H, Han H, Na JH, Huh MS, Park JH, et al. The movement of self-assembled amphiphilic polymeric nanoparticles in the vitreous and retina after intravitreal injection. *Biomaterials*. 2012;33(12):3485–93. doi:10.1016/j.biomaterials.2012.01.030.
35. ClinicalTrials.gov [Internet]. Bethesda (MD): National Library of Medicine (US). 2000 [cited 2016 April 14]. NLM Identifier: NCT00535054, NCT02420834, NCT01987323, NCT02466399, NCT02599688, NCT00072384, NCT00335738, NCT01115192, NCT02006147. Available from: <http://clinicaltrials.gov>
36. Natarajan JV, Ang M, Darwitan A, Chattopadhyay S, Wong TT, Venkatraman SS. Nanomedicine for glaucoma: liposomes provide sustained release of latanoprost in the eye. *Int J Nanomedicine*. 2012;7:123–31. doi:10.2147/IJN.S25468.
37. Habib FS, Fouad EA, Abdel-Rhman MS, Fathalla D. Liposomes as an ocular delivery system of fluconazole: in-vitro studies. *Acta Ophthalmologica*. 2010;88(8):901–4. doi:10.1111/j.1755-3768.2009.01584.x.
38. Fujisawa T, Miyai H, Hironaka K, Tsukamoto T, Tahara K, Tozuka Y, et al. Liposomal diclofenac eye drop formulations targeting the retina: formulation stability improvement using surface modification of liposomes. *Int J Pharm*. 2012;436(1–2):564–7. doi:10.1016/j.ijpharm.2012.07.024.
39. Abrishami M, Zarei-Ghanavati S, Soroush D, Rouhbakhsh M, Jaafari M, Malaekheh-Nikouei B. Preparation, characterization, and in vivo evaluation of nanoliposomes-encapsulated bevacizumab (avastin) for intravitreal administration. *Retina*. 2009;29(1):699–703.
40. Wang J-I, Y-I L, Li Y, W-b D, Guo Z-m, Wang Z-h, et al. EphA2 targeted doxorubicin stealth liposomes as a therapy system for

- choroidal neovascularization in rats. *Invest Ophthalmol Vis Sci*. 2012;53(11):7348–57. doi:10.1167/iov.12-9955.
41. Chen C-W, Lu D-W, Yeh M-K, Shiao C-Y, Chiang C-H. Novel RGD-lipid conjugate-modified liposomes for enhancing siRNA delivery in human retinal pigment epithelial cells. *Int J Nanomedicine*. 2011;6:2567–80. doi:10.2147/IJN.S24447.
  42. Cho YW, Han YS, Chung IY, Kim SJ, Seo SW, Yoo JM, et al. Suppression of laser-induced choroidal neovascularization by intravitreal injection of tristetraprolin. *Int J Ophthalmol*. 2014;7(6):952–8. doi:10.3980/j.issn.2222-3959.2014.06.07.
  43. Chen C-W, Yeh M-K, Shiao C-Y, Chiang C-H, Lu D-W. Efficient downregulation of VEGF in retinal pigment epithelial cells by integrin ligand-labeled liposome-mediated siRNA delivery. *Int J Nanomedicine*. 2013;8:2613–27. doi:10.2147/IJN.S39622.
  44. Liu HA, Liu YL, Ma ZZ, Wang JC, Zhang Q. A lipid nanoparticle system improves siRNA efficacy in RPE cells and a laser-induced murine CNV model. *Investig Ophthalmol Vis Sci*. 2011;52(7):4789–94. doi:10.1167/iov.10-5891.
  45. Honda M, Asai T, Umamoto T, Araki Y, Oku N, Tanaka M. Suppression of choroidal neovascularization by intravitreal injection of liposomal su5416. *Arch Ophthalmol*. 2011;129(3):317–21. doi:10.1001/archophth.2011.12.
  46. Li T, Hou X, Deng H, Zhao J, Huang N, Zeng J, et al. Liposomal hypocrellin B as a potential photosensitizer for age-related macular degeneration: pharmacokinetics, photodynamic efficacy, and skin phototoxicity in vivo. *Photochem Photobiol Sci*. 2015;14(5):972–81. doi:10.1039/C4PP00412D.
  47. Davis BM, Normando EM, Guo L, Turner LA, Nizari S, O'Shea P, et al. Topical delivery of avastin to the posterior segment of the eye in vivo using annexin A5-associated liposomes. *Small*. 2014;10(8):1575–84. doi:10.1002/sml.201303433.
  48. Gross N, Ranjbar M, Evers C, Hua J, Martin G, Schulze B, et al. Choroidal neovascularization reduced by targeted drug delivery with cationic liposome-encapsulated paclitaxel or targeted photodynamic therapy with verteporfin encapsulated in cationic liposomes. *Mol Vis*. 2013;19:54–61.
  49. Shimazaki H, Hironaka K, Fujisawa T, Tsuruma K, Tozuka Y, Shimazawa M, et al. Edaravone-loaded liposome eyedrops protect against light-induced retinal damage in mice. *Investig Ophthalmol Vis Sci*. 2011;52(10):7289–97. doi:10.1167/iov.11-7983.
  50. Hironaka K, Inokuchi Y, Fujisawa T, Shimazaki H, Akane M, Tozuka Y, et al. Edaravone-loaded liposomes for retinal protection against oxidative stress-induced retinal damage. *Eur J Pharm Biopharm*. 2011;79(1):119–25. doi:10.1016/j.ejpb.2011.01.019.
  51. Salehi-Had H, Roh MI, Giani A, Hisatomi T, Nakao S, Kim IK, et al. Utilizing targeted gene therapy with nanoparticles binding alpha v beta 3 for imaging and treating choroidal neovascularization. *PLoS ONE*. 2011;6(4):e18864. doi:10.1371/journal.pone.0018864.
  52. Maurice DM, Mishima S. Ocular pharmacokinetics. In: Sears M, editor. *Pharmacology of the eye*. Handbook of experimental pharmacology. Berlin: Springer; 1984. p. 19–116.
  53. Curtis LH, Hammill BG, Schulman KA, Cousins SW. Risks of mortality, myocardial infarction, bleeding, and stroke associated with the therapies for age-related macular degeneration. *Arch Ophthalmol*. 2010;128(10):1273–9. doi:10.1001/archophth.2010.223.
  54. Kawczyk-Krupka A, Bugaj AM, Potempa M, Wasilewska K, Latos W, Sieroń A. Vascular-targeted photodynamic therapy in the treatment of neovascular age-related macular degeneration: clinical perspectives. *Photodiagn Photodyn Ther*. 2015;12(2):161–75. doi:10.1016/j.pdpdt.2015.03.007.
  55. Yamauchi H, Yano T, Kato T, Tanaka I, Nakabayashi S, Higashi K, et al. Effects of sialic acid derivative on long circulation time and tumor concentration of liposomes. *Int J Pharm*. 1995;113(2):141–8. doi:10.1016/0378-5173(94)00188-B.
  56. Maeda H, Nakamura H, Fang J. The EPR effect for macromolecular drug delivery to solid tumors: improvement of tumor uptake, lowering of systemic toxicity, and distinct tumor imaging in vivo. *Adv Drug Deliv Rev*. 2013;65(1):71–9. doi:10.1016/j.addr.2012.10.002.
  57. Kimura H, Yasukawa T, Tabata Y, Ogura Y. Drug targeting to choroidal neovascularization. *Adv Drug Deliv Rev*. 2001;52(1):79–91.
  58. Ideta R, Yanagi Y, Tamaki Y, Tasaka F, Harada A, Kataoka K. Effective accumulation of polyion complex micelle to experimental choroidal neovascularization in rats. *FEBS Letters*. 2004;557(1–3):21–5. doi:10.1016/S0014-5793(03)01315-2.
  59. Mura S, Nicolas J, Couvreur P. Stimuli-responsive nanocarriers for drug delivery. *Nat Mater*. 2013;12(11):991–1003. doi:10.1038/nmat3776.
  60. Li P-Y, Shih J, Lo R, Saati S, Agrawal R, Humayun MS, et al. An electrochemical intraocular drug delivery device. *Sensors Actuators A Phys*. 2008;143(1):41–8. doi:10.1016/j.sna.2007.06.034.
  61. Peng K, Tomatsu I, van den Broek B, Cui C, Korobko AV, van Noort J, et al. Dextran based photodegradable hydrogels formed via a Michael addition. *Soft Matter*. 2011;7(10):4881–7. doi:10.1039/C1SM05291H.
  62. Pirmoradi FN, Jackson JK, Burt HM, Chiao M. On-demand controlled release of docetaxel from a battery-less MEMS drug delivery device. *Lab Chip*. 2011;11(16):2744–52. doi:10.1039/C1LC20134D.
  63. Phan S, Fong W-K, Kirby N, Hanley T, Boyd BJ. Evaluating the link between self-assembled mesophase structure and drug release. *Int J Pharm*. 2011;421(1):176–82.
  64. Lee K-W, Nguyen T-H, Hanley T, Boyd BJ. Nanostructure of liquid crystalline matrix determines in vitro sustained release and in vivo oral absorption kinetics for hydrophilic model drugs. *Int J Pharm*. 2009;365(1–2):190–9.
  65. Clogston J, Caffrey M. Controlling release from the lipidic cubic phase. Amino acids, peptides, proteins and nucleic acids. *J Contr Release*. 2005;107(1):97–111.
  66. Malmsten M. Soft drug delivery systems. *Soft Matter*. 2006;2:760. doi:10.1039/b608348j.
  67. Nguyen T-H, Hanley T, Porter CJH, Boyd BJ. Nanostructured liquid crystalline particles provide long duration sustained-release effect for a poorly water soluble drug after oral administration. *J Control Release*. 2011;153:180–6. doi:10.1016/j.jconrel.2011.03.033.
  68. Israelachvili JN, Mitchell DJ, Ninham BW. Theory of self-assembly of hydrocarbon amphiphiles into micelles and bilayers. *J Chem Soc Faraday Trans*. 1976;72:1525–68.
  69. Dong Y-D, Dong AW, Larson I, Rappolt M, Amenitsch H, Hanley T, et al. Impurities in commercial phytantriol significantly alter its lyotropic liquid-crystalline phase behavior. *Langmuir*. 2008;24:6998–7003. doi:10.1021/la8005579.
  70. Fong W-K, Hanley T, Boyd BJ. Stimuli responsive liquid crystals provide 'on-demand' drug delivery in vitro and in vivo. *J Control Release*. 2009;135:218–26. doi:10.1016/j.jconrel.2009.01.009.
  71. Muir BW, Zhen G, Gunatillake P, Hartley PG. Salt induced lamellar to bicontinuous cubic phase transitions in cationic nanoparticles. *J Phys Chem B*. 2012;116:3551–6. doi:10.1021/jp300239g.
  72. Du JD, Liu Q, Salenting S, Nguyen T-H, Boyd BJ. A novel approach to enhance the mucoadhesion of lipid drug nanocarriers for improved drug delivery to the buccal mucosa. *Int J Pharm*. 2014;471(1–2):358–65. doi:10.1016/j.ijpharm.2014.05.044.
  73. Negrini R, Fong WK, Boyd BJ, Mezzenga R. pH-responsive lyotropic liquid crystals and their potential therapeutic role in cancer treatment. *Chem Commun*. 2015;51(30):6671–4. doi:10.1039/c4cc10274f.
  74. Arruebo M, Fernández-Pacheco R, Ibarra MR, Santamaría J. Magnetic nanoparticles for drug delivery. *Nano Today*. 2007;2:22–32. doi:10.1016/S1748-0132(07)70084-1.

75. Fong W-K, Hanley TL, Thierry B, Kirby N, Boyd BJ. Plasmonic nanorods provide reversible control over nanostructure of self-assembled drug delivery materials. *Langmuir*. 2010;26(9):6136–9. doi:10.1021/la100644s.
76. Fong W-K, Hanley TL, Thierry B, Kirby N, Waddington LJ, Boyd BJ. Controlling the nanostructure of gold nanorod–lyotropic liquid-crystalline hybrid materials using near-infrared laser irradiation. *Langmuir*. 2012;28(40):14450–60. doi:10.1021/la302901q.
77. Yavlovich A, Smith B, Gupta K, Blumenthal R, Puri A. Light-sensitive lipid-based nanoparticles for drug delivery: design principles and future considerations for biological applications. *Mol Membr Biol*. 2010;27(7):364–81. doi:10.3109/09687688.2010.507788.
78. Leung SJ, Romanowski M. Light-activated content release from liposomes. *Theranostics*. 2012;2(10):1020–36. doi:10.7150/thno.4847.
79. Yavlovich A, Singh A, Tarasov S, Capala J, Blumenthal R, Puri A. Design of liposomes containing photopolymerizable phospholipids for triggered release of contents. *J Therm Anal Calorim*. 2009;98(1):97–104. doi:10.1007/s10973-009-0228-8.
80. Weissleder R, Ntziachristos V. Shedding light onto live molecular targets. *Nat Med*. 2003;9(1):123–8.
81. Cao J, Huang S, Chen Y, Li S, Li X, Deng D, et al. Near-infrared light-triggered micelles for fast controlled drug release in deep tissue. *Biomaterials*. 2013;34(26):6272–83. doi:10.1016/j.biomaterials.2013.05.008.
82. Fong W-K, Hanley TL, Thierry B, Tilley A, Kirby N, Waddington LJ, et al. Understanding the photothermal heating effect in non-lamellar liquid crystalline systems, and the design of new mixed lipid systems for photothermal on-demand drug delivery. *Phys Chem Chem Phys*. 2014;16(45):24936–53. doi:10.1039/C4CP03635B.
83. Du JD, Fong W-K, Salentinig S, Caliph SM, Hawley A, Boyd BJ. Phospholipid-based self-assembled mesophase systems for light-activated drug delivery. *Phys Chem Chem Phys*. 2015;17:14021–7. doi:10.1039/C5CP01229E.
84. Barun VV, Ivanov AP, Volotovskaya AV, Ulashchik VS. Absorption spectra and light penetration depth of normal and pathologically altered human skin. *J Appl Spectrosc*. 2007;74(3):430–9. doi:10.1007/s10812-007-0071-2.
85. Kotliar K, Maier M, Bauer S, Feucht N, Lohmann C, Lanzl I. Effect of intravitreal injections and volume changes on intraocular pressure: clinical results and biomechanical model. *Acta Ophthalmol*. 2007;85(7):777–81. doi:10.1111/j.1600-0420.2007.00939.x.



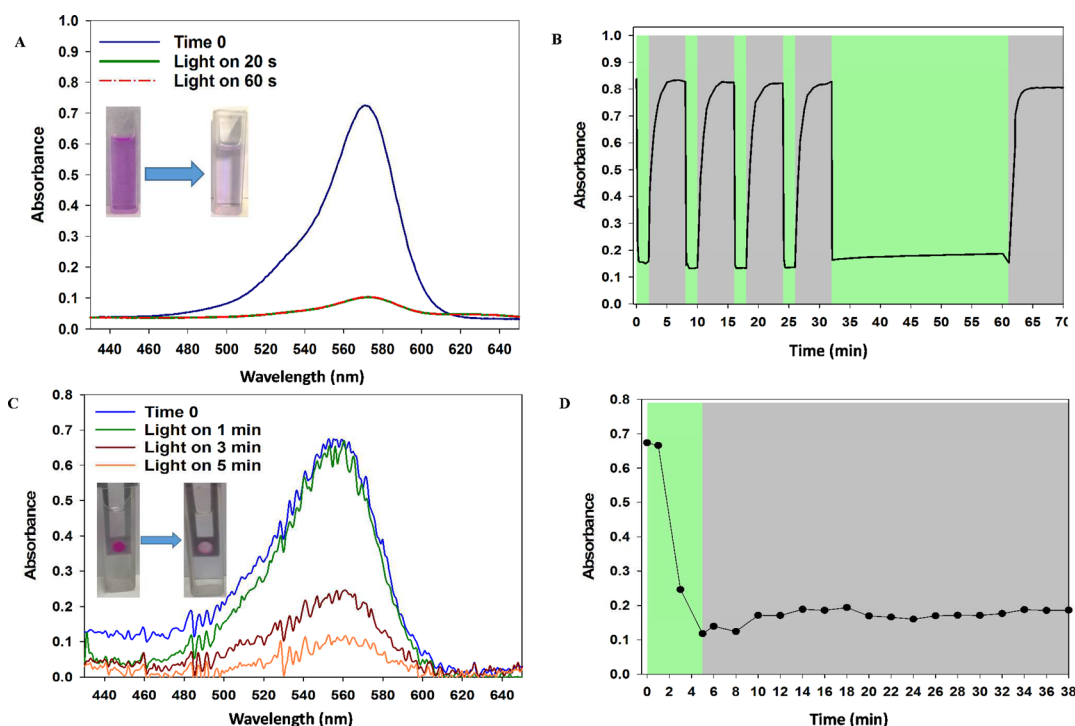


**Figure 2.** (A) Absorbance spectra of **D1** in toluene ( $4 \mu\text{g mL}^{-1}$ ) upon cold LED light irradiation ( $12 \text{ mW cm}^{-2}$ ). (B) Multiple cycles of photoswitching of **D1** in toluene ( $4.5 \mu\text{g mL}^{-1}$ ). The absorbance was monitored at  $570 \text{ nm}$  every  $10 \text{ s}$ . The solution of **D1** was exposed to cold LED light for  $2 \text{ min}$  (green) and then kept in the dark for  $5 \text{ min}$  (gray). (C) Absorbance spectra of **D1** doped into phytantriol-based LLC matrix ( $0.06\% \text{ w/w}$ ) upon irradiation with green light ( $532 \text{ nm}$ ,  $57 \text{ mW cm}^{-2}$ ). (D) Absorbance of **D1** doped in phytantriol-based LLC matrix during irradiation (green) and after irradiation (gray).

lipids can self-assemble into one-, two-, and three-dimensional mesophases, such as the lamellar ( $L_a$ ), hexagonal ( $H_2$ ), and bicontinuous cubic phases ( $V_2$ ).<sup>21</sup> The  $V_2$  and  $H_2$  mesophases are of most interest in the field of drug delivery.<sup>22,23</sup> The  $H_2$  phase is composed from cylindrical micelles that are packed in a hexagonal lattice with a negative mean curvature toward the aqueous interior.<sup>24</sup> The  $V_2$  phase comprises two separate, continuous, but nonintersecting hydrophilic regions, divided by a lipid bilayer, which are contorted into a periodic minimal surface with zero average curvature.<sup>24,25</sup> This phase possesses extremely high viscosity due to its regular structural connectivity, which is an advantage for slowing diffusion.<sup>25</sup> Liquid crystals are capable of incorporating a diverse variety of therapeutic cargos<sup>26,27</sup> and have excellent biocompatibility.<sup>28</sup>

Different LLC mesophases provide dramatically different rates of drug release, so stimuli-responsive versions of mesophases may provide on–off drug release behavior. The use of stimuli including pH<sup>29</sup> and temperature,<sup>30</sup> which reflect physiological differences in disease states such as cancer and inflammation, have been reported. The manipulation of these factors disturbs the lipid packing and so can induce a phase transition, dramatically altering the release rate of encapsulated cargo. To overcome the practical drawbacks of these stimuli, the use of noninvasive stimuli like irradiation is drawing increasing attention, with the aim to spatially and temporally control the drug release in a noninvasive manner.<sup>31–33</sup>

In this contribution, we investigate the effect of photoisomerization of an alkylated DASA molecule, **D1** (Figure 1B), upon the lyotropic self-assembly of a host cubic phase matrix based on phytantriol. Phytantriol (Figure 1C) is one of the most commonly used materials for preparing stimuli responsive lipid-based liquid crystalline matrices as the molecule itself has a

relatively high resistance to chemical degradation or oxidation. Additionally, phytantriol forms the  $V_2$  phase in excess water, whose structure and dimensions are very sensitive to changes in lipid packing, particularly when dopant molecules insert at the interface, where they can have the greatest impact upon lipid self-assembly.<sup>32,34</sup> Hence, phytantriol-based cubic phase was used in this context as a host for studying the photoisomerization of **D1** to understand the potential benefits and drawbacks of using DASAs as photoswitches in lipid systems more generally. Small-angle X-ray scattering (SAXS) was used to detect changes to self-assembly induced by photoisomerism of **D1** upon irradiation, while spectroscopic investigations were undertaken to examine the photoisomerization behavior of **D1**.

## EXPERIMENTAL SECTION

**Materials and Methods.** **D1** was synthesized following the methods described by Helmy et al.,<sup>17,18</sup> with only minor modifications (the full synthesis is described in the Supporting Information).

The liquid crystalline samples were prepared by predissolving **D1** in chloroform and adding to phytantriol to give the desired final concentration of **D1**. This mixture was then homogenized by vortexing. The chloroform was subsequently removed under vacuum. McIlvaine's buffer (pH 4.8) was then added to the lipid phase with a ratio of 1:1 (w/w) to ensure full hydration of the LLC matrix.<sup>21,35</sup> A control sample without **D1** was also prepared. The samples were heated transiently to  $70 \text{ }^\circ\text{C}$  to enable vortex mixing ( $\times 3$ ) and then left to equilibrate for  $70 \text{ h}$  before SAXS measurements.

**Absorption Spectrophotometry.** Absorption spectra ( $400\text{--}600 \text{ nm}$ ) were measured on a Cary-50 spectrophotometer at a scan rate of  $720 \text{ nm s}^{-1}$ . The instrument was fitted with a Peltier temperature-controlled cell. For photoswitching experiments in solvent, a solution of **D1** in toluene ( $4 \mu\text{g mL}^{-1}$ ) was placed in a quartz cuvette (Hellma Analytics, 100-QS,  $20 \text{ mm}$ ) and irradiated with a cold LED light ( $12 \text{ W cm}^{-2}$ ) from above. For photoswitching experiments in LLC matrix, the

D1-doped phytantriol-based liquid crystal (0.06%, w/w) was loaded into a 3D printed chip (1 mm depth). The chip was placed in a quartz cuvette (Hellma Analytics, 100-QS, 20 mm) and irradiated with green light laser (532 nm, 57 mW cm<sup>-2</sup>) from the side.

**Small-Angle X-ray Scattering (SAXS).** SAXS experiments were performed on the SAXS/WAXS beamline of the Australian Synchrotron.<sup>33</sup> All liquid crystalline samples were loaded into a flat stainless steel metal plate (96 sample positions with a thickness of 0.5 mm) sealed on both sides with Kapton tape, which was attached to a thermostated heating block and mounted on the SAXS/WAXS beamline. An X-ray beam wavelength ( $\lambda$ ) of 1.0322 Å (12 keV) was passed through the sample, and the 2D scattering patterns were collected on a 1M Pilatus detector with an acquisition time of 10 ms every 10 s. The computer software ScatterBrain Analysis was used to reduce 2D scattering patterns to the one-dimensional scattering function  $I(q)$ . The  $d$ -spacing of the liquid crystalline lattice was derived from Bragg's law ( $2d \sin \theta = n\lambda$ ), where  $n$  is an integer,  $\lambda$  is the wavelength, and  $\theta$  is the scattering angle. The absolute location of the peaks allows for the calculation of mean lattice parameter,  $a$ , of the matrices, from the corresponding interplanar distance,  $d$  ( $d = 2\pi/q$ ), using the appropriate scattering law for the phase structure. Detailed information about sample loading and analysis is reported in the Supporting Information.

## RESULTS AND DISCUSSION

**Spectrophotometric Analysis of Photoisomerization Behavior of D1 in Toluene and in LLC Matrix.** The photoswitchable capacity of D1 was first examined in toluene solution. Upon irradiation with a white LED light (12 mW cm<sup>-2</sup>), a rapid color change from purple to light pink was observed, associated with a decrease in absorbance at  $\lambda_{\text{max}} = 570$  nm (Figure 2A) and corresponding to the isomerization of D1 from the triene form to the cyclopentenone form (Figure 1A), as has been reported previously.<sup>17,18</sup> A photostationary state was reached within 20 s of irradiation. D1 was then found to fully revert back to the triene form (within 2 min) upon removal of light (Figure 2A and Figure S3B). Multiple photoswitching cycles of D1 in toluene were conducted under ambient conditions, including a prolonged irradiation of 30 min (Figure 2B). The results precluded significant material degradation, indicating D1 exhibits substantial fatigue resistance.

D1 doped into the phytantriol LLC matrix was also initially purple in color ( $\lambda_{\text{max}} = 560$  nm) and exhibited a decrease in absorbance upon exposure to green light irradiation (532 nm, 57 mW cm<sup>-2</sup>) (Figure 2C), consistent with phototriggered cyclization of the triene form of D1 to its cyclopentenone form. The decrease in absorbance accompanying photoisomerization was slower than in toluene, perhaps due to the microviscosity of the bilayer comprising the cubic phase hindering the rate of molecular rearrangement of D1. Nevertheless, it was complete after 5 min irradiation time. In contrast to the rapid and full reversion seen in toluene, there was limited reversion of D1 to the triene form in the LLC matrix (Figure 2D). A likely explanation is that the zwitterionic headgroup of the colorless cyclopentanone form of D1 partitioned into the surrounding aqueous phase, preventing reversion to the colored triene form. It has already been shown that the photoswitching of DASAs from their triene to cyclopentenone forms is irreversible in protic solvents (e.g., methanol and water).<sup>19,20</sup>

**SAXS Analysis of D1-Doped LLC Mesophases.** *Effect of Addition of D1 on Equilibrium Phase Behavior of LLC Mesophases.* The SAXS scattering profiles of different phases formed from phytantriol–water systems with increasing temperature are well-known and hence allow precise structure

identification and detection of subtle changes. LLC matrices doped with increasing concentrations of D1 (0, 0.13%, 0.25%, 2.5%, and 5%, w/w) were prepared. The effects of D1 on the temperature-dependent structure of the phytantriol cubic phase in the absence of irradiation were examined via a temperature ramp experiment. All samples were heated from 25 to 65 °C and SAXS scattering patterns recorded at various temperatures (Figure S5). The phytantriol–water matrix prepared without D1 showed a phase transition from the V<sub>2</sub> phase to the H<sub>2</sub> phase at 50 °C and then to the reverse micelle (L<sub>2</sub>) phase at 65 °C (Figure 3). These phase transitions and the measured lattice

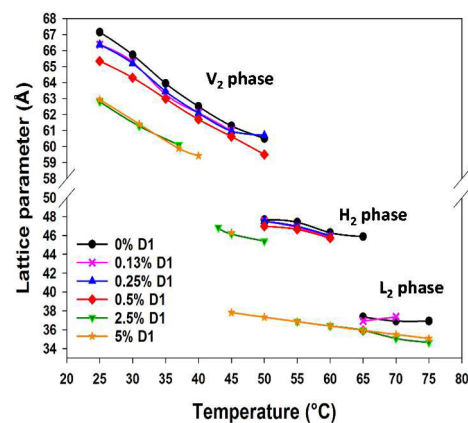


**Figure 3.** Influence of D1 on the temperature-dependent phase behavior of phytantriol-based LLC matrix. Lattice parameter versus temperature plots for LLC matrix doped with increasing concentrations of D1 (% w/w): phytantriol only (0%) (black line with filled circles), 0.13% (pink line with cross), 0.25% (blue line with up triangles), 0.5% (red line with diamonds), 2.5% (green line with down triangles), and 5% (orange line with stars). Symbols corresponding to the V<sub>2</sub> (*Pn3m* space group), H<sub>2</sub>, and L<sub>2</sub> phases are labeled on the plot.

parameters are consistent with those previously reported.<sup>28,35,33</sup> When D1 was added at concentrations of 0.13% and 0.25%, there was no influence on the liquid crystalline structure or the V<sub>2</sub>-to-H<sub>2</sub> phase transition temperature. Increasing the concentration of D1 to 0.5% resulted in slightly reduced lattice parameters but did not affect the transition temperature. Doping of the LLC matrix with 2.5% or 5% D1, however, produced a significant reduction in phase transition temperatures, with these systems existing in the H<sub>2</sub> and L<sub>2</sub> phase, respectively, at around 45 °C.

**Effects of Irradiation upon Nanostructure.** Time-resolved SAXS was used to study the dynamic phase behavior of the LLC systems with and without D1 upon exposure to green light (532 nm, 57 mW cm<sup>-2</sup>). A schematic of the dynamic irradiation experiments is shown in Figure 4.

The SAXS profiles recorded of the structures before irradiation, after 60 s of continuous irradiation, and 1 or 5 min after irradiation was completed are compared in Figure 5. The full profiles with six frames acquired every 10 s during irradiation and two frames acquired every 1 min after irradiation are shown in Figure S6. The scattering profiles show that all samples exhibited the *Pn3m* type of V<sub>2</sub> cubic phase prior to irradiation at 37 °C, with peaks at spacing ratios of  $\sqrt{2}:\sqrt{3}:\sqrt{4}:\sqrt{6}:\sqrt{8}:\sqrt{9}$ . When exposed to visible light irradiation, the phytantriol-only control sample exhibited no significant change in its scattering profiles (Figure 5a). For samples containing  $\leq 0.5\%$  D1, the peaks in the diffractograms

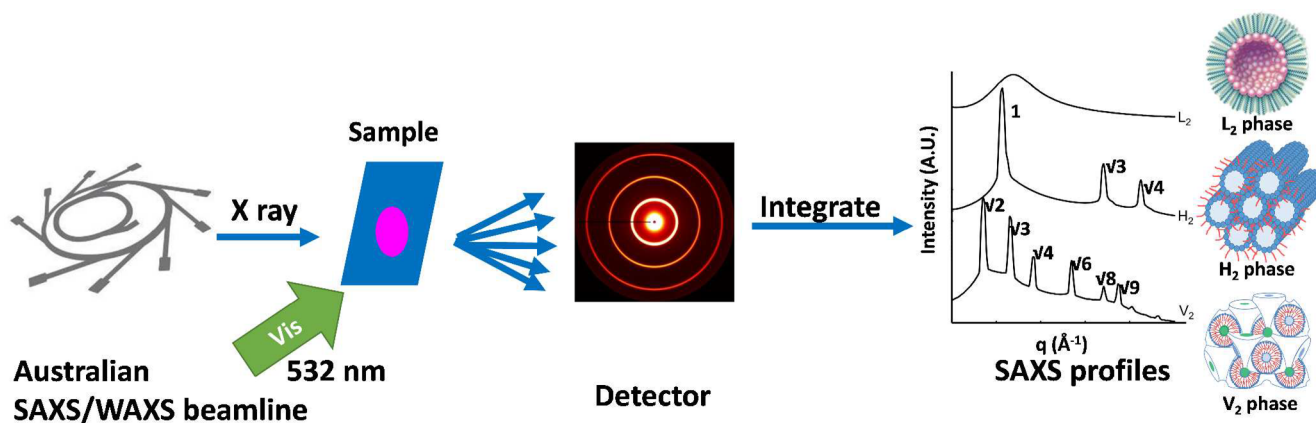


**Figure 4.** Schematic of the synchrotron SAXS and irradiation set up to identify the mesophase structure of the phytantriol-based LLC matrix with and without D1 dopant. The phase structures corresponding to the SAXS scattering profiles are shown at the left side (reproduced with permission from ref 22).

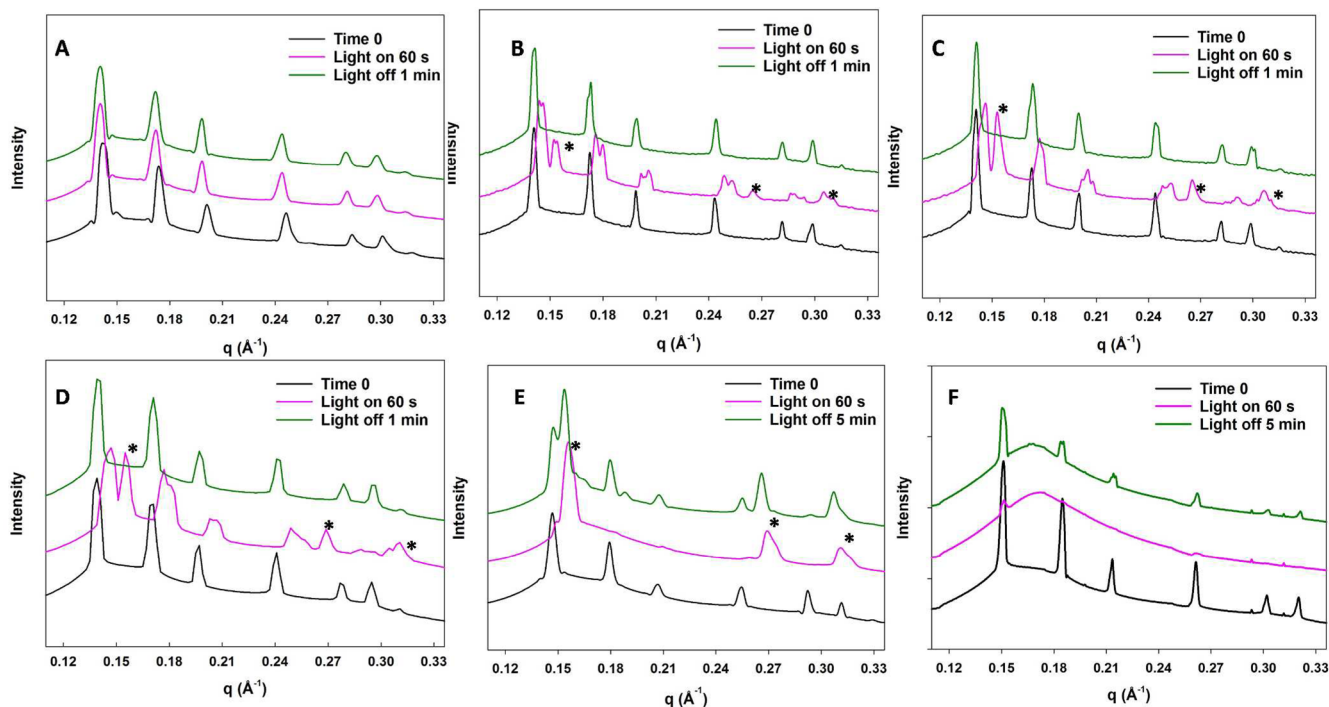


**Figure 5.** Influence of irradiation (532 nm,  $57 \text{ mW cm}^{-2}$ ) on D1-doped phytantriol-based LLC matrix. SAXS scattering profiles for the LLC matrix doped with increasing concentrations of D1 (% w/w): (A) phytantriol only (0%), (B) 0.13%, (C) 0.25%, (D) 0.5%, (E) 2.5%, and (F) 5%. The SAXS profiles are at 0 s (black line) and 60 s irradiation (pink line) and after irradiation was ceased (green line). Peaks in the SAXS profiles that indicate the presence of the  $H_2$  phase are marked with an asterisk.

exhibited a clear shift to higher  $q$  values, and a new series of peaks assigned to a  $H_2$  phase appeared after 10 s of irradiation (spacing ratio  $1:\sqrt{3}:\sqrt{4}$ , indicated with an asterisk in Figure 5b–d). Increasing the concentration of D1 led to a greater change in the phase of the LLC matrix. Irradiation of the 2.5% D1 sample led to complete conversion to  $H_2$  phase not achievable at the lower concentrations (Figure 5e), while at 5% D1 there was melting of the  $H_2$  phase to partially form the inverse micellar  $L_2$  phase (Figure 5f). This phase progression ( $V_2$  to  $H_2$  to  $L_2$ ) is well-known on heating of the phytantriol–water cubic phase, but such a significant level of disruption by a photochromic compound indicates its high potential utility in these systems, as discussed below.

The relaxation behavior of the samples after irradiation can be divided into two types. For samples containing  $\leq 0.5\%$  D1, complete reversion to the  $V_2$  phase occurred within 30 s, indicating that irradiation of D1 induced a completely reversible effect on the liquid crystalline structure. (Figure S7 shows the changes in the scattering profiles of one D1-doped sample upon two cycles of irradiation.) For samples containing higher concentrations of D1, only partial return to the  $V_2$  phase was observed. We believe that the effect here is irreversible, as the profile did not show any obvious changes over a 5 min period.

Figure 6A illustrates the changes in lattice parameter upon irradiation, with increasing concentration of D1. The lattice parameter of the phytantriol-only control sample remained

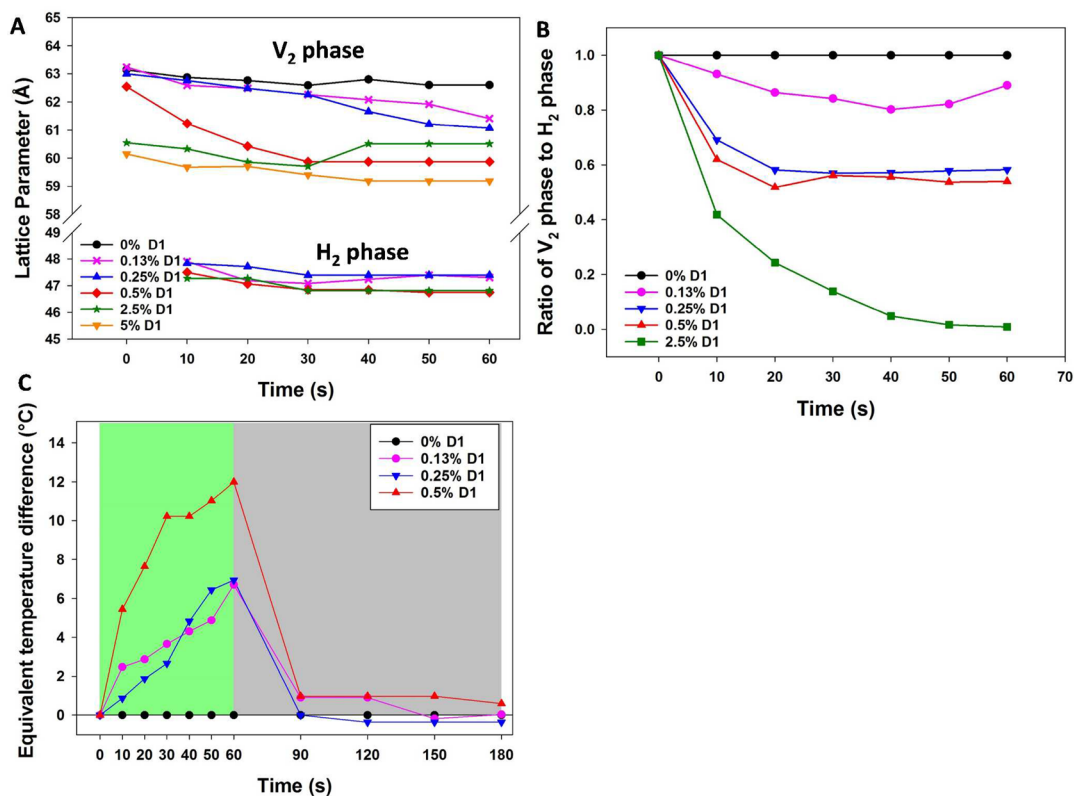


**Figure 6.** Effects of irradiation (532 nm, 57 mW cm<sup>-2</sup>) on (A) the lattice parameter of phytantriol-based LLC matrix containing 0%, 0.13%, 0.25%, 0.5%, 2.5%, and 5% D1 (w/w); (B) the ratio of intensity of first peak for V<sub>2</sub> phase to that of H<sub>2</sub> phase, as an indication of proportion of the two phases present. (C) The equivalent temperature of the samples during irradiation (green) and after irradiation (gray). Symbols corresponding to the V<sub>2</sub> (*Pn3m* space group), and H<sub>2</sub> phases are labeled on the plot.

constant throughout. For samples containing  $\leq 0.5\%$  D1, the lattice parameter of the V<sub>2</sub> phase decreased from 63 to  $\sim 60$  Å upon irradiation, while for samples containing higher levels of D1, it did not change. The lattice parameter of the visible light-induced H<sub>2</sub> phase was similar for the samples containing 0.13%, 0.25%, 0.5%, and 2.5% D1 (46–48 Å) and consistent with previous reports for the H<sub>2</sub> phase in phytantriol–water systems.<sup>28,35,37</sup>

Figure 6B shows the increase in the ratio of intensity of the first peak for the V<sub>2</sub> phase to that of the H<sub>2</sub> phase (see Supporting Information for calculation) versus irradiation time for each sample (except for the 5% D1-doped sample, whose phase behavior was distinctly different from the others). It is clear that increasing the concentration of D1 promoted formation of H<sub>2</sub> phase upon irradiation.

The equivalent temperature is derived using the temperature ramp as a calibration curve to describe the degree of disruption of packing under irradiation “equivalent” to a direct temperature change.<sup>31</sup> Figure 6C shows changes in the equivalent temperature versus irradiation time for samples containing  $\leq 0.5\%$  D1, based on the measured lattice parameter of the V<sub>2</sub> phase. After 60 s of irradiation, the 0.25% and 0.5% D1-doped samples exhibited disruption of lipid packing equivalent to increasing the equivalent temperature from 37 °C (63 Å) to 44 °C (61.1 Å) and 47 °C (59.9 Å), which is just below the complete transition temperature observed in the temperature ramp (50 °C, see Figure 3). This effect on packing is similar to that previously reported for gold nanorod-doped or graphene-doped liquid crystalline systems, where the gold nanorods and graphene provided rapid photothermal heating effects to the

system upon NIR irradiation.<sup>31,33</sup> From a potential *in vivo* application point of view, a distinct advantage of using a photoisomerization process (as for D1), rather than a photothermal heating effect to achieve a light-triggered phase change, is that it can avoid local hyperthermal effects on tissues.

The disruption observed upon irradiation is understood to result from the photoinduced isomerization of D1. When doping hydrophobic molecules into the phytantriol V<sub>2</sub> phase, they are expected to reside within the bilayer region, imparting a more negative curvature on the lipid packing and potentially inducing the formation of the H<sub>2</sub> phase at equilibrium. This effect has been seen previously for vitamin E acetate loaded into phytantriol V<sub>2</sub> phase. On the other hand, conversion to the more hydrophilic form would lead to less negative critical packing parameter, therefore normally be expected to drive the packing away from the H<sub>2</sub> phase toward the V<sub>2</sub> phase or even further to lamellar packing. However, the opposite effect was observed with addition of D1 in this case. We anticipated that D1 in its initial extended triene form is likely to reside fully within the phytantriol bilayer due to its hydrophobic nature. The disruption, however, is not sufficient to induce the phase transition due to the small molarity of D1. Although the irradiation generated the more hydrophilic cyclopentenone form, the consequent bulkier structure may induce greater disruption of the bilayer than the linear, yet more hydrophobic form, if it is still retained in the bilayer. This is in line with the photochemical response of mesophases incorporating alkylated spiropyran molecules.<sup>32,34</sup>

The spectroscopic data (*vide supra*) indicate that once D1 has undergone photoinduced conversion to the zwitterionic

cyclopentanone form within the LLC matrix, the bulk of it is unable to revert to the initial triene form. As noted earlier, a possible explanation is that the hydrophilic headgroup of **D1** in its cyclopentanone form tends to partition into the aqueous phase after irradiation was ceased, since protic surroundings are known to favor this isomer.<sup>19,20</sup> The fast reversion of most of the **D1**-doped LLC samples back from the coexisting H<sub>2</sub> phase to the V<sub>2</sub> phase upon cessation of irradiation is consistent with this proposal, since the matrix might otherwise be expected to remain in the H<sub>2</sub> phase if the cyclopentanone form was retained fully within the bilayer.

We speculate that the photoisomerization of **D1** may also be accompanied by heating effects which would account for structural reversibility without essential spectroscopic reversibility. This photothermal property has reported previously for an azobenzene-functionalized liquid crystal polymer.<sup>38</sup> Hence, when the **D1**-doped LLC samples are irradiated, the observed phase changes may be at least partially associated with an actual increase in temperature.

The study here has confirmed the hypotheses that (1) visible light has sufficient penetration to trigger the isomerization of the **DASA** doped into lyotropic liquid crystals and (2) the isomerization (likely together with a photothermal effect) provides sufficient disruption of the packing that it may be a useful photoactuator for future deployment in actual drug delivery systems. As already well reported, the phase transition of the phytantriol/water system from V<sub>2</sub> phase to H<sub>2</sub> phase represents a change from fast release pattern to slow release.<sup>29,30</sup> Hence, to achieve the goal of using light to trigger a slow-to-fast release pattern, **DASAs** will be incorporated into a more appropriate lipid system in future, with desired transitions enabled by the findings in this article. Future work will also involve using **DASAs** with alkyl chains of different length or bulky alkyl chains, which could induce greater steric effects and hence greater disruption of packing within the lipid bilayer.

## CONCLUSIONS

We have demonstrated that **DASAs** have a possible role as actuators for photoswitching in lipid-based drug delivery systems. Upon irradiation with 532 nm light, **D1** can induce a rapid and reversible phase transition within a phytantriol-based liquid crystalline system, with the impact on phase behavior being dependent on the concentration of **DASA**. The photochemical behavior of the **D1** compound in a LLC environment, however, is not straightforward, with spectroscopic studies indicating a degree of irreversibility in the photoswitching process. It is likely that the **DASA** systems impart, at least in part, a photothermal effect in addition to a photoisomerization effect on lipid packing. Further studies investigating the incorporation of structurally varied **DASAs** into different liquid crystalline systems are underway to obtain systems that display a complete phase transition upon visible light irradiation. It is anticipated that this approach has potential to enable control of drug release rate from LLC matrices and hence the development of novel, visible light-sensitive, “on-demand” drug delivery systems.

## ASSOCIATED CONTENT

### Supporting Information

The Supporting Information is available free of charge on the ACS Publications website at DOI: 10.1021/acs.langmuir.6b03726.

Detailed materials and methods, synthetic procedures for **D1**, analysis of photoswitching behavior of **D1** in toluene, studies of **D1** absorbance over time in phytantriol-based LLC systems, detailed structural characterization of LLC phases using SAXS, SAXS analysis of the effects of **D1** on the nanostructure of phytantriol-based LLC systems (PDF)

## AUTHOR INFORMATION

### Corresponding Authors

\*(B.G.) E-mail [Bim.Graham@monash.edu](mailto:Bim.Graham@monash.edu).

\*(B.J.B.) E-mail [Ben.Boyd@monash.edu](mailto:Ben.Boyd@monash.edu).

### ORCID

Wye-Khay Fong: 0000-0002-0437-9332

Ben J. Boyd: 0000-0001-5434-590X

### Notes

The authors declare no competing financial interest.

## ACKNOWLEDGMENTS

Some of this research was conducted on the SAXS/WAXS beamline at the Australian Synchrotron. B.B. and B.G. are recipients of Australian Research Council Future Fellowships. A China Scholarship Council (CSC) scholarship to S.J. is greatly acknowledged. We thank Michael D. Lee for proofreading this manuscript and Stephen Mudie (Australian Synchrotron) for his technical assistance.

## REFERENCES

- (1) Chen, H.; Liao, Y. Photochromism Based on Reversible Proton Transfer. *J. Photochem. Photobiol., A* **2015**, *300*, 22–26.
- (2) Ube, T.; Ikeda, T. Photomobile Polymer Materials with Crosslinked Liquid-Crystalline Structures: Molecular Design, Fabrication, and Functions. *Angew. Chem., Int. Ed.* **2014**, *53* (39), 10290–10299.
- (3) Aznar, E.; Oroval, M.; Pascual, L.; Murguía, J. R.; Martínez-Mañez, R.; Sancenón, F. Gated Materials for On-Command Release of Guest Molecules. *Chem. Rev.* **2016**, *116* (2), 561–718.
- (4) Croissant, J.; Chaix, A.; Mongin, O.; Wang, M.; Clement, S.; Raehm, L.; Durand, J. O.; Hugues, V.; Blanchard-Desce, M.; Maynadier, M.; et al. Two-Photon-Triggered Drug Delivery via Fluorescent Nanovalves. *Small* **2014**, *10* (9), 1752–1755.
- (5) Bandara, H. M. D.; Burdette, S. C. Photoisomerization in Different Classes of Azobenzene. *Chem. Soc. Rev.* **2012**, *41* (5), 1809–1825.
- (6) Puntoriero, F.; Ceroni, P.; Balzani, V.; Bergamini, G.; Vögtle, F. Photoswitchable Dendritic Hosts: A Dendrimer with Peripheral Azobenzene Groups. *J. Am. Chem. Soc.* **2007**, *129* (35), 10714–10719.
- (7) Klajn, R. Spiropyran-Based Dynamic Materials. *Chem. Soc. Rev.* **2014**, *43* (1), 148–184.
- (8) Xing, Q. J.; Li, N. J.; Chen, D. Y.; Sha, W. W.; Jiao, Y.; Qi, X. X.; Xu, Q. F.; Lu, J. M. Light-Responsive Amphiphilic Copolymer Coated Nanoparticles as Nanocarriers and Real-Time Monitors for Controlled Drug Release. *J. Mater. Chem. B* **2014**, *2*, 1182–1189.
- (9) Matsuda, K.; Irie, M. Diarylethene as a Photoswitching Unit. *J. Photochem. Photobiol., C* **2004**, *5* (2), 169–182.
- (10) Van Der Molen, S. J.; Liao, J.; Kudernac, T.; Agustsson, J. S.; Bernard, L.; Calame, M.; Van Wees, B. J.; Feringa, B. L.; Schönenberger, C. Light-Controlled Conductance Switching of Ordered Metal-Molecule-Metal Devices. *Nano Lett.* **2009**, *9* (1), 76–80.
- (11) Bléger, D.; Hecht, S. Visible-Light-Activated Molecular Switches. *Angew. Chem., Int. Ed.* **2015**, *54* (39), 11338–11349.
- (12) Stolik, S.; Delgado, J. A.; Pérez, A.; Anasagasti, L. Measurement of the Penetration Depths of Red and near Infrared Light in Human “Ex Vivo” Tissues. *J. Photochem. Photobiol., B* **2000**, *57* (2–3), 90–93.

- (13) Beharry, A. A.; Sadovski, O.; Woolley, G. A. Azobenzene Photoswitching without Ultraviolet Light. *J. Am. Chem. Soc.* **2011**, *133* (49), 19684–19687.
- (14) Samanta, S.; Beharry, A. A.; Sadovski, O.; McCormick, T. M.; Babalhavaeji, A.; Tropepe, V.; Woolley, G. A. Photoswitching Azo Compounds in Vivo with Red Light. *J. Am. Chem. Soc.* **2013**, *135* (26), 9777–9784.
- (15) Bléger, D.; Schwarz, J.; Brouwer, A. M.; Hecht, S. O. -Fluoroazobenzenes as Readily Synthesized Photoswitches Offering Nearly Quantitative Two-Way Isomerization with Visible Light. *J. Am. Chem. Soc.* **2012**, *134* (51), 20597–20600.
- (16) Johns, V. K.; Peng, P.; DeJesus, J.; Wang, Z.; Liao, Y. Visible-Light-Responsive Reversible Photoacid Based on a Metastable Carbanion. *Chem. - Eur. J.* **2014**, *20* (3), 689–692.
- (17) Helmy, S.; Leibfarth, F. A.; Oh, S.; Poelma, J. E.; Hawker, C. J.; Read de Alaniz, J. Photoswitching Using Visible Light: A New Class of Organic Photochromic Molecules. *J. Am. Chem. Soc.* **2014**, *136* (23), 8169–8172.
- (18) Helmy, S.; Oh, S.; Leibfarth, F. A.; Hawker, C. J.; Read De Alaniz, J. Design and Synthesis of Donor-Acceptor Stenhouse Adducts: A Visible Light Photoswitch Derived from Furfural. *J. Org. Chem.* **2014**, *79* (23), 11316–11329.
- (19) Lerch, M. M.; Wezenberg, S. J.; Szymanski, W.; Feringa, B. L. Unraveling the Photoswitching Mechanism in Donor-Acceptor Stenhouse Adducts. *J. Am. Chem. Soc.* **2016**, *138* (20), 6344–6347.
- (20) Singh, S.; Friedel, K.; Himmerlich, M.; Lei, Y.; Schlingloff, G.; Schober, A. Spatiotemporal Photopatterning on Polycarbonate Surface through Visible Light Responsive Polymer Bound DASA Compounds. *ACS Macro Lett.* **2015**, *4* (11), 1273–1277.
- (21) Alexandridis, P.; Olsson, U.; Lindman, B. A Record Nine Different Phases (Four Cubic, Two Hexagonal, and One Lamellar Lyotropic Liquid Crystalline and Two Micellar Solutions) in a Ternary Isothermal System of an Amphiphilic Block Copolymer and Selective Solvents (Water and Oil). *Langmuir* **1998**, *14* (10), 2627–2638.
- (22) Chen, Y.; Ping, M. A.; Shuangying, G. Cubic and Hexagonal Liquid Crystals as Drug Delivery Systems. *BioMed Res. Int.* **2014**, *2014*, 815981.
- (23) Phan, S.; Fong, W. K.; Kirby, N.; Hanley, T.; Boyd, B. J. Evaluating the Link between Self-Assembled Mesophase Structure and Drug Release. *Int. J. Pharm.* **2011**, *421* (1), 176–182.
- (24) Hyde, S. T. Identification of Lyotropic Liquid Crystalline Mesophases. *Handb. Appl. Surf. Colloid Chem.* **2001**, 299–332.
- (25) Spicer, P. T. Cubosomes: Bicontinuous Cubic Liquid Crystalline Nanostructured Particles. *Encycl. Nanosci. Nanotechnol.* **2004**, *1* (1), 727.
- (26) Angelova, A.; Angelov, B.; Mutafchieva, R.; Lesieur, S.; Couvreur, P. Self-Assembled Multicompartment Liquid Crystalline Lipid Carriers for Protein, Peptide, and Nucleic Acid Drug Delivery. *Acc. Chem. Res.* **2011**, *44* (2), 147–156.
- (27) Mulet, X.; Boyd, B. J.; Drummond, C. J. Advances in Drug Delivery and Medical Imaging Using Colloidal Lyotropic Liquid Crystalline Dispersions. *J. Colloid Interface Sci.* **2013**, *393* (1), 1–20.
- (28) Dong, Y. D.; Dong, A. W.; Larson, I.; Rappolt, M.; Amenitsch, H.; Hanley, T.; Boyd, B. J. Impurities in Commercial Phytantriol Significantly Alter Its Lyotropic Liquid-Crystalline Phase Behavior. *Langmuir* **2008**, *24* (13), 6998–7003.
- (29) Negrini, R.; Mezzenga, R. pH-Responsive Lyotropic Liquid Crystals for Controlled Drug Delivery. *Langmuir* **2011**, *27* (9), 5296–5303.
- (30) Fong, W. K.; Hanley, T.; Boyd, B. J. Stimuli Responsive Liquid Crystals Provide “on-Demand” Drug Delivery in Vitro and in Vivo. *J. Controlled Release* **2009**, *135* (3), 218–226.
- (31) Fong, W. K.; Hanley, T. L.; Thierry, B.; Kirby, N.; Boyd, B. J. Plasmonic Nanorods Provide Reversible Control over Nanostructure of Self-Assembled Drug Delivery Materials. *Langmuir* **2010**, *26* (9), 6136–6139.
- (32) Fong, W. K.; Malic, N.; Evans, R. A.; Hawley, A.; Boyd, B. J.; Hanley, T. L. Alkylation of Spiropyran Moiety Provides Reversible Photo-Control over Nanostructured Soft Materials. *Biointerphases* **2012**, *7* (1–4), 3–7.
- (33) Quinn, M. D. J.; Du, J.; Boyd, B. J.; Hawley, A.; Notley, S. M. Lipid Liquid-Crystal Phase Change Induced through near-Infrared Irradiation of Entrained Graphene Particles. *Langmuir* **2015**, *31* (24), 6605–6609.
- (34) Tangso, K. J.; Fong, W.; Darwish, T.; Kirby, N.; Boyd, B. J.; Hanley, T. L. Novel Spiropyran Amphiphiles and Their Application as Light-Responsive Liquid Crystalline Components. *J. Phys. Chem. B* **2013**, *117* (35), 10203–10210.
- (35) Barauskas, J.; Landh, T. Phase Behavior of the Phytantriol/water System. *Langmuir* **2003**, *19* (23), 9562–9565.
- (36) Kirby, N. M.; Mudie, S. T.; Hawley, A. M.; Cookson, D. J.; Mertens, H. D. T.; Cowieson, N.; Samardzic-Boban, V. A Low-Background-Intensity Focusing Small-Angle X-Ray Scattering Undulator Beamline. *J. Appl. Crystallogr.* **2013**, *46* (6), 1670–1680.
- (37) Dong, Y. D.; Larson, I.; Hanley, T.; Boyd, B. J. Bulk and Dispersed Aqueous Phase Behavior of Phytantriol: Effect of Vitamin E Acetate and F127 Polymer on Liquid Crystal Nanostructure. *Langmuir* **2006**, *22* (23), 9512–9518.
- (38) Lee, K. M.; White, T. J. Photochemical Mechanism and Photothermal Considerations in the Mechanical Response of Monodomain, Azobenzene-Functionalized Liquid Crystal Polymer Networks. *Macromolecules* **2012**, *45* (17), 7163–7170.

## Supporting information

# Investigation of Donor Acceptor Stenhouse Adducts as New Visible Wavelength-Responsive Switching Elements for Lipid-Based Liquid Crystalline Systems

*Shiyang Jia,<sup>†</sup> Joanne D. Du,<sup>‡</sup> Adrian Hawley,<sup>§</sup> Wye-Khay Fong,<sup>‡</sup> Bim Graham,<sup>\*†</sup> and Ben J. Boyd<sup>\*‡||</sup>*

<sup>†</sup>Medicinal Chemistry, Monash Institute of Pharmaceutical Sciences, Monash University (Parkville Campus), 381 Royal Parade, Parkville, VIC 3052, Australia.

<sup>‡</sup>Drug Delivery, Disposition and Dynamics, Monash Institute of Pharmaceutical Sciences, Monash University (Parkville Campus), 381 Royal Parade, Parkville, VIC 3052, Australia

<sup>§</sup>SAXS/WAXS beamline, Australian Synchrotron, Clayton, VIC, Australia

<sup>||</sup>ARC Centre of Excellence in Convergent Bio-Nano Science and Technology, Monash Institute of Pharmaceutical Sciences, Monash University, Parkville Campus, 381 Royal Parade, Parkville, VIC 3052, Australia

## Table of Contents

<b>1. Materials and methods</b> .....	2
<b>2. Synthesis of D1</b> .....	2
<b>3. Analysis of photoswitching behavior of D1 in toluene</b> .....	6
<b>4. Absorbance of DASA in liquid crystalline matrix over time</b> .....	6
<b>5. Structural characterization of LLC phases using small angle X-ray scattering (SAXS)</b> .....	7
<b>5.1 Temperature-dependent phase behavior</b> .....	7
<b>5.2 Dynamic irradiation experiments</b> .....	7
<b>6. SAXS analysis of the effects of D1 on the nanostructure of phytantriol-based LLC systems</b> .....	8
<b>7. Phase-switching kinetics</b> .....	10

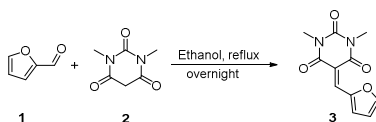


## 1. Materials and methods

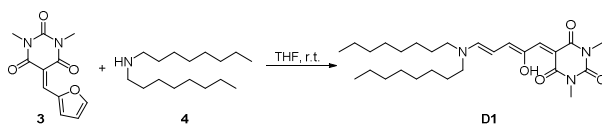
All chemicals were purchased from Sigma-Aldrich Pty, Matrix Scientific, or Merck Group Ltd and used without purification. All solvents were reagent grade. *Flash chromatography* was carried out using Merck 38 Silica gel 60, 230–400 mesh ASTM. *Thin layer chromatography (TLC)* was performed on Merck Silica Gel 60 F254 plates. TLC plates were visualized using a UV lamp at 254 nm or through the use of  $\text{KMnO}_4$  or ninhydrin staining agent.  $^1\text{H}$  and  $^{13}\text{C}$  nuclear magnetic resonance (NMR) spectra were recorded using an Avance III Nanobay 400 MHz Bruker spectrometer coupled to the BACS 60 automatic sample changer at 400.13 MHz and 100.61 MHz, respectively. Data acquisition and processing was managed using Topspin software package version 3. Additional processing was handled with MestReNova software (PC). Chemical shifts ( $\delta$ ) were measured in parts per million (ppm) referenced to an internal standard of residual solvent. Spectroscopic data are given using the following abbreviations: s, singlet; d, doublet; dd, doublet of doublets; t, triplet; q, quartet; m, multiplet; br, broad;  $J$ , coupling constant. *Analytical high-performance liquid chromatography (HPLC)* was carried out on an Agilent 1260 series modular HPLC equipped with the following modules: G1312B binary pump, G1316A thermostated column compartment equipped with an Agilent Eclipse Plus C18 3.5  $\mu\text{m}$ , 4.6 x 100 mm column and a G1312B diode array detector. The following elution protocols were used. “PP gradient”: 0–10 min, gradient from 5% buffer B/95% buffer A to 100% buffer B (buffer A = 99.9%  $\text{H}_2\text{O}$ , 0.1% TFA, and buffer B = 99.9% ACN, 0.1% TFA); flow rate = 1 mL  $\text{min}^{-1}$ . “PP hydrophobic”: 0–10 min, gradient from 80% buffer B/20% buffer A to 100% buffer B (buffer A = 99.9%  $\text{H}_2\text{O}$ , 0.1% TFA, and buffer B = 99.9% ACN, 0.1% TFA); flow rate = 1 mL  $\text{min}^{-1}$ . *High-resolution mass spectrometric (HRMS) analyses* were performed on a Waters LCT TOF LC-MS mass spectrometer coupled to a 2795 Alliance Separations module. All data were acquired and mass corrected via a dual-spray Leucine Enkephaline reference sample. Mass spectra were generated by averaging the scans across each peak and background subtraction of the TIC. Acquisition and analysis were performed using the MassLynx software version 4.1. The mass spectrometer conditions were as follows: electrospray ionization mode, desolvation gas flow of 550 L  $\text{h}^{-1}$ , desolvation temperature of 250 °C, source temperature of 110 °C, capillary voltage of 2400 V, sample cone voltage of 60 V, scan range acquired between 100–1500  $m/z$ , one sec scan times and internal reference ions for positive ion mode (Leucine Enkephaline) of 556.2771.

## 2. Synthesis of D1

**D1** was synthesized following the methods described by Helmy *et al.*,<sup>1</sup> with minor modifications. Furfural was reacted with barbituric acid through a Knoevenagel condensation to obtain the furylidene-barbituric acid **3**. Helmy *et al.* reported that treating **3** with dioctylamine (1 equiv.) in tetrahydrofuran affords the triene form of **D1** as a purple solid, which can be purified by washing with cold diethyl ether. However, we consistently obtained a viscous liquid. Attempts to purify **D1** via silica gel chromatography were hampered by the fact that **D1** appeared unstable on silica gel. Using halogenated solvent and ethyl acetate for elution could stabilize **D1** to some extent, affording **D1** with 85% purity by analytical HPLC (245 nm).



**5-(Furan-2-ylmethylene)-1,3-dimethylpyrimidine-2,4,6(1H,3H,5H)-trione (3):** Furfural **1** (2.16 g, 22.5 mmol) was added dropwise to a solution of barbituric acid **2** (2.34 g, 15 mmol) in EtOH (30 mL) and the mixture refluxed overnight. After cooling to room temperature, the mixture was concentrated under reduced pressure and the residue taken up into H<sub>2</sub>O (20 mL) and washed with EtOAc (3 × 30 mL). The organic layers were combined, washed with H<sub>2</sub>O (20 mL), dried with anhydrous Na<sub>2</sub>SO<sub>4</sub> and concentrated under reduced pressure. The crude residue was purified by silica gel flash chromatography (EtOAc/petroleum spirits) to yield the product as a yellow solid. Yield: 2.68 g, 76%. <sup>1</sup>H NMR (400 MHz, CDCl<sub>3</sub>): δ 8.61 (d, *J* = 3.8 Hz, 1H), 8.40 (s, 1H), 7.83 (d, *J* = 0.9 Hz, 1H), 6.72 (d, *J* = 2.9 Hz, 1H), 3.38 (s, 3H), 3.37 (s, 3H). <sup>13</sup>C NMR (101 MHz, CDCl<sub>3</sub>): δ 162.52, 160.91, 151.45, 151.23, 150.50, 141.03, 128.11, 115.24, 111.50, 29.06, 28.30. HRMS (ESI) *m/z* calcd. [M+H]<sup>+</sup>, M = C<sub>11</sub>H<sub>10</sub>N<sub>2</sub>O<sub>4</sub>: 235.0713, found: 235.0718.



**5-((2Z,4E)-5-(diocetyl-amino)-2-hydroxypenta-2,4-dien-1-ylidene)-1,3-dimethylpyrimidine-2,4,6(1H,3H,5H)-trione (D1):** Diocetylamine **4** (0.36 g, 1.5 mmol) was added dropwise to a suspension of the activated furan **3** (0.35 g, 1.5 mmol) in THF (5 mL). The color of the mixture rapidly changed from yellow to pink, then to dark red. Stirring at room temperature was continued until the reaction was judged to be complete by analytical HPLC (PP, hydrophobic). The solvent was removed under reduced pressure and the crude residue was purified by silica gel flash chromatography (1:1 → 2:1 EtOAc/CH<sub>2</sub>Cl<sub>2</sub>) to yield **D1** as a viscous purple oil. Yield: 0.51 g, 71%. <sup>1</sup>H NMR (400 MHz, CD<sub>2</sub>Cl<sub>2</sub>): δ 7.29 (d, *J* = 12.2 Hz, 1H), 7.04 (s, 1H), 6.81 (d, *J* = 12.4 Hz, 1H), 6.08 (t, *J* = 12.3 Hz, 1H), 3.41 (m, 4H), 3.29 (s, 3H), 3.26 (s, 3H), 1.67 (m, 4H), 1.40–1.22 (m, 20H), 0.89 (t, *J* = 6.6 Hz, 6H). <sup>13</sup>C NMR (101 MHz, CD<sub>2</sub>Cl<sub>2</sub>): δ 165.62, 163.55, 158.62, 151.86, 146.73, 137.86, 103.48, 98.02, 58.31, 50.27, 32.28, 29.72, 29.67, 29.64, 29.43, 28.58, 28.47, 27.66, 27.45, 26.94, 23.16, 14.39. HRMS (ESI) *m/z* calcd. [M+H]<sup>+</sup>, M = C<sub>27</sub>H<sub>45</sub>N<sub>3</sub>O<sub>4</sub>: 476.3483, found: 476.3467. [M+Na]<sup>+</sup>: 498.3302, found: 498.3276. Analytical HPLC: 85% purity (254 nm).

**Figure S1.**  $^1\text{H}$  and  $^{13}\text{C}$  NMR spectra of 5-(furan-2-ylmethylene)-1,3-dimethylpyrimidine-2,4,6(1H,3H,5H)-trione (**3**) in  $\text{CDCl}_3$ .

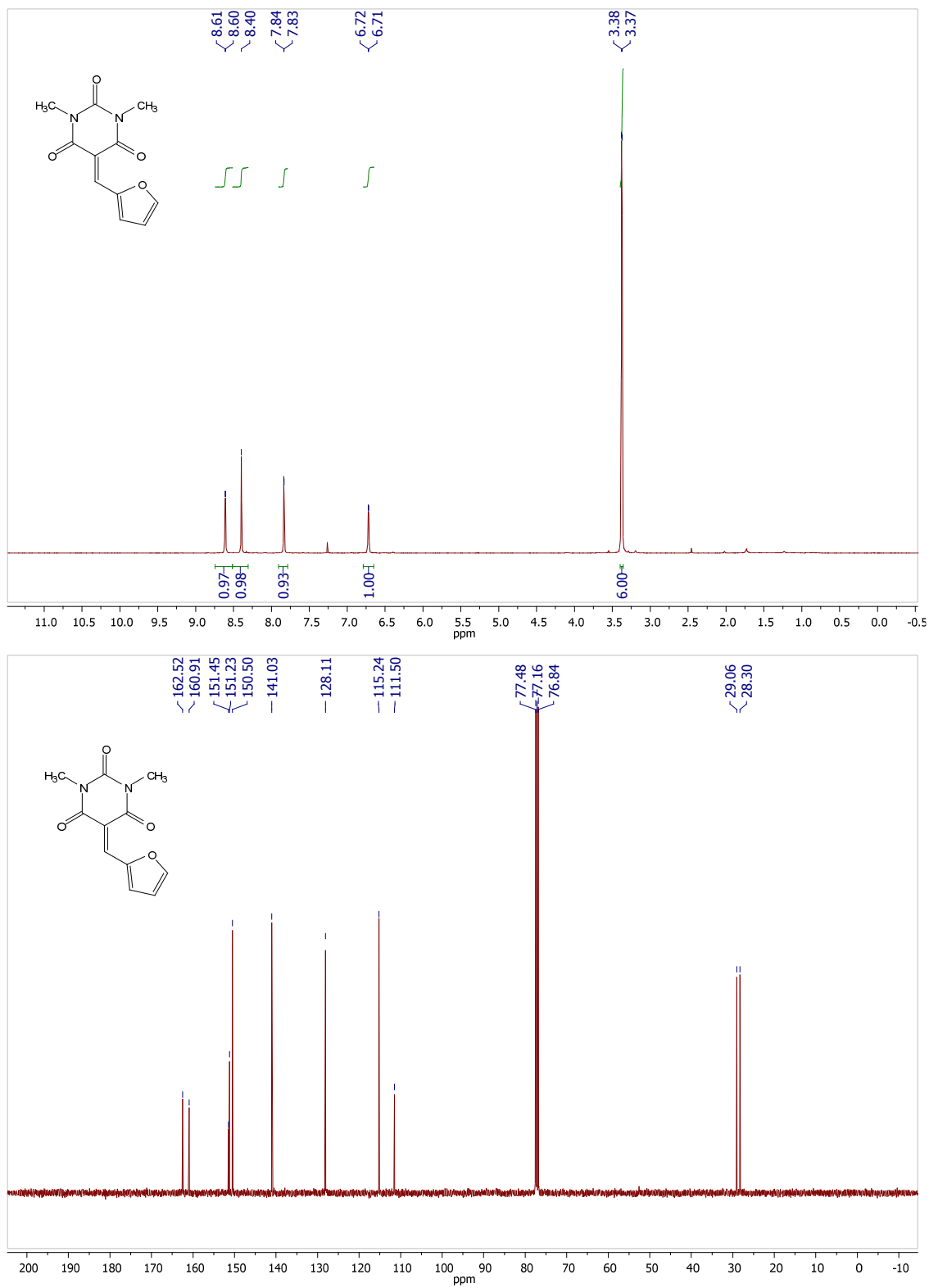
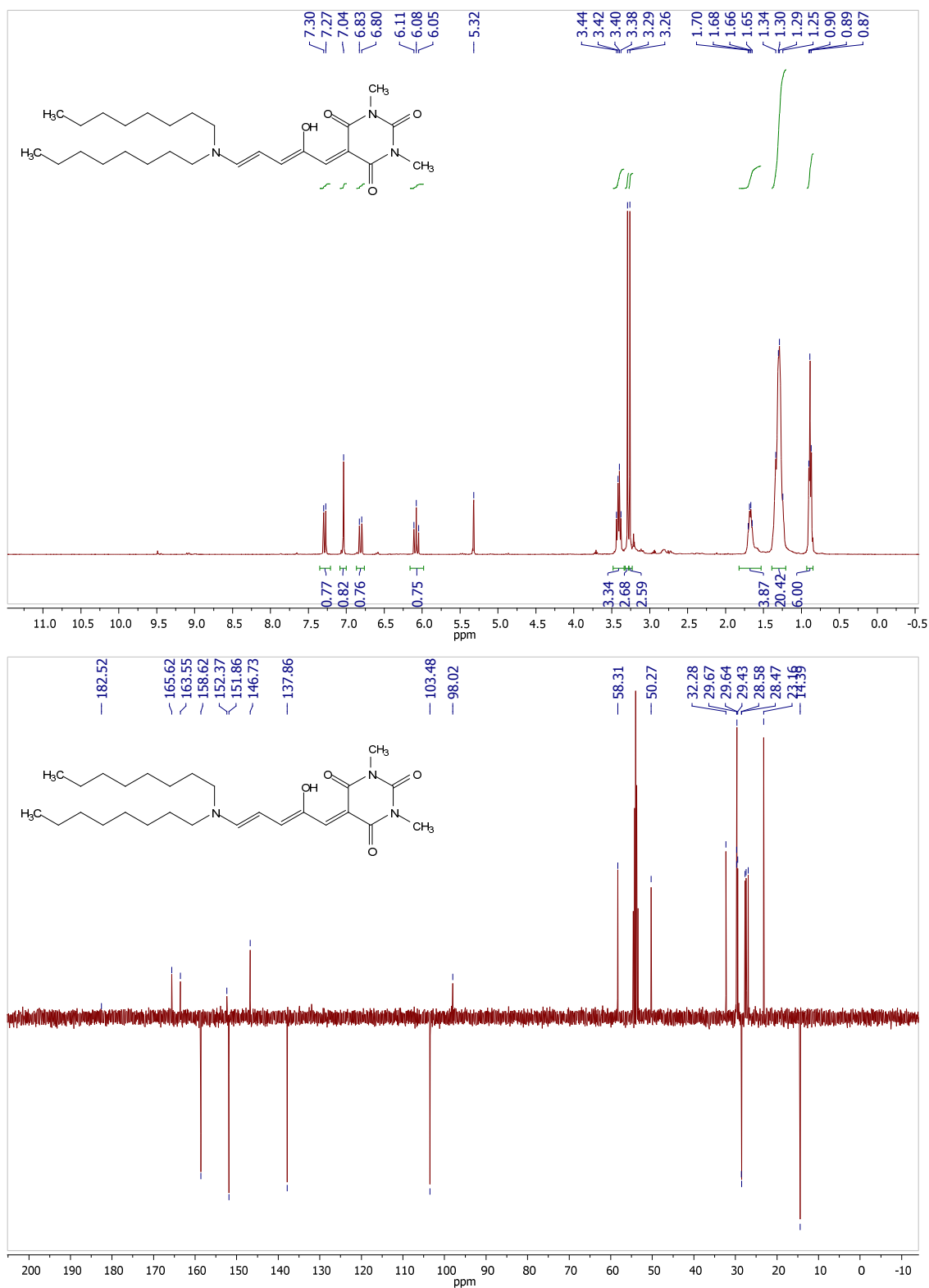


**Figure S2.**  $^1\text{H}$  and  $^{13}\text{C}$  NMR spectra of 5-((2Z,4E)-5-(dioctylamino)-2-hydroxypenta-2,4-dien-1-ylidene)-1,3-dimethylpyrimidine-2,4,6(1H,3H,5H)-trione (**D1**) in  $\text{CD}_2\text{Cl}_2$ .



### 3. Analysis of photoswitching behavior of D1 in toluene

A solution of **D1** in toluene ( $4 \mu\text{g mL}^{-1}$ ) was placed in a quartz cuvette (Hellma Analytics, 100-QS, 20 mm) and irradiated with a cold LED light ( $12 \text{ W cm}^{-2}$ ) from above. The absorption spectra was measured periodically using an Agilent Cary 50 UV-Vis spectrophotometer, with a recording time of approximate 20 s.

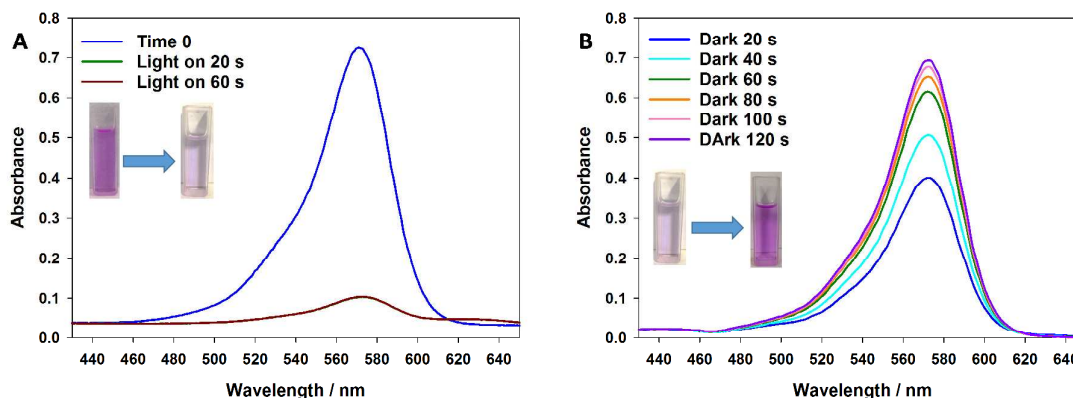


**Figure S3.** Absorption spectra of **D1** in toluene ( $4 \mu\text{g mL}^{-1}$ ) before (A) and after (B) cold LED light irradiation ( $12 \text{ mW cm}^{-2}$ ).

### 4. Absorbance of D1 in liquid crystalline matrix over time

We investigated the stability of **D1** in phytantriol-based liquid crystalline sample by absorbance measurements. The sample was presented to the green laser beam as a fully hydrated thin layer on the inside of a quartz cuvette. The result is shown below in Figure S4 A, showing some initial decrease in absorbance then a plateau after approximately 5 hr and was constant for three days (72 hrs). All SAXS measurements were undertaken at 70 hr after preparation. It is possible that the thickness of the layer may decrease over time due to gravity inducing the decrease in absorbance. To address this problem, we doped **D1** into liposomes that were prepared from DLPC and lauric acid with the same buffer that was used in this manuscript. The absorbance change of **D1** in liposome over time is shown in Figure S4 B. As can be seen from the plots below, the absorbance of **D1** also plateaued after 5 hours. Even though a drop on the absorbance occurred, the remaining triene form of **D1** after a long term still induced sufficient disruption on the nanostructure of the host material upon irradiation.

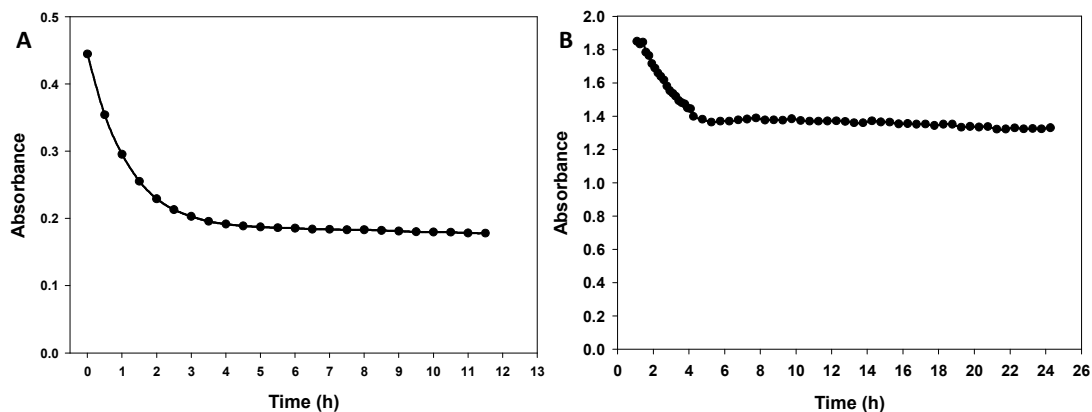


**Figure S4** (A) The absorbance of D1 doped into phytantriol-based liquid crystalline (0.02 %, w/w) matrix was monitored over time. The sample was presented to the beam as a fully hydrated thin layer on the inside of a quartz cuvette (Hellma Analytics, 100-QS, 20 mm). (B) The absorbance of D1 doped into DLPC/lauric acid-based liposome (4 %, w/w) matrix was monitored over time.

## 5. Structural characterization of LLC phases using small angle X-ray scattering (SAXS)

### 5.1 Temperature-dependent phase behavior

Phytantriol-based bulk phase samples were loaded into a flat stainless steel metal plate (96 sample positions with a thickness of 0.5 mm) sealed on both sides with Kapton tape, which was attached to a thermostated heating block and mounted on the SAXS/WAXS beamline at the Australian Synchrotron. The holder was equilibrated at 25 °C for at least 30 min before acquiring the first scattering pattern, with 10 min equilibration at each  $5.0 \pm 0.2$  °C temperature increment from 25 to 65 °C, with the actual temperature recorded to within 0.2 °C with a thermocouple. Radiation with wavelength ( $\lambda$ ) of 1.0322 Å (12 keV) was selected and an acquisition time of 0.5 s was used. The 2D scattering patterns were collected on a 1 M Pilatus detector, which covered the  $q$  range of interest from 0.0021 to  $1.0986 \text{ \AA}^{-1}$ , where  $q = 4\pi \sin(\theta/\lambda)$  and  $\theta$  is the scattering angle.

### 5.2 Dynamic irradiation experiments

Time-resolved irradiation experiments using synchrotron SAXS were conducted to assess the efficiency and reversibility of phase transitions induced by **D1**.

Bulk sample matrices prepared in McIlvaine's buffers (pH 4.8) containing varying concentrations (0, 0.13%, 0.25%, 0.5%, 2.5% and 5%) of photochromic additive **D1** were loaded into a flat stainless steel metal plate (96 sample positions with a thickness of 0.5 mm) sealed on both sides with Kapton tape and irradiated with green light (200 mW, 532 nm) at 60 s exposure times. The green light was delivered to the samples using an MGL-532(FC)-1W laser and fiber optic cable, with the end of the fiber optic cable positioned approximately 5 cm from the sample at a slight tangent to the X-ray beam. The irradiation studies were conducted at 37 °C at the SAXS beamline at the Australian Synchrotron, with the samples mounted inside a temperature controlled capillary holder. The 2D scattering patterns were acquired for 0.5 s every 10 s for the first 1 min, then every minute for 3

min, using a 1 M Pilatus detector (active area  $169 \times 179 \text{ mm}^2$  with a pixel size of  $172 \mu\text{m}$ ) located 956 mm from the sample position.

The computer software ScatterBrain Analysis was used to reduce 2D scattering patterns to the one-dimensional scattering function  $I(q)$ . The d-spacing of the liquid crystalline lattice is derived from Bragg's law ( $2d \sin \theta = n\lambda$ ), where  $n$  is an integer,  $\lambda$  is the wavelength, and  $\theta$  is the scattering angle). Since the scattering profiles of the  $V_2$ ,  $H_2$ , and  $L_2$  phases have been well characterized using SAXS, by observing the difference in relative positions of the Bragg peaks, correlated by the Miller indices of known phases, we can confirm the phase identity of the system being analyzed. The  $V_2$  phase with Pn3m spacegroup has the Bragg reflections  $\sqrt{2}:\sqrt{3}:\sqrt{4}:\sqrt{6}:\sqrt{8}:\sqrt{9}$ , etc., while the  $H_2$  phase can be identified by the Bragg reflections  $1:\sqrt{3}:\sqrt{4}$ , etc. The  $L_2$  phase is identified by a singular characteristic broad peak. The absolute location of the peaks allows for the calculation of mean lattice parameter,  $a$ , of the matrices, from the corresponding interplanar distance,  $d$  ( $d = 2\pi/q$ ), using the appropriate scattering law for the phase structure. For cubic phases,  $a = d(h^2 + k^2 + l^2)^{1/2}$ , while for the  $H_2$  phase,  $a = 4d/3(h^2 + k^2)^{1/2}$ , where  $h$ ,  $k$ , and  $l$  are the Miller indices for the particular structure present. Since the  $L_2$  phase shows only one broad peak,  $d$  is termed the characteristic distance.<sup>2</sup>

## 6. SAXS analysis of the effects of D1 on the nanostructure of phytantriol-based LLC systems

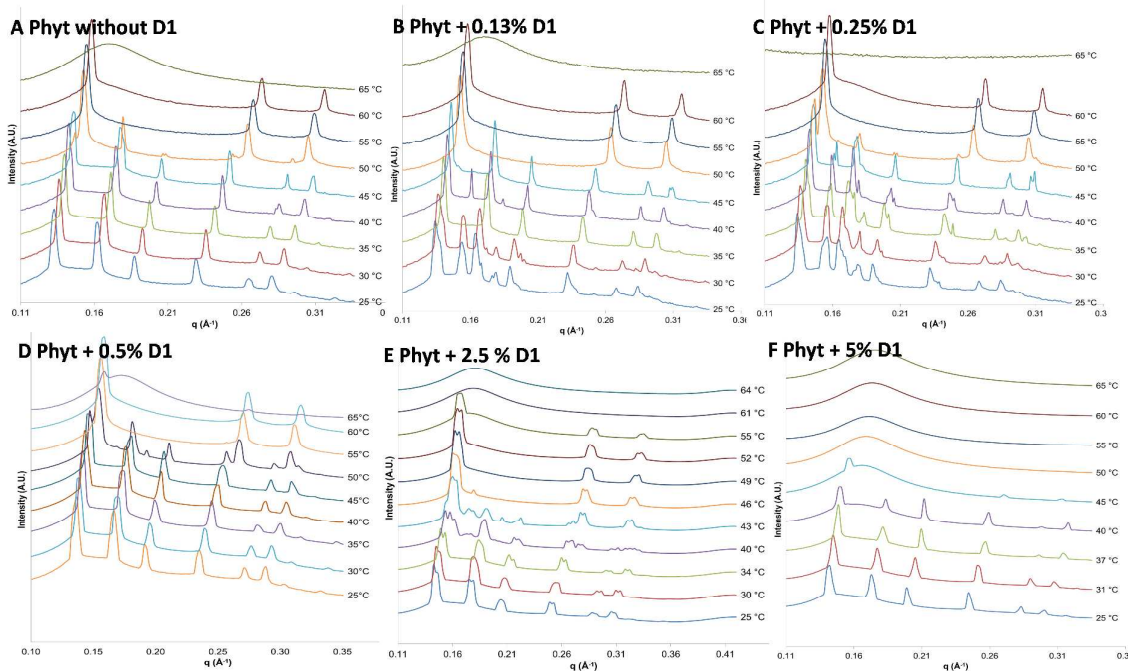


**Figure S5.** The influence of **D1** on the temperature-dependent phase behavior of phytantriol-based LLC matrix. Phase behavior of LLC matrix doped with increasing concentrations of **D1** (%w/w): (A) phytantriol-only (0%), (B) 0.13%, (C) 0.25%, (D) 0.5%, (E), 2.5%, and (F) 5%.

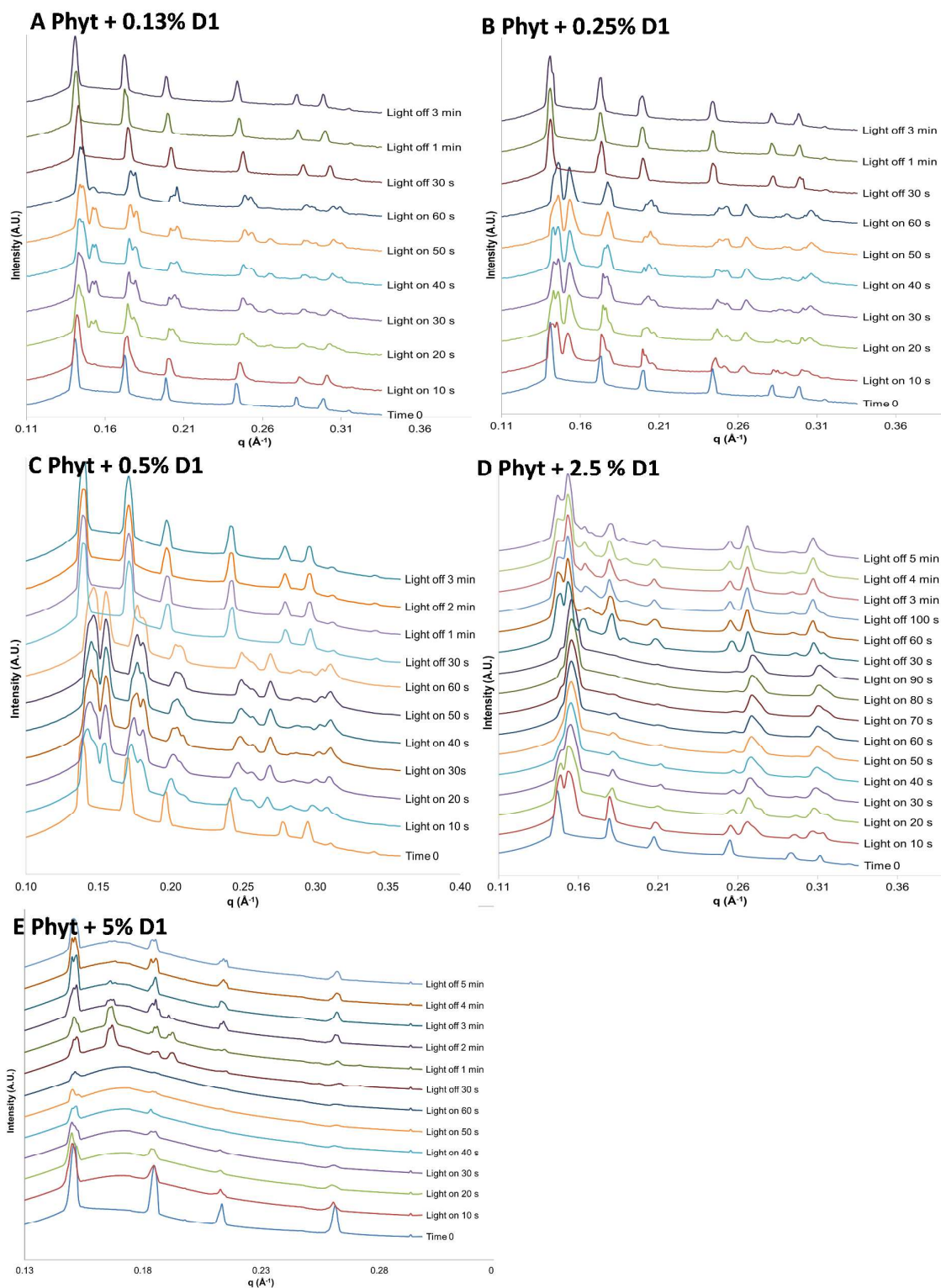


**Figure S6.** SAXS scattering profiles of phytantriol-based LLC matrix doped with increasing concentrations of **D1** (%w/w): (A) 0.13%, (B) 0.25%, (C) 0.5%, (D), 2.5%, and (E) 5%. The matrices were exposed to 60 s of green light (532 nm, 57 mW cm<sup>-2</sup>). The SAXS profiles are recorded at 0 s and every 10 s during 60 s irradiation, and after irradiation ceased.

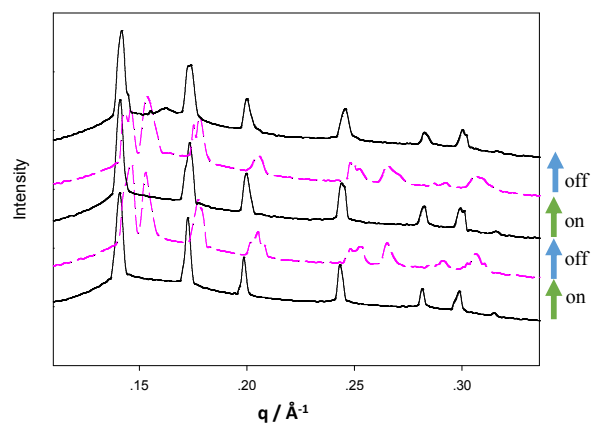


**Figure S7.** Time-resolved SAXS profiles showing the reversible phase transition of the **D1** (0.25% w/w)-containing phytantriol-based LLC matrix. The sample was exposed to irradiation (532 nm, 57 mW cm<sup>-2</sup>) for two cycles (60 s laser on, 60 s laser off, 30 s laser on, 30 s laser off) (from bottom to top).

## 7. Phase-switching kinetics

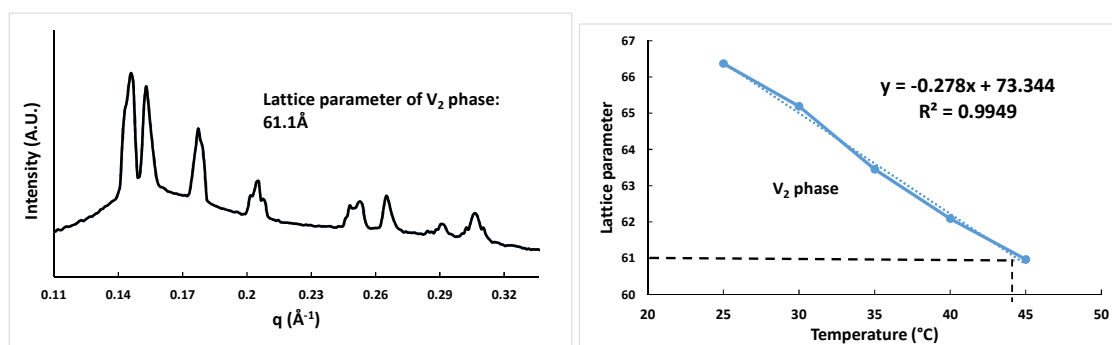
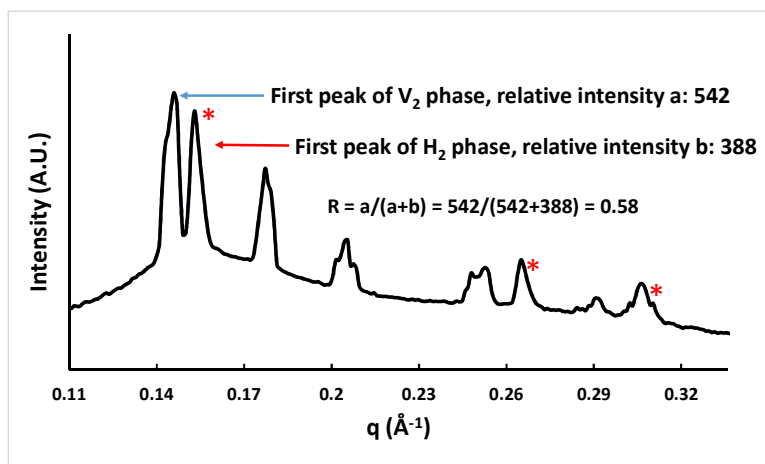


**Figure S8.** Schematic showing how equivalent temperature can be derived from the lattice parameter vs. temperature calibration plot (generated from equilibrium temperature scans) by determining the lattice parameter of the phase identified from the SAXS scattering profile. Example for **D1** (0.25% w/w)-containing phytantriol-based LLC sample after 60 s of irradiation (532 nm, 57 mW cm<sup>-2</sup>).



Equation:  $R = a/(a+b)$ , where  $R$  is the relative amount of  $V_2$  phase,  $a$  is the intensity of the first peak for the  $V_2$  phase, and  $b$  is the intensity of the first peak for the  $H_2$  phase.

**Figure S9.** Schematic showing how relative amount of  $V_2$  phase is approximated from the intensities of peaks corresponding to the  $V_2$  and  $H_2$  phases in the SAXS scattering profile. Example for **D1** (0.25% w/w)-containing phyantriol-based LLC sample after 60 s of irradiation (532 nm, 57 mW cm<sup>-2</sup>). The peaks that correspond to the  $H_2$  phase are marked with an asterisk.

## References

1. S. Helmy, F. Leibfarth, S. Oh, J. E. Poelma, C. J. Hawker and J. Read de Alaniz, *J. Am. Chem. Soc.*, 2014, **136**, 8169–8172.
2. Hyde, S. T. In *Handbook of Applied Surface and Colloid Chemistry*; Holmberg, K., Ed.; **2001**; Chapter 16, pp 299–332.

# Lipid Liquid-Crystal Phase Change Induced through near-Infrared Irradiation of Entrained Graphene Particles

Matthew D. J. Quinn,<sup>†</sup> Joanne Du,<sup>‡</sup> Ben J. Boyd,<sup>‡</sup> Adrian Hawley,<sup>§</sup> and Shannon M. Notley<sup>\*||</sup>

<sup>†</sup>Department of Chemistry and Biotechnology, Faculty of Science, Engineering and Technology, Swinburne University of Technology, Hawthorn, Victoria 3122, Australia

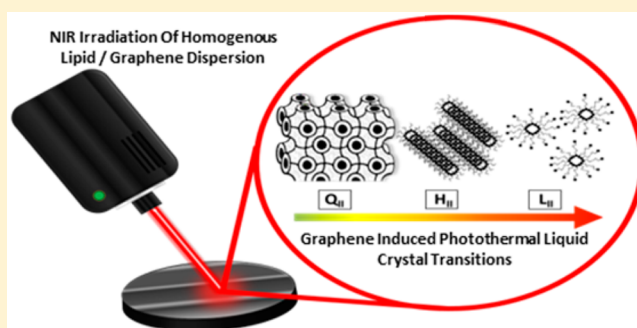
<sup>‡</sup>Drug Delivery, Disposition and Dynamics and ARC Centre of Excellence in Convergent Bio-Nano Science and Technology, Monash Institute of Pharmaceutical Sciences, Monash University (Parkville Campus), 381 Royal Parade, Parkville, Victoria 3052, Australia

<sup>§</sup>SAXS/WAXS Beamline, Australian Synchrotron, Clayton, Victoria, Australia

<sup>||</sup>Department of Applied Mathematics, Research School of Physics and Engineering, The Australian National University, Canberra, ACT 0200, Australia

## S Supporting Information

**ABSTRACT:** Lipid packing is intimately related to the geometry of the lipids and the forces that drive self-assembly. Here, the photothermal response of a cubic liquid-crystalline phase formed using phytantriol in the presence of low concentrations of pristine graphene was evaluated. Small-angle X-ray scattering showed the reversible phase changes from cubic to hexagonal to micellar due to localized heating through irradiation with near-infrared (NIR) light and back to cubic after cooling.



## INTRODUCTION

Amphiphilic lipid molecules are capable of forming highly structured liquid-crystalline (LC) matrices in the presence of water,<sup>1,2</sup> other surfactants,<sup>3,4</sup> and a range of nanoparticles.<sup>5,6</sup> The ability of these lipid molecules to form such structures opens up a range of potential applications such as LC templating for enhanced photocatalytic<sup>7,8</sup> and photothermal<sup>9–11</sup> conversions as well as many well-established roles in drug delivery and release strategies.<sup>12–15</sup>

Nanoparticles such as gold and graphene derivatives have been explored in recent years as photothermal agents,<sup>16–19</sup> particularly in biomedical applications because of their high optical absorption in the near-infrared (NIR) region<sup>16</sup> along with the inherent advantages associated with the substantial surface area to volume ratio provided by nanoscale materials. Graphene, as a truly 2D material, shows great promise in photothermal applications because every atom in the material is exposed and hence can absorb incident radiation, unlike 3D materials where the internal “dead volume” does not contribute to light absorption. Defect-free graphene or pristine graphene also has an ultrahigh thermal conductivity leading to enhanced heat distribution. There has hence been many proposed uses for graphene in biomedical applications such as thermal ablative therapy<sup>20</sup> and stimuli-responsive drug delivery<sup>21,22</sup> because of these attractive photothermal properties.

The photothermal ability of graphene can be directly demonstrated by introducing the nanosheets into the lipid

LC dispersion. Defects of the graphene sheets must be minimized during production in order to maximize the polyaromatic structure, allowing for greater NIR light absorption and thermal transport.<sup>23</sup> Surfactant-assisted liquid-phase exfoliation of graphite is highly suited to the production of defect-free graphene<sup>24,25</sup> and has been used herein.

Synchrotron small-angle X-ray scattering (SAXS) allows the direct determination of the structural evolution of these lipid systems through the identification of phase transitions occurring during NIR exposure. The phytantriol–water system provides a useful, chemically stable tool for proof of concept of photothermal phase behavior (Figure 1). This system forms a bicontinuous cubic phase (Q<sub>II</sub>) at low temperatures and transitions to a reversed hexagonal phase (H<sub>II</sub>) at higher temperatures with incremental decreases in the lattice dimension during the heating process in excess water environments. Further temperature increases result in the formation of an isotropic reverse micellar phase.<sup>26</sup>

## EXPERIMENTAL SECTION

The LC phytantriol matrices were prepared by incorporating aqueous pristine graphene suspensions stabilized by the triblock nonionic copolymer surfactant Pluronic F108 (PEO<sub>141</sub>PPO<sub>44</sub>PEO<sub>141</sub>) into neat phytantriol in a ratio of 1:1 (% w/w) as described in the Supporting

Received: April 19, 2015

Revised: June 8, 2015

Published: June 9, 2015

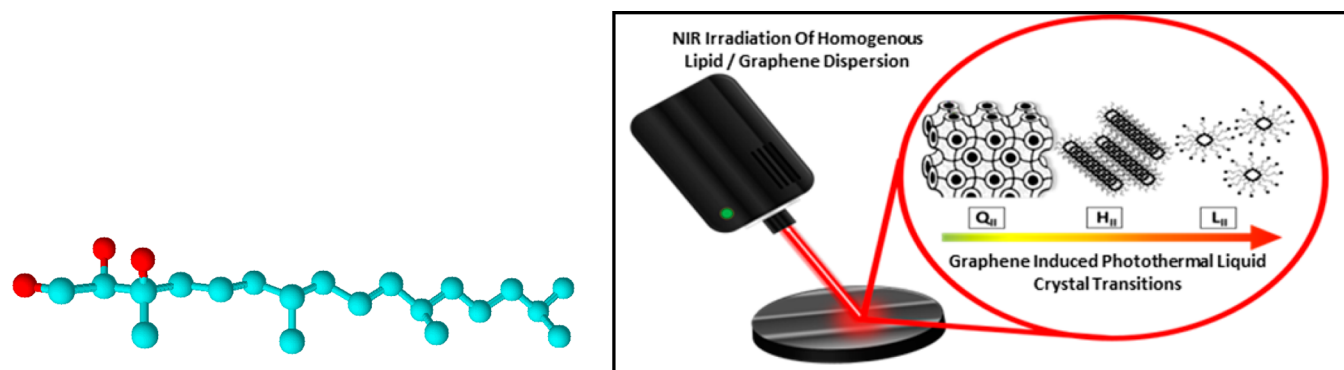


**Figure 1.** (Left) Phytantriol molecular structure, a chemically stable lipid used for all photothermal experiments (carbon, blue; oxygen, red). (Right) Schematic diagram showing the change in phase upon photothermal heating of the phytantriol–water liquid crystal.

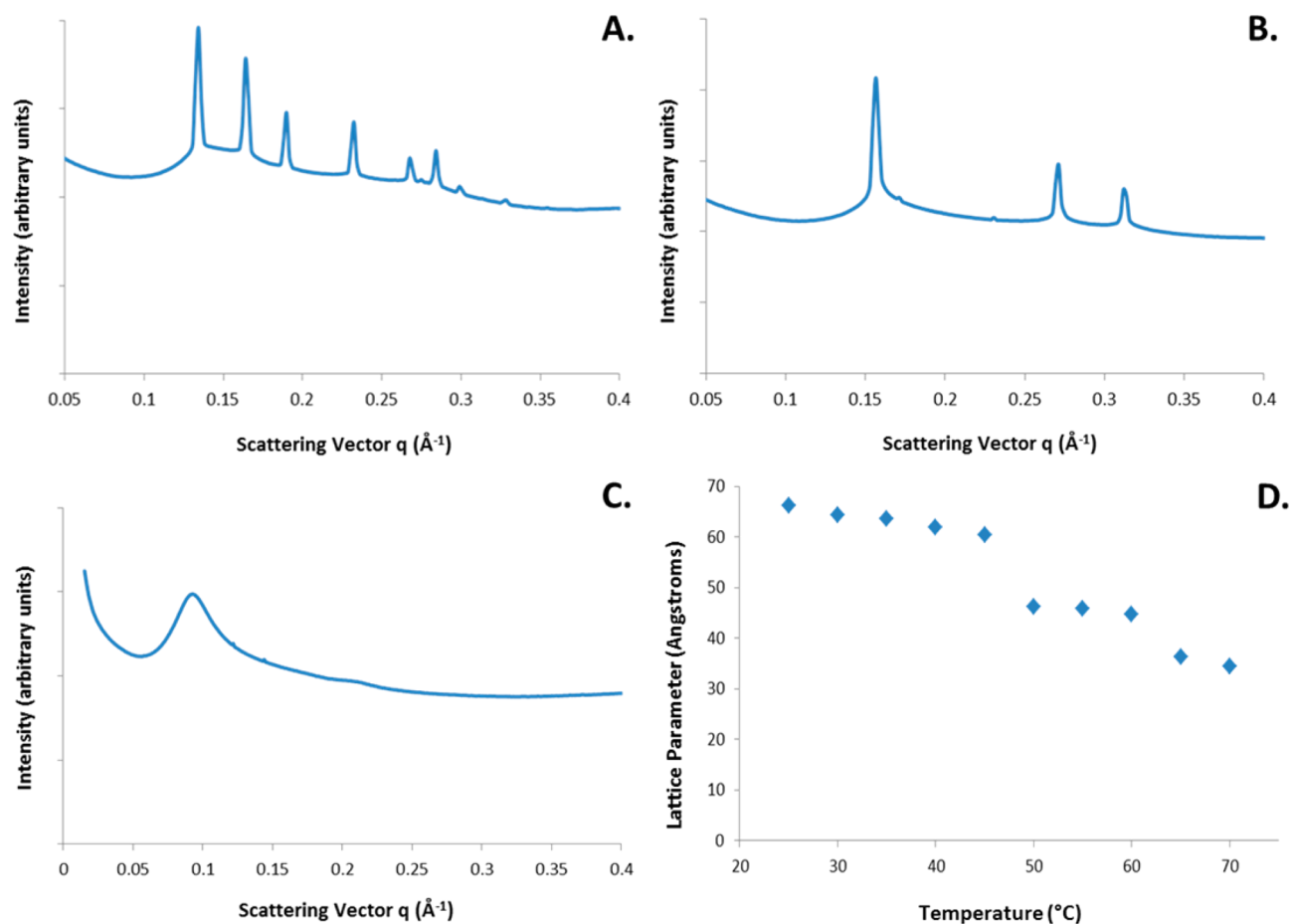


**Figure 2.** SAXS pattern for the phytantriol 0.5 g·L<sup>-1</sup> F108-graphene dispersions at (A) 25 °C, (B) 50 °C, and (C) 65 °C and (D) the lattice parameter of 0.5 g·L<sup>-1</sup> graphene phytantriol.

Information (SI). Surfactant-stabilized graphene was prepared using a procedure described by Notley<sup>24</sup> (preparation and characterization of graphene details provided in the SI). Information on the SAXS experiments conducted at the Australian Synchrotron is also provided in the SI.

## RESULTS AND DISCUSSION

Initial SAXS patterns of the cubic phase in the presence and absence of graphene were collected with 100 ms snapshots to preclude any effect on the packing structure of the phytantriol due to the presence of the nanosheets (Figure S4). These preliminary scattering snapshots indicated that the graphene

sheets did not significantly alter the initial packing at room temperature because there were no identifiable changes to the collected SAXS patterns. With average lateral dimensions in the range of 100–500 nm it is likely that the sheets are too large to interact with the nanostructure itself and more likely that the sheets are present in the aqueous phase. The positioning within the aqueous phase is further supported when the surfactant employed is considered. Surfactant molecule F108 would impart strong hydrophilic properties to the sheets with the PPO segments adsorbed to the basal planes while the PEO segments would be exposed in solution. Furthermore, the high flexural stiffness of graphene would suggest that the particles

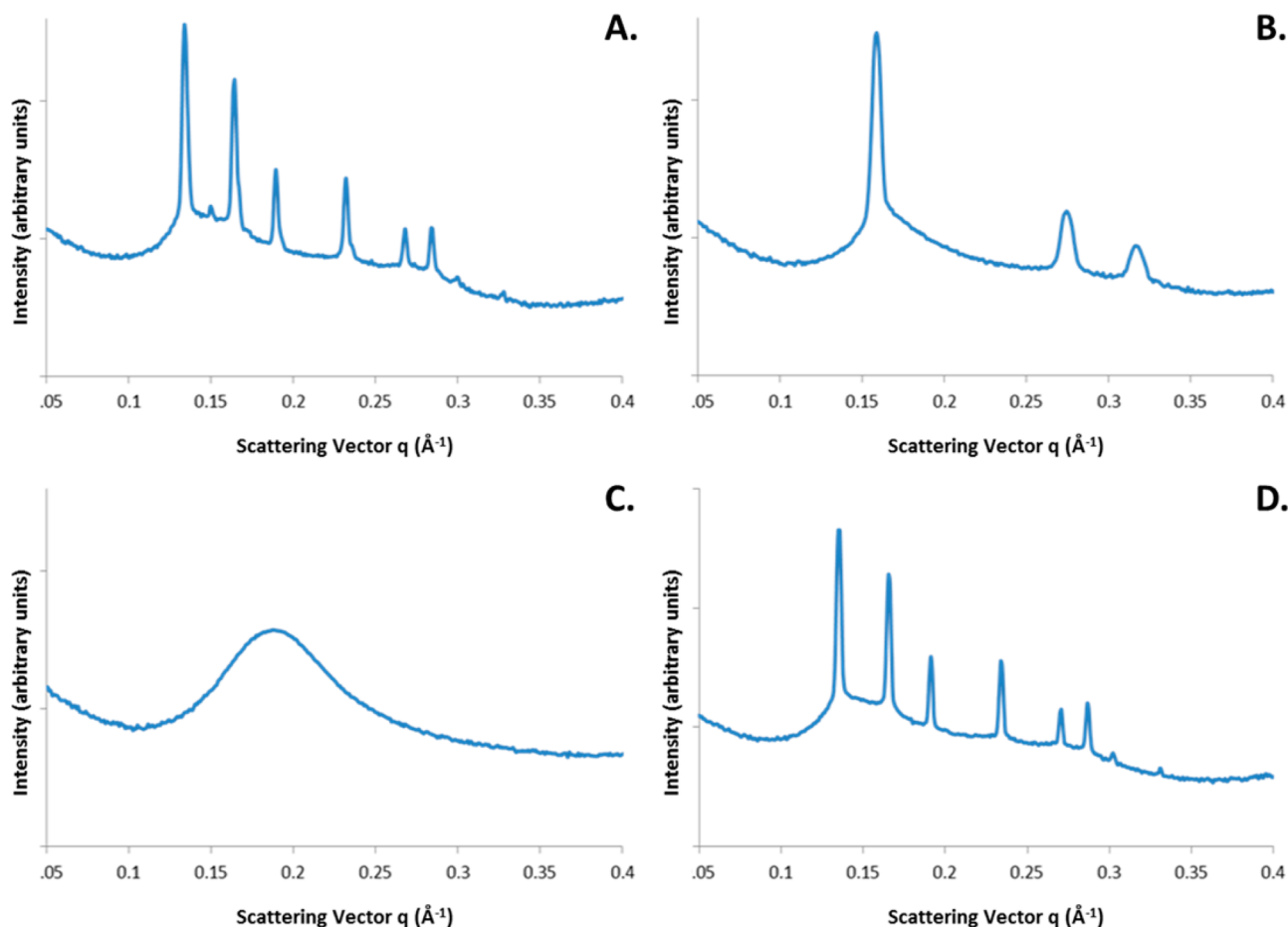


**Figure 3.** SAXS pattern for the phytantriol 0.5 g·L<sup>-1</sup> F108-graphene dispersions after (A) 0, (B) 15, and (C) 50 s of 400 mW 808 nm exposure and (D) 60 s after the laser was switched off.

cannot bend to fit the shape induced by the LC template. Attempts to determine the location of the molecularly thin graphene sheets relative to the liquid crystals are ongoing.

To further investigate any impact of graphene on the structure of the self-assembled phytantriol systems in water and to enable the construction of a lattice parameter versus temperature calibration plot, a temperature ramp was conducted where the samples at equilibrium were incrementally heated and the structure at each temperature was determined using SAXS. The transitions shown in Figure 2 are readily identified by their Bragg peak positions in the diffractograms. Figure 2A shows the Bragg reflections at a spacing ratio of  $2^{1/2}:3^{1/2}:4^{1/2}:6^{1/2}:8^{1/2}:9^{1/2}$  which indicates a reversed “double diamond-type” cubic phase, with a  $Pn3m$  space group, which consists of contorted bilayers that partition hydrophobic and hydrophilic regions into continuous but nonintersecting spaces.<sup>13,27</sup> At approximately 50 °C, Figure 2B shows reflections at a spacing ratio of  $1:3^{1/2}:4^{1/2}$ , indicating a transition to the reversed hexagonal phase which is a dense packing of water-filled rods, arranged on a 2D hexagonal lattice and separated by lipid bilayers. Finally, Figure 2C shows the transition to the isotropic reversed micellar phase, characterized by a singular broad peak. Figure 2D indicates the temperature-dependent changes in the structure and lattice parameter. The temperature ramp showed that the cubic phase converted almost completely to a  $H_{II}$  phase between 45 and 50 °C. Between 60 and 65 °C the characteristic hexagonal-phase peaks disappeared as the lipid dispersion converted to the  $L_{II}$  phase.

The photothermal studies were performed by exposing the graphene/phytantriol bulk dispersion to NIR radiation while collecting 100 ms SAXS patterns periodically over 60 s. Scattering snapshots were collected for a 2 min cool-down period after irradiation was stopped, mapping the reversibility of the phase transitions. Full transitions in excess water from reversed cubic space group  $Pn3m$  to the reversed hexagonal phase and through to a fluid isotropic reversed micellar phase were observed over the 60 s exposure period and are shown in Figure 3. The maximum temperature for this system was achieved after approximately 40 s, corresponding to a heating effect of over 35 °C and a dispersion temperature of 58.5 °C. Full reversibility of the LC phase formation was shown by capturing periodic SAXS snapshots once the laser irradiation was ceased and the samples were allowed to cool and returned to room temperature.

Using the calibration curves of lattice parameter versus temperature established via the temperature ramp study<sup>5</sup> using the approach described by Fong et al., the apparent temperatures ( $T_{app}$ ) of the sample during irradiation could be determined. The key phase-transition boundaries,  $Q_{II}$  to  $H_{II}$  to  $L_{II}$ , were identified as occurring at 52.29 and 72.08 °C for the irradiated 0.5 g·L<sup>-1</sup> graphene phytantriol dispersions. Figure 4 shows the irradiation-induced heating curve for the 0.5 g·L<sup>-1</sup> graphene phytantriol dispersion calculated from the collected scattering patterns and the lattice parameter calibration curves.

Key reasons to explore the use of graphene as a photothermal agent include the advantages of the surface area

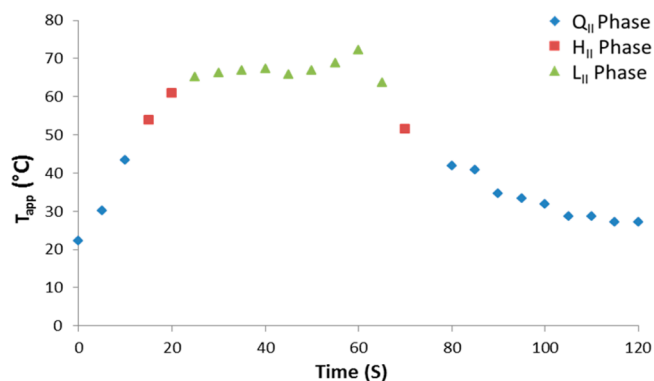


**Figure 4.** Apparent temperature ( $T_{app}$ ) of irradiated  $0.5 \text{ g}\cdot\text{L}^{-1}$  F108-graphene phytantriol dispersions as a function of irradiation time calculated from the equilibrium lattice parameter versus temperature calibration curve.

to volume ratio presented by such materials and the excellent thermal transport properties. It is clear from Figure 3 that the high absorptivity of NIR radiation of the graphene sheets leads to rapid temperature increases within the liquid-crystalline matrix. No heating or any phase transitions were observed upon equivalent irradiation of the phytantriol–water system in the absence of graphene (Figure S5). Previously it was shown that gold nanoparticles can induce phase changes in LC materials upon irradiation with NIR light.<sup>5</sup> Typically the optical density in the infrared region is tuned through controlling the particle size and shape; however, recent studies have demonstrated that at high temperatures a loss of the target morphology can occur, rendering the tunable absorbance potentially impractical for some photothermal applications.<sup>28</sup> Gold nanoparticles are highly efficient photothermal transducers, though they are relatively expensive, but the costs associated with graphene are continually decreasing and are already significantly less than for gold of a given mass. Another distinct advantage of using graphene in photothermal applications comes from the particle geometry. Statistically, it is more likely that an incident photon will be absorbed by a 2D sheet than a 3D particle for a given volume of particles. This allows reduced light flux to be used to generate the same amount of heat and a greater chance of effectiveness in deeper tissues in biomedical applications. Graphene is hence an interesting alternative to gold nanoparticles in photothermal applications.

Ensuring the graphene particles are evenly distributed throughout the dispersion is critical as any aggregation or inhomogeneity can act to either decrease the efficiency of NIR absorption or show exaggerated heating effects due to a higher localized concentration of photothermal transducers. A previous study on gold nanorods dispersed in a phytantriol–water LC dispersion produced via the same method showed a homogeneous distribution.<sup>5</sup> In addition the entire LC graphene dispersion was irradiated during the experiment, removing potential nonrepresentative increases in temperature and localized phase changes.

This system of photothermally stimulated phase transitions could be optimized by lowering the required phase-transition temperature through small alterations to the lipid compositions, such as the addition of GMO which has been previously demonstrated.<sup>5</sup> A lower phase-transition temperature will subsequently reduce the required concentration of graphene to heat the system (or alternatively allow a reduced light flux) and increase the overall efficiency of target applications.

The findings from this study demonstrate that exfoliated graphene is an efficient NIR photothermal agent that is highly capable of inducing full phase transitions in phytantriol lipid LC systems. The temperatures achieved represent a significant advance toward using graphene to produce phase changes due to light stimulation in other lipid liquid-crystalline systems.

## ■ ASSOCIATED CONTENT

### 📄 Supporting Information

Additional materials and experimental details as well as graphene characterization data. The Supporting Information is available free of charge on the ACS Publications website at DOI: 10.1021/acs.langmuir.5b01308.

## ■ AUTHOR INFORMATION

### Notes

The authors declare no competing financial interest.

## ■ ACKNOWLEDGMENTS

This research was undertaken on the SAXS/WAXS beamline at the Australian Synchrotron, Victoria, Australia. S.M.N. and B.J.B. acknowledge financial support under the ARC Future Fellowship scheme.

## ■ REFERENCES

- (1) Barauskas, J.; Johnsson, M.; Tiberg, F. Self-assembled lipid superstructures: Beyond vesicles and liposomes. *Nano Lett.* **2005**, *5*, 1615–1619.
- (2) Barauskas, J.; Landh, T. Phase behavior of the phytantriol/water system. *Langmuir* **2003**, *19*, 9562–9565.
- (3) Dong, Y. D.; Larson, I.; Barnes, T. J.; Prestidge, C. A.; Allen, S.; Chen, X.; Roberts, C. J.; Boyd, B. J. Understanding the interfacial properties of nanostructured liquid crystalline materials for surface-specific delivery applications. *Langmuir* **2012**, *28*, 13485–13495.
- (4) Boyd, B. J.; Dong, Y. D.; Rades, T. Nonlamellar liquid crystalline nanostructured particles: Advances in materials and structure determination. *J. Liposome Res.* **2009**, *19*, 12–28.
- (5) Fong, W. K.; Hanley, T. L.; Thierry, B.; Kirby, N.; Waddington, L. J.; Boyd, B. J. Controlling the nanostructure of gold nanorod-lyotropic liquid-crystalline hybrid materials using near-infrared laser irradiation. *Langmuir* **2012**, *28*, 14450–14460.
- (6) Fong, W. K.; Hanley, T. L.; Thierry, B.; Kirby, N.; Boyd, B. J. Plasmonic nanorods provide reversible control over nanostructure of self-assembled drug delivery materials. *Langmuir* **2010**, *26*, 6136–6139.
- (7) Sreethawong, T.; Puangpetch, T.; Chavadej, S.; Yoshikawa, S. Quantifying influence of operational parameters on photocatalytic  $\text{H}_2$  evolution over Pt-loaded nanocrystalline mesoporous  $\text{TiO}_2$  prepared by single-step sol-gel process with surfactant template. *J. Power Sources* **2007**, *165*, 861–869.
- (8) Kibsgaard, J.; Chen, Z.; Reinecke, B. N.; Jaramillo, T. F. Engineering the surface structure of  $\text{MoS}_2$  to preferentially expose active edge sites for electrocatalysis. *Nat. Mater.* **2012**, *11*, 963–969.
- (9) Wu, D.; Duan, J.; Zhang, C.; Guo, K.; Zhu, H. Sacrificial template synthesis and photothermal conversion enhancements of hierarchical and hollow  $\text{CuInS}_2$  microspheres. *J. Phys. Chem. C* **2013**, *117*, 9121–9128.
- (10) Wu, D.; Duan, J.; Lin, Y.; Meng, Z.; Zhang, C.; Zhu, H. Photothermal conversion of copper sulfide hollow structures with different shape and thickness. *J. Nanosci. Nanotechnol.* **2015**, *15*, 3191–3195.
- (11) Han, J.; Li, J.; Jia, W.; Yao, L.; Li, X.; Jiang, L.; Tian, Y. Photothermal therapy of cancer cells using novel hollow gold nanoflowers. *Int. J. Nanomed.* **2014**, *9*, 517–526.
- (12) Yang, P.; Quan, Z.; Li, C.; Kang, X.; Lian, H.; Lin, J. Bioactive, luminescent and mesoporous europium-doped hydroxyapatite as a drug carrier. *Biomaterials* **2008**, *29*, 4341–4347.

- (13) Spicer, P. T. Progress in liquid crystalline dispersions: Cubosomes. *Curr. Opin. Colloids Interface Sci.* **2005**, *10*, 274–279.
- (14) Shah, J. C.; Sadhale, Y.; Chilukuri, D. M. Cubic phase gels as drug delivery systems. *Adv. Drug Delivery Rev.* **2001**, *47*, 229–250.
- (15) Kono, K. Thermosensitive polymer-modified liposomes. *Adv. Drug Delivery Rev.* **2001**, *53*, 307–319.
- (16) Tian, B.; Wang, C.; Zhang, S.; Feng, L.; Liu, Z. Photothermally enhanced photodynamic therapy delivered by nano-graphene oxide. *ACS Nano* **2011**, *5*, 7000–7009.
- (17) Huang, X.; El-Sayed, I. H.; Qian, W.; El-Sayed, M. A. Cancer cell imaging and photothermal therapy in the near-infrared region by using gold nanorods. *J. Am. Chem. Soc.* **2006**, *128*, 2115–2120.
- (18) Jain, P. K.; Lee, K. S.; El-Sayed, I.; El-Sayed, M. A. Calculated absorption and scattering properties of gold nanoparticles of different size, shape, and composition: Applications in biological imaging and biomedicine. *J. Phys. Chem. B* **2006**, *110*, 7238–7248.
- (19) Yang, K.; Feng, L.; Shi, X.; Liu, Z. Nano-graphene in biomedicine: Theranostic applications. *Chem. Soc. Rev.* **2013**, *42*, 530–547.
- (20) Yang, K.; Zhang, S.; Zhang, G.; Sun, X.; Lee, S. T.; Liu, Z. Graphene in mice: Ultrahigh in vivo tumor uptake and efficient photothermal therapy. *Nano Lett.* **2010**, *10*, 3318–3323.
- (21) Hu, S. H.; Fang, R. H.; Chen, Y. W.; Liao, B. J.; Chen, I. W.; Chen, S. Y. Photoresponsive protein-graphene-protein hybrid capsules with dual targeted heat-triggered drug delivery approach for enhanced tumor therapy. *Adv. Funct. Mater.* **2014**, *24*, 4144–4155.
- (22) Guo, M.; Huang, J.; Deng, Y.; Shen, H.; Ma, Y.; Zhang, M.; Zhu, A.; Li, Y.; Hui, H.; Wang, Y.; Yang, X.; Zhang, Z.; Chen, H. PH-responsive cyanine-grafted graphene oxide for fluorescence resonance energy transfer-enhanced photothermal therapy. *Adv. Funct. Mater.* **2015**, *25*, 59–67.
- (23) Robinson, J. T.; Tabakman, S. M.; Liang, Y.; Wang, H.; Sanchez Casalongue, H.; Vinh, D.; Dai, H. Ultrasmall reduced graphene oxide with high near-infrared absorbance for photothermal therapy. *J. Am. Chem. Soc.* **2011**, *133*, 6825–6831.
- (24) Notley, S. M. Highly concentrated aqueous suspensions of graphene through ultrasonic exfoliation with continuous surfactant addition. *Langmuir* **2012**, *28*, 14110–14113.
- (25) Hernandez, Y.; Nicolosi, V.; Lotya, M.; Blighe, F. M.; Sun, Z.; De, S.; McGovern, I. T.; Holland, B.; Byrne, M.; Gun'ko, Y. K.; Boland, J. J.; Niraj, P.; Duesberg, G.; Krishnamurthy, S.; Goodhue, R.; Hutchison, J.; Scardaci, V.; Ferrari, A. C.; Coleman, J. N. High-yield production of graphene by liquid-phase exfoliation of graphite. *Nat. Nanotechnol.* **2008**, *3*, 563–568.
- (26) Bender, J.; Ericson, M. B.; Merclin, N.; Iani, V.; Rosén, A.; Engström, S.; Moan, J. Lipid cubic phases for improved topical drug delivery in photodynamic therapy. *J. Controlled Release* **2005**, *106*, 350–360.
- (27) Hyde, S. T.; Andersson, A.; Ericsson, B.; Larsson, K. A cubic structure consisting of a lipid bilayer forming an infinite periodic minimum surface of the gyroid type in the glycerolmonooleat-water system. *Z. Kristallogr.* **1984**, *168*, 213–219.
- (28) Xie, J.; Lee, J. Y.; Wang, D. I. C. Seedless, surfactantless, high-yield synthesis of branched gold nanocrystals in HEPES buffer solution. *Chem. Mater.* **2007**, *19*, 2823–2830.

## **Electronic Supplementary Information**

### **Using graphene to control nanostructure in photoresponsive self-assembled graphene-lipid drug delivery materials**

*Matthew D. J. Quinn<sup>1</sup>, Joanne Du<sup>2</sup>, Ben J Boyd<sup>2</sup>, Adrian Hawley<sup>3</sup>, Shannon M. Notley<sup>4\*</sup>*

#### **Graphene Exfoliation**

The graphene suspension was prepared via surfactant assisted liquid exfoliation. 1 % w/w of graphite flakes was added to a 0.1 % w/w F108 MilliQ solution and was sonicated with the Q700 Qsonica ultrasonicator with a 13mm diameter probe attached at an amplitude of 40 for 4 hours. The suspension produced was then centrifuged at 1500 rcf for 5 min. Previous studies have shown that this length of sonication and subsequent separation through centrifugation results in highly concentrated aqueous suspensions of single and few layer graphene [1].

Following this, the supernatant was decanted and the graphene suspension and particles characterised. The concentration of graphene was 0.524 mg/mL determined from absorptivity at 660 nm using an extinction coefficient of 2460 L g<sup>-1</sup> m<sup>-1</sup> [2].

#### **Graphene Characterisation**

Raman spectra of the dried F108-graphene particles deposited on a glass slide were measured using an alpha 300A Raman (Witec) with a laser wavelength of 532nm. Three distinct peaks at 1352.96, 1584.77 and 2701.60 cm<sup>-1</sup> corresponding to the D, G and 2D modes are observed. The presence of the D peak at 1352.96 cm<sup>-1</sup> indicates the presence of non-sp<sup>2</sup> carbon principally from edge defects as previously described for measurements on particles with

nanometre lateral dimensions [3]. Furthermore the 2D peak has shifted in comparison to graphite and is Lorentzian in shape indicating that the sample is highly exfoliated. The relative intensities of the G to 2D peak also indicated that the measured sample is of single to few layer thickness [4].

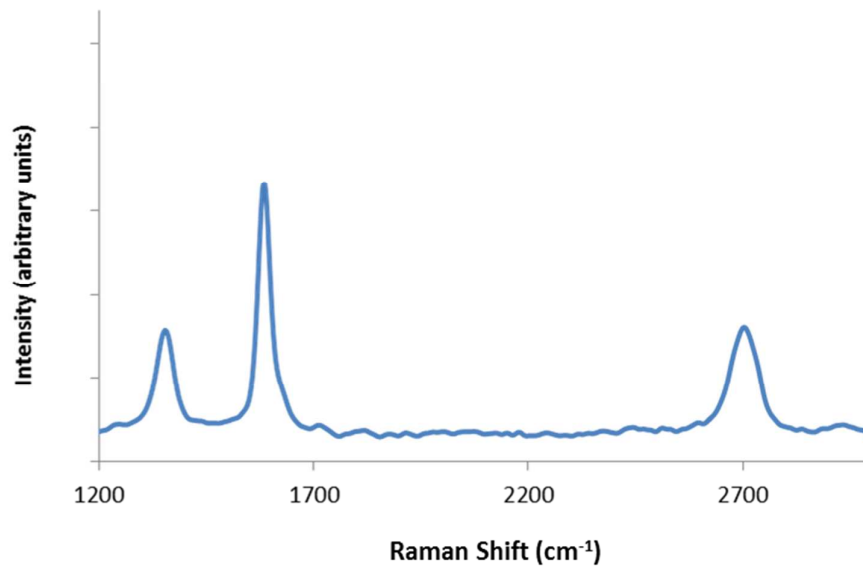


**Figure S1.** Raman spectra showing the characteristic peak position and shapes for exfoliated graphene sheets.

Particle sizing measurements were performed using the dynamic light scattering (DLS) technique driven by a 90Plus Particle Size Analyzer (Brookhaven Instruments). The mean lateral diameter measured was 344.3nm. It is of importance to note though that DLS gives the equivalent sphere hydrodynamic radius. Clearly, the geometry of the graphene sheets deviates significantly from this model and hence DLS cannot distinguish on the basis of particle thickness.

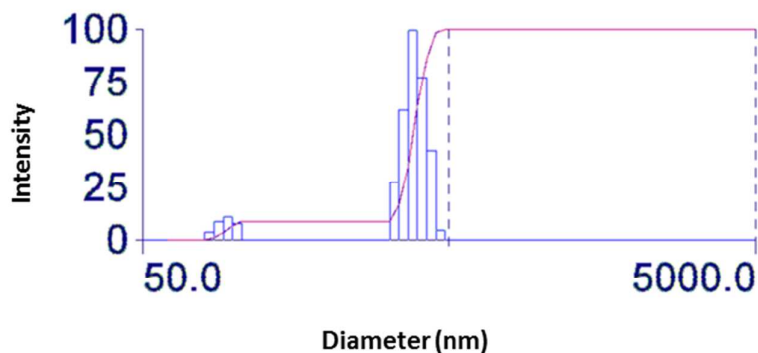


**Figure S2.** A representative particle sizing multimodal size distribution graph, the poly disperse nature of the dispersions should be taken into account when a single lateral size is stated.

The light absorption of the graphene suspension was investigated using UV-visible spectrophotometry. The spectrum for the F108-graphene is shown in Figure S3. The peak in absorptivity was observed at 270 nm indicating that the graphene sheets have few to no basal plane defects [5]. Furthermore, there is significant absorption across all wavelengths investigated here showing the highly conjugated nature of the carbon bonding of the graphene particles again providing compelling evidence for the lack of significant defects. For this particular study, absorption of light in the IR region (wavelength of the incident laser used was 808 nm) is of great importance. As can be seen from the data in Figure S3, the graphene particles strongly absorb light of this wavelength promoting the efficacy of this material in photothermal applications.

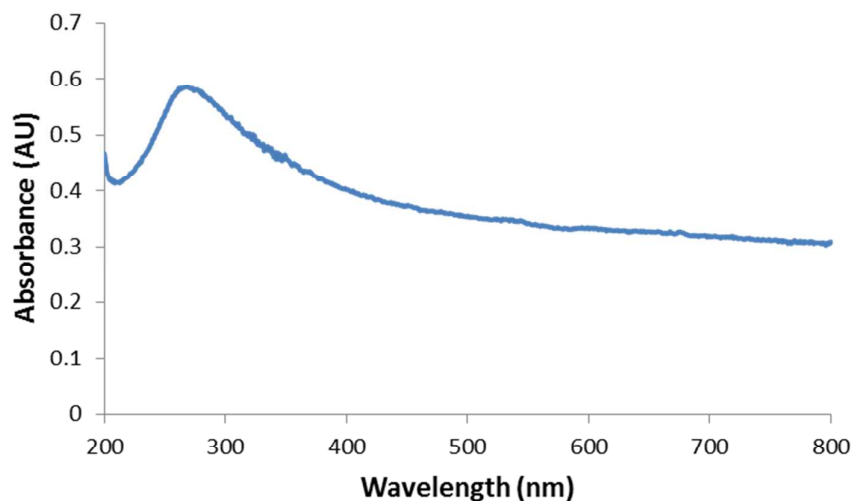


**Figure S3.** Absorbance spectrum for  $0.0131 \text{ g.L}^{-1}$  F108 (100 fold dilution of stock suspension) stabilised graphene suspension showing the characteristic peak at 270nm.

The photoresponsive liquid crystalline nanoparticles were prepared by dispersing a graphene suspension stabilised by a triblock copolymer F108 (Purchased from Sigma Aldrich, Australia, and used without further purification), into phytantriol at a ratio of 1:1. The phytantriol (a gift from DSM Nutritional Products (Singapore) and used without further purification) was warmed in a  $60 \text{ }^{\circ}\text{C}$  drying oven in order to allow easy handling and 500 mg was weighed into 4 mL glass vials. A  $0.524 \text{ g.L}^{-1}$  (determined via the extinction coefficient  $2460 \text{ L g}^{-1}\text{m}^{-1}$  [2]) suspension of F108 stabilised graphene suspension was prepared in MilliQ filtered water and appropriate volumes were added to the respective lipid samples.

After addition of the aqueous graphene phase to the lipids, the samples were heated to  $75 \text{ }^{\circ}\text{C}$  for 30 min, followed immediately by 10 sec vortexing (whilst warm and viscosity is minimised). The samples are then allowed to cool to room temperature (approximately 15 min on the bench) and the heating, vortexing, cooling steps are repeated (3 times). Samples are placed on a “roller” overnight to allow equilibration and then stored at  $4 \text{ }^{\circ}\text{C}$ .

## SAXS Experimental Data

Dynamic SAXS data was collected on the SAXS/WAXS beamline at the Australian Synchrotron [6]. An X-ray beam with a wavelength of 0.103 Å (12 keV) was selected. A silver behenate standard (d-spacing = 58.38 Å) was used for the  $q$  range calibration. The scattering patterns were acquired using a Pilatus 1M detector with active area 169 x 179 mm<sup>2</sup> and with a pixel size of 172 μm. The total  $q$  range for the instrument configuration was 0.02 <  $q$  < 1.00 Å<sup>-1</sup>.

Bulk (50 mg) samples were loaded into capillary holders, sealed with Kapton tape and mounted in front of the X-ray beam with the 400 mW 808 nm laser positioned 12 mm from the sample in order to achieve full sample coverage.

The 100 ms acquisition time was selected in order to minimise the potential of any radiation damage. Due to the high flux of the synchrotron radiation the resolution of the diffractograms obtained were all more than sufficient.

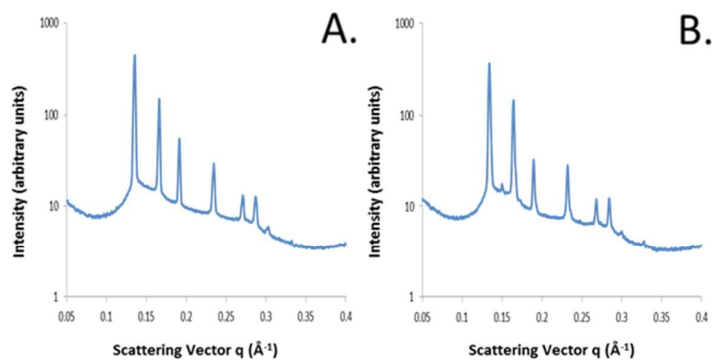


**Figure S4.** The two series presented represent the initial SAXS snapshot for (A) 0.5 g L<sup>-1</sup> F108 graphene phytantriol and (B) graphene free phytantriol water dispersion

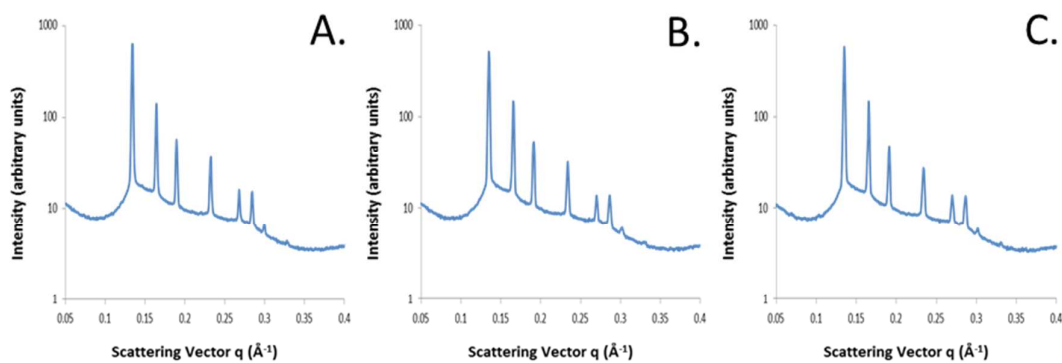


**Figure S5.** The three series presented here are for the phytantriol in MilliQ 1:1 (A) prior to laser exposure, (B) after 1 minute of exposure and (C) after a two minute “cool down” period.

### Surfactant Selection

A range of preparation methods for lipid liquid crystalline systems have been previously studied with a number of different parameters including in the presence of surfactants such as F127 [7] and other amphiphilic lipids such as glyceryl monooleate (GMO) [8]. The systems produced via these preparation methods have been confirmed, usually by SAXS, to be stable and reproducible. It has been shown that phytantriol in the presence of high concentrations of large and high hydrophobe lipophobe balance (HLB) pluronic surfactants such as F127 (PEO<sub>101</sub>PPO<sub>56</sub>PEO<sub>101</sub>), will maintain its Q<sub>II</sub> Pn3m structure [9] and have greater stability [10]. The non-ionic surfactant F108 (PEO<sub>141</sub>PPO<sub>44</sub>PEO<sub>141</sub>), which is larger than the F127 copolymer studied previously and of a similar HLB, was selected for exfoliation of the graphene.

## References

1. Notley, S.M., *Highly concentrated aqueous suspensions of graphene through ultrasonic exfoliation with continuous surfactant addition. Langmuir*, 2012. 28(40): p. 14110-14113.
2. Hernandez, Y., Nicolosi, V., Lotya, M., Blighe, F. M., Sun, Z., De, S., McGovern, I. T., Holland, B., Byrne, M., Gun'ko, Y. K., Boland, J. J., Niraj, P., Duesberg, G., Krishnamurthy, S., Goodhue, R., Hutchison, J., Scardaci, V., Ferrari, A. C., Coleman, J. N., *High-yield production of graphene by liquid-phase exfoliation of graphite. Nat. Nanotechnol.*, 2008. 3(9): p. 563-568.
3. Lotya, M. Hernandez, Y., King, P. J., Smith, R. J., Nicolosi, V., Karlsson, L. S., Blighe, F. M., De, S., Zhiming, W., McGovern, I. T., Duesberg, G. S. Coleman, J. N., *Liquid phase production of graphene by exfoliation of graphite in surfactant/water solutions. J. Am. Chem. Soc.*, 2009. 131(10): p. 3611-3620.
4. Wang, J., Manga, K. K., Bao, Q., Loh, K. P., *High-Yield Synthesis of Few-Layer Graphene Flakes through Electrochemical Expansion of Graphite in Propylene Carbonate Electrolyte. J. Am. Chem. Soc.*, 2011. 133(23): p. 8888-8891.
5. Dan, L., Müller, M. B., Gilje, S., Kaner, R. B., Wallace, G. G., *Processable aqueous dispersions of graphene nanosheets. Nat. Nanotechnol.*, 2008. 3(2): p. 101-105.
6. Kirby, N.M., Mudie, S. T., Hawley, A. M., Cookson, D. J., Mertens, H. D. T., Cowieson, N., Samardzic-Boban, V., *A low-background-intensity focusing small-angle X-ray scattering undulator beamline. J. App. Crystallogr.*, 2013. 46(6): p. 1670-1680.
7. Landh, T., *Phase behavior in the system pine oil monoglycerides-poloxamer 407-water at 20°C. J. Phys. Chem.*, 1994. 98(34): p. 8453-8467.
8. Boyd, B.J., Rizwan, S. B., Dong, Y., Hook, S., Rades, T., *Self-Assembled Geometric Liquid-Crystalline Nanoparticles Imaged in Three Dimensions: Hexosomes Are Not Necessarily Flat Hexagonal Prisms. Langmuir*, 2007. 23(25): p. 12461-12464.
9. Dong, Y.D., Larson, I., Hanley, T., Boyd, B. J., *Bulk and dispersed aqueous phase behavior of phytantriol: Effect of vitamin E acetate and F127 polymer on liquid crystal nanostructure. Langmuir*, 2006. 22(23): p. 9512-9518.
10. Boyd, B.J., Y.D. Dong, and T. Rades, *Nonlamellar liquid crystalline nanostructured particles: Advances in materials and structure determination. J. Liposome Res.*, 2009. 19(1): p. 12-28.

*Keep Going!*

*The best is yet to come...*